Cardiff University
School of Medicine
Systems Immunity Research Institute

Prifysgol Caerdydd
Yr Ysgol Meddygaeth
Sefydliad Ymchwil Systemau Imiwnedd

Identification of novel cancer-specific T cell targets by dissection of successful tumour-infiltrating lymphocyte therapy

Cristina Rius Rafael

A thesis submitted to Cardiff University
in candidature for the degree of
Doctor of Philosophy

August 2019

Statements and declarations

STATEMENT 1

This thesis is being submitted in partial fulfilment of the requirements for the degree of PhD.

Signed: …… Date ……

STATEMENT 2

This work has not been submitted in substance for any other degree or award at this or any other university or place of learning, nor is it being submitted concurrently for any other degree or award (outside of any formal collaboration agreement between the University and a partner organisation)

Signed: …… Date ……

STATEMENT 3

I hereby give consent for my thesis, if accepted, to be available in the University's Open Access repository (or, where approved, to be available in the University's library and for inter-library loan), and for the title and summary to be made available to outside organisations, **subject to the expiry of a University-approved bar on access**.

Signed: …… Date ……

DECLARATION

This thesis is the result of my own independent work, except where otherwise stated, and the views expressed are my own. Other sources are acknowledged by explicit references. The thesis has not been edited by a third party beyond what is permitted by Cardiff University's Use of Third Party Editors by Research Degree Students Procedure.

Signed: …… Date ……

WORD COUNT: 43,823 words

(Excluding summary, acknowledgements, declarations, contents pages, appendices, tables, diagrams and figures, references, bibliography, footnotes and endnotes)

This thesis is dedicated to the memory of Juan Rafael Martinez (1931-2018)

Acknowledgements

The research conducted in this thesis would not have been possible without the contribution of my supervisory team, my colleagues, collaborators and my funding body Cancer Research Wales. To all, thank you for the role you played in the development of this project.

First of all, I would like to thank my supervisor **Professor Andrew K. Sewell** for accepting my candidature to enrol in this exciting project. Thank you for always making sure that I "keep smiling", addressing my questions and providing the necessary support through these years. I look forward to generating further ground-breaking scientific discoveries in your team! A very special thanks to my supervisor **Dr Garry Dolton** for training and support, and for being an inspiration of dedication and perseverance. I thank **Dr Meriem Attaf**, who taught me so much about TCR clonotyping. Thank you all for the continued support provided, as it has guided me through completion of my PhD.

I would like to acknowledge all my colleagues from the **T cell modulation group**, present and past, for creating such a constructive and positive environment. A special mention to **Dr Mateusz Legut**, **Dr Sophie Wheeler-Morris** and soon-to-be-Dr **Sarah Galloway** and **Marine Caillaud** for the great times spent together in Cardiff, but most importantly, thank you for your friendship. An important thanks to **Anna Fuller**, who's management of the lab made sure everything ran like clockwork, while always being so helpful and supportive. I would also like to acknowledge the support received with cell sorting from **Catherine Naseriyan** and **Ann Kift-Morgan** from the CBS Flow Cytometry Facility; and **Dr Barbara Szomolay** for the development of the PS-CPL webtool that was crucial for my studies.

Special thanks to **Professor Ann Ager**, **Dr James Mathews** and **Dr Eddie Wang** for taking the time to provide feedback on my annual progress reports and for much-appreciated advice. I would also like to thank **Professor Ron Chakraverty** and **Professor Awen Gallimore** for kindly agreeing to examine me.

Last but not least, I would like to express my most solemn gratitude to my family. A very special thank you to my Mother, who has always put my sister and me first, and who made sure I would get to wherever I wanted to be; to my aunt, who has always encouraged me and believed in me, and to my *yaya*, who would have preferred I had chosen a more convenient profession so I wouldn't have to move away from home, but who I know is proud of what I have achieved. A massive thanks to my partner Alex, for being so patient, supportive and caring with me all these years. I cannot even put into words how much you've all helped me get to this point, thank you. My last expression of gratitude is to my *yayo*, to whom this thesis is dedicated, for the many years of love and inspiration to be both the person and the researcher I want to be.

To each and all of you, thank you.

Summary

Background – T cell-based cancer immunotherapy has emerged as the biggest development in cancer treatment since radiotherapy and is capable of inducing complete, durable remissions in end-stage cancer patients. It is believed that the key effector cells are cytotoxic $CD8^+$ T cells, which can detect anomalies in the proteome of cells that have undergone cancerous transformation, through the recognition of peptides presented at the cell surface bound to human leukocyte antigen (HLA) class I molecules. Recognition of peptide-HLA is controlled by the αβ T cell receptor (TCR). My work focussed on successful tumour infiltrating lymphocyte (TIL) therapy for the treatment of melanoma, which involves *in vitro* expansion of T cells from a tumour lesion to large numbers ($>10^{10}$ cells) and reinfusion back into the patient's blood. I had access to stored samples from a cohort of patients that underwent a complete durable remission following TIL therapy for stage IV melanoma. These samples included the TIL infusion product, an autologous melanoma cell line and peripheral blood mononuclear cells before treatment and after cancer clearance. The main focus of my thesis was to dissect the persistent tumour-reactive TCR repertoire in an HLA*02:01 melanoma patient successfully treated by TIL therapy and to identify the antigenic-specificity of key T cell clonotypes using a combination of High throughput sequencing (HTS), combinatorial peptide library (CPL) screening and CRISPR/Cas9 technology.

Results – When I initiated my studies, it became apparent that the current "gold standard" for the identification of antigen-specific T cells, fluorochrome-conjugated peptide-HLA multimers (usually tetramers) failed to detect many fully functional T cells bearing low affinity TCRs. I therefore set out to optimise this technique so that it was capable of detecting all cancer-specific T cells within patient-derived samples. HTS of the TCRs that responded to the patient-autologous cancer line allowed me to identify cancer-specific TCRs in the TIL infusion product that persisted in patient blood after successful treatment. Disruption of the *HLA A*0201* allele revealed that most of this response was operated through HLA A2. Some persistent clonotypes were shown to respond to a wide range of HLA $A2^+$ cancer cell lines from a range of different tissue origins. This broad tumoricidal activity suggested that these T cell clones responded to unknown, common, shared antigens. Application of a bespoke CPL-based epitope discovery pipeline identified two new HLA A2-restricted epitopes. Further analysis of one persistent clonotype identified an important new property that allowed it to recognise most types of cancer cell via HLA A*02:01.

Conclusions – I showed that peptide-HLA tetramers can fail to detect relevant functional T cell clonotypes and that this technology underestimates biologically relevant antigen-reactive T cell populations. Dissection of the cancer-specific T cell response in the TIL infusion product and blood following complete remission identified T cell clonotypes that responded to cancer cell lines from a range of different tissue origins, suggesting that these T cells respond to unknown shared antigens. I showed that a bespoke CPL-based ligand presentation platform could identify new broadly-expressed HLA A*02:01-restricted epitopes. TCRs with these specificities might protect from a wide range of cancer types and make exciting candidates for further therapeutic exploration.

Work incorporated in this thesis

Rius, C., Attaf, M., Tungatt, K., Bianchi, V., Legut, M., Bovay, A., Donia, M., Thor Straten, P., Peakman, M., Svane, I. M., Ott, S., Connor, T., Szomolay, B., Dolton, G. and Sewell, A. K. (2018) 'Peptide-MHC Class I Tetramers Can Fail To Detect Relevant Functional T Cell Clonotypes and Underestimate Antigen-Reactive T Cell Populations.', *Journal of immunology*, 200(7), pp. 2263–2279. doi: 10.4049/jimmunol.1700242.

Other work published during my PhD

Bagaev D. V, Vroomans M.A, Samir J, Stervbo U, **Rius C**, Dolton G, Greenshields-Watson A, Attaf M, Evgeny S. Egorov, E. S, Zvyagin, I. V, Babel N, Cole D. K, Godkin A. J, Sewell A. K, Kesmir C, Chudakov, D. M., Luciani F, Shugay M. 'VDJdb in 2019: database extension, new analysis infrastructure and a TCR motif compendium'. Nucleic acids research. Pending of publication.

Galloway SAE, Dolton G, Attaf M, Wall A, Fuller A, **Rius C**, Bianchi V, Theaker S, Lloyd A, Caillaud ME, Svane IM, Donia M, Cole DK, Szomolay B, Rizkallah P and Sewell AK (2019) 'Peptide Super-Agonist Enhances T cell Responses to Melanoma.' *Frontiers in Immunology.* 10:319. doi: 10.3389/fimmu.2019.00319

Dolton, G., Zervoudi, E., **Rius, C**., Wall, A., Thomas, H. L., Fuller, A., Yeo, L., Legut, M., Wheeler, S., Attaf, M., Chudakov, D. M., Choy, E., Peakman, M. and Sewell, A. K. (2018) 'Optimized Peptide–MHC Multimer Protocols for Detection and Isolation of Autoimmune T cells', *Frontiers in Immunology*, 9, p.1378. doi: 10.3389/fimmu.2018.01378.

Shugay, M., Bagaev, D. V, Zvyagin, I. V, Vroomans, R. M., Crawford, J. C., Dolton, G., Komech, E. A., Sycheva, A. L., Koneva, A. E., Egorov, E. S., Eliseev, A. V, Van Dyk, E., Dash, P., Attaf, M., **Rius, C.,** Ladell, K., McLaren, J. E., Matthews, K. K., Clemens, E. B., Douek, D. C., Luciani, F., van Baarle, D., Kedzierska, K., Kesmir, C., Thomas, P. G., Price, D. A., Sewell, A. K. and Chudakov, D. M. (2018) 'VDJdb: a curated database of T cell receptor sequences with known antigen specificity.', Nucleic acids research, 46(D1), pp. D419–D427. doi: 10.1093/nar/gkx760.

Theaker, S. M., **Rius, C**., Greenshields-Watson, A., Lloyd, A., Trimby, A., Fuller, A., Miles, J. J., Cole, D. K., Peakman, M., Sewell, A. K. and Dolton, G. (2016) 'T cell libraries allow simple parallel generation of multiple peptide-specific human T cell clones.', Journal of immunological methods. 430, pp. 43–50. doi: 10.1016/j.jim.2016.01.014.

Presentations of the results described in this thesis

Next Generation Immuno-Oncology Congress, poster presentation (London – UK, 2019)

Division of Infection and Immunology Seminar Series, Invited speaker (Cardiff – UK, 2018)

University of Utah, Invited speaker (Salt Lake City - USA, 2018)

Cardiff University Post-Graduate Day Seminar, Invited speaker (Cardiff – UK, 2018)

Monash University Seminar, Invited speaker (Cardiff – UK, 2017)

Cancer Research Wales, Invited speaker (Cardiff – UK, 2017)

Division of Infection and Immunology Annual meeting, poster presentation (Cardiff – UK, 2017)

List of abbreviations

aa	amminoacid
BsAb	Bispecific antibody
mAb	Monoclonal Antibody
ACT	Adoptive Cell Therapy
ALL	Acute lymphoblastic leukaemia
AML	Acute myeloid leukaemia
APC	Antigen Presenting Cell
aPC	Allophycocyanin
APL	Altered peptide ligand
APM	Antigen Presentation Machinery
ATCC	American-Type Culture Collection
BITE	Bi-specific T cell engager
bp	base pair
BSA	Bovine Serum Albumin
BST-2	Bone Marrow Stromal Cell Antigen 2
BTLA	B- and T- lymphocyte attenuator
C	Constant Region of the TCR
°C	Celsius
CAF	Cancer Associated Fibroblasts
CART T cells	Chimeric Antigen Receptor Transduced T cells
CCIT	Center for Cancer Immune Therapy
CCL (number)	Chemokine Ligand (number)
CCR (number)	Chemokine receptor (number)
CD (number)	Cluster Differentiation (number)
CDR (number)	Complementary Determining Region (number)
CFSE	Carboxyfluorescein succinimidyl ester
CMV	Cytomegalovirus
Cr	Chromium
CR	Complete Remission
CRISPR	Clustered regularly interspaced short palindromic repeats
crRNA	Complementary RNA
CTA	Cancer-Testis Antigens
CTL	Cytotoxic $\alpha\beta$ T-Lymphocytes
CTLA-4	Cytotoxic T-Lymphocyte-associated protein 4
DC	Dendritic Cells
DMEM	Dulbecco modified eagle's minimal essential media
DMSO	Dimethyl sulphoxide
DN	Double Negative
DNA	Deoxyribonucleic Acid
DP	Double positive
Dr	Doctor
DTT	Dithiothreitol

EBV	Epstein Barr Virus
ECM	Extracellular Matrix
EDTA	Ethyl-enediaminetetra acetic acid
ELISA	Enzyme-Linked Immunosorbent Assay
ELISpot	Enzyme-Linked ImmunoSpot
ER	Endoplasmic Reticulum
ERAAP	Endoplasmic Reticulum Aminopeptidase associated with Antigen Processing
E:T	Effector to target
ETP	Early committed Thymic Precursor
FACS	Fluorescence-Activated Cell Sorting
FBS	Foetal Bovine Serum
FDA	Food and Drug Administration
FITC	Fluorescein Isothiocyanate
FMO	Fluorescence minus one
FSC	Forward scatter
g	gram
h	hour
HCV	Hepatitis C Virus
HHV	Human Herpes Virus
HIV	Human Immunodeficiency Virus
HLA	Human leukocyte Antigen
HPV	Human Papilloma Virus
HSC	Hematopoietic Stem Cells
HTS	High Throughput Sequencing
irAEs	Immune-related adverse effects
IAV	Influenza A Virus
ICAM	Intercellular Adhesion Molecule
ICOS(L)	Inducible T cell co-stimulator (ligand)
IDO	Indoleamine-pyrrole 2,3-dioxygenase
IFN	Interferon
IGF2BP2	Insulin-Like Growth Factor 2 mRNA Binding Protein (a.k.a. IMP2)
IL	Interleukin
ITAM	Immunoreceptor Tyrosine-based Activation Motif
IU	International Units
K_D	Dissociation constant
LAG-3	Lymphocyte-activation gene
LFA-1	Lymphocyte function-associated antigen-1
MBP	Myelin Basic Protein
MDSC	Myeloid-Derived Suppressor Cells
MHC	Main Histocompatibility Complex
MIP-1β	Macrophage inflammatory protein 1-beta
MM	Malignant Melanoma
M	Molar
mM	milli Molar
N	non-template nucleotides

NGS	Next Generation Sequencing
NK	Natural Killer cell
NKT	Natural Killer T cell
NS	Non-structural
NSCLC	Non-small-cell lung carcinoma
OR	Objective Response
P	palindromic nucleotides
p	peptide
PB	Pacific blue
PAM	Protospacer Adjacent Motif
PBMC	Peripheral blood mononuclear cell
PBS	Phosphate Buffer Saline
PCR	Polymerase chain reaction
PDB	Protein Data Bank
PD-1	Programmed death receptor 1
PD-L1	Programmed death receptor Ligand 1
PE	R-phycoerythrin
PE Cy7	R-phycoerythrin CyChrome 7
PerCP	Peridinin chlorophyll protein
PHA	Phytohemagglutinin
PI	Protease Inhibitor
PKI	Protein Kinase Inhibitor
pMHC	Peptide-MHC complex
PS-CPL	Positional Scan Combinatorial Peptide Library
RACE	Rapid Amplification of cDNA Ends
RAG	Recombinase-Activating Gene
rCD2	Rat Cluster Differentiation 2
RNA	Ribonucleic Acid
rpm	Revolutions per minute
RPMI	Roswell Park Memorial Institute medium
RSS	Recombination Signal Sequence
RT	Room temperature
RT	Reverse Transcriptase
RVE	Rubella Virus
scFv	Single-chain fragment variable
SP	Single Positive
SSC	Side scatter
T1D	Type 1 Diabetes
TAA	Tumour Associated Antigens
TAM	Tumour Associated Macrophages
TAPI	TNF processing inhibitor
TCR	T Cell Receptor
TDSF	Tumour-derived Soluble Factors
TGFβ	Transforming Growth Factor Beta
TIL	Tumour Infiltrating Lymphocytes

TIM-3	T cell Immunoglobulin and Mucin domain-3
TME	Tumour Micro Environment
TNF	Tumour necrosis factor
tracRNA	Trans-activating RNA
tra/trb/trg/trd	TCR receptor alpha/beta/gamma/delta chain
TRAJ	T cell receptor alpha joining gene
TRAV	T cell receptor alpha variable gene
TRBD	T cell receptor beta diversity gene
TRBJ	T cell receptor beta joining gene
TRBV	T cell receptor beta variable gene
Treg	Regulatory T cell ($CD4^+$)
TSA	Tumour Specific Antigens
UV	Ultraviolet
V	Variable Region of the TCR
V	Volts
V(D)J	Variable, Diverse and Joining regions of the TCR
VISTA	V-domain Ig suppressor of T cell activation
WT	Wild-type
YFV	Yellow Fever virus
xg	G force or relative centrifugal force
β2m	Beta-2-microglobuliln
µ	micro
µg	micro grams
µL	micro litre
-ve	Untransduced

Table of contents

List of figures

List of tables

– Chapter 1 –

Introduction

1.1. Overview of the Adaptive Immune System

The Immune System acts as an inherent protection system in all vertebrates, including humans, by recognising exogenous (i.e. infections) and/or endogenous (i.e. malignancies) threats and by activating immune effector and regulation functions to ensure effective containment/elimination of the threat without causing damage to the body. Initial defence against a pathogen is carried out through the **Innate Immune System** arm (or non-specific immunity) which has evolved to generate a fast response against a limited number of molecules, most of which are unique to microbes. In contrast, the **Adaptive Immune System** arm (or specific immunity) is initiated when the non-specific response fails to eliminate a threat. The components of the Adaptive arm (B and T lymphocytes) are capable of recognizing a much wider array of foreign substances through highly diverse and specialised antigen receptors, which persist in the body and generate immunological memory, allowing a more rapid and effective response to a pathogen that has been previously encountered[1].

Adaptive immune responses are built on the foundations set by the innate immunity. Effective cross-talk between the two arms of the immune system plays a pivotal role in successful immunity. In general terms, adaptive humoral responses are mediated by production of antibodies by B lymphocytes and their progeny, whereas cellular responses are characterised by T lymphocytes recognising antigenic peptides presented by **Major Histocompatibility Complex (MHC)** molecules on **Antigen Presenting Cells (APCs)**[1]. Yet, this broad description cannot even start to cover the vast complexity of such fine-tuned system; instead, different subtypes of T lymphocytes can be found in the periphery based on their effector functions and molecular phenotype.

In the context of malignancies, elements from both arms of the immune system are present within the tumour microenvironment[2–4], however the focus of this thesis is the role of a specific subset of Lymphocytes: **Cytotoxic αβ T-Lymphocytes (CTLs).** CTLs are known to be of primary importance in anticancer immunity for two main reasons: firstly, CTLs are able to detect changes in the internal proteome that can give rise to cancerous transformation; secondly, they can directly eliminate malignant cells through a variety of mechanisms. Many studies have shown how immune infiltration shapes tumour progression and its response to therapy[5–8]. In fact, both pathogens and tumour malignancies have developed advanced mechanisms of evading the immune response, some of which will be further discussed in **Section 1.4** with a special focus in cancer immunity. According to the focus of this thesis, this section describes conventional αβ T cells and mechanisms of actions in tumour clearance.

1.1.1. T cell development

T cells are generated from a pool of hematopoietic progenitor cells that differentiate and proliferate to generate a diverse range of cell types[9]. The T cell differentiation programme can be characterised by changes in the cell-surface phenotype, proliferation status and functionality. The two key events in T cell development include commitment to the αβ or γδ T cell lineage through the rearrangement and expression of the T cell receptor (TCR) genes, and positive/negative selection of immature TCR repertoire by recognition of self-peptide-MHC complexes.

Several T cell subsets arise from the differentiation program and contribute to immune surveillance based on the somatically rearranged TCR expressed on their surface. In humans, conventionally MHC-restricted αβ T lymphocytes are the most abundant T cell subset, whereas unconventional T lymphocytes comprise non-MHC restricted γδ T cells and constitute 1-10% of all circulating T cells. However this ratio can significantly change during infections[10] and varies widely depending on tissue[11]. Additionally, there is a subset of unconventional αβ T cells that are not MHC-restricted and can recognise lipids, small molecule metabolites or specifically modified peptides[12]. However, these aspects fall beyond the scope of this introduction; consequently, sections below will provide an overview of conventional αβ T cell immunity, unless stated otherwise.

1.1.1.1. αβ T cell differentiation

Bone marrow-derived hematopoietic stem cells (HSCs) give rise to all lineages of blood cells, including B and T Lymphocytes, in a tightly regulated multi-step process. Commitment to a lymphoid lineage depends on the instructions received from several cell surface receptors to induce specific transcriptional regulators that drive a common lymphoid progenitor to specifically assume a B cell or T cell fate[13]. Whereas precursors of B lymphocytes stay in the bone marrow, precursors of T lymphocytes migrate to the thymus to complete their differentiation and maturation[14].

The early committed thymic precursors (ETP) that migrate to the thymus lack expression of TCR and co-receptors, and are termed Double Negative (DN: $CD8^-$ $CD4^-$) thymocytes. As illustrated in **Figure 1-1**, DN cells can be further subdivided into four stages of differentiation based on the expression of CD44, CD25, CD3, CD4 and CD8 molecules. Cells in the αβTCR pathway, progress through DN-stage 2 to DN-stage 4 by expressing a pre-TCR formed by a rearranged TCRβ-chain paired with a non-rearranged pre-TCRα chain. Transition into DN-stage 4 is determined by successful pre-TCR expression and active signalling leading to a substantial T cell proliferation and further maturation into Double Positive (DP: $CD8^+$ $CD4^+$) cells, followed by replacement of the pre-TCRα chain by a rearranged TCRα chain. In the event of initial non-productive TCRα chain gene rearrangement, the developing T cell can be rescued by a subsequent successful TCRα rearrangement that enables signalling by a self-pMHC complex[1,15–18].

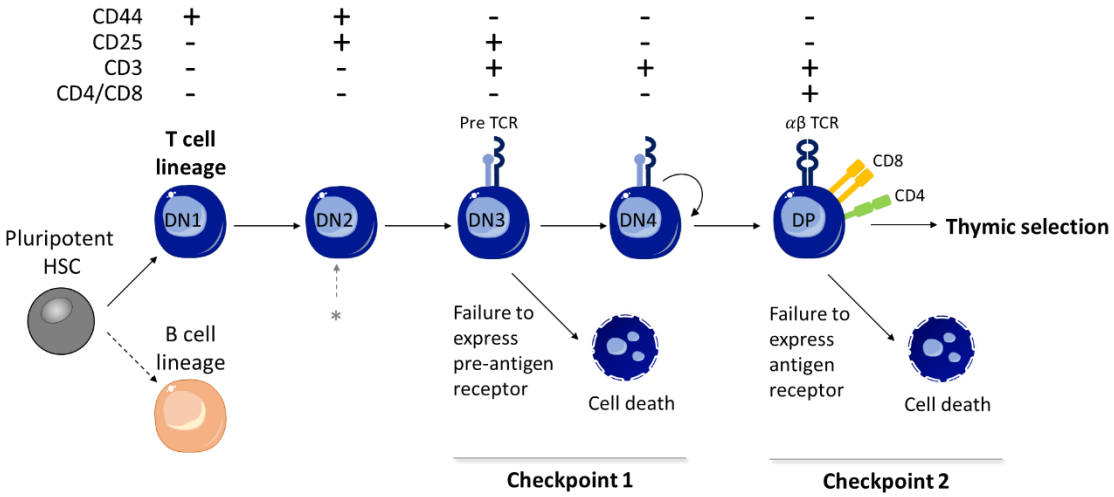

Figure 1-1. αβ T cell differentiation. During T Lymphocyte development in the thymus, early committed T cells lacking the expression of the TCR and the CD4/CD8 co-receptors (Double Negative, DN) undergo several developmental checkpoints. The first checkpoint occurs at the DN3 stage when thymocytes are required to signal through a pre-TCR (β selection). At this stage, checkpoint selects cells for survival, proliferation and further differentiation, but the pre-TCR is incapable of antigen recognition. The second checkpoint occurs with the expression of the CD4 and CD8 co-receptors (Double Positive, DP) and evaluates TCR and co-receptor matching in an interaction with self-peptide-MHC-class I or II complexes presented by thymic epithelial cells and dendritic cells. This interaction determines the fate of the developing T cell. Asterisk (*) indicates initiation of somatic rearrangement of the *Trb*, *Trg* and *Trd* TCR gene loci.

1.1.1.2. T cell receptor rearrangement

Conventional T cell immunity relies on the specific recognition of antigenic peptides through the TCR. The generation of a highly diverse TCR repertoire is essential for an effective immune cover[19,20]. It is estimated that the somatic gene rearrangement process described below can produce as many as 10^{20} different TCRs in theory; however, only a small fraction of these possibilities could ever be used as there are only 10^{12} T cells in the human body[21]. As the TCR repertoire is sometimes dominated by abundant clonotypes that have been subjected to strong selection events[22], it is clear that the extent of the TCR repertoire must be considerably smaller. The diversity of the TCR repertoire is thought to be ~10^8 T cells and will be further discussed in **section 1.2.** The process by which this diversity is initially generated is described below.

The TCR is a heterodimeric surface molecule made of two chains with N' terminal variable and a C' terminal constant domains. The variable domain of each TCR chain contains three hypervariable loops that include the Complementary Determining Regions (CDRs) generated by a semi-stochastic process of recombination and joining of germline encoded non-functional Variable (V) and Junctional (J) gene segments at the *tra* and *trg* loci, and an additional Diverse (D) segment at the *trb* and *trd* loci[23]. As depicted in **Figure 1-2.A,** for αβ TCRs the first recombination event in the *tra* loci on human chromosome 14 takes place between V and J segments, whereas in the *trb* loci on chromosome 7 the first recombination event in takes place between the D and J segments, followed by a second recombination event between V-DJ segments. Additional diversity is generated by the deletion of template nucleotides generated during the DNA cleavage, or the addition of palindromic (P) or non-template nucleotides (N) at

the junction of each recombined region[23]. The sequence between the recombined V(D)J exon and the C segment is further spliced to form a full length TCR chain transcript.

V(D)J recombination is initiated by the binding of lymphocyte specific Recombination-Activation Genes 1 and 2 (RAG-1 and RAG-2) endonucleases to a Recombination Signal Sequence (RSS) that is found flanking each individual gene segment. RAG-mediated cleavage introduces double strand breaks, causing the activation of a multifunctional genetic programme and activating pro-survival signals that prolong the lifespan of immature lymphocytes, while ensuring the assembly of a broad repertoire and inhibiting further initiation of the V(D)J recombination[24] (**Figure 1-2.B**).

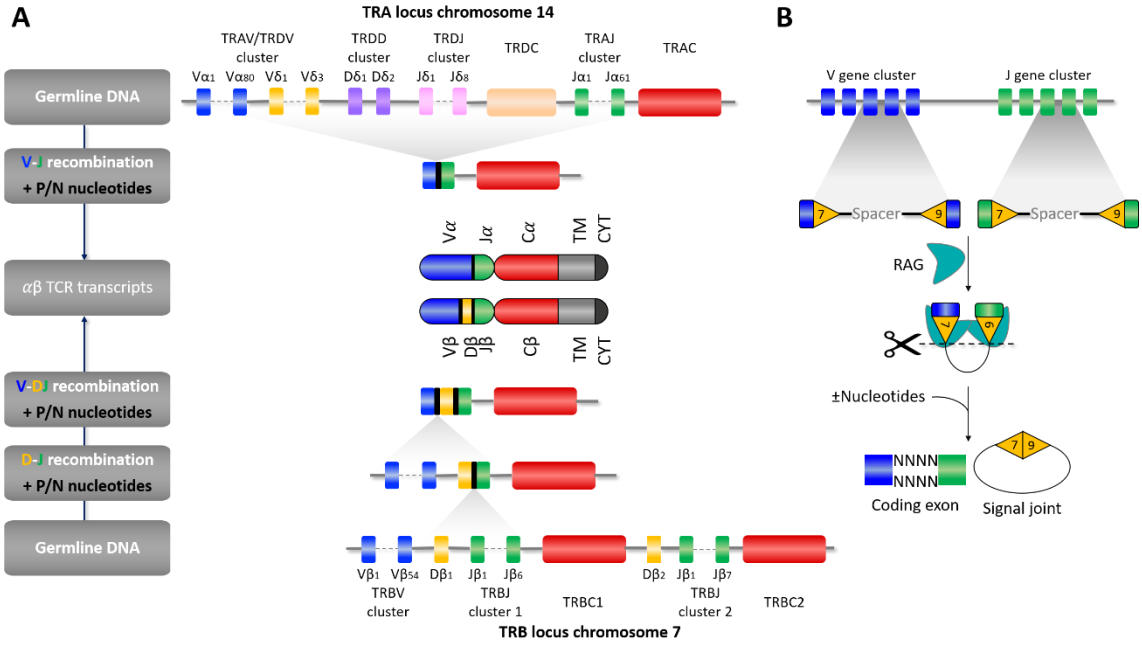

Figure 1-2. Schematic overview of the V(D)J gene recombination process. (A) T cell receptors are form through the somatic recombination of V(D)J gene segments found in the germline DNA of *tra* and *trb* loci. Non-germline addition/deletion of nucleotides can occur at the recombination junctions (V/J and V/D/J). Finally, V(D)J segments are spliced with the constant region (TRAC and TRBC1 or TRBC2), containing transmembrane (TM) and cytoplasmic domains (CYT) to form α-chain and β-chain transcripts. Notably, recombination at the *tra* loci leads to the deletion of *trd* segments. **(B)** Individual gene segments are flanked by RSS motifs (RSS: heptamer – 12/23bp spacer – nonamer) that are recognised by RAG endonucleases. DNA hairpins result from the cleavage of non-coding segments and broken ends are brought together and ligated by DNA repair enzymes through the addition of P- and N-nucleotides[23,25].

While the V(D)J recombination was commonly believed to be a "random" process, the presence of "public" (shared by more than one individual) and "private" (specific to an individual) TCRs strongly suggests an inherent bias in the V(D)J recombination process, facilitating some recombination events over others. To explain such distortion, some studies suggest that public TCRs might be easier to generate because they require minimal or non-random nucleotide additions[26,27]. Other studies suggest that this bias could be explained by a V(D)J recombination modulation through differential accessibility of RSSs to the RAGs, or accessibility of the *tra* and *trb* loci, as well as differential individual gene segment promoter activities[23,28]. For example, the TCRα enhancer (Eα) and TCRβ enhancer (Eβ) are required for efficient rearrangement of the *tra* and *trb* loci, respectively, and various markers of accessible chromatin have been associated with

V(D)J recombination gene bias[29,30]. Furthermore, Single Nucleotide Polymorphisms (SNPs) in the RSS and spatial distances between clusters appear to determine the frequency of TCRβ segment usage[31,32]. Pairing efficiency of the pre-TCR and convergent recombination may also play a role in skewing the T cell repertoire[33]. In summary, while many factors might contribute to V(D)J generation biases, the precise nature of how the TCR repertoire is generated and maintained remains to be fully elucidated.

As mentioned above, the heterodimeric TCR molecule is composed of a variable and a constant domain. The diversity in the TCR is determined by the CDR loops in the variable domain of the α and β chains **(Figure 1-3A**). In the most common mode of ligand engagement, the CDR1 and CDR2 loops that make direct contact with the MHC surface and the hypervariable CDR3 loop interacts with the peptide cargo[34]. CDR1 and CDR2 are encoded in the V gene segments, and CDR3 encoded in the (D)J genes **(Figure 1-3B**)[35]. The size and position of certain residues in the CDR1 and CDR2 loops are semi-conserved to allow a roughly conserved diagonal docking on the MHC molecule[36], although certain exceptions have been described[37–39] (see **section 5.1.1**). Most of the diversity resides in the CDR3 loops due to nucleotide insertion and deletions in the junction sites of joining gene segments and form the centre of the antigen-binding site[40,41].

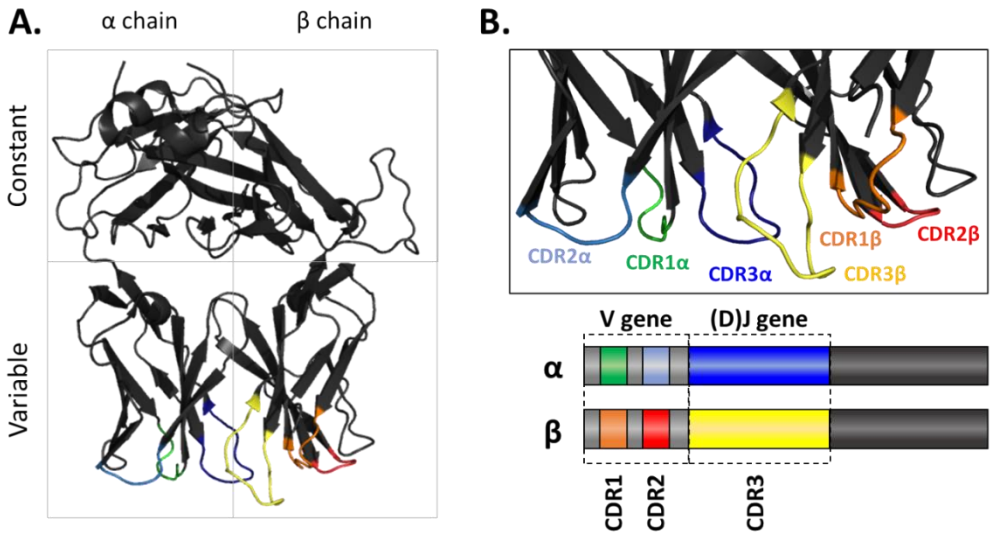

Figure 1-3. Structure of an αβ TCR. **(A)** Crystal tertiary structure of an αβ TCR. The diversity is encompassed by the six CDR loops (coloured) which reside at the membrane-distal end of the molecule. **(B)** Zoom into the CDRα and CDRβ loops in the antigen-binding Variable domain of a TCR tertiary structure (top). Graphical representation of the αβ CDR1 and CDR2 loops mRNA encoded by the Variable (V) gene, CDR3α encoded by Joining (J) and CDR3β encoded by J and Diversity (D) genes; in addition to random deletion and addition of template and non-template nucleotides at the junction of recombined V(D)J gene segments (bottom). Protein Data Bank (PDB) code: **3H9S**. This figure was adapted from *Attaf et al.,* 2015.

TCR-pMHC interactions during thymic selection shape the binding affinity ranges of the TCR repertoire (measured as the dissociation constant K_D) to their cognate pMHC complexes[42] (see **section 1.1.1.3** below). An optimal TCR-pMHC binding affinity and dwell time will ensure sufficient contact time for the T cell to activate the corresponding responding signals while enabling a single pMHC to serially trigger multiple TCRs[43].

1.1.1.3. Thymic selection

After T cell lineage commitment, somatic DNA rearrangement and TCR chain pairing, thymic selection (also known as **central tolerance**) determines which precursor lymphocytes will successfully mature (positive selection) and ensures that thymocytes expressing potentially autoreactive TCRs are deleted (negative selection)[17]. From this point onward, developmental decisions in the αβ T cell lineage are dependent on the interaction of their TCR with a pMHC ligand in the thymic microenvironment[1]. Selection of αβ T cells occurs in specific compartments of the thymus through the interaction of T cells in the DP stage ($CD4^+$ $CD8^+$) with cortical thymic epithelial cells (cTECs) presenting a large self-antigen-MHC ligandosome[44]. Positively selected thymocytes acquire an MHC restriction so that MHC-I-restricted DP cells become $CD4^-$ $CD8^+$ (CTLs) SP and MHC-II-restricted DP cells become $CD4^+$ $CD8^-$ (Helper T Lymphocytes) SP[45]. Thus, thymic selection also determines the cell-surface phenotype and functional potential of the mature T cell as depicted in **Figure 1-4**[1].

During thymic selection T cell fate is determined by the strength of the interaction of the T cell receptor with a self-peptide-MHC complex[46]. As **Figure 1-4** shows, T cells that are positively selected show low TCR affinity to the selecting self-pMHC ligand, and are therefore allowed to mature and migrate to peripheral lymphoid tissues to exert immunosurveilance. However, T cells that fail to interact with self-pMHC complexes fail to activate survival signals and undergo programmed cell death (death by neglect). Thymic selection, also ensures that TCRs with a relatively high affinity for self-ligands are eliminated[47]. This process of central tolerance ensures that only T cells with TCRs within a narrow affinity range for self-peptide MHC will be rescued from clonal deletion and allowed to populate the periphery. Subsequent peripheral tolerance mechanisms operate to ensure that T cells become apoptotic or unresponsive after self-antigen encounter in the periphery[48].

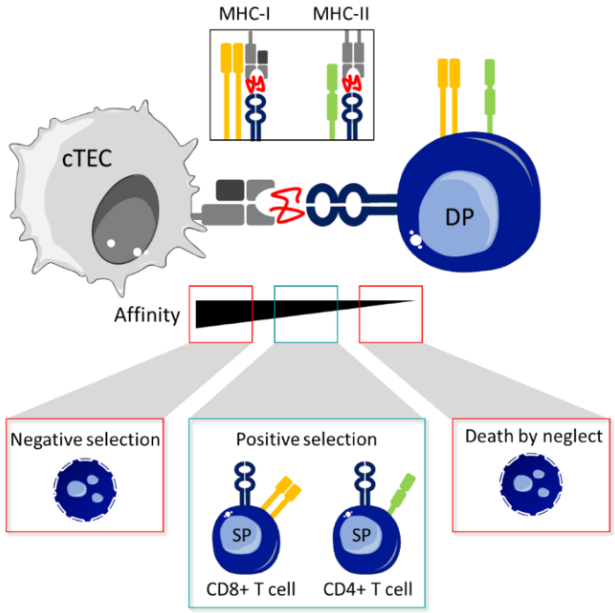

Figure 1-4. Positive and Negative selection of T cells. In the thymus, cTECs audit DP T cells for reactivity against pMHC complexes and determines their death or survival. The pMHC reactivity of positively selected T cells also determines their fate towards the $CD4^+$ or $CD8^+$ lineage based on the MHC restriction.

1.1.2. Antigen presentation by MHC proteins to αβ T cells

As discussed above and depicted in **Figure 1-4**, antigenic peptide ligands recognised by conventional T cells are presented by classical Major Histocompatibility Complex (MHC) molecules expressed on the surface of an APC or target cell. Recognition of anomalies by αβ T cells therefore requires that protein antigens are processed and presented in the MHC as peptides.

1.1.2.1. Antigen processing

Peptides originating from either intracellular or internalised extracellular proteins are degraded by the proteasome or endocytic and phagocytic pathways, respectively. Peptides are then loaded onto the appropriate Class I or Class II MHC molecules in the endoplasmic reticulum (ER) or acidified endocytic vesicles, respectively, and transported to the cell surface for presentation to T cells (**Figure 1-5**). Notably, Dendritic Cells (DCs) can cross-present peptides generated from endocytosed or phagocytosed exogenous proteins through Class I MHC molecules[49,50]. DC cross-presentation of exogenous antigens to $CD8^+$ T cells has been correlated with the maintenance of self-tolerance[51,52], the generation of anti-viral CTL immunity[53] and tumour immunosurveilance[54,55].

1.1.2.2. Antigen presentation through classical MHC molecules

In humans, MHC molecules are encoded on chromosome 6 in a cluster of genes within the highly polymorphic Human Leukocyte Antigen (HLA) locus, including classical MHC class I molecules (HLA-A, -B and -C) and class II (HLA-DR, -DP and -DQ). The high polymorphism at the MHC locus reflects the strong evolutionary pressure from highly mutable pathogens, and ensures diversity in peptide presentation at the population level.

Class I HLA molecules are expressed by almost all nucleated cells to allow T cell scanning of the internal proteome. In contrast, class II HLA molecules expression is tissue-specific with constitutive expression generally restricted to B cells, dendritic cells, macrophages and the thymic epithelium. Class I and class II HLA molecules bear an overall structural similarity (**Figure 1-5**). Class I HLA molecules consist of a highly-variable heavy chain composed by three alpha domains associated to a conserved β2 microglobulin (β2m), forming a closed-end binding groove that restricts the length of presented peptides. Generally, classical $CD8^+$ T cells recognise intracellular-derived antigenic peptides of 8-10 aa long bound to the α1 and α2 helices of HLA class I molecules; however, longer peptides can be presented by class I molecules although these protrude outside or bulge out the binding cleft in order to accommodate the extra length. Class II molecules are characterised by an open-ended peptide-binding cleft conformation, thus allowing the presentation of exogenously-derived antigenic peptides of 10-25 aa long to $CD4^+$ T cells[38,56] (**Figure 1-5**). Peptide binding to the MHC is achieved through a series of pockets within the peptide-binding groove. MHC polymorphisms are concentrated around these pockets and ensure that different MHCs can present differing subsets of peptides to T cells[38,57,58].

As mentioned above, polymorphisms in the HLA genes lead to non-synonymous amino acid changes in the peptide-binding groove, thus indicating that a selective pressure is sustained to increase the variety of peptides displayed[59]. In effect, each specific HLA molecule binds a set of specific peptides, thus the expression of a wide variety of HLA molecules ensures that individuals across the population present different antigenic peptides and provides the greatest chance that some individuals may survive any emerging infection[60]. Indeed, the HLA-I molecule has been historically associated with differential immune responses to infection, inflammation and autoimmunity[61–63]. For instance, HLA-B27$^+$ and HLA-B57$^+$ delay progression to AIDS in HIV infection[64]; whereas other alleles, including HLA-B35 and HLA-B7 have been associated accelerated disease[65]. On the other hand, HLA-B27 appears to increase the risk of ankylosing spondylitis, and HLA-B57 is associated with a higher risk of autoimmune psoriasis in patients infected with HIV. The contribution of HLA genotype is also being explored in the context of immunotherapies. In a recent study, *Chowell and colleagues*[66] showed that HLA class I genotype influences the response to treatment with checkpoint inhibitors in melanoma patients.

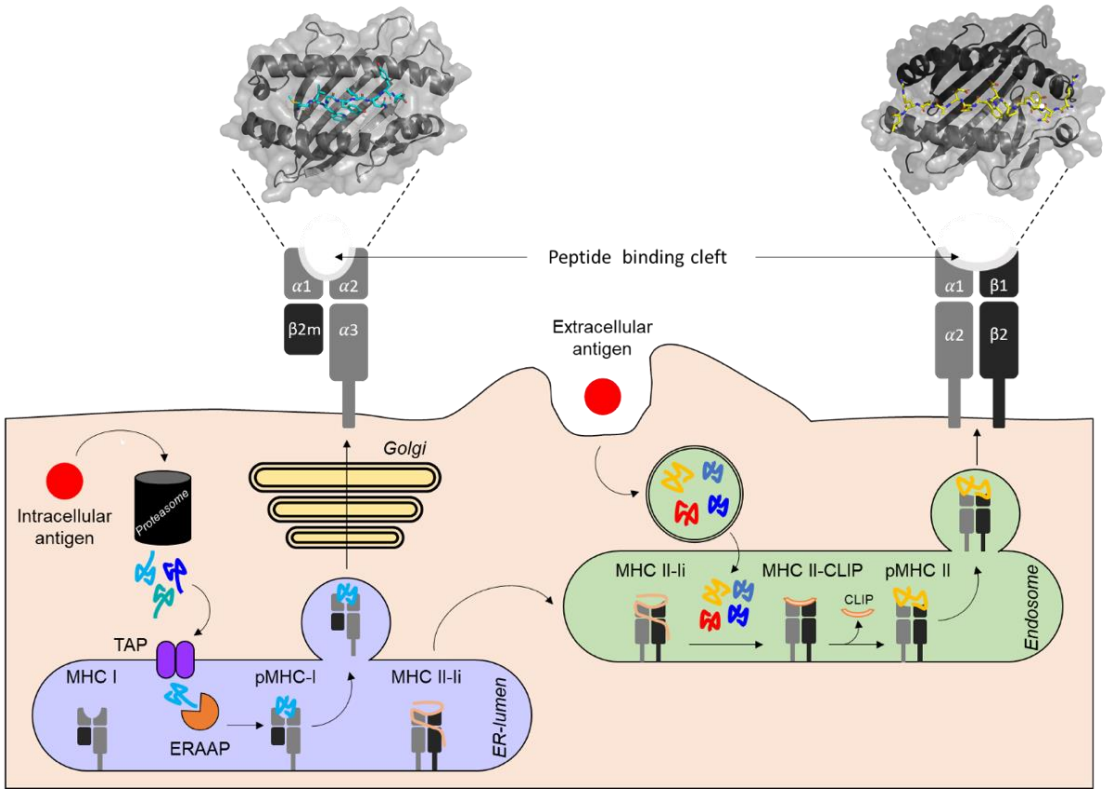

Figure 1-5. **Antigen processing and presentation through Class I and II MHC molecules. (A)** Intracellular self or foreign proteins are fragmented into peptide precursors by degradation through the proteasome, followed by TAP-induced translocation to the ER lumen where ERAAP aminopeptidases trim the peptide precursors to the optimal length for MHC I presentation. In the ER, the peptide is assembled with a newly synthesised MHC class I molecule and migrates through the Golgi to the cell surface. **(B)** Binding of peptides to class II MHC is accomplished through the proteolysis of endocytosed extracellular antigens. Class II MHC assembles in the ER-lumen, but only captures peptides after arriving to the endocytic compartment. To prevent premature peptide loading in the ER lumen, the invariant chain (Ii) binds the MHC II peptide-binding groove. The complex is then directed to the endocytic system where Ii is cleaved leaving only the CLIP fragment bound to the MHC II molecule. CLIP is then substituted by other peptides present in the endosomal lumen, and the peptide-loaded MHC II molecule is liberated to the plasma membrane. **TAP**: Transporter associated with Antigen Processing; **ER**: Reticulum Endoplasmatic; **CLIP**: Class-II-associated Invariant Chain Peptide.

1.1.3. T cell activation and signal transduction

Following thymic selection, naïve $CD8^+$ T cells recirculate through secondary lymphoid organs until encountering cognate pMHC on the surface of APCs and becoming activated effector CTLs. Both co-inhibitory and co-stimulatory ligands are present at the surface of APCs delivering secondary signalling to T cells (see **Table 1-1**), a balance that is tightly regulated to both maximise protective immune responses while preventing autoimmunity by inducing T cell tolerance[67]. While costimulatory signalling is required for activation of $CD4^+$ naïve T cells[68], naïve $CD8^+$ T cells can be activated and differentiate into effector CTLs without co-stimulation[69]. More recent reports indicate the importance of CD28 co-stimulation in the activation of naïve $CD8^+$ CTLs through an increased production of cytokines, such as IL-2[70]. Co-stimulatory molecules are of therapeutic interest due to the ability to enhance or terminate an immune response (see **section 1.5.2**)

Table 1-1. Some of the known T cell co-receptors with corresponding co-stimulatory or co-inhibitory ligands[67,71]

Co-receptor	Ligand	Co-signalling
CD28	B7-1 (CD80), B7-2 (CD86)	Stimulatory
ICOS	B7-H2 (ICOSL)	Stimulatory
OX40	OX40L	Stimulatory
LFA-1	ICAM	Stimulatory
CD27	CD70	Stimulatory
CD40	CD40L	Stimulatory
TIM3	TIM4, TIM1	Stimulatory
CD48	CD244	Stimulatory
CD155	CD226	Stimulatory
CD173	CD173L	Stimulatory
CTLA-4	B7-1 (CD80), B7-2 (CD86)	Inhibitory
PD-1	PD-L1, PD-L2	Inhibitory
TIM2	SEMA4A, H-ferritin	Inhibitory
TIM3	Galectin9	Inhibitory
LAG-3	FGL1	Inhibitory
CD155	CD96	Inhibitory
BTLA (CD272)	HVEM, (CD270)	Inhibitory

The αβTCR-pMHC interaction initiates highly specialised molecular organisation at the T cell-target interface called the **immunological synapse** (**IS**). IS formation results in a rapid multi-layered cascade of signals transmitted through the cytosol to the nucleus. As depicted in **Figure 1-6**, the α and β chains of the TCR associate with the CD3 complex (δ, ε, γ and ζ chains) that transmit antigen-binding events into a signal through their immunoreceptor tyrosine-based activation motifs (ITAMs). Binding of the CD8 and CD4 co-receptors to the invariant sites on MHC class I and II, respectively, acts to recruitment further signalling molecules to the TCR-CD3 complex. The CD8 molecule also acts to stabilise TCR-pMHC binding, thus modulating the binding kinetics (on- and off- rates) and mediating distinct biological outcomes[72].

In order to initiate an adaptive immune response against an antigenic peptide, naïve T cells are continuously recirculating through the peripheral lymphoid tissues, surveying the APC/target cells for foreign antigens. Once in the periphery, weak stimulation of mature T cells with self-pMHC triggers signals that are crucial to maintain a restorative state of T cell reactivity towards foreign antigens[73]. Encounter with a cognate foreign pMHC complex results in a stronger interaction leading to signalling and cellular activation. The highly fine-tuned specificity and complexity of the TCR signal-transduction network determines the quality and quantity of the outcome of a T cell response, including long term functional outcomes that can lead to effector, memory or tolerant T cells[74].

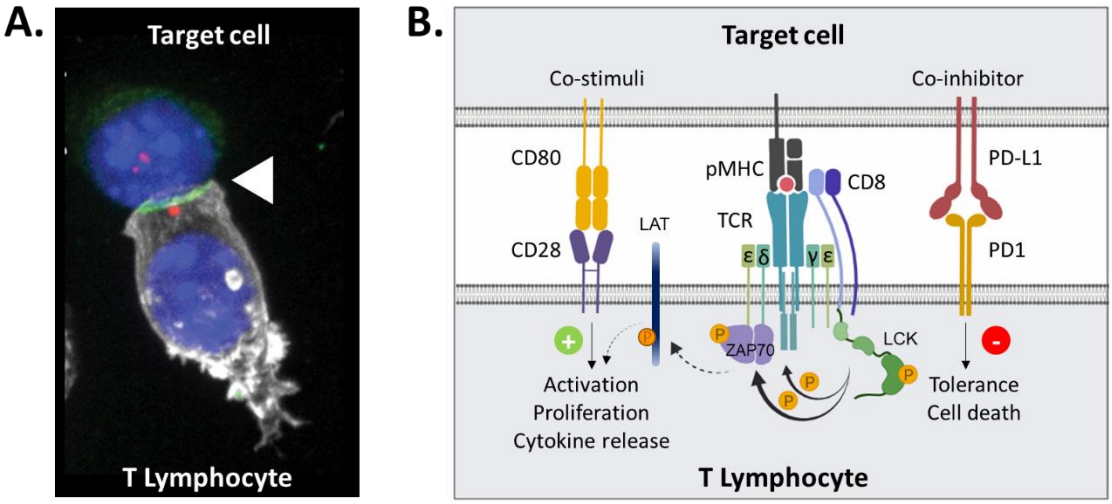

Figure 1-6. **The TCR-mediated signalling results in the activation of various signal transduction pathways. (A)** the immunological synapse (IS) (white arrow) forming between the T cell and the target cell or APC is integrated by three main components: the TCR, adhesion molecules and costimulatory or inhibitory ligands[75]. **(B)** At the IS, the TCRαβ heterodimer is coupled to a CD3 molecule, which is composed of epsilon (ε), gamma (γ), delta (δ), and zeta (ζ) chains containing ITAM domains for signalling. Following TCR engagement, signal transduction begins with the recruitment of LCK by the CD4 or CD8 co-receptor to mediate ITAM phosphorylation of CD3 chains. This results in the recruitment and activation of ZAP-70, that in turn phosphorylates LAT starting a signal amplification and diversification that is responsible for most of the responses that derive from TCR engagement[74,76,77]. **ZAP-70:** zeta (ζ) -chain-associated protein of 70 kDa. **LAT:** Linker for Activation of T cells, **LCK:** Tyrosine-protein kinase.

1.1.3.1. Key features of T cell signalling

As discussed above, in classically MHC-restricted αβ T cells, TCR recognition of cognate antigenic pMHC complex present at the surface of APCs or target cells is the key event for the mediation of the adaptive immune response to pathogens and cancer, and plays a decisive role in allergy, autoimmunity and transplant rejection[78]. The outcome of a T cell response is determined by the biochemical parameters of the TCR-pMHC interaction. In physiological conditions, such TCR-pMHC interactions are usually characterised by an affinity within a range K_D from 1 to 50 μM[79]. Exceptions have been described to escape thymic deletion, possibly as a consequence of TCR cross-reactivity[80] (see **section 5.1.1**).

The duration of this interaction, also known as binding kinetics (or dwell time), is dependent on the affinity of the TCR-pMHC interaction[81]. Binding kinetics must fall within a specific range to enable efficient intracellular signal transduction, while allowing each pMHC complex to be engaged by multiple TCRs in series[82]. A combination of TCR-pMHC binding affinity and kinetics has been used to describe T cell activation[43,83,84]. In their studies, *Galvez et. al.* suggest that T cells bearing higher affinity TCRs would receive stronger and more prolonged signalling, offering a competitive advantage during the immune response over those T cells bearing lower affinity TCRs[78]. However, contradictory evidence where TCR binding affinities do not correlate with biological potency has been presented. For instance, *Cole et. al.* suggest that more efficient serial triggering may occur with TCRs exhibiting weaker affinity, as weaker binding could allow such TCRs to contact multiple pMHC molecules in series more quickly than TCRs with greater affinity[82]. This would result in sustained TCR signalling. Overall, several studies have shown that there is not a direct relationship between TCR affinity and T cell response, but rather an optimal TCR-pMHC binding affinity and dwell time that ensures sufficient contact time for the T cell to initiate T cell-mediated functions such as proliferation, cytokine secretion or cytotoxicity, while enabling a single pMHC to serially trigger multiple TCRs[43,80,82,85,86].

Beyond the initial TCR-pMHC contact, many additional key molecules recruited to the immune synapse (see **Figure 1-6**) have been described to be involved in the activation of T cells bearing low affinity TCRs. For instance, the CD8 co-receptor has been long acknowledged to stabilise the TCR-pMHC interaction, and is a requirement for the functionality of low affinity TCRs[85]. A more recent study conducted by *Cemerski and colleagues*[87] suggests a role for the immune synapse in the amplification of signals from weak TCR-pMHC interactions, resulting in enhanced T cell proliferation. Further work reporting serial activation and translocation of ZAP-70 indicates it could lower the affinity threshold required for T cell activation[88]. Furthermore, in early T cell activation events mobilisation of intracellular calcium (Ca^{2+}) is required for signal transduction and modulation of the strength and fitness of the T cell response[89]. Studies conducted by *Chen and colleagues*[90] demonstrated that Ca^{2+} mobilisation and consequent T cell proliferation is dependent on the affinity and binding kinetics of the TCR-pMHC interaction.

The interacting properties of a TCR-pMHC are of high relevance for the outcome of a T cell response. To date, numerous studies have attempted to elucidate the precise binding parameters that correlate with a given response with the aim of developing therapeutic strategies to generate an optimal T cell response to pathogen and tumour antigens, while preventing autoimmunity. A requirement of such strategies is the identification of optimal TCR affinity ranges.

1.1.4. Establishment of T Cell Memory

A key feature of the adaptive immunity is the capacity of creating an immunological memory towards the encountered antigens during the individual's lifespan. Upon encounter with cognate antigen, recirculating naïve T cells cease to migrate and undergo clonal expansion and differentiation into effector T cells. Following elimination of antigen, effector T cells undergo a contraction phase of apoptosis-driven T cell death; however, a relatively small percentage of 5-10% T cells survive to further differentiate into memory T cells (see **Figure 1-7**). The determinants of T cell differentiation towards the memory phenotype remain still unclear, however evidence suggests that the signals received during the αβTCR-pMHC interaction play a determinant role in the formation of the memory T cell population[91,92].

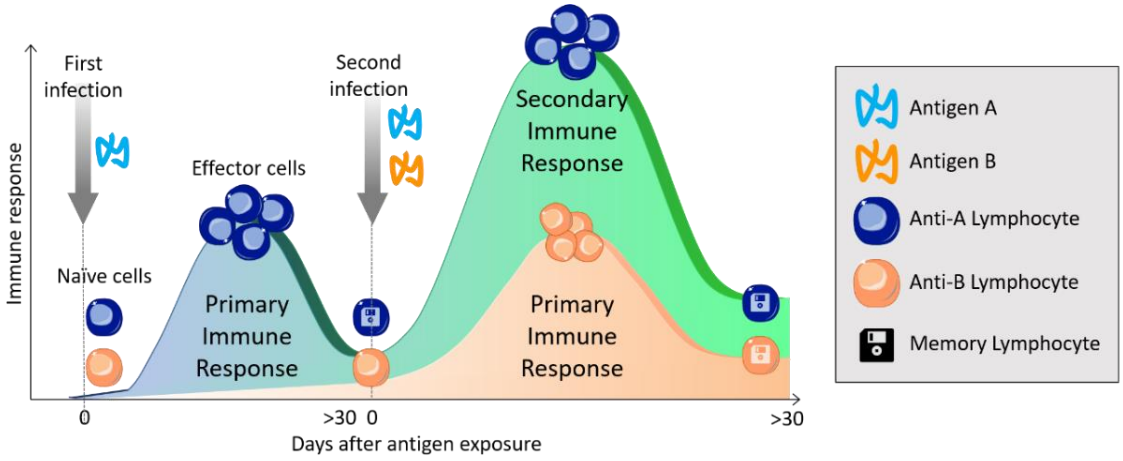

Figure 1-7. The phases of a CD8⁺ T cell response. During a primary encounter with a cognate antigen, activated T cells differentiate into effector T cells and clonally expand. Upon antigenic clearance, short-lived effector cells undergo a contraction phase by apoptosis, and only a small subset with potential for long-term survival stablishes in the secondary lymphoid organs, persisting long after antigenic clearance. This subset is termed memory T cells. Upon re-exposure to antigen, memory T cells undergo a secondary immune response with faster expansion and more robust effector functions when compared with the primary immune response, leading to faster clearance of the threat.

On some occasions, the memory pool can also provide further protection against pathogens and malignancies through the intrinsic ability of a TCR to recognise multiple antigenic peptides, known as TCR cross-reactivity (see **section 1.2**). For example, *Lee et al.*[93] showed detection of CD4⁺ and CD8⁺ H5N1-specific memory T cell subsets in healthy individuals with no prior exposure to the avian influenza strain H5N1 virus. Further evidence is presented by *Davis and colleagues*[94] by describing the presence of HIV-specific memory T cells in HIV-negative individuals. The accumulation of memory T cells throughout a lifespan plays an important role in protective immunity, however increasing numbers of memory T cells would overwhelm the body, unless homeostatic mechanisms controlling the size of the memory T cell pool were put in place. These mechanisms explain the dynamic changes in the memory T cell pool throughout an individual's lifetime[95].

1.2. The T cell receptor repertoire

T cells are required to respond to all possible infections without prior knowledge of what these might be or what peptide antigens they might present in the context of self MHC molecules. In the event of infection, T cells are required to respond rapidly and there is not time to generate new pathogen-specific TCRs. Consequently, existing naïve T cells must be capable of responding to all possible foreign peptides that can bind to self MHC molecules. Failure to cover all possible foreign peptides would leave T cell 'blind spots' that could be rapidly exploited by pathogens, which can evolve millions of times faster than their mammalian hosts.

The *Clonal Selection Theory* of adaptive immunity was widely accepted for many years. The theory suggested that the immune system was capable of successfully providing immunity to all foreign peptides in a "one clonotype one specificity" paradigm. However, this theory has been challenged by several authors throughout the years and there is now a body of evidence supporting the fact that individual TCRs are capable of recognising vast numbers of ligands (reviewed in [60]). According to the calculations made by Mason[96], the human TCRs repertoire is capable of recognising $>10^{17}$ potential foreign peptides that could bind to self MHC molecules. This simple arithmetic dictates that the number of potential foreign pMHC complexes that T cells might encounter vastly exceeds the number of available TCRs in the immune system[60,96,97]. Recent advances in TCR repertoire sequencing have illuminated the relatively small size of the TCR repertoire in relation to the potential gamut of foreign peptides it must respond to. As previously discussed, the V(D)J rearrangement, together with nucleotide addition/deletion at the junction sites and the pairing of the two separately rearranged chains results in a calculated *theoretical* repertoire of over 10^{20} in humans[98] (see **section 1.1.1.2**). However, there are only 10^{12} T cells in a human, and more recent studies have estimated that the naïve T cell pool is composed by $<10^{8}$ distinct TCRs[21]. Therefore, the theoretically achievable TCR repertoire is many orders of magnitude larger than could be expressed in any given individual at any given moment[42] suggesting that, in order to confer a comprehensive immune protection, T cells *must* be cross-reactive[60] (i.e. each T cell and each TCR must be capable of responding to millions of different peptides[99]).

The features of a healthy TCR repertoire can be summarised as the following: (1) the repertoire must be able to respond to a vast number of foreign pMHC ligands; (2) the specificity of the response must be in the optimal range to selectively recognise the foreign pMHC ligand and not cross-react with self-peptides; and (3) the frequency of reactive T cells for a given pMHC ligand must be large enough to allow a rapid response to infection. It is somewhat paradoxical that a healthy TCR repertoire must be simultaneously degenerate and specific, albeit the process of thymic selection ensures the removal of TCRs with high sensitivity for self-derived peptides[42] (see **section 1.1.1.3**). Indeed, studies conducted by *Bendelac and colleagues*[100] show that cross-reactive αβ TCRs are predominant targets of thymocyte negative selection, and *Chao and colleagues*[101] showed that negative selection decreases the average cross-reactivity of the pre-thymic selection repertoire by fivefold.

The flexibility of the TCR antigen-binding site is believed to be a key element contributing to T cell cross-reactivity. Structural and functional data has demonstrated that the CDR loops of a TCR can adopt different conformations to accommodate binding to different pMHC ligands[39,102], however the peptide itself can also adapt to the TCR[103]. Because of the importance of TCR cross-reactivity in immuno-surveillance, the fundamental mechanisms of cross-recognition of targets has been subjected to study using functional and structural data. At the outset of my studies I did not anticipate how important T cell cross-reactivity might be to successful immunotherapy. I now believe that this property could play a pivotal role in successful immunotherapy. This aspect will be further expanded on in relation to cancer immunotherapy in **Chapter 4**.

1.3. Tumour-specific effector CTLs

Genomic instability and accumulation of genetic alterations are intrinsic characteristics of tumorigenesis and provide selective advantages for the survival of cancer cells. The activation of oncogenic drivers and the inactivation of proliferation/suppression genes leads to the generation of heterogenic signalling that enables cancer progression and survival[104]. These events result in the expression of protein antigens with high (tumour specific) or low (tumour associated) tumour specificity that are not normally expressed in healthy cells, and can be targeted by CTLs (see **Table 1-2**).

Table 1-2. Classes of human tumour antigens that are recognized by T lymphocytes. Key for cancer histology: Colon (♦), Prostate (♣), Cervix (♥), Melanoma (♠), Renal (↔), Many cancers (∞)

	Tumour antigens	Definition	Examples (histology)	Ref
Tumour Specific Antigens (TSAs)	Oncoviral antigens	Antigen derived from viral oncogenic proteins that are produced in the infected transforming cells.	HPV E6 (♥) HPV E7 (♥) EBV (∞)	105 106 107
	Cancer-Testis Antigens (CTAs)	Antigen which expression is limited to adult reproductive tissues that do not express HLA I molecules (i.e. testis, placenta), and cancer cells.	MAGE-1 (∞) CTAG1B (∞) NY-ESO1 (∞)	108 109 110
	Neo-antigens	Antigen expression is exclusive to tumour cells, usually as a result of a tumour-specific mutation.	$P53_{M234I}$ (∞) $B\text{-catenin}_{S37P}$ (∞) $BRAF_{V600E}$ (∞) $KRAS_{G12D}$ (∞)	111 112 113 114
Tumour Associated Antigens	Oncofetal antigens	Proteins present during the period of embryogenesis can also be expressed by tumour cells.	5T4 (∞) CEA (♦) TAG-72 (♣)	115 116 117
	Differentiation Antigens	Antigen expression is tissue-restricted and limited to lineage-specific tumour or healthy cells.	MART-1 (♠) Gp100 (♠) PSA (♣)	118 119 120
	Overexpressed Antigens	Antigens are expressed by both healthy and cancerogenic tissue, but levels of antigen expression in cancer are highly elevated.	HER2 (∞) WT1 (∞) MUC1 (↔)	121 122 123

An effective cancer-specific T cell response is believed to depend on the immune infiltration into the tumour microenvironment, leading to a cancer recognition and an antigen spread cycle that expands reiteratively as depicted in **Figure 1-8**: Immuno-stimulatory tumour-infiltrating dendritic cells (DCs) capture and process tumour antigens and present them bound to the surface of HLA molecules. Antigen-bearing DCs then travel to the secondary lymphoid organs and present their peptide cargo to naïve T cells. Upon activation, T cells differentiate into effector $CD4^+$ or $CD8^+$, proliferate and circulate to the tumour site, where they recognise tumour antigens expressed by cancer cells through the interaction of the TCR with the cognate peptide-bound HLA complex. $CD8^+$ differentiated T cells (CTLs) recognising HLA class I-bound peptide mediate tumour clearance using effector mechanisms such as cell-mediated cytotoxicity using perforin and granzymes, which result in the release of further secondary TAAs that can be taken up and processed by resident APCs (i.e. macrophages and dendritic cells)[124–126].

Clinical studies supporting the concept of cancer-immunity cycle (or antigen spread process) indicate that this might be a key event in the immune-mediated elimination of malignancies[127–129]. Thus, an initial immune response against the primary antigens propagates and aids an adaptive response towards secondary tumour antigens thereby strengthening and widening the anti-cancer response[130–132].

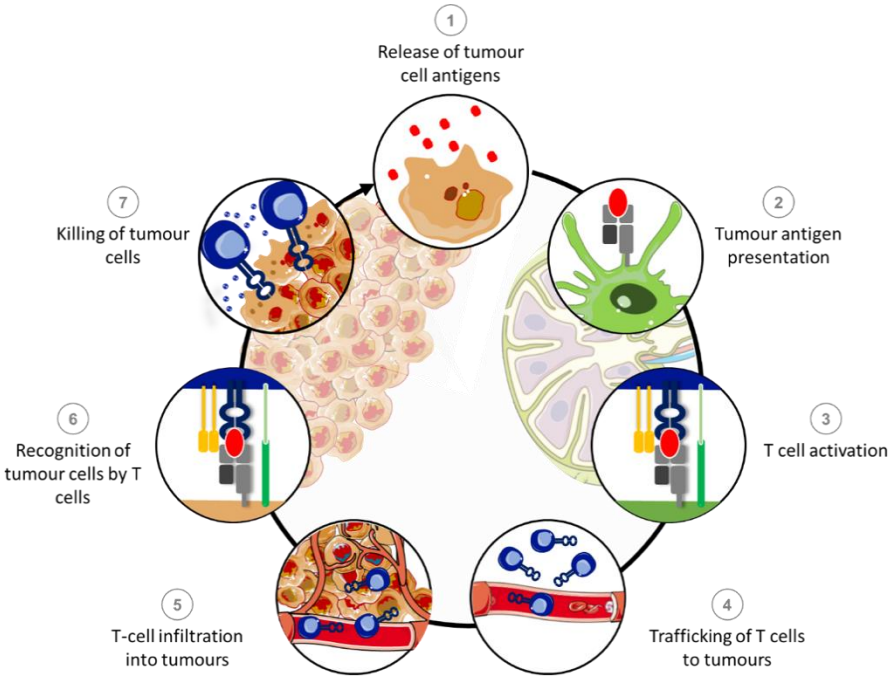

Figure 1-8. **Schematic diagram of epitope spreading following successful CTL-mediated anti-tumour response**. The cancer immunity cycle can be divided in seven major steps, starting with the release of antigens as a consequence of the pro-inflammatory environment induced by the tumour growth and the recruitment of immune cells that will induce the production of tumour cell debris. Cancer antigens are ingested by local dendritic cells, thus initiating a reiterative response that amplifies and propagates until successful elimination of the tumour. Each step is described in the text above.

Unfortunately, avoiding immune destruction is a hallmark of cancer, and cancer populations escaping Immunosurveillance are biased towards the production of immuno-escaping mechanisms[104,133] (see below **section 1.4**).

1.4. Tumour immunoevasion

As previously discussed, central tolerance shapes immunological specificity by depleting T cells that express high affinity TCRs for self-antigens. As most TAAs are derived from over-expressed or aberrantly expressed self-proteins, thymically-selected anti-tumour T cells exhibit low affinity TCRs that might be sub-optimal for tumour clearance[134]. Indeed, studies indicate that anticancer TCRs bind with ~5-fold lower affinity than equivalent antiviral TCRs[82]. Other studies indicate that the strength of TCR binding is of critical importance to the effector functions exhibited by anticancer T cells[135,136]. As a result, most tumour-associated peptide-HLAs represent challenging targets for the immune system. In addition, successful cancers have developed strategies to escape and suppress the immune system, resulting in a failure to initiate and maintain the corresponding anti-tumour immune response, facilitating tumour survival and progression[137]. This section describes mechanisms by which cancer cells deceive the immune system to allow the progression of tumorigenesis.

1.4.1. Immunosurveillance, Immuno-editing and Immuno-escape

Tumours are heterogenic populations of cells subjected to the selective pressure of the immune system, which results in intra-tumour Darwinian mechanisms known as “Immuno-editing” by which the “fittest clones” survive and expand[138]. The alterations occurring during the immunologic sculpting of the developing tumours are closely related to their inherent genetic instability, resulting in the production of tumour cells that better endure the anti-tumour pressure exerted by immune cells, which ends up shaping the tumour to confer immune-escape[133,139].

As depicted in **Figure 1-9**, elimination of cancer cells requires a cross-talk between the innate and adaptive immune branches to detect and suppress tumour cells before clinical evidence of disease. Effective elimination of highly immunogenic cancer cells while neglecting low immunogenic cells results in the persistence of neoplastic elements leading to a stage of “dynamic equilibrium” characterised by a state of “tumour dormancy” in which variant cancer cells that have adopted features that enhance the potential for immune-escape predominate[140].

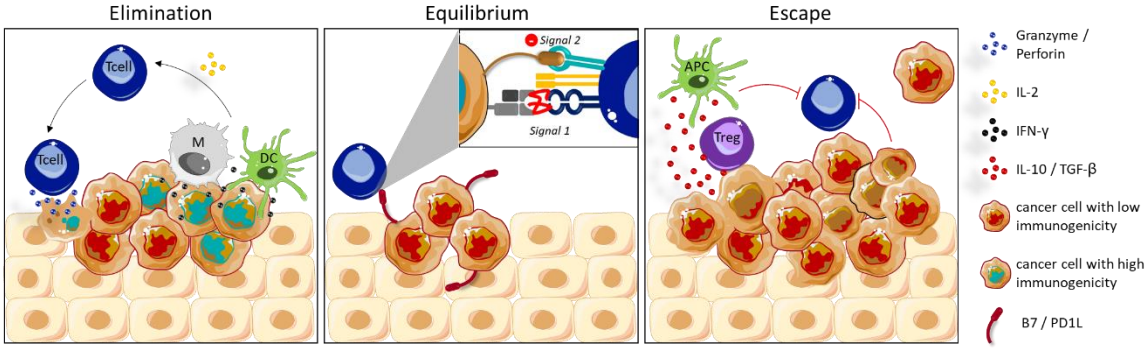

Figure 1-9. The three phases of cancer immuno-editing: Elimination, Equilibrium and Escape. When healthy cells undergo transformation, transforming events can lead to the production of highly or poorly immunogenic antigens. Immunosurveillance involves synergetic effect of innate and adaptive immune cells that recognise and eliminate transformed cells. However, poorly immunogenic persistent neoplastic cells can remain in a dynamic equilibrium controlled by immune effectors (usually conventional αβ T cells and unconventional γδ and NK cells) that exert potent selection pressure on the tumour cells, which might be characterised high mutational ratios. Eventually, surviving cancer cells carry mutations that provide them with increased resistance to immune attack. According to the immuno-editing model, the selective pressure of the immune system shapes tumorigenesis by failing to supress and eliminate neoplastic cells. M: Macrophage; DC: Dendritic cell; APC: Antigen Presenting Cell.

1.4.2. Mechanisms of tumour-mediated immune suppression

Multiple factors, mainly facilitated by the inherent genetic instability in tumours, contribute to immunoevasion (see **Figure 1-10**). Tumour immune suppression factors extend to all branches of the immune system from recruitment of infiltrating immune cells to forming a suppressive tumour microenvironment (TME)[141,142]. Although initial pro-inflammatory TME and the consequent recruitment of cells from the innate immune system to the tumour site produces tumour death, necrotic cells can recruit further inflammatory cells of the immune system that, in the context of neoplasia, can promote tumour angiogenesis, proliferation and invasiveness by creating an immunosuppressive milieu that impairs CTL reactivity.

Tumours can escape from anti-cancer CTLs through mutations that affect the antigenic peptide, the HLA molecule or any of the proteins involved in the antigen presentation machinery. Indeed, abnormalities in the HLA class I antigen presentation machinery have been associated with poor prognosis in several malignant diseases and may play a role in the resistance to immune checkpoint inhibitor-based immunotherapy[66,143–145]. Successful cancers also exploit T cell costimulatory pathways by failing to express key costimulatory molecules such as CD80 or CD86, while upregulating expression of ligands for immune checkpoints such as PD-L1, PD-L2 and CTLA-4.

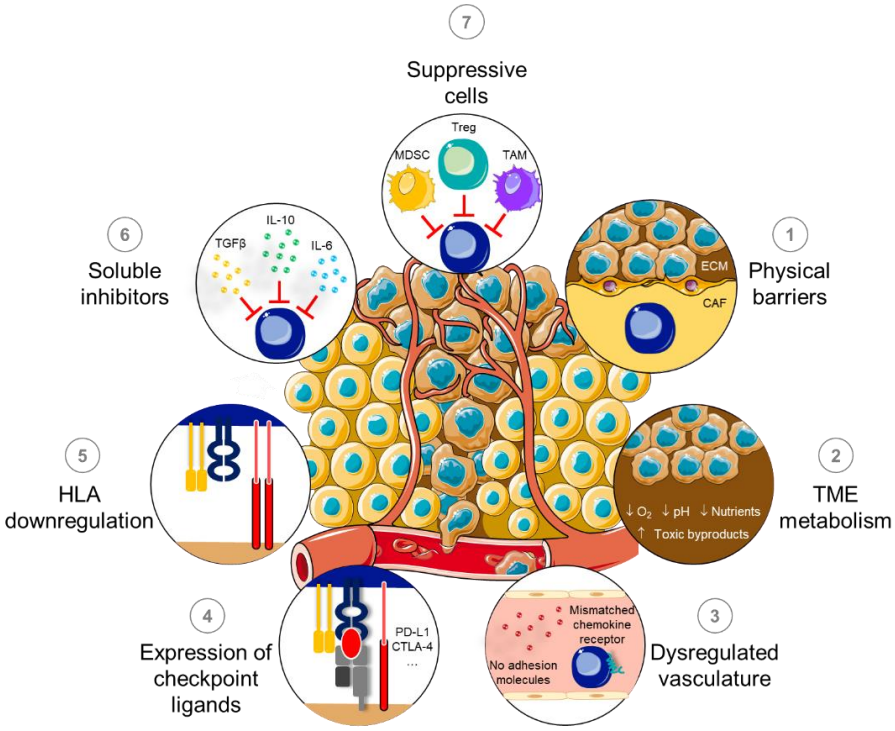

Figure 1-10. Mechanisms of immune suppression in the tumour micro environment. The development of an immunosuppressive TME is determined by the presence of factors that allow cancer cells to grow **(1-3).** Tumours embrace the expression of immune-suppressive signals **(4)** and downregulation of MHC machinery **(5)** to dampen the CTL-based immune response. The growth of the tumour causes minor disruptions in the surrounding tissue that induce inflammatory signals that lead to the recruitment of cells of the innate immune system. Infiltrating cells release soluble inhibitors **(6)** that attract suppressive cells **(7)** that in turn decrease or inhibit the local immune response[146]. **TME**: Tumour Micro Environment, **ECM**: Extra Cellular Matrix, **CAF**: Cancer Associated Fibroblasts, **MDSC**: Myeloid-derived suppressor cells, **TAM**: Tumour Associated Macrophages.

1.5. Cancer immunotherapy

Although the role of the immune system in preventing tumorigenesis was firstly described in 1909 by Paul Ehrlich[147] and the formal hypothesis of cancer immunosurveilance was proposed in 1957 by Burnet and Lewis Thomas[146], only lately has the importance of cancer immunosurveilance become widely acknowledged and immunoevasion considered a Hallmark of Cancer[104]. The success of immunotherapy-based clinical trials in patients with multiple metastases where conventional treatments had failed was finally acknowledged by *Science* magazine as Breakthrough of the year 2013[148] and the 2018 Nobel prize for Physiology or Medicine was awarded for the discovery for cancer therapy by inhibition of negative immune regulation[149].

Several immunotherapies have been exploited to generate an anti-tumour immune response. As depicted in **Figure 1-11**, the most promising immunotherapy approaches could be broadly classified as: **(A)** Active immunisation through vaccination; **(B)** Reversal of immunosuppression using checkpoint inhibitors; **(C)** Non-specific immune stimulation (or cytokine therapy); and, **(D)** Adoptive cell transfer. These approaches will be briefly discussed below with a particular focus on $CD8^+$ T cell-mediated immunotherapies for malignant melanoma that formed the basis of my own studies.

The principal goal of cancer immunotherapy is to harness the immune system of the patient to successfully achieve the permanent eradication of tumour cells. Successful cancer immunotherapy will require an understanding of the immunologic mechanisms involved in tumour recognition and elimination, as well as an insight into the mechanisms favouring tumour escape.

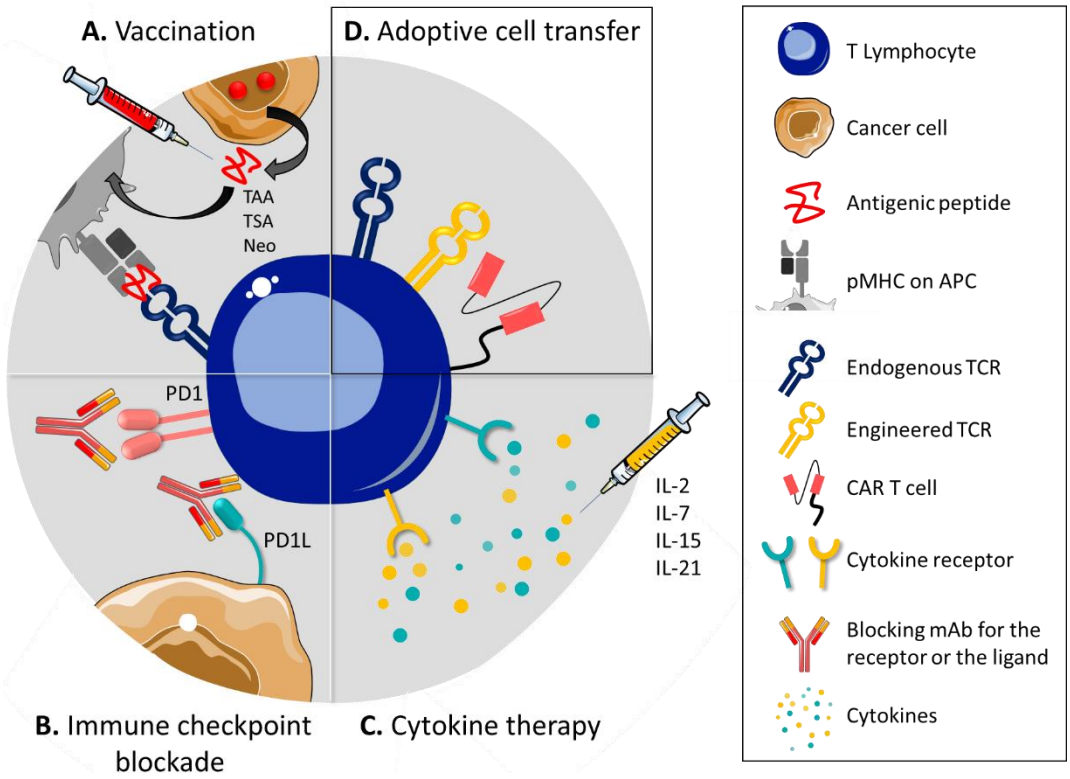

Figure 1-11. Cancer immunotherapies. Current cancer immunotherapies can be grouped in four modalities: **(A)** Cancer vaccines (Active Immunisation), **(B)** Adoptive Cell Transfer, **(C)** Immune checkpoint blockade (Reversal of Immunosuppression) and **(D)** Cytokine therapy (Non-specific Immune Stimulation). The therapy used to treat the patients presented in this thesis, adoptive cell transfer, is shown boxed.

1.5.1. Cancer vaccines

As discussed in **Section 1.3**, an effective anti-tumour response is characterised by the activation (or priming) of naïve antigen-specific T cells through APCs, such as DCs. Several cancer vaccines modalities have been pursued, however clinical results for therapeutic cancer vaccines have been less impressive in comparison with other immunotherapy modalities, often due to the lack of an optimally immunogenic antigen capable of breaking self-tolerance. For instance, the use of DC as professional APCs have been used as an alternative method to bypass T cell tolerance to self-antigen derived TAAs that bear low immunogenicity. In 2010 the autologous DC-based vaccine *Sipuleucel-T* (Provenge®) was approved for the treatment of metastatic hormone-refractory prostate cancer[150]; however, the DC-production challenges and the modest clinical effect of *Sipuleucel-T* has manifested the need for more effective cancer vaccines[119,151].

Current successes with cancer vaccines encompass the use of short antigenic peptides (although other modalities have been developed recently[152]) with or without adjuvants and delivery systems,

thus delivering a target antigen to Class I and II MHC molecules on APCs at the injection site and promoting $CD8^+$ and $CD4^+$ T cell responses, respectively. Easy administration of synthetic peptides as an "off-the-shelf" reagent is inexpensive and highly attractive. Unfortunately, results with cancer vaccines have generally been disappointing, with the main exception of prophylactic vaccination against oncoviruses, mainly because of the difficulty in antigen selection and tumour immunoevasion (see **section 1.4**).

The sections below provide an overview of the most promising antigen-based cancer vaccines modalities that induce strong tumour-specific T cell responses.

1.5.1.1. Prophylactic vaccination against oncoviruses

Cancer vaccination has shown some promising successes in settings where the induced T cell response is unlikely to impact on immune-suppressive mechanisms[153]. Accordingly, successes in prophylactic vaccination against oncogenic viruses (or oncoviruses) stems from treatment of a *cause* for cancer rather than via vaccination against cancer antigens themselves. Two notorious successes in prophylactic vaccination are Heptabax-B® (Merk, approved in 1981) against the hepatitis B virus (HBV) for the prevention of hepatocellular carcinoma (HCC)[154], and *Gardasil*® (Merk, approved in 2006) for the prevention of infection by human papilloma virus (HPV) strains 6, 11, 16 and 18, acknowledged as the main cause of cervix cancer[155]. In 2014 followed the approval of *Gardasil-9*® which included immunisation towards HPV strains 31, 33, 45 and 58, thus including protection to HPV-associated anal and vaginal cancers[156]. Although prophylactic vaccination offers an attractive solution for the treatment of virus-associated cancers, this approach cannot be applied to the majority of cancers.

1.5.1.2. Vaccination with neoantigens

Effective anti-tumour immunity can be directed towards peptides encoded by random non-synonymous somatic mutations exclusively present in tumour cells, also known as *neoantigens*. Such mutations are recognised as non-self by the immune system, as they are no longer subjected to the constraints of central tolerance. Indeed, several studies have positively correlated a high mutational load with stronger T cell responses, increased numbers of tumour-specific T lymphocytes and improved patient survival[157–160].

The development of whole-exome sequencing and HLA-binding epitope prediction algorithms has illuminated the potential use of neoantigens in immunotherapy. For instance, adopting these techniques, *Ott and colleagues*[161] demonstrated the immunogenicity of a peptide-based vaccine (NeoVax) that targeted up to 20 predicted personal neoantigens in stage III-IV melanoma patients (NCT03929029). Another study conducted by *Sahin and colleagues*[152] demonstrated that personalised RNA-based vaccines targeting neoepitopes can also prevent melanoma recurrence in metastatic patients (NCT02035956). Interestingly, both studies demonstrated that neoantigen vaccination exerts a dual effect: it strengthens existing $CD4^+$ and $CD8^+$ anti-neoepitope responses and activates naïve cells.

As demonstrated by *Nicholaou and colleagues*[162], neoantigen vaccination can elicit tumour-specific responses, but it can also influence tumour immunoevasion. Failure to impact on tumour immune-suppressive mechanisms has now been acknowledged as one of the main reasons for the lack of success with cancer vaccines (reviewed in [153]). Indeed, Sahin[152] revealed upregulation of PD-1L expression in vaccinated patients with recurrent tumours, and PD1 expression of the neoepitope-specific T cell population. These results highlight the selective pressure induced by neoantigen cancer vaccines. Accordingly, many clinical trials have started exploring combination therapy by delivering a neoantigen vaccine with checkpoint inhibitors. For instance, NeoVax in combination with anti-CTL-4 antibody is starting to be explored in a phase 1 study as a possible treatment for metastatic melanoma (NCT03929029) and renal cell carcinoma (NCT02950766).

So far, studies encompassing neoantigen vaccines have focused on cancers with a high mutation load and successes in cancers with a low mutation load has yet to be demonstrated[163]. Additionally, whereas vaccination with neoantigens that are prevalent across patients and tumour types is a highly attractive therapy, the majority of neoantigens are patient-unique. Thus, a customised therapy would be required to target the exact mutations present in each individual's tumour and thus be highly personalised[159,164]. Such, patient-personalised vaccination strategies pose significant hurdles in terms of cost and time of manufacture in comparison to the "off the shelf" notion of cancer vaccines. Another pressing concern is the potential cross-reactive responses induced by neoantigen vaccination that could cause potential unforeseen side effects. All of these considerations must be taken into account in the design of targets for cancer vaccination.

1.5.1.3. Vaccination against TAAs

The identification of a large collection of tumour-associated antigens (TAAs)[165] resulted in hope that therapeutic cancer vaccines could be used to boost tumour immunity by expansion of cancer-specific memory T cells[166]. Unfortunately, this approach has been largely disappointing. Suboptimal clinical responses may relate to the absence of high-affinity tumour-specific T cells available for DC-priming as a result of thymic deletion, or to the poor immunogenicity of natural epitopes expressed by Melanoma cells (with exception of immunodominant Melan-A[118] and gp100[167]), possibly as a consequence of tumour-escape mechanisms.

To circumvent low peptide immunogenicity, substitutions on the peptide backbone that translate into an increased affinity for cognate TCRs or MHC molecules have been developed, and are referred to as Altered Peptide Ligands (APLs). Examples of such "heteroclitic peptides" are shown in **Table 1-3**). Being non-self, APL may encompass a better prospect for breaking immune tolerance. In fact, studies show that vaccination with tumour-derived peptides harbouring amino acid substitutions that elicit a higher avidity T cell response broadens the clonal diversity of the anti-tumour response, which serves as driver for spreading other subdominant determinants with lower avidity T cell clones[168,169]. Consequently, optimised peptide antigens offer a highly attractive, relatively inexpensive option for cancer vaccination.

Table 1-3. List of current natural human HLA A*0201-restricted melanoma antigens and their related heteroclitic peptides. Anchor residue modifications are underlined (adapted from [170]).

TAA (protein)	Natural peptide	Heteroclitic peptide	Reference
Melan-A_{26-35}	EAAGIGILTV	EL<u>A</u>GIGILTV	[171]
NY-ESO-$1_{157-165}$	SLLMWITQC	SLLMWITQ<u>L</u>	[172]
$gp100_{209-217}$	ITDQVPFSV	I<u>L</u>DQVPFSV	[173]
$gp100_{280-288}$	YLEPGPVA	YLEPGPV<u>V</u>	[173]
$gp100_{154-162}$	KTWGQYWQV	K<u>L</u>WGQYWQV	[174]

While APLs can induce a greater expansion of T cells *in vitro* and *in vivo* when compared to the WT peptide, these T cells may not optimally recognise the WT epitope present on the tumour[141,175,176]. APL-induced TCR clonotypes must therefore be carefully evaluated after *ex vivo* priming to ensure their efficacy. My laboratory recently pioneered a new approach to peptide vaccination against cancer called TCR optimised peptide skewing of the repertoire of T cells (TOPSORT)[177]. This approach aims to use an APL that is optimised to induce the most-effective T cell clonotypes. Our recently published study demonstrated that the an APL of sequence <u>MTSA</u>IGIL<u>P</u>V induced a Melan-A_{26-35} -specific T cell population that was far more effective at recognising melanoma cells than those induced by the natural epitope[178]. Importantly, we showed that this APL could prime T cells from the blood of melanoma patients that were more potent at eliminating autologous cancer cells. This same approach has since shown *in vitro* success for renal cell carcinoma, ovarian cancer and chronic lymphocytic leukaemia (*Galloway et al. unpublished*). It remains to be seen whether these promising *in vitro* results can be replicated *in vivo.*

1.5.2. Antibody based immunotherapies

Antibody-based therapies are the most important recent development in cancer immunotherapy. Over the last two decades, the FDA has approved more than ten monoclonal antibodies (mAbs) for the treatment of hematologic and solid malignancies. In addition, there are over 50 mAbs in different phases of clinical trials being tested either as a monotherapy or in combination with other treatments (reviewed in [179]). These recent advances are partially due to the successes in humanised antibody engineering techniques, that have allowed the alteration of antibody characteristics, such as size, affinity, functional avidity and half-life[179] and several antibody formats with distinctive architectures are currently being used in the clinic.

As with all types of immunotherapy, a key challenge for mAb-based therapies is the identification of suitable antigens. For direct recognition of cancer, the targeted antigen should be specifically expressed by malignant cells, and antigen secretion should be minimal to prevent *off situ* antibody capture; examples of cancer antigens targeted by therapeutic monoclonal antibodies include CD20 (Non-Hodgkin's lymphoma), CD30 (Hodgkin's lymphoma), Her-2 (HER-2 overexpressing tumours), EpCAM (breast, colon and lung tumours), PSMA (prostate carcinoma), EGFR (glioma, lung, breast, colon, head and neck tumours), ERBB2 and ERBB3 (breast, colon, lung, ovarian

and prostate tumours), amongst others (reviewed in [179]). The safety and efficacy of the therapeutic antibody is highly dependent on the nature of the target antigen.

Many therapeutic antibodies are currently being tested, however they fall beyond the scope of this introduction. Here, I will focus on antibody cancer immunotherapies that involve T cells. These comprise: (i) immune checkpoint inhibitors and (ii) bi-specific antibodies.

1.5.2.1. Immune checkpoint inhibitors

Whereas other cancer immunotherapies require knowledge of the antigenic targets recognized by a patient's T cells, the use of T cell checkpoint inhibitor monoclonal antibodies for immunotherapy is not limited by this constraint. Checkpoint inhibition targets negative immunoregulatory ligands on T cells such as PD-1, CTLA-4 and TIM3. (see **sections 1.1.3** and **1.4.2**). Successful cancers exploit these negative regulators of T cell immunity by expressing their cognate ligands to produce a highly suppressive microenvironment for T cell immunity. Blocking of T cell checkpoints has produced some remarkable clinical results with some cancers as described below.

The CTLA-4-targeted antibody *Ipilimumab* (**Yervoy,** 2011) was the first immune checkpoint to be clinically tested in melanoma, with patient objective responses up to 11%, from which 60% of the patients showed long-term responses[180]. The first FDA-approved antibody targeting PD-1 was *Pembrolizumab* (**Keytruda**) in 2014 for the treatment of melanoma with reported OR rates of 33%[181]. Use of *Pembrolizumab* has since been extended to the treatment of metastatic NSCLC[182] and recurrent head and neck squamous cell carcinoma[183]. Another anti-PD1 antibody, *Nivolumab* (**Opdivo**) was also FDA-approved in 2014 for the treatment of melanoma[184], followed by extension of approval to treat squamous cell lung cancer[183], renal cell carcinoma[185] and Hodgkin's lymphoma[186]. Further checkpoint antibodies targeting PD-L1 have been FDA approved to treat several malignancies, including *Atezolizumab* (**Tecentriq**, 2016) for the treatment of lung and bladder cancer[187], *Avelumab* (**Bavencio**, 2016) for Merkel-cell carcinoma[188], *Durvalumab* (**Imfinzi**, 2017) for NSCLC and urothelial cancer[189], and *Cemiplimab* (**REGN-2810**, 2018) for the treatment of squamous cell skin carcinoma, myeloma and lung cancer[190]. Overall, OR rates suggest that treatment with T cell checkpoint inhibitors produces a low but durable response rate. However, modulation of regulatory events in order to maintain overall T cell activation increases the risk for autoimmune side effects, as reported by the incidence of Immune-related adverse effects (irAEs) in up to 60% of the patients treated with CTLA-4 blockade therapy, and in over 20% of the patients receiving anti-PD-1/PD-L1 inhibitors[191,192].

In addition to monotherapy, checkpoint inhibitors are being tested in combination therapies. For instance, combination therapy of Anti-PD1/PD-L1 with anti-CTLA-4 has shown OR rates of >40% in melanoma patients[193]. However, data from clinical trials on patients with melanoma and NSCLC suggest that the therapeutic success of checkpoint inhibition depends on the mutational load and the neoantigen abundance in the tumour[194], the nature of the immune filtrate[195] and the initial

diversity of peripheral TCR repertoire therapy[196]. Tumours have now been defined in two categories, with those that have a large T cell infiltrate being described as “hot” in contrast to “cold” tumours which lack T cells. Current combination therapies encompass the use of chemotherapy or targeted therapy (BRAF and MEK inhibitors) to achieve transition from “cold” to “hot” tumours in order to enhance responses to checkpoint inhibitors. Furthermore, as mentioned in **section 1.5.1**, combination of checkpoint inhibitor antibodies with cancer vaccines encompasses the potential of both generating strong T cell responses towards immunogenic antigens while releasing effector cells from a suppressed state.

Overall, mono-therapy with T cell checkpoint inhibitors produces long-term responses, although in a minority of patients, and is associated with acute cases of irAEs. Nonetheless, this therapy can be supplied in combination with other immunotherapies including cancer vaccines as described above. The success of T cell checkpoint inhibitor therapy was recently underscored with the award of the Nobel Prize in Physiology or Medicine 2018 to Dr James P Allison and Dr Tasuku Honjo for their pioneering investigations encompassing inhibition of CTLA-4 and PD-1, respectively. Importantly, the successes of checkpoint inhibition highlight the potential of T cells to eradicate cancer and have resulted in considerable investment into all aspects of cancer immunotherapy.

1.5.2.2. T cell-engaging/redirecting

T cell-redirecting bispecific antibodies (BsAb) are another emerging immunotherapy modality that exploits engineered molecules (usually antibodies) with multiple binding sites to link and recruit immune cells. The first two FDA approvals for bispecific antibodies were granted to *Catumaxomab* (Removab®) in 2009 and to *Blinatumomab* (Blincyto®) in 2017. Removab® is an anti-CD3 antibody paired with an anti-epithelial cell adhesion molecule (EpCAM), while its Fc domain recruits innate immune cells to tumours, thus enhancing T- B- and DC cell interactions[197] (**Figure 1-12A**). Removab® was initially approved for the treatment of malignant ascites in adults with $EpCAM^+$ ovarian cancer, and clinical trials are currently on going for the treatment of malignant ascites in gastric adenocarcinomas (NCT01504256) and epithelial cancer (NCT01065246).

T cell-engager bispecific antibodies (BITE®) represent a different category of BsAb. BITEs®, such as Blincyto®, differ from BsAbs in their mechanistic action as they are designed to engage CD3 molecules (part of the TCR) and activate T cells. Such CD3 fusion antibodies can be used the ‘leash’ polyclonal T cells to cancer cells and ‘hijack’ their effector functions. Consequently, such molecules can be used to redirect cytotoxic T cells to kill tumour cells *in vivo*. Blincyto® crosslinks CD3 and CD19 present in B cell malignancies[198] (**Figure 1-12B**). Blincyto® was initially approved for the treatment of B-acute lymphoblastic leukemia (B-ALL) in adults, but current clinical trials explore its benefits in paediatric ALL (NCT01471782) and diffuse large B-cell lymphoma (DLBCL) (NCT01741792).

More recently, Immune-mobilising monoclonal TCRs (ImmTACs) have been explored in efficacy studies as “off-the-shelf” reagents. ImmTACs constitute a platform of novel bispecific fusions comprising a soluble affinity-enhanced TCR fused to an anti-CD3 single-chain variable fragment (scFv); which achieve redirection of T cell activation and secretion of pro-inflammatory cytokines leading to a particularly potent tumour cell killing, even for tumours that display very low numbers of antigen[199] (**Figure 1-12C**). Promising results have already been achieved in a Phase 1 trial for the treatment of melanomas with the gp100-targeting ImmTAC IMCgp100 (NCT01211262), and the Phase 2 trial for the treatment of melanoma, meningioma, breast cancer, NSCLC and hepatocellular cancer with the NY-ESO-targeting ImmTAC-NYE (NCT01967823). Yet, *in vivo* ImmTAC-redireced T cells are still subjected to the immunosuppressive effects of the TME, thus current research is exploring ImmTAC-NYE and IMCgp100 with α-PD-1 antibody combination therapy to enhance killing of cancer cells by reversing regulatory T cell-mediated immunosuppression[200,201].

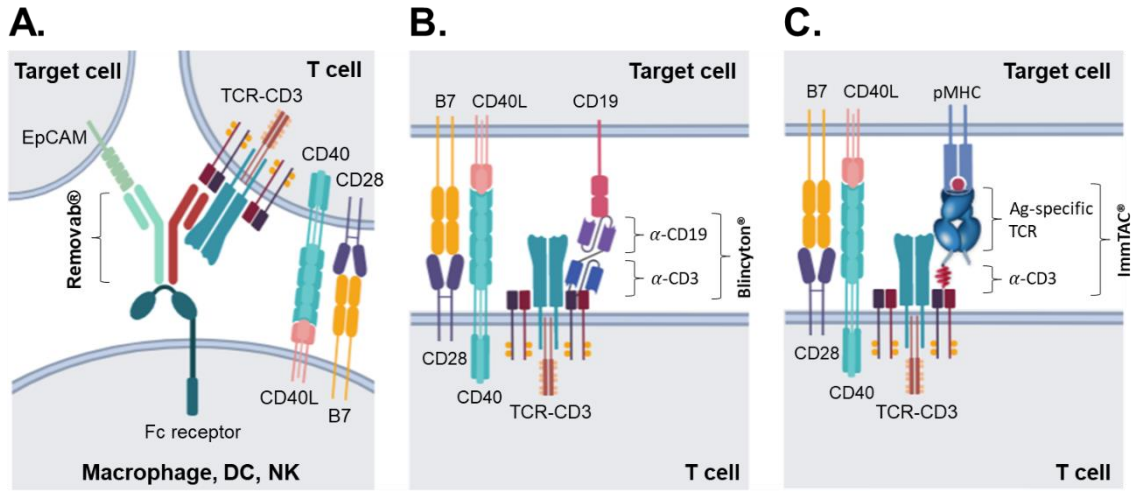

Figure 1-12. **Novel T cell-redirecting immunotherapy approaches.** Graphic representation of bispecific antibodies Removab® **(A)** Blincyto® **(B)** and the TCR-based soluble therapy ImmTACs **(C)** used to attract immune cells to the tumour niche to create an immune synapse that result in T cell activation. These fusion molecules form a central molecular complex that establishes an artificial immune synapse for activating CD3+ T cells in the proximity of tumour cells in the TME, which allow cytokine production for tumour killing. Reviewed in [202,203].

1.5.3. Cytokine therapy

Cytokines act as messengers to the elements of the innate and adaptive immune system and control many behaviours of immune cells including proliferation, differentiation, survival and effector function. The administration of cytokines to enhance T cell therapy has been explored in T cell therapy. Clinical trials of cytokine therapy started in 1986 with the use of IFNα for the treatment of hairy cell leukaemia (HCL)[204]. In 1992, treatment with IL-2 was approved for metastatic renal cell cancer[205], and later in 1998 for the treatment of advanced melanoma[206]. Currently, cytokines including IL-2, IL-7, IL-15, IL-21 and IFNα have been long exploited for therapeutic applications in the treatment of cancer malignancies[207]. However, systemic

administration of immunomodulation has toxic effects[208]. To bypass this hurdle, *Irvine and colleagues*[209–211] developed a "T cell backpack" system based on drug-loaded protein nanogels conjugated to the plasma membrane of ACT T cells that selectively release cytokine cargos in response to T cell activation. It must also be noted that, for many cytokines, each tumour-elimination approach is paralleled with the induction of immunological checkpoints inducing inhibitory factors such as PD-L1, IL-10 and TGFβ.

To date, high-dose IL-2 therapy has been extensively studied for treating several metastatic cancers as both a monotherapy and in combination with other immuno-approaches including peptide vaccines (gp100)[212], chemotherapeutic agents (*cisplatin* and *dacarbazine*)[213], monoclonal antibodies (i.e*. ipilimumab*)[214], and with TIL therapy[215]. The high dosage required in the treatment can be associated to severe toxicity[207].

1.5.4. Adoptive cell transfer (ACT)

ACT is a highly-personalised form of immunotherapy based on the transfer of *ex vivo* expanded autologous T cells with optional genetic engineering or selection of tumour-reactive cells. Pioneered by *Rosenberg and colleagues*[216] at the National Cancer Institute (NCI), this T cell-based immunotherapy has been shown to be one of the most effective treatments in metastatic melanoma, renal cell carcinoma and lymphoma with diverse degrees of tumour regression[132]. The presence of $CD8^+$ and $CD4^+$ Th1 Tumour-Infiltrating Lymphocytes (TILs) subtypes in the tumour niche has been related to a positive prognostic factor in melanoma[217,218], ovarian[219,220], colorectal[221], urothelial[222], pancreatic cancer[223] and other solid cancers. In contrast, infiltration of MDSC, Th2 and Th17 $CD4^+$ T cells and $Foxp3^+$ $CD4^+$ regulatory T cells (Tregs) have been generally associated with negative prognosis[224].

In general, ACT with T cells requires patient pre-conditioning by non-myeloablative lymphodepleting chemotherapy to create a niche space for the transferred T cells[225]. The use of minimally cultured TILs (or Young TILs)[226] offers an attractive source of T cells for ACT, especially in melanoma, as the therapy enhances the natural anti-tumour immune response by removing the cancer-specific cells from the immunosuppressive tumour microenvironment, followed by GMP-compliant *in vitro* expansion and re-infusion to a pre-conditioned patient (**Figure 1-13**). Pre-conditioning usually involves temporary ablation of the patient's immune system, including the removal of potential immunoregulatory cells from the tumour microenvironment, using non-myeloablative lymphodepleting systemic chemotherapy alone[227] or in combination with total-body radiation to activate the innate immune system[228].

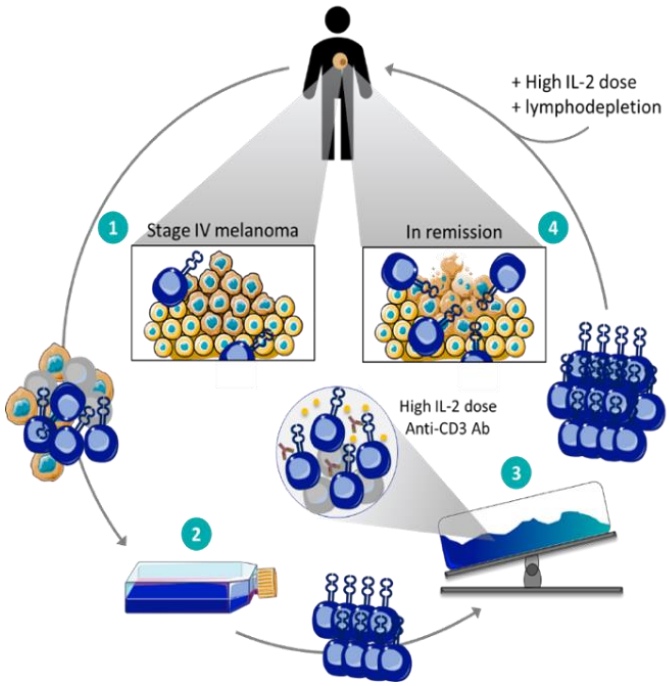

Figure 1-13. **Schematic diagram of Adoptive cell transfer using Young Tumour Infiltrating Lymphocytes (TILs).** (1) Tumour lesions containing several cell types are surgically resected and fragmented (1-3mm^3 fragments) or digested. (2) Tumour-infiltrating lymphocytes (TILs) are further expanded by co-culture with high dose of interleukin-2 (IL-2), irradiated feeders and anti-CD3 antibody in a Wave® bioreactor for 14 days (3). Cells are then re-infused into a lymphodepleted patient together with high dose of IL-2 (4). The overall generation of a TIL infusion product takes on average 3-4 weeks.

Young TIL therapy is limited to tumours that are easily and safely accessed by surgery and that contain sufficient TIL to allow rapid expansion[132]. The range of cancers that can be treated by ACT can be extended by equipping blood-derived patient T cells with a tumour-specific antigen receptor. Two main genetic engineering approaches have been utilised in the clinic: chimeric antigen receptor (CAR-T) therapy and TCR gene transfer (TCR-T). These genetic engineering-based approaches enable rapid generation of autologous T cell products that can target patient tumour cells.

1.5.4.1. CAR-T therapy

Chimeric antigen receptors (CARs) are hybrid proteins that fuse a tumour targeting extracellular domain (usually an antibody) with a manufactured T cell signalling domain. Thus, CAR-T cells encompass both an extracellular domain for antigen binding and an intracellular domain with T cell activating functions in a single, chimeric receptor. In 2017, the first CD19-targeted CAR T cell therapy *Axicabtagene ciloucel* (**Yescarta**) was approved by the FDA for the treatment of CD19$^+$ B-cell lymphomas[229]. This was quickly followed by *Tisagenlecleucel* (**Kymriah**) in 2018 for treatment of CD19$^+$ non-Hodgkin Lymphomas[230]. Currently active clinical trials are using engineered bi-specific CD19-targeted CAR-T cells in combination with other targets, including CD20 and CD22[231–233]. Early testing has shown promising results in the eradication of B cell malignancies while reducing off-target effects[231,233–235]. Despite this promise, CAR-T therapies have yet to show efficacy for solid tumours[236]. A new modality of “armoured CAR-T cells”, which

are modified to co-express immunomodulatory ligands such as CD40L[237], secrete PD-1-blocking scFv[238], or constitutively secrete cytokines[239], have been shown to allow an enhanced efficacy of the CAR-T in cancers with an immune-suppressive TME.

In contrast, evidence from TIL therapy and checkpoint inhibitor therapy has demonstrated that T cells bearing natural TCRs can eradicate some solid tumours. Consequently, there are numerous trials in progress using T cells that have been engineered to express cancer-specific TCRs; so-called TCR-T therapy.

1.5.4.2. TCR-T therapy

T cells transduced with TCRs of various affinities have been used in human adoptive T cell trials with variable efficacy and safety as listed in **Table 1-4**. Natural TCRs against shared tumour antigens express weak TCRs as the result of central tolerance as described in **section 1.3** above. TCR affinity is known to be important for cancer recognition[135,136]. Consequently, many studies have utilised TCRs that have been engineered to enhance their binding affinity to levels seen with natural anti-pathogen TCRs or greater. Engineered, sequence-modified TCRs, might exhibit improved recognition of cancer cells but these receptors have bypassed the rigors of the natural thymic selection process and thereby carry the risk of unexpected autoimmune reactivity. There is also the further possibility that transduced TCR chains might mis-pair with the natural endogenous chains. Thus, and TCR transduced T cells can express up to 4 different TCRs: (i) The transduced TCR; (ii) the endogenous TCR; (iii) the transduced TCR α chain paired with the endogenous TCR β chain; and, (iv) the transduced TCR β chain paired with the endogenous TCR α chain. The specificity of the latter two hybrids is unknown and they have the capacity to recognise self peptide-MHC complexes[240].

Table 1-4. **Active clinical trials using TCR-transduced T cells for cancer immunotherapy**. Data collected from www.clinicaltrials.gov. **MSD**: Myelodysplastic Syndromes; **AML**: Acute Myeloid Leukaemia; **NSCLC**: Non-Small Cell Lung Cancer

Transduced TCR	Cancer type	Trial stage	HLA-restriction	Identifier
NY-ESO-1	NSCLC	Recruiting	A*02:01	NCT03029273
NY-ESO-1^{c259} TCR	Malignant melanoma	Phase 1 Phase 2	A*02:01	NCT01350401
NY-ESO-1	Bladder Carcinoma Breast Cancer Oesophagus Carcinoma Lung Cancer Melanoma Multiple Myeloma Neuroblastoma Ovarian Cancer Synovial Sarcoma	Phase 1	A*02	NCT02457650
MAGE-A3/A6 (KITE-718)	Solid tumour	Phase 1	DPB1*04:01	NCT03139370
WT1	MDS AML	Phase 1 Phase 2	A*02:01	NCT02550535
WT1	Stage III-IV NSCLC Mesothelioma	Phase 1 Phase 2	A*02:01	NCT02408016
HERV-E	Kidney Cancer	Phase 1	A*11:01	NCT03354390
IMCgp100	Uveal melanoma Malignant melanoma	Phase 1 Phase 1b/2	A*02:01	NCT02570308 NCT02535078
IMCnyeso	NY-ESO-1^{+} and/or LAGE-1A^{+} cancers Melanoma NSCLC Urothelial carcinoma Synovial sarcoma	Phase 1 Phase 2	A*02:01	NCT03515551
MAGE A4	Urothelial cancer Melanoma Head and Neck cancer Ovarian cancer NSCLC Oesophageal cancer Gastric cancers Synovial sarcoma	Phase 1	A*02 Except for A*02:05 or A*02: 07	NCT03132922
MAGE-A10	Urothelial cancer Melanoma Head and Neck cancer	Phase 1	A*02:01 or A*02:06 Except for A*02:05, B*15:01 or B*46:01	NCT02989064
AFP	Hepatocellular cancer	Phase 1	A*02:01 or A*02:642	NCT03132792
E6 E7	HPV-associated epithelial cancers	Phase 1 Recruiting	A*02:01 A*02:01	NCT03578406 NCT02858310

These theoretical risks were proven to be very real during the trial of an engineered TCR by Adaptimmune in 2013 (NCT01350401) that resulted in fatal adverse effects due to an unanticipated cross-reactivity with a self peptide from Titin[241] (discussed in **Chapter 5**). More recent studies by my own group have demonstrated that redirection of primary $CD8^+$ and $CD4^+$ T cells with pan-cancer reactive natural TCRs is substantially improved when CRISPR/Cas9 gene editing is used to disrupt the endogenous TCR chains[240]. Such "TCR replacement" has multiple benefits as in addition to removing the capacity for TCR chain mispairing it also ensures that more of the transduced TCR is expressed at the T cell surface. Indeed, *Legut et. al.*[240] demonstrated that T cells manufactured by TCR replacement could be over 1000-fold more sensitive to cognate antigen than T cells engineered as currently used in the clinic. The optimal TCR affinity for recognition of cancer cells as previously described by my laboratory[135] requires reassessment as it maybe that the use of affinity enhanced engineered TCRs, and their associated risks, is unnecessary if TCR replacement is used.

A critical limitation of conventional αβTCR therapies is antigen presentation by specific MHC molecules, restricting treatment to HLA-eligible patients. In addition, downregulation of MHC molecules has been described as a mechanism of avoiding TCR recognition (see **section 1.4**)[242]. An alternative approach of transducing T cells with cancer-specific γδTCR with the aforementioned methodology, showing some initial promise *in vitro*[240]. However, understanding of the molecular mechanisms and anti-tumour targeting mechanisms of γδ T cells is still very limited and most therapies in the clinic make use of αβTCRs despite the obvious limitation of HLA-restriction.

In summary, multiple approaches are being developed for the immunotargeting of cancer with each therapeutic modality proving efficacious for some patients with some cancers. While these successes are hugely promising with one having already seen the award of a Nobel prize, there is clearly room for substantial improvement. The successes shown by antibody-based checkpoint inhibitors to modulate T cell immunosuppression have aroused a renewed interest in cancer immunotherapy, yet "releasing the breaks" on general T cell activation has led to reported immune-related toxicities. Similarly, the popularity of successes using CAR-T cells has also been compromised by several reported incidences of cytokine release syndrome ranging from 35% to >90% in treated patients[243]. Bispecific T cell engaging antibodies on the other hand are designed to specifically target tumour cells, thus reducing the risk of adverse events resulting from non-specific immune activation; however the limited number of tumour-specific surface-presented antigens highly restricts the application of these therapies. TIL-based ACT therapy is highly unsuitable for cold tumours; and TCR-engineering of autologous T cells suffers the major drawback of MHC restriction limiting the use of any specific therapeutic modality to a minority of patients. Consequently, there is room for considerable improvement in cancer immunotherapy. One potential way to generate such improvements could come by dissecting successful immunotherapy to establish which antigens are recognised by successful T cells as I aimed to do here.

1.6. Project aims

T cell immunotherapy has shown some remarkable success in some patients with some cancers. The next step will be to extend the number of patients that respond to treatment and the range of cancers that can be treated. While it is known that $CD8^+$ T cells underlie the success of both checkpoint inhibitor and TIL therapy, no detailed dissection of the T cells and TCRs that respond to the autologous cancer when these therapies succeed has been provided. Thus, the question of what successful T cells target remains largely unanswered. I set out to dissect successful immune therapy for malignant melanoma using a cohort of patients with stage IV disease who were successfully treated by tumour-infiltrating lymphocyte (TIL) therapy. I hypothesised that the targets recognised by persistent T cell clonotypes (i.e. those T cells within the TIL infusion product that were expanded in patient blood during and after complete remission) might illuminate how this therapy succeeds and enable this success to be replicated in other patients with other cancers. This discovery-driven project took me in several unanticipated and exciting directions.

I began my project by interrogating antigen-specific TCR repertoire from a melanoma patient using pMHC multimer staining. The rationale for this start point was that it would allow me to stain and capture cancer-specific T cells in the TIL infusion product and patient blood following complete remission. During my early studies, it became apparent that standard peptide-MHC tetramer staining was failing to detect fully functional T cells. I thus set out to formally prove that the "gold standard" of T cell detection using peptide-MHC tetramers has a very serious deficiency by comparing T cell populations that were stained with conventional technology (as generally used elsewhere) and an optimal protocol developed within my laboratory. This work resulted in a first author paper in the *Journal of Immunology*[244] and is the subject of **Chapter 3**. I next used the techniques I had learned during this pMHC multimer-based work, especially high throughput sequencing of antigen-specific TCRs, to examine the entire response to an autologous cancer line in an HLA A*02:01^+ patient who underwent a complete and durable remission following TIL therapy at the *Center for Cancer Immune Therapy* (CCIT) in Copenhagen. Sequencing of cancer-specific TCRs present in the TIL infusion product used to treat the patient and patient blood following complete remission allowed me to identify *persistent* HLA A*02:01-restricted T cell clonotypes of unknown specificity. Some of these clonotypes were observed to respond to many HLA A*02:01^+ cancer lines of many different origins. A bespoke "epitope discovery pipeline" encompassing Positional Scanning Combinatorial Peptide Library (PS-CPL) screening in conjunction with bioinformatic interrogation of a cancer proteomics database was successful in identifying new broadly-expressed HLA A*02:01-restricted cancer epitopes. This work is the subject of **Chapter 4**.

– Chapter 2 –

Materials and Methods

2.1. Cell culture media and buffers

Table 2-1. Composition of cell culture media. All media was filter-sterilised through a 0.22 µm filter, stored at 4°C and used within 30 days after preparation. Cells were cultured with the appropriate media volume in 6, 24, 48, 96 multi well plates or T25, T75 and T175 flasks (Greiner Bio-One) as specified.

Media	Composition
R0	RPMI-1640 (Life Technologies), 100 U/mL Penicillin (Life Technologies), 100µg/mL Streptomycin (Life Technologies), 2mM L-Glutamine (Life Technologies)
R5	R0 supplemented with 5% Heat-Inactivated Foetal Bovine Serum (FBS) (Life Technologies)
R10	R0 supplemented with 10% FBS
D10	DMEM supplemented with 10% FBS, 100 U/ml penicillin, 2 mM L-Glutamine
D10/F12	DMEM/F12 supplemented with 10% FBS, 100 U/ml penicillin, 2 mM L-glutamine, 10 mM HEPES (Life Technologies)
T cell culture media (IU200)	R10, 10mM HEPES (Life Technologies), 1mM Sodium Piruvate (Life Technologies), 1X MEM Non-essential amino acids (NEAA) solution (Life Technologies), 25 ng/mL IL-15 (PeproTech), 200 IU/mL IL-2 (Aldesleukin, brand name Proleukin; Prometheus)
T cell expansion media (IU20)	R10, 10 mM HEPES (Life Technologies), 1 mM Sodium Piruvate (Life Technologies), 1X MEM Non-essential amino acids (NEAA) solution (Life Technologies), 25 ng/mL IL-15 (PeproTech), 20 IU/mL IL-2 (Aldesleukin, brand name Proleukin; Prometheus)
T cell priming media	R10 supplemented with 10 mM HEPES, 1 mM sodium pyruvate, 1x non-essential amino acids, and 20 IU IL-2 (Proleukin; Prometheus, San Diego, CA)

Table 2-2. Composition of Buffers. All buffers were filter-sterilised through a 0.22 µm filter, stored at 4°C and used within 30 days of preparation. Reagents were purchased from Sigma Aldrich (unless otherwise specified)

Buffers and reagents	Composition
Freezing buffer	90% FBS, 10% DMSO
Red Blood Cell (RBC) lysis buffer	155 mM NH_4Cl, 10 mM $KHCO_3$, 0.1 mM EDTA, pH 7.2-7.4
PBS-EDTA	Dubecco's PBS, 2 mM EDTA
FACS buffer	PBS, 4% FCS
MACS buffer	2 mM EDTA, 0.5% BSA in D-PBS
Fixing buffer	4% PFA in PBS
Tris-EDTA (TE) Buffer	10 mM Tris, 1 mM EDTA in ddH_2O (pH=8.0)
Buffered water	2.5 mM HEPES in ddH_2O (pH=7.3)
2X HEPES-buffered saline (HeBS)	0.28 M NaCl, 0.05 M HEPES, 1.5 mM Na_2HPO_4 in ddH_2O (pH=7.0)

2.2. Mammalian Cell culture

2.2.1. Immortalised Cell line culture

Cell lines were grown at 37°C, 5% CO_2 in the correspondent culture media (see **Table 2-1** for media composition). Cell lines were routinely fed every 2 days and passaged when reaching 80% confluence and/or turned the media yellow due to waste-product accumulation[245].

Adherent cell lines were passaged by removing old media, washing with Dulbecco's PBS and detaching with PBS-EDTA at 37°C. Detached cells were collected in a sterile tube, centrifuged at 400 × g for 5 minutes, and the supernatant aspired. Cell pellet was resuspended in the corresponding media and plated into a flask at the appropriate density (20-30%).

For suspension cultures, cells were re-suspended, harvested and plated with fresh media in a new flask (additional centrifugation and pellet resuspension in fresh media was followed for cell counting when required). All cell lines were routinely tested for Mycoplasma using a MycoAlert™ Mycoplasma Detection Kit (Lonza) and found to be negative. A summary of the cell lines used in this thesis and their characteristics can be found in **Table 2-3**.

Table 2-3. Cell lines used throughout the study. Cell lines were procured from ATCC and cultured according to manufacturer's recommendation or grown from primary patient tumour at the Centre of Cancer Immune Therapy in Copenhagen.

Cell line	HLA-A2	Tissue (Disease)	Culture	Media
MM909.11	-	Malignant Melanoma	Adherent	R10
MM909.22	-	Malignant Melanoma	Adherent	R10
MM909.24	+	Malignant Melanoma	Adherent	R10
MM909.37	+	Malignant Melanoma	Adherent	D10 F12
MM909.45	-	Malignant Melanoma	Adherent	D10 F12
ACHN	-	Kidney (Carcinoma)	Adherent	D10
RCC17	+	Kidney (Carcinoma)	Adherent	D10 F12
HePG	+	Normal Hepatocyte	Adherent	D10
MRC-5	+		Adherent	D10
Colo 205	+	Colon (Carcinoma)	Adherent	R10
SiHa	-	Cervix (Carcinoma)	Adherent	D10
A 2780	-	Ovarian (Carcinoma)	Adherent	R10
LnCap	+	Prostate (Carcinoma)	Adherent	D10
PC-3	-	Prostate (Carcinoma)	Adherent	D10 F12
H69	+	Lung (carcinoma)	Adherent	R10
MCF-7	+	Breast (Adenocarcinoma)	Adherent	R10
MDA-MB-231	+	Breast (Adenocarcinoma)	Adherent	R10
SaOS	+	Bone (Osteosarcoma)	Adherent	D10
T2	+	Lymphoblast	Suspension	R10
C1R	-	Lymphoblast	Suspension	R10
0439 LCL	+	Lymphoblast	Suspension	R10
MM909.24 LCL	+	Lymphoblast	Suspension	R10
MOLT3	-	T cell Leukaemia	Suspension	R10

2.2.2. Cell counting

Cells were resuspended at an estimated density of between $0.5x10^6$ and $3x10^6$ cells/mL. 10 µL of cell suspension was mixed 1:1 with 0.4% trypan blue solution (Sigma Aldrich) and loaded into the haemocytometer. Live cells on a 16-square grid were counted twice based on trypan blue exclusion. Cell density calculated according to the following formula:

$$\frac{cells}{mL} = \frac{count\ 1 + count\ 2}{2} \times dilution\ factor \times 10^4$$

2.2.3. Cryopreservation

For cryopreservation, cells were harvested, washed with R0 by centrifugation at 400 × g for 5 minutes to remove culture media, and then counted by trypan blue exclusion. Cell pellets were resuspended in freezing buffer (**Table 2-2**) at the density of 1-2×10^6 cells/mL. 1 mL aliquots were transferred to cryovials (Nunc™) and cooled down to -80°C using a controlled-rate freezing device (Mr. Frosty® freezing pot, Nalgene) following manufacturer's instructions. For long term storage, frozen cells were moved from -80°C to liquid nitrogen.

For cryopreservation removal, cells were moved from liquid nitrogen and thawed in a water bath at 37°C for 1 minute. Thawed cells were transferred to 15 mL centrifuge tubes containing 10 mL pre-warmed R10 media, centrifuged at 400 × g for 5 minutes and supernatant aspired. Cell pellet was resuspended in respective media, counted by trypan blue exclusion and plated into the appropriate tissue culture flask or plate.

2.2.4. Isolation of Peripheral Blood Mononuclear Cells (PBMCs)

PBMCs were routinely isolated from healthy donors' peripheral blood, provided either as buffy coats by the Welsh Blood Service, or obtained through venepuncture from local donors, in accordance with the Human Tissue Act governance and corresponding local ethics. Buffy coats were seronegative tested for HIV-1, HBV and HCV by the Welsh Blood Service before delivery. Briefly, whole blood was separated by density gradient centrifugation by layering 25 mL of blood on top of 13 mL Lymphoprep™ in SepMate™ tubes (STEMCELL Technologies). Tubes were then centrifuged at 1,200 × g for 10 minutes, and the supernatant containing PBMC was collected, diluted 1:1 with R0 and centrifuged at 700 × g for additional 10 minutes. Red blood cells were lysed by resuspending cell pellet in 25 mL of RBC lysis buffer for 10 minutes in a water bath at 37ºC. After lysis, 25 mL of R0 was added to each tube, and centrifuged at 300 × g for 6 minutes to remove platelets. RBC lysis was repeated when necessary. The resulting PBMC pellet was resuspended in R10 and cell density was established by counting (see **section 2.2.2).** Purified PBMC were either processed immediately or kept at 4°C.

For T cell expansion, irradiated PBMC from at least three donors was used to provide sufficient stimulus due to HLA mismatching. PBMC were irradiated with Cesium-137 for 3100 centigrays (cGy). After irradiation, cells were washed and recounted for pooling of 1:1:1 ratio.

2.2.5. Generation of T cell clones

Antigen-specific $CD8^+$ T cell clones were produced by single cell cloning from freshly prepared PBMC, T cell lines or frozen TIL samples following tetramer-based cell sorting by flow cytometry on a BD FACSARIA III (see **section 2.4**) or Magnetic enrichment (see **section 2.3.9**). Briefly, T cells were plated in a 96 U-bottom culture plate in 100 µL 20IU T cell expansion media at 0.5 T cells per well density with 50,000 allogenic irradiated PBMC and 1µg/mL PHA. Cells were incubated at 37°C 5% CO_2 for 7 days and topped up with 100 µL 20IU following 7 more days of incubation. On day 14, wells containing visibly growing T cell clones were screened in the appropriate functional assays or re-stimulated if necessary (**Figure 2-1**). TCR clonotyping of T cell clones was routinely performed (see **section 2.5**). A summary of the T cell clones used in this thesis can be found in **Table 2-4**.

2.2.6. Expansion and culture of T cells

T cell clones and lines were routinely expanded in T25 flasks at 37°C, 5% CO_2. Briefly, T cells were harvested, washed and counted by trypan blue exclusion. Up to 1×10^6 T cells per flask were cultured with 15×10^6 allogenic irradiated feeder mix containing PBMCs from three individuals (see **section 2.2.4**) and 1 µg/mL Phytohaemagglutinin (PHA, Sigma Aldrich) in 15 mL of 20IU expansion media (**Table 2-1**) in approximately 45° angle to allow cell-to-cell contact. On day 5 post-expansion, half the media was replaced with fresh 20IU expansion media. On day 7 post-expansion, cells were harvested, washed, resuspended in 200IU T cell culture media (**Table 2-1**), counted and plated at the appropriate density ($1\text{-}2\times 10^6$ cells/well in 48 well plates, $3\text{-}4 \times 10^6$ cells/well in 24-well plates). T cells were feed every 48h by replacing half the media from the well with fresh 200IU media. T cells were used in functional assays after day 14 post-expansion up to 4 weeks or frozen until further use.

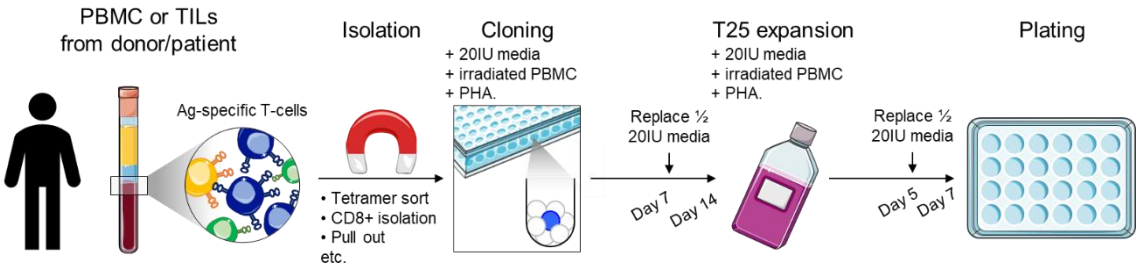

Figure 2-1. **Procurement of $CD8^+$ T cell clones workflow.** Graphical representation of the workflow followed in the generation of T cell clones from healthy or diseased donors based on FACS ARIA sort or magnetic enrichment of CD8 co-receptor expressing cells, antigen-specific cells using multimerised pMHCs, or cytokine secretion upon antigen/tumour challenging (described in the sections below). Following isolation, cells were plated as indicated with the required stimuli for 14 days, then tested and re-stimulated as required for 7 more days. T cell clones to be used in assays were plated at the appropriate density and used in functional assays as specified.

Table 2-4. HLA A2-restricted T cell clones used throughout the study. All T cell clones were tested for $CD8^+$ expression and antigen-specificity validated by tetramer staining.

Clone name	Specificity	αβ TCR clonotype			
CR0439.GLC	EBV BMLF1	TRAV5 TRBV29-1	TRBD2	TRAJ15 TRBJ1-5	CDR3α: CAEKGAGTALIF CDR3β: CSVAGTGDLNQPQHF
GD.GLC17	EBV BMLF1	TRAV5 TRBV20-1	TRBD2	TRAJ31 TRBJ1-3	CDR3α: CAEDNNARLMF CDR3β: CSARVGVGNTIYF
CR24	Melan-A; BST2; IMP-2	TRAV12-2 TRBV6-5	TRBD2	TRAJ8 TRBJ2-7	CDR3α: CAVQKLVF CDR3β: CASSYSFTEATYEQYF
CR0439.NLS	IMP-2	TRAV40 TRBV11-3	TRBD2	TRAJ53 TRBJ2-5	CDR3α: CLTPSGGSNYKLTL CDR3β: CASAAYGETQYF
LIMON	IMP-2; Melan-A	TRBV5-4	TRBD2	TRBJ2-3	CDR3β: CASSLDNSVLTTDTQYF
MANUELA	IMP-2; Melan-A	TRAV12-2 TRBV2	TRBD1	TRAJ45 TRBJ2-6	CDR3α: CAAYSGGGVDGLTF CDR3β: CASSPTELGANVLTF
CACTUS	IMP-2; Melan-A	TRAV12-2 TRBV25-1	TRBD1	TRAJ31 TRBJ2-5	CDR3α: CAVNNARLMF CDR3β: CASSGPFGAQYF
TESLA	IMP-2	TRAV12-2 TRBV2	TRBD2	TRAJ49 TRBJ2-1	CDR3α: CAVTGNQFYF CDR3β: CASGDSNSYNEQFF
MARIA	Melan-A	TRAV12-2 TRBV28	TRBD2	TRAJ45 TRBJ2-1	CDR3α:CAVSTGNQFYF CDR3β: CASTLPGLAGNEQFF
CR124	Melan-A	TRAV12-2 TRBV19	TRBD1	TRAJ9 TRBJ1-5	CDR3α: CAVHTGGFKTIF CDR3β: CASTVAGVGQPQHF
CR324	Melan-A	TRAV38-2 TRBV28	TRBD1	TRAJ41 TRBJ2-2	CDR3α: CAYRRVDALNF CDR3β: CASRQQGLSTGELFF
B7.24	Melan-A	TRBV9	TRBD1	TRBJ2-7	CDR3β: CASSVGVQGSWEQYF
B17.24	Melan-A	TRAV12-2 TRBV12-4	TRBD1	TRAJ45 TRBJ2-7	CDR3α: CAVPRGAQKLVF CDR3β: CASSWAGPVEQYF
CR31	Melan-A	TRAV12-2 TRBV30	TRBD1	TRAJ49 TRBJ1-5	CDR3α: CGSNTGNQFYF CDR3β: CAWSSQGLGQPQHF
VB6G4.24	Melan-A	TRAV36 TRBV24-1	TRBD1	TRAJ34 TRBJ2-1	CDR3α: CAVQTDKLIF CDR3β: CATSDRGQGANWDEQF
VB16F1.24	Melan-A	TRAV12-2 TRBV6-2	TRBD2	TRAJ6 TRBJ1-3	CDR3α: CAVKEGGSYIPTF CDR3β: CASSYAGSGNTIYF
VB10F5.24	Melan-A	TRAV8-6 TRBV5-6	TRBD2	TRAJ49 TRBJ2-3	CDR3α: CALNTGNQFYF CDR3β: CASSLGILTDTQYF
MEL 5	Melan-A; BST2; IMP-2	TRAV12-2 TRBV30	TRBD2	TRAJ27 TRBJ2-2	CDR3α: CAVNVAGKSTFG CDR3β: CAWSETGLGTGELFFG

2.3. Functional T cell assays

2.3.1. Peptides

Synthetic crude peptides (purity 50-60%) (see **Table 4-1**, **Table 4-3** and **Supplementary table 12**) were manufactured by GL Biochem Ltd. (Shanghai, China). Synthetic pure peptides (purity >90%) (see **Table 2-5**) were synthesized by Peptide Protein Research Ltd. (Hampshire, UK). Lyophilised peptides were reconstituted in DMSO (Sigma Aldrich) to a final concentration of 20mg/mL and stored at -80°C. For T cell functional assays, reconstituted peptides were thawed on ice and working concentrations freshly prepared in R0.

Table 2-5. List of HLA A2 restricted peptides (purity >90%) used. Underlined first three amino acid residues were used as shorted versions of these sequences throughout this thesis.

Protein	Length	Residues	Peptide sequence
Melan-A	10 mer	26 - 35	EAAGIGILTV
Melan-A (heteroclitic)	10 mer	26 - 35	ELAGIGILTV
BST2	10 mer	22 - 31	LLLGIGILVL
IMP-2	10 mer	366 - 376	NLSALGIFST
NS4b (Yellow Fever Virus)	9 mer	214 - 222	LLWNGPMAV
BMLF1 (Epstein Barr Virus)	9 mer	280 - 288	GLCTLVAML
LMP2A (Epstein Barr Virus)	9 mer	426 - 434	CLGGLLTMV
pp65 (Cytomegalovirus)	9 mer	495 - 503	NLVPMVATV
M1 (Influenza Virus)	9 mer	58 - 66	GILGFVFTL

2.3.2. Peptide priming of T cells

Following $CD8^+$ subset isolation from PBMC (see **section 2.3.9.1**), T cells were plated at a density of 2×10^6 or $3\text{-}4\times 10^6$ T cells/well into 48-well or 24-well plates, respectively, in 0.5 mL priming media. Next, autologous PBMC or $CD8^{neg}$ cells were pulsed with 25 µM peptide in pre-warmed R10 for 1 hour at 37°C under slow continuous rotation, followed by irradiation with Cesium-137 for 3,100 centigrays (cGy). After irradiation, cells were washed in pre-warmed R0, counted and added to $CD8^+$ cells at a density of 4×10^6 or $6\text{-}8\times 10^6$ T cells/well into 48-well or 24-well plate respectively, together with 2 µg/mL anti-CD28 antibody (Beckman Coulter Ltd., UK). On day 3 of culture, 1 mL of T cell priming media was added per well followed by media exchange three times a week. On day 14 post-priming, T cells were supplemented with 25 ng/mL of IL-15, and were ready for downstream analysis.

2.3.3. Chromium-51 (^{51}Cr) release cytotoxicity assay

Short term cytotoxic activity of T cells against target cells was measured by ^{51}Cr release assay. Briefly, target cells (2,000 cells/well, usually in duplicates) were harvested and washed with D-PBS, then labelled for 1 hour at 37°C with 30 µCi ^{51}Cr (sodium chromate, Perkin Elmer) per 1x10^6 cells. After labelling, cells were washed in D-PBS, resuspended in R10 and incubated for 1 hour at 37°C to allow ^{51}Cr leaching from cells. Following excess removal, cells were washed again, resuspended in R10 at the desired confluence and plated in 96U-well plates (typically 2,000 cells/well). For Maximum and Spontaneous ^{51}Cr release controls, target cells were also incubated with 5% Triton X-100 and medium only, respectively. Effector cells, already in R10, were then added at the desired E:T ratios in a final volume of 150 µL, and incubated for 4- and/or 16-hours at 37°C, 5% CO_2. Following incubation times, 15 µL supernatant was collected and mixed with 150 µL Optiphase Supermix Scintillation Cocktail (Perkin Elmer) in disposable polyethylene terephthalate plates (Perkin Elmer). ^{51}Cr release was measured indirectly on a 1450-Microbeta™ counter (Perkin Elmer). Cytotoxic activity of T cells against target was calculated with the following formula:

$$\%\ Specific\ Lysis = \frac{Experimental\ ^{51}Cr\ release - Spontaneous\ ^{51}Cr\ release}{Maximum\ ^{51}Cr\ release - \ Spontaneous\ ^{51}Cr\ release} \times 100$$

2.3.4. Long term killing assay

Long term killing assays were performed to assess T cell mediated cytotoxicity against tumour cells at longer time points (>16 h) where other assays were unfeasible. Target tumours were plated at 10,000 cells/well alone (to serve as 100% survival control) and in the presence of T cells at the desired E:T ratios in a final volume of 200 µL 20IU medium. Each condition was set up in triplicate. At the chosen time points (usually after 3-7 days of co-incubation) 50,000-100,000 CFSE labelled C1Rs were added to each well to serve as an internal control. Cells in wells were then washed three times in dPBS-EDTA and stained with Vivid, anti-CD3 and anti-CD8 antibody (to exclude T cells). Samples were then acquired on a FACS Canto II with at least 3,000 CFSE-labelled C1R events acquired per sample. The representative gating strategy is shown in **Figure 2-2**, and % of cytotoxic activity was calculated according to the following formula:

$$\%\ Lysis = 100 - \left(\frac{experimental\ tumour\ cell\ events \div experimental\ CFSE\ labelled\ C1R\ events}{control\ tumour\ cell\ events \div control\ CFSE\ labelled\ C1R\ events}\right) \times 100$$

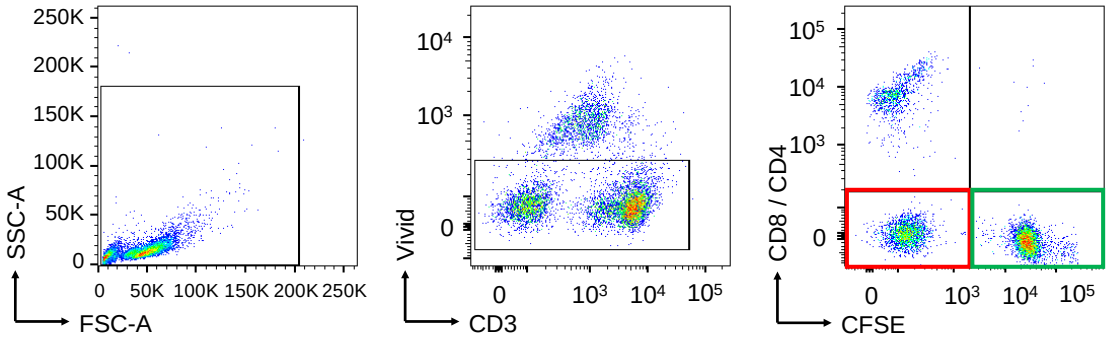

Figure 2-2. Gating strategy for long-term killing assays by flow cytometry. Cells were gated based on forward and side scatters with the voltage adjusted so that both T cells and tumour cells could be captured, then gated on $CD3^{+}$ and $CD3^{neg}$ alive cells, and CD8/CD4 and CFSE. Populations were then separated in quadrants and a minimum of 3,000 events of CFSE-labelled C1Rs (the $CFSE^{+}$ $CD8/CD4^{neg}$ quadrant) were required. The number of cells in the correspondent quadrants were used in the equation above. Red: Experimental/control tumour cells ($CFSE^{neg}$ $CD8/CD4^{neg}$), Green: experimental/control CFSE labelled C1R cells ($CFSE^{+}$ $CD8/CD4^{neg}$).

2.3.5. IFNγ Enzyme-Linked ImmunoSpot Assay (ELISpot)

PVDF-backed plates (Millipore) were incubated overnight at 4°C with 10 µg/mL (50 µL/well) Mouse anti-human IFNγ antibody 1-DIK (Mabtech). Coated plates were washed three times with 250 µL/well sterile PBS and blocked with 100 µL/well R10 medium for a minimum of 1 hour at RT. Freshly isolated PBMC (200,000 cells/well) or T cell clones (50,000 cells/well) were co-incubated with peptide (10^{-5} M) and/or target cells (30,000 cells/well) in R5 to a final volume of 200 µL/well. Experiments were performed in duplicate. 2 pg/mL PHA was added as a positive control with no peptide as a negative control. Plates were wrapped in tin foil and incubated overnight at 37°C.

Plates were then washed with PBS as described above and incubated with 100 µL/well sterile ddH_2O for 10 min at room temperature to lyse remaining bound cells, then washed twice with PBS. 50 µL/well of 1 µg/mL secondary biotinylated mouse antibody 7-B6-1 Biotin (Mabtech) was added and incubated in the dark at room temperature for 2 hours, followed by three PBS washes. 50 µL/well of 1 µg/mL Streptavidin-Alkaline phosphatase was added and incubated in the dark at room temperature for 2 hours. Plates were then washed three times in PBS and developed using the Alkaline Phosphatase Conjugate Substrate Kit (Bio-rad). Solution was added at 50 µL/well and developed in the dark until spots were clearly visible. Reaction was then stopped by washing the plates with tap water; plates were air dried in the dark before spot counting using the automated ImmunoSpot® S6 Analyser.

2.3.6. Enzyme Linked Immunosorbent Assay (ELISA)

T cells were washed in R0 and rested in R5 medium overnight before co-incubation with stimuli. When using peptides, APCs were pulsed with 100 µM peptide in the adequate volume to give a concentration of 1×10^6 cells/mL in a 15 mL falcon tube. Incubation was performed for 1 h at 37°C with rotation to avoid cell sedimentation, followed two washes in R0 and resuspension of cells in R10. T cells were co-incubated with target cells at 1:2 ratio (usually 30,000 T cells and 60,000 target cells per well) in a 96 U-well plates for 18 h at 37°C in 100 µL R5 medium. After co-incubation, plates were centrifuged (400xg 5 minutes) and 50 µL of supernatant was harvested, avoiding harvesting cells, and diluted with 70 µL of R0.

T cell activation upon antigenic stimulation was measured using MIP-1β, TNF or IFNγ outputs. T cell secretion of the chemoattractant chemokine MIP-1β recruits additional immune cells, including NK cells, monocytes and macrophages. Although MIP-1β is not a direct measure of T cell-induced death, previous data in our laboratory has shown that minimal ligand concentration is required to elicit a MIP-1β T cell response[246,247], and is therefore used in this thesis as a marker of T cell activation.

ELISAs for MIP-1β, TNF or IFNγ were performed according to manufacturer's instructions (DuoSet® human ELISA kits, R&D Systems). All washes were performed three times with 200 µL of 0.05% Tween 20-PBS, and incubations performed at room temperature. Briefly, a half area flat bottom 96 well plate was coated overnight with 50 µL mouse anti-human MIP-1β / TNF capture antibody (1.5 µg/mL in PBS). Plate was then blocked with 150 µL Reagent diluent (1% BSA in PBS) for at least 1 h. After washing, 50 µL of diluted supernatants were added in parallel with 50 µL of recombinant standards (range concentrations 1,000 to 8 pg/µL) used to plot a standard curve to calculate experimental concentration of MIP-1β or TNF in the sample. Supernatants and standards were incubated for 75 min and then washed. The plate was then incubated with 50 µL of biotinylated goat anti-human MIP-1β / TNF detection antibody (50 ng/mL) for 75 min, washed and incubated in the dark for 20 min with 50 µL horse radish peroxidase (HRP)-conjugated streptavidin. After washing, 50 µL of colour reagents A (tetramethylbenzidine) and B (Hydrogen peroxide) at 1:1 ratio was added and incubated for as long as needed to allow colour to be sufficiently developed. Reaction was then stopped by adding 25 µL of 1 M Sulphuric acid and the OD of each well measured at 450 nm with 570 nm correction in an iMark microplate reader (Bio-Rad).

2.3.7. Peptide size-scan

Peptide mixtures (Pepscan Presto Ltd) of X^8, X^9, X^{10}, X^{11}, X^{12} and X^{13} (where X is any of the 19 proteogenic L-amino acids excluding cysteine) described in **Table 2-6** were used to define the MHCI-peptide length preference of individual TCRs. Each peptide scan mixture was pulsed in duplicate at 1 mM with 60,000 APCs for 1hour at 37°C, prior to the addition of 30,000 overnight rested $CD8^+$ clonal T cells, and followed by overnight incubation at 37°C. Supernatant was collected and assayed by MIP-1β ELISA (see **section 2.3.6**).

Table 2-6. **Sizing scan parameters in scan mixture.** Superscript "n" indicates the number of degenerate positions in accordance to the length of the peptide. Adapted from [248].

Length	Total no. of peptides (19^n)	Concentration of each peptide*
8 mer	1.7×10^{10}	5.9×10^{-15} M
9 mer	3.2×10^{11}	3.1×10^{-16} M
10 mer	6.1×10^{12}	1.6×10^{-17} M
11 mer	1.2×10^{14}	8.6×10^{-19} M
12 mer	2.2×10^{15}	4.5×10^{-20} M
13 mer	4.2×10^{16}	2.4×10^{-21} M

*When mixtures are used at a concentration of 100µM.

2.3.8. Combinatorial peptide library (CPL) scans

Overnight rested $CD8^+$ T cells were challenged with 10 amino acid length combinatorial peptide library (CPL) (Pepscan Presto Ltd). In brief, the CPL library employed contained a total of 9.36×10^{12} different decamer peptides at equimolar concentrations. Library was divided into 200 different peptide mixtures where one L-amino acid residue position was fixed, but all other positions were degenerate, excluding cysteine to avoid disulphide bonds and peptide aggregation.

Antigen presenting cells were pulsed with library mixtures (60,000 cells / 100 µM peptide per well) for 1 hour at 37°C. T cells (30,000 per well) were then added to a final volume of 100 µL, and incubated overnight at 37°C. Activation towards each mixture was measured by MIP-1β release ELISA as described in **section 2.3.6**.

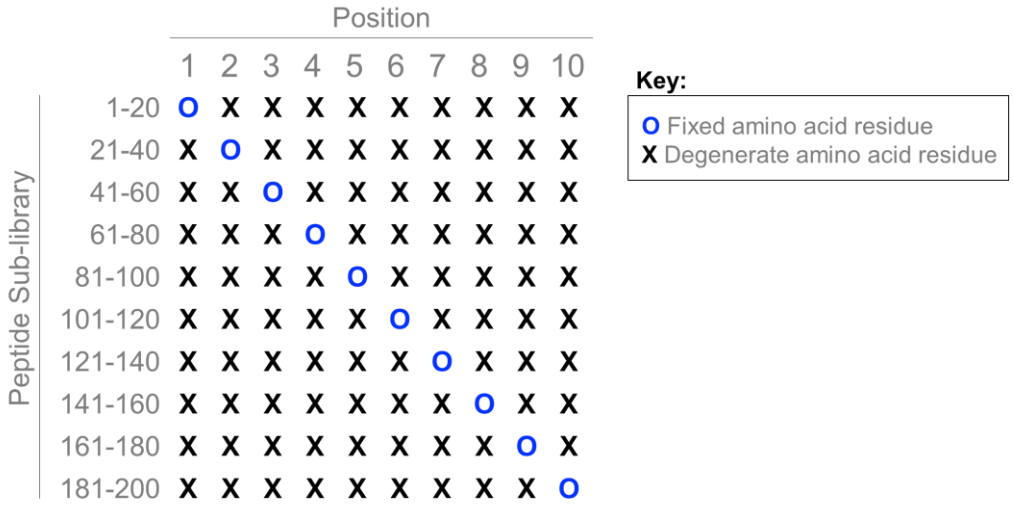

Figure 2-3. **Schematic representation of a Decamer (10mer) CPL**. Each of 200 mixtures included one of the 20 natural L-aminoacids in a defined position (O) and all possible combinations of other amino acids in the rest of the backbone in an equimolar mix. Cysteine was included as a fixed amino acid residue but excluded as a degenerate residue to limit the possibilities for oxidation.

2.3.9. Magnetic Activated Cell Sorting (MACS)

Labelling and isolation of desired T cell population was performed using Immunomagnetic beads from Miltenyi Biotec according to manufacturer's instructions in combination with high magnetic gradient MACS MS (maximum capacity 10^7 cells) or LS (maximum capacity 10^9 cells) columns. Washes were performed on pre-chilled MACS Buffer, and centrifugation steps were conducted for 5 min at 400xg 4ºC to prevent bead internalisation.

2.3.9.1. Isolation based on CD8 surface marker

Magnetic beads isolation was conducted according to manufacturer´s instructions. In brief, a maximum of 10^7 PBMC were resuspended in 80 µL MACS Buffer and incubated with 20 µL CD8 MicroBeads for 15 min at 4ºC. Following incubation, cells were washed with pre-chilled MACS buffer and passed through a 0.22 µm filter (if required) prior to application onto a MACS column to remove cell clumps. The column was washed three times with pre-chilled MACS buffer, and the $CD8^+$ enriched cell fraction was then eluted by applying a plunger to the column. The positively selected fraction was resuspended in T cell complete medium and treated as required for downstream applications. If downstream applications included peptide priming, $CD8^{neg}$ fraction was collected in a separate tube (see **section 2.3.2**).

2.3.9.2. TNF and/or IFNγ based magnetic pull-out

Enrichment of tumour-reactive or antigen-reactive T cells was achieved using a combination of the TNF and IFNγ Secretion Assay Kits to maximise the number of recovered antigen-reactive cells. Briefly, overnight rested T cells were co-incubated at 1:1 ration with target tumour cells or stimulated with 10^{-5} M peptide (typically 50,000 T cells and 50,000 target cells per well in a 96U-well plate) for 4 h. After incubation, cells were harvested and washed twice in MACS buffer, followed by resuspension in 80 µL MACS Buffer and incubated with 20 µL IFNγ and TNF Catch Reagents for 5 minutes on ice. After labelling with the Catch Reagents, cells were diluted in 5mL of warm R5 medium and incubate for 45 min at 37°C under slow continuous rotation to allow cytokine secretion. Cells were then washed in pre-chilled MACS buffer, resuspended in 100 µL MACS buffer and incubated with 75 µL IFNγ and TNF Enrichment Reagent for 15 min at 4°C. Labelled cells were subsequently washed with pre-chilled MACS Buffer and run in a MACS column (according to specifications). Column-bound cells were eluted by applying a plunger to the column and enriched antigen-reactive T cells were resuspended in T cell culture medium at the right density. On the following day, T cells were expanded as lines or cloned.

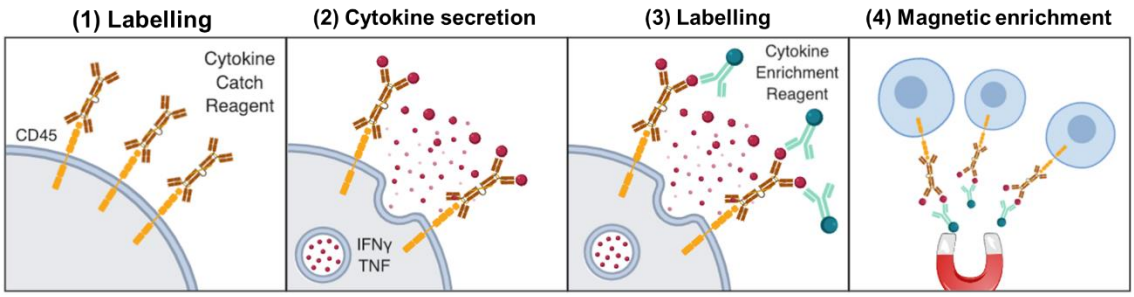

Figure 2-4. IFNγ and TNF secretion assay. **(1)** Stimulated T cells were incubated with the TNF and/or IFNγ Cytokine Catch Reagent, which specifically binds to CD45 molecule expressed at the surface of all leukocytes. Catch reagent consists of an anti-IFNγ or anti-TNF monoclonal antibody conjugated to an anti-CD45 monoclonal antibody. **(2)** A short period for cytokine secretion was allowed to achieve binding of the secreted IFNγ and/or TNF to the Catch Reagent on the antigen-specific secreting cells. **(3)** Cells were labelled with IFNγ and TNF Cytokine Enrichment Reagent, consisting of an anti-IFNγ or anti-TNF monoclonal antibody conjugated to MACS® MicroBeads. **(4)** Labelled cell suspension is positively selected by loading onto a MACS Column and placing in a magnetic field, allowing unlabelled cells to run through and conserving magnetically retained IFNγ and/or TNF secreting cells.

2.4. Flow cytometric analysis

Cells were washed in FACS buffer or PBS (700xg 3 min), counted by trypan blue exclusion (see **section 2.2.2**) and transferred to 5 mL FACS tubes (Elkay Laboratory Products Ltd, UK). About 50,000-100,000 T cells, LCLs or tumour cells and $\sim 3 \times 10^6$ PBMC were normally stained per tube. Staining was always performed on ice and in the dark unless indicated otherwise. Fluorescence Minus One (FMO) were always conducted in parallel to sample staining as negative control.

Events were acquired on FACS Canto II (BD Bioscience) or acquired and sorted using FACSAria Sort, and analysed using FlowJo Software v10.2 (Tree Star, Inc; Ashland, OR). Compensation was performed by single staining of anti-mouse Ig Compensation Particles (BD Bioscience).

2.4.1. Labelling cells with antibodies

PBS washed cells were stained for 5 min at room temperature in the dark with LIVE/DEAD® Fixable Violet Dead Stain Kit (Thermofisher), hereon referred to as *Vivid*, for dead cell exclusion before surface staining. Following incubation, primary fluorochrome-conjugated antibodies (for staining of surface proteins) were added to the cells and incubated for 20 min. Cells were then washed with PBS and kept on ice in the dark until flow cytometric analysis. If necessary, cells were fixed in 2% PFA for 20 min followed by two washes with PBS.

Surface-staining based phenotyping was performed to confirm phenotype of T cell clones and lines prior to functional experiments. The gating strategy utilised for T cell clones and PBMC samples is outlined in **Figure 2-5**, and a list of all used antibodies can be found in table **Table 2-7.**

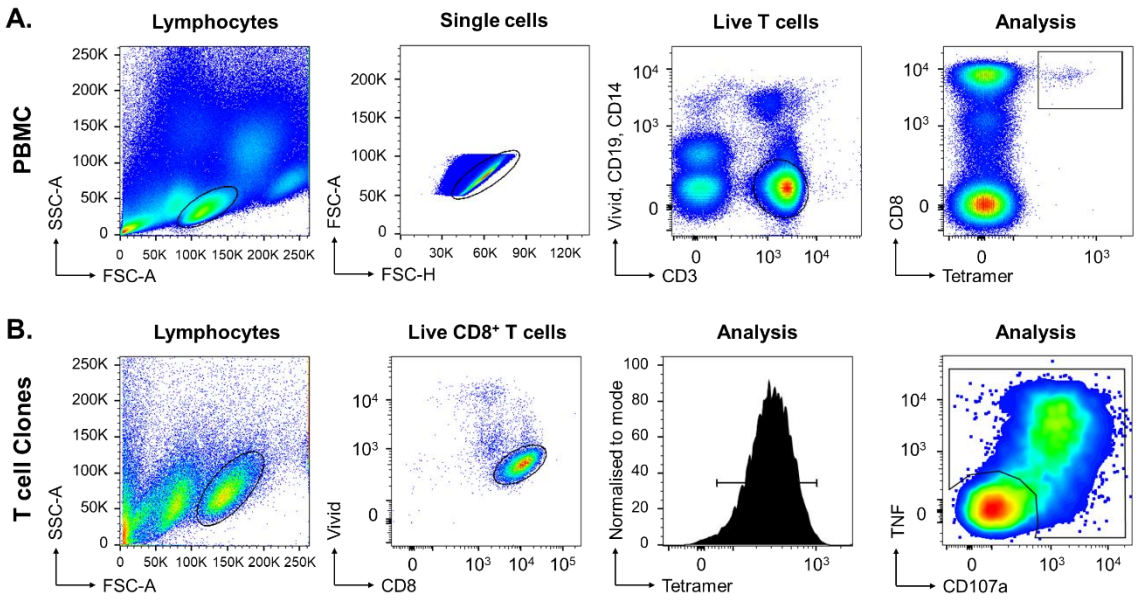

Figure 2-5 **Gating strategy for acquisition of antibody/tetramer labelled samples.** Assayed T cells stained with antibodies and/or tetramer were gated based on characteristic Forward (FSC-A) and side (SSC-A) scatter area properties of lymphocytes, followed by selection of single cells and live $CD3^{+}$ $CD14^{neg}$ $CD19^{neg}$ in PBMC samples **(A)**, or based on live $CD8^{+}$ staining for T cell clones **(B)**. Further analysis was conducted depending on the assay. Representative plots for PBMC **(A)** and T cell clone **(B)** staining with tetramer and antibodies is shown.

Staining with primary unconjugated antibodies (for single staining of non-surface proteins) was performed by permeabilization of the cells using Cytofix/Cytoperm™ (BD Biosciences), according to manufacturer's instructions. After permeabilization, cells were stained intracellularly with unconjugated antibodies for 20 minutes on ice, then washed with PBS followed by secondary antibody staining with conjugated donkey anti-rabbit antibody for 20 minutes on ice. The cells were subsequently washed with PBS and stored on ice in the dark until flow cytometric analysis.

Table 2-7. List of antibodies used for flow cytometry staining. All the employed antibodies were generated in mouse and were reactive against human proteins, unless specified otherwise. *Used in conjunction with secondary donkey anti-rabbit Ig.

Specificity	Fluorochrome	Clone	Provider
CD3	PerCP	BW264/56	Miltenyi Biotec
CD4	aPC Vio77	M-T466	Miltenyi Biotec
CD8	aPC Vio77	REA734	Miltenyi Biotec
CD14	Pacific Blue	M5E2	Biolegend
CD19	Pacific Blue	HIB19	Biolegend
HLA-A2	FITC	MCA2090F	Bio-Rad
IFNγ	aPC	45-15	Miltenyi Biotec
TNF	PE-Vio770	cA2	Miltenyi Biotec
CD107a	PE	H4A3	BD Biosci
Rat CD2	PE	OX-34	Biolegend
BST-2	PE	RS38E	Biolegend
Melan-A* (Rabbit)	Unconjugated	EP1422Y	Abcam
Anti-PE	Unconjugated	PE001	Biolegend
Donkey anti-Rabbit	PE	Polyclonal	ThermoFisher

2.4.2. pMHC multimer staining protocol

Biotinylated peptide-MHC (pMHC) monomers were produced in house as previously described[249]. When used for direct comparison, the same monomeric pMHC protein was employed to make tetramers and dextramers. Tetramers were assembled by co-incubation of streptavidin-PE with pMHC monomers at 1:4 ratio in 5 consecutive steps separated by 20 min incubation on ice, whereas dextramers were assembled by co-incubation of pMHC monomers with dextran-streptavidin-PE at a molar ratio of 3:1 for 30 minutes at room temperature. Once assembled, protease inhibitors (Set 1; Merck, London, UK) and PBS (tetramers) or dextramer buffer and were added to the mix for a working concentration of 0.1 mg/mL. Multimerised pMHC were stored at 4°C in the dark and used within a week after assembly.

For standard staining, cells were washed with FACS buffer followed by incubation with 0.2-0.5 µg tetramer (with respect to pMHC content) on ice for 30 min, followed by two washes with PBS and surface staining as described in **section 2.4.1**. For optimised tetramer staining, cells were resuspended in 50 nM PKI (Protein Kinase Inhibitor, Dasatinib, Azon Medchen, Reston) and incubated for 5 to 30 min at 37°C prior to staining[250]. Following tetramer or dextramer staining, cells were washed and stained with primary mouse anti-PE unconjugated antibody (PE001; BioLegend) and surface markers for 20 min as described. Besides staining with cognate tetramer, irrelevant tetramer and primary antibody cocktail staining were used as controls.

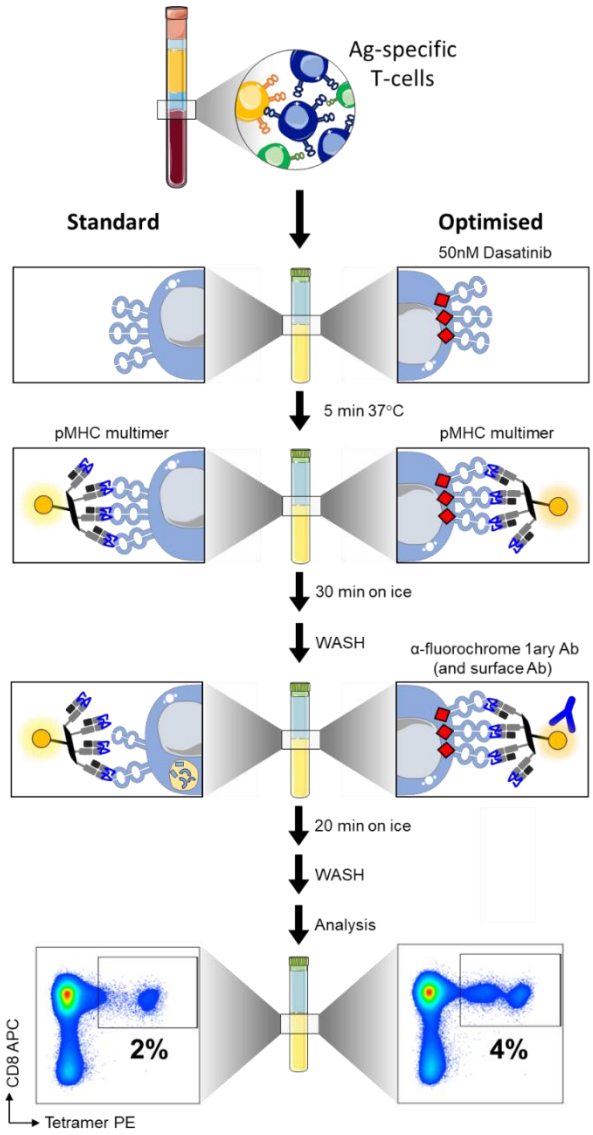

Figure 2-6. **Schematic representation of Standard and Optimised pMHC multimer staining.** Alongside the standard pMHC multimer staining, the Optimised protocol includes incubation with PKI to avoid TCR downregulation and binding of anti-PE unconjugated antibody to stabilise TCR-pMHC complex and prevent multimer off-rate.

2.4.3. TNF processing inhibitor-0 (TAPI-0) assay

Isolation of viable cytotoxic T cells based on the activation marker TNF was performed using a TAPI assay. TNF is produced by activated T cells within the first few hours of TCR engagement, primarily as a membrane-bound form that is subsequently cleaved by TNF-converting enzyme (TACE)[251]. Therefore, membrane-bound TNF can be captured by preventing of such cleavage using TNF processing inhibitor 0 (TAPI-0, TAPI hereon), thus allowing the labelling of the T cells from which it originated from.

Briefly, overnight rested T cells (usually 15,000 per condition) were co-incubated with or without target cells for 4h at 37°C at 1:2 ratio in R5 containing TAPI (Abcam), anti-TNF and anti-CD107a antibodies. After incubation, cells were washed 3X with PBS and stained with Vivid and surface antibodies as described in **section 2.4.1**.

2.5. Sequencing of human αβTCR repertoire

All the procedures involving RNA or DNA handling were conducted in the corresponding clean, nuclease-free space designated for work. Filtered tips and nuclease-free reagents were used throughout the procedures to ensure no degradation of the sample, and to decrease the chances of contamination. RNA samples were stored at -80°C, and DNA at +4°C for immediate use or at -20°C for long term. **Figure 2-7** provides a schematic representation of the experimental workflow. A more detailed description of procedures is described in the sections below. Of note, sequencing of T cell clones from culture was performed using "Bugs to Bases" protocol, which required DNA cloning into a vector and bacteria amplification (see **section 2.5.5**); whereas TCR profiling of heterogenous samples was performed by sequencing a PCR product on the Illumina Miseq platform (see **section 2.5.6**)

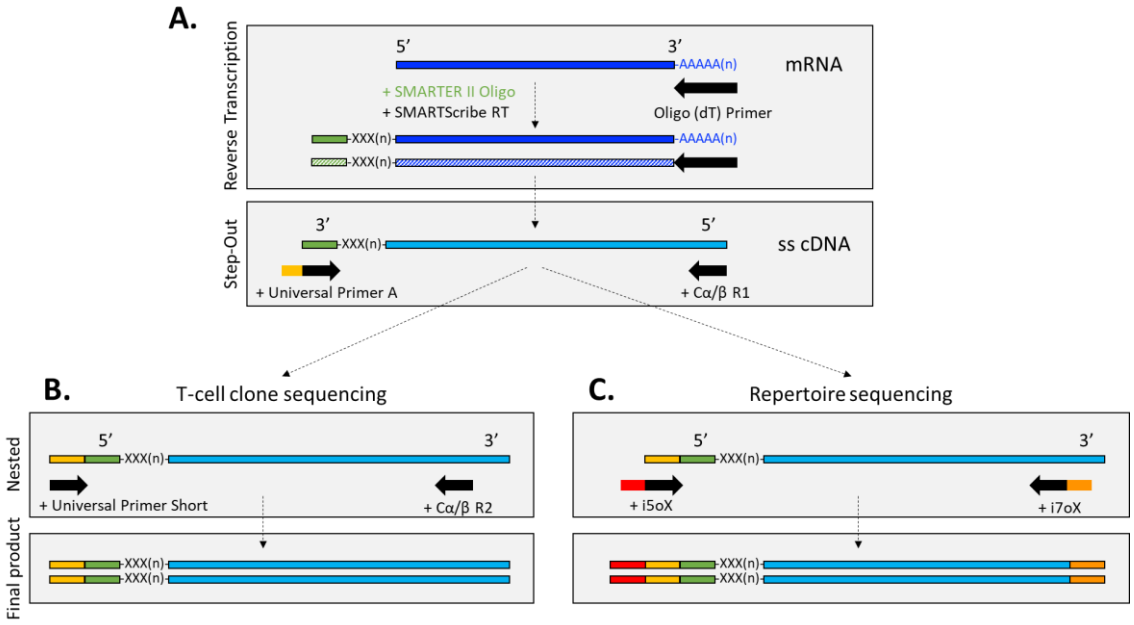

Figure 2-7. Schematic representation of TCR Sequencing workflow. **(A)** Complementary single stranded DNA (ss cDNA) was generated by reverse transcription using MMLV-derived reverse transcriptase (SMARTScribe RT) and an Oligo (dT) primer binding mRNA poly(A) tail. When reaching the end of the mRNA transcript, SMARTScribe adds non-template residues (indicated as "XXX(n)") to the cDNA strand, creating an annealing site for SMARTER II Oligonucleotide to perform a template switch. Generated cDNA molecules contain a universal anchor at the 5' end (in green) that allows subsequent PCR steps using a 5' Universal Primer and a 3' TCR chain specific primer (Step Out reaction) targeting the α or β chain Constant domain of the TCR. **(B)** For T cell clone sequencing, nested PCR was performed using internal 5' Universal Primer and 3' TCR chain specific, and final product cloned into a commercial vector, transformed into bacterial cells and sent for sequencing to *Eurofins Genomics*. **(C)** For Next Generation Sequencing (NGS) of TCR repertoires, a nested PCR was performed using the barcoded primers described in Table 2-9. Final product was sequenced using MiSeq Illumina platform.

2.5.1. Primers

Table 2-8. Primers used for TCR sequencing. Green: guanine ribonucleotide for template switch. Underlined: Anchor specific region.

Oligo	Step	Sequence (5' → 3')
Oligo-dT	cDNA	(T)n
Smarter II	cDNA	AAGCAGTGGTATCAACGCAGAGTACXXX(n)
CA-R1	Step Out	CTGTGCTAGACATGAGGTCTATGG
CB-R1	Step Out	GA GAC CCT CAG GCG GCT GCT C
Universal Primer A	Step Out	CTAATACGACTCACTATAGGGCAAGCAGTGGTATCAACGCAGAGT
CA-R2	Nested	GACAAGTCTGTCTGCCTATTCACC
CB-R2	Nested	TGT GGC CAG GCA CAC CAG TGT G
Universal Primer Short	Nested	CTAATACGACTCACTATAGGGC
CA-R3	Sequencing	CCTGCCGTGTACCAGCTGAGAG
CB-R3	Sequencing	TTC TGA TGG CTC AAA CAC AGC GAC

Table 2-9. Primers used for sample indexing of TCR Repertoires run in a MiSeq platform. Blue: Flow cell binding, Black: Barcode, Green: Sequencing Pad, Orange: Internal primer

Primer	(5' → 3')
i5o1	AATGATACGGCGACCACCGAGATCTACACTATAGCCTACACTCTTTCCCTACACGACGCTCTTCCGATCTCTAATACGACTCACTATAGGGC
i5o2	AATGATACGGCGACCACCGAGATCTACACATAGAGGCACACTCTTTCCCTACACGACGCTCTTCCGATCTCTAATACGACTCACTATAGGGC
i5o3	AATGATACGGCGACCACCGAGATCTACACCCTATCCTACACTCTTTCCCTACACGACGCTCTTCCGATCTCTAATACGACTCACTATAGGGC
i5o4	AATGATACGGCGACCACCGAGATCTACACGGCTCTGAACACTCTTTCCCTACACGACGCTCTTCCGATCTCTAATACGACTCACTATAGGGC
i5o5	AATGATACGGCGACCACCGAGATCTACACAGGCGAAGACACTCTTTCCCTACACGACGCTCTTCCGATCTCTAATACGACTCACTATAGGGC
i5o6	AATGATACGGCGACCACCGAGATCTACACTAATCTTAACACTCTTTCCCTACACGACGCTCTTCCGATCTCTAATACGACTCACTATAGGGC
i5o7	AATGATACGGCGACCACCGAGATCTACACCAGGACGTACACTCTTTCCCTACACGACGCTCTTCCGATCTCTAATACGACTCACTATAGGGC
i5o8	AATGATACGGCGACCACCGAGATCTACACGTACTGACACACTCTTTCCCTACACGACGCTCTTCCGATCTCTAATACGACTCACTATAGGGC
I7o1 α	CAAGCAGAAGACGGCATACGAGATCGAGTAATGTGACTGGAGTTCAGACGTGTGCTCTTCCGATCTCTCTCAGCTGGTACACGGCAGG
I7o2 α	CAAGCAGAAGACGGCATACGAGATTCCGGAGAGTGACTGGAGTTCAGACGTGTGCTCTTCCGATCTCTCTCAGCTGGTACACGGCAGG
I7o3 α	CAAGCAGAAGACGGCATACGAGATAATGAGCGGTGACTGGAGTTCAGACGTGTGCTCTTCCGATCTCTCTCAGCTGGTACACGGCAGG
I7o4 α	CAAGCAGAAGACGGCATACGAGATGGAATCTCGTGACTGGAGTTCAGACGTGTGCTCTTCCGATCTCTCTCAGCTGGTACACGGCAGG
I7o5 β	CAAGCAGAAGACGGCATACGAGATTTCTGAATGTGACTGGAGTTCAGACGTGTGCTCTTCCGATCTTTCTGATGGCTCAAACACAGCGAC
I7o6 β	CAAGCAGAAGACGGCATACGAGATACGAATTCGTGACTGGAGTTCAGACGTGTGCTCTTCCGATCTTTCTGATGGCTCAAACACAGCGAC
I7o7 β	CAAGCAGAAGACGGCATACGAGATAGCTTCAGGTGACTGGAGTTCAGACGTGTGCTCTTCCGATCTTTCTGATGGCTCAAACACAGCGAC
I7o8 β	CAAGCAGAAGACGGCATACGAGATGCGCATTAGTGACTGGAGTTCAGACGTGTGCTCTTCCGATCTTTCTGATGGCTCAAACACAGCGAC

2.5.2. Total RNA extraction

Total RNA from T cell clones and lines was extracted using the RNEasy Micro Plus Kit (Qiagen, Heidelberg, Germany) according to manufacturer's instructions. Briefly, $<0.5\times 10^6$ T cell clone pellet or Aria-sorted lines were resuspended in 350 µL of RLT Plus buffer supplemented with 20 mM DTT for lysis. Genomic DNA was eliminated using a gDNA Eliminator spin column, and 70% ethanol was added to the flow through at 1:1 ratio. RNA was then bound onto the RNEasy MinElute spin column, washed with the supplied buffers and eluted with 20 µL RNAse-free water. RNA was stored at -80ºC or used directly for cDNA synthesis.

2.5.3. SMARTerTM RACE cDNA amplification

Full length cDNA synthesis from whole cell RNA was performed using the 5' SMARTer™ (Switching Mechanism At 5' end of RNA Transcript) RACE (Rapid Amplification of cDNA Ends) kit (Clontech) according to manufacturer's instructions and as described in **Figure 2-7A.** Samples and reagents were kept on ice at all times. The following mix was prepared for each sample:

Reagent	Volume per reaction
RNA template	10 µL
Oligo dT Primer	1 µL
Final volume	**11 µL**

Reaction tubes were placed in the thermocycler and incubated 72°C for 3 min and 42°C for 2 min to allow synthesis primer annealing. The following mastermix was prepared for n reactions and 8 µL added to each tube:

Reagent	Volume per reaction
5X First Strand Buffer	4 µL
DTT (100 mM)	0.5 µL
dNTP (10 mM)	1 µL
RNAse Inhibitor (20U)	0.5 µL
SMARTScribe RT (100U)	2 µL
SMARTer II Oligo	1 µL
Final volume	**8 µL**

Reaction tubes were placed in the thermocycler and incubated 42°C for 90 minutes and 70°C for 10 min.

2.5.4. TCR specific chain amplification

PCR was designed to capture the whole variable region of TCR α or β chain using forward primers binding to 5' universal anchor-bound cDNA and chain-specific 3' primers targeting the constant domain of the TCR. This primer combination was chosen to allow unbiased amplification of all TCRs within the sample, regardless of their variable region. Used primers are listed in **Table 2-8** as indicated. No template controls (NTC) were set up alongside samples substituting DNA with water in order to test presence of contamination. PCR mastermix was prepared as follows:

Step-Out PCR

Reagent	Volume per reaction
5X Phusion® High Fidelity Buffer	10 µL
DMSO	0.5 µL
dNTP (20 mM)	1 µL
Chain specific primer (see **Table 2-8**)	1 µL
10X Universal Primer A	5 µL
Phusion® High Fidelity DNA polymerase	0.5 µL
Nuclease-free H_2O	29.5 µL
cDNA template	2.5 µL
Final volume	**50 µL**

Then, a nested PCR was performed using two sets of primers that anneal upstream of the sequence amplified by the first set of primers on the Step-Out PCR. Primer sequences are listed in **Table 2-8** for T cell clones sequenced by "Bugs to Bases" and **Table 2-9** for TCR repertoires sequenced by MiSeq Illumina, as indicated. In order to test presence of contaminations, no template controls (NTC) were set up alongside samples with the water control from the previous PCR. A mastermix was prepared as follows:

Nested PCR for T cell clones sequenced by Bugs to Bases

Reagent	Volume per reaction
5X Phusion® High Fidelity Buffer	10 µL
DMSO	0.5 µL
dNTP (20 mM)	1 µL
Chain specific primer (see **Table 2-8**)	1 µL
10X Universal Primer Short	1 µL
Phusion® High Fidelity DNA polymerase	0.5 µL
Nuclease-free H_2O	29.5 µL
Step-Out PCR template	2.5 µL
Final volume	**50 µL**

Nested PCR for T cell repertoires sequenced by MiSeq Illumina

Reagent	Volume per reaction
5X Phusion® High Fidelity Green Buffer	10 µL
DMSO	0.5 µL
dNTP (20 mM)	1 µL
i5o Gene specific primer (see **Table 2-9**)	1 µL
i7o Gene specific primer (see **Table 2-9**)	1 µL
Phusion® High Fidelity DNA polymerase	0.5 µL
Nuclease-free H_2O	29.5 µL
Step-Out PCR template	2.5 µL
Final volume	**50 µL**

Cycling conditions for specific primers are indicated below:

	Cα R1	Cβ R1	Cα R2	Cβ R2	I7o i5o	Time	
Initial denaturation	94	94	94	94	94	5 min	
Denaturation	94	94	94	94	94	30 s	30 cycles
Annealing	63	66	63	63	62	30 s	
Extension	72	72	72	72	72	45 s	
Final extension	72	72	72	72	72	5 min	

PCR products were run in 1% agarose gel prepared from UltraPure™ agarose powder (ThermoFisher) dissolved in 1X TAE buffer. Midori Green nucleic acid dye (GeneFlow) was added (1:100) to the gel before solidifying. 5 µL of 1kb DNA HyperLadder™ (Bioline) was run in parallel to samples for 45 min at 80 V and then visualised under a LED illuminator (FastGene) to facilitate cutting out the DNA bands using a disposable scalpel and without the risk of UV-induced DNA damage. A representative gel for TCR clonotyping is shown in **Figure 2-8**. DNA was purified from the agarose slices using the NucleoSpin® Gel and PCR Clean-up Kit (Clontech), following manufacturer's instructions. Pure DNA was eluted in 20 µL 0.5 M Tris-Cl (pH 8.5) buffer and stored -20°C.

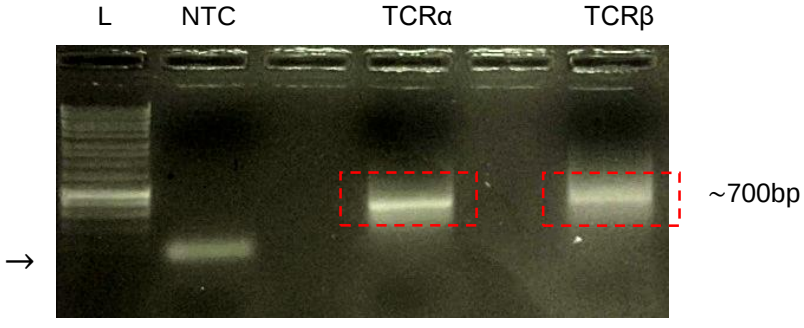

Figure 2-8. **Representative agarose gel electrophoresis of PCR amplified products for αβTCR clonotyping.** Nested PCR products were run in a 1% agarose gel, visualised and cut out of the gel for purification. Empty lanes were kept between samples to avoid sample cross-contamination during loading. Water was used as negative control (NTC). Downstream sequencing was only performed when NTC was clear. Arrow indicates primer annealing in the water control. **L** – 1kb DNA ladder, **NTC** – No Template Control, **TCRα** – representative α chain, **TCRβ** – representative β chain at the expected size of approximately 700bp.

2.5.5. Molecular cloning and bacterial transformation of T cell clones

PCR products were cloned into a vector using topoisomerase-based Zero Blunt® TOPO PCR Cloning kit (Invitrogen) following manufacturer's instructions. Briefly, 1 µL PCR™ Blunt II-TOPO vector and 5 µL purified PCR product were combined in the presence of 1 µL Salt Solution, followed by 5 min incubation at room temperature to allow insertion of blunt-ended PCR products into the plasmid vector containing a cassette for Kanamycin selection.

OneShot™ TOP10 Chemically Competent *E. coli* cells (Invitrogen) were transformed with ligation mixture following manufacturer's instructions. Briefly, 6 µL ligation was incubated with 50 µL TOP10 cells and incubated on ice for 30 min, heath-shocked for 30 s at 42°C, and placed back on ice. 250 µL of pre-warmed Super Optimal Broth (SOC, Clontech) was added to cells and incubated for 1 h at 37°C in the orbital shaker (220rpm) to allow cell recovery. Next, 150 µL from each transformation was plated on LB-agar plates containing 50µg/mL Kanamycin and incubated overnight at 37°C. Growing colonies were screened for insert-presence by colony PCR **(Figure 2-9**). The following mastermix was prepared for n reactions:

Reagent	**Volume per reaction**
M13 Forward (TGT AAA ACG ACG GCC AGT)	1 µL
M13 Reverse (CAG GAA ACA GCT TG ACC)	1 µL
DreamTaq 2X MasterMix	12.5 µL
H_2O	10.5 µL
Bacterial colony on sterile p10 tip	1 colony
Final volume	**25 µL**

The following cycling programme was used:

	Temperature	Time	
Initial denaturation	94°C	10 min	
Denaturation	94°C	20 s	30 cycles
Annealing	57°C	20 s	
Extension	72°C	45 s	
Final extension	72°C	5 min	

25 µL reactions were run in a 1% agarose gel as described before (see **section 2.5.4**). Colonies containing the right sized inserts were selected for sequencing (**Figure 2-9**). At least 8 insert-containing colonies per sample were sequenced using the PlateSeq Kit Clone service (Eurofins Genomics) and Cα-R3 or Cβ-R3 primers (see **Table 2-8**). Results were analysed using IMGT/V-QUEST software.

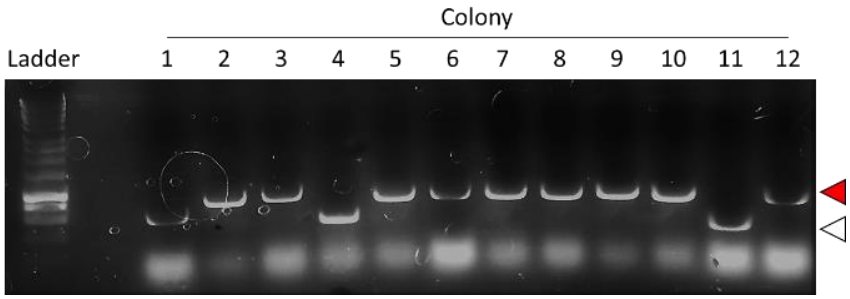

Figure 2-9 **Colony PCR run in a 1% agarose gel.** Colonies containing the right size insert are indicated with a **red** arrow (◀). Colonies that have incorporated an empty vector are indicated with a **white** arrow (◁).

2.5.6. Next Generation Illumina Sequencing of T cell repertoires

2.5.6.1. Library preparation

PCR products amplified with primers listed in **Table 2-9** already contained Illumina adaptors and sample specific barcodes, thus did not required further preparation. Libraries were diluted to 4 nM and pulled together for denaturalisation following the manufacturer's instructions. Briefly, 5 µL 4 nM library was incubated with 5 µL 0.2M NaOH for 5 minutes, followed by dilution with HT1 buffer to obtain a 10 pM denatured library. PhiX at 10 pM was spiked at 8% as internal sequencing control as suggested by manufacturer. Libraries were multiplexed and run on Illumina Miseq using MiSeq v2 kit (Illumina), with 2×250 bp paired end reads.

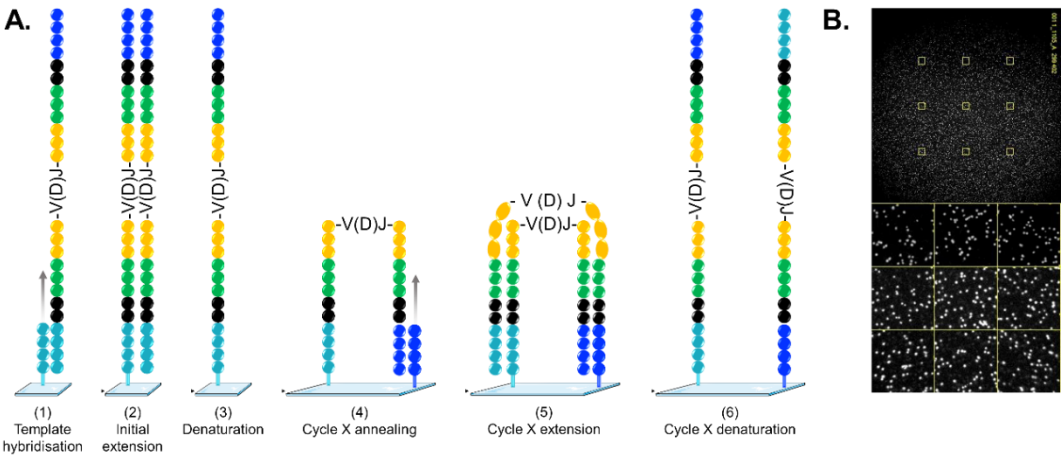

Figure 2-10. **Generation of clusters by bridge amplification in Illumina MiSeq. (A)** Flow cell is coated with adapter sequences that bind the denatured template DNA. Bound libraries are extended to form a double-stranded DNA molecule, followed by denaturation and removal of the original template. After this process, the newly synthesised DNA strand was covalently attached to the flow cell surface. Next, this DNA strand formed a bridge by hybridising to an adjacent complementary adapter oligo on the flow cell, followed by polymerase extension (bridge amplification). The double-stranded bridge was then denatured to generate two copies of covalently bound single-stranded molecules. The bridge amplification cycle was repeated multiple times. Primers used: Blue: Flow cell binding sequence, **Black**: Barcode, Green: Sequencing Pad, Orange: Internal primer. **(B)** Representative image of a cluster of clonally amplified DNA fragments from a successful MiSeq run.

2.5.6.1. Figures and Data analysis

TCR gene usage was determined using reference sequences from the ImMunoGenetics (IMGT) database (www.imgt.org) and all TCR gene segments were designated according to the IMGT nomenclature using MiXCR software (v1.8.1). Data was filtered according to our quality requirements: low quality reads, and TCRs present at <5 reads (for PBMC analysis) were not included in the analysis. The web-based graphical interface application VDJviz (https://vdjviz.cdr3.net/)[252] was used to visualise the results of MiXCR processed TCR data. The V-J chord diagram function was used to represent Variable and Joining gene usage combinations of the analysed clonotype set. Each arc represents a scaled V or J segment to the relative number of reads. Public clonotypes were annotated according to the web-based application VDJdb.CDR3 (https://vdjdb.cdr3.net/search)[253].

2.6. Western Blot protein analysis

2.6.1. Reagents and Buffers

Cells and reagents were kept on ice at all times during the course of the protocol. All buffers were stored at 4°C for a maximum of one week. Ponceau-S stain was stored at room temperature.

Table 2-10. Buffers and reagents used in western blot analysis.

Reagent	Composition
RIPA Lysis Buffer	150 mM NaCl, 5 mM EDTA (pH 8.0), 50 mM Tris (pH 8.0), 1% NP-40, 0.5% v/v sodium deoxycholate, 0.1% v/v SDS.
Transfer Buffer	192 mM Glycine, 25 mM Tris, 0.25% SDS, 20% CH_3OH
Ponceau-S stain	0.1% Ponceau-S, 5% v/v acetic acid
Membrane Wash Buffer (PBS-T)	PBS 1X supplemented with 0.1% Tween
Blocking Buffer	PBS-T supplemented with 5% non-fat milk

2.6.2. Sample preparation

Tumour cells were harvested from culture as previously described (see **section 2.2.1**) and washed twice in dPBS to remove any proteins from the supernatant. Up to 10^6 cells were resuspended in 50 µL RIPA buffer supplemented with 0.1 µL 100X Halt protease phosphatase inhibitor cocktail, followed by 30 min incubation on ice. To ensure complete membrane disruption, cells were sonicated at 50% amplitude (Branson Digital Sonifier) three times for 20 s with 1 min rest on ice between each pulse. Lysate was then centrifuged at 13,000rpm in a benchtop microcentrifuge (Eppendorf™) for 30 min at 4°C and protein-containing supernatant was collected and transferred to a pre-chilled tube. Protein concentration was measured using a spectrophotometer (NanoPhotometer®, Geneflow) at 280 nm wavelength.

2.6.1. Gel electrophoresis

50 µg of protein was pre-mixed with reducing loading buffer (10% DTT) and incubated at 90°C for 5 min before loading onto a pre-cast 10% Bis/Tris gel (NuPAGE,nvitrogen) with 1X running buffer (NuPAGE, Invitrogen). BLU Wide Range (10 to 245kDa) protein ladder (Geneflow Ltd) was used as a band size (kDa) reference. Gels were run at 90V for 90 min. To prevent excessive heating, gels were run on blocks of ice.

2.6.2. Semi-dry Western Blot transfer

Proteins from the gel were electro-transferred to a polyvinylidene difluoride (PVDF) membrane (Invitrolon™, ThermoFisher Scientific) at 10V for 30 min, according to manufacturer's instructions. PVDF was previously activated with 100% methanol for 1 min, followed by a 1 min wash in ddH_2O, then equilibrated for 15 min with transfer buffer together with blotting filter papers and the SDS-page gel. After transfer, the protein-containing membrane was stained with Ponceau-S for 5 min to confirm successful transfer through the visualisation of whole lysate proteins, and then de-stained with ddH_2O for 10 min followed by three washes with PBS-T.

2.6.3. Membrane preparation and antibody staining

The PVDF membrane was blocked for 1 h at room temperature (or overnight at 4°C) with blocking buffer and continuous rotation. Following three washes of 5 min each with PBS-T in continuous rotation, blocked membrane was incubated with IMP-2 (ab124930, Abcam) primary antibody (1:2000 dilution in blocking buffer) for 1 h at room temperature (or overnight at 4°C). The membrane was then washed for 5 min three times with PBS-T and continuous rotation, followed by 1 h incubation with HRP-conjugated secondary goat anti-rabbit IgG antibody (ab205718, Abcam) (1:20,000 dilution in blocking buffer) at room temperature. The membrane was washed three times with PBS-T (5 minutes each wash) and continuous rotation before development. Pierce™ ECL Plus Western Blotting Substrate kit (#32132, Thermofisher) was used for signal development, according to manufacturer's protocol. After 5 min incubation, detection was performed using CCD-based imager (MyECL imager, ThermoFisher Scientific) with 10 min exposure time. β-Actin (1:50,000 dilution, ab8227 Abcam) staining was performed as a positive loading control at the end.

2.7. Lentiviral transduction of human cells

All the procedures involving lentiviral handling were conducted in the designated space for work. Filtered tips were used throughout the procedures to ensure no contamination of materials and minimise risk of exposure. Lentivirus supernatants were stored double-contained at -80°C in 1 mL aliquots.

The naturally HLA A2^{neg} tumours and LCL lines used throughout this thesis were transduced with the 3rd generation lentivirus *pELNS* in order to attain permanent expression of HLA A*02:01. The human-derived lymphoblastoid line MOLT3 was transduced with 3rd generation lentivirus in order to attain permanent expression of Melan-A, BST2 and IMP-2 proteins, and/or HLA-A 02:01. Permanent expression of collagen was used as negative control. The melanoma tumour line MM909.24 was transduced with the 2nd generation lentivirus *pLentiCRISPRv2* to silence the expression of the *MLANA* gene. A workflow overview is represented in **Figure 2-11** and described in more detail in the sections below.

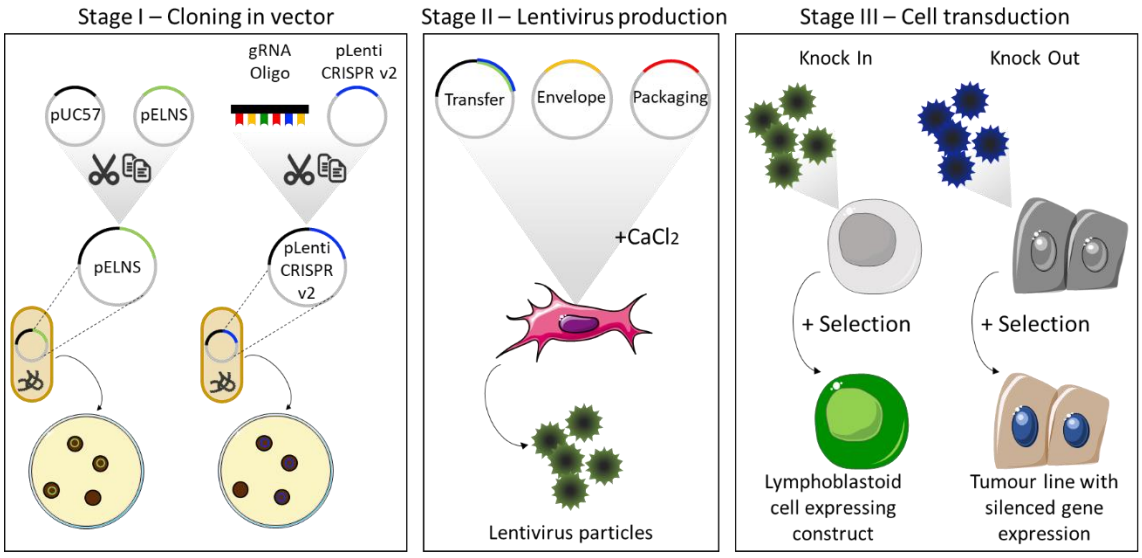

Figure 2-11. Workflow for stable artificial expression of genes in human cells. Constructs for gene expression or silencing were cloned into the corresponding plasmid vector by enzymatic digestion and ligation, and then transformed into chemically competent bacteria under antibiotic selection. Growing colonies were screened by sequencing and insert-containing bacteria used for escalated production of insert-containing plasmids. Purified transfer plasmids were used to co-transfect HEK-293T with envelope and packaging plasmids required for lentiviral production. After 16 h media was replaced, and at time points 48 h and 72 h post-transduction, lentivirus-containing supernatant was collected, concentrated and used for infection of target cells.

2.7.1. Vectors used for lentivirus production

Gene expression (Knock In) was performed by cloning of codon-optimised mRNA transgene (see **section 2.7.2.1**) of interest into the 3rd generation transfer plasmid pELNS[254] (kindly provided by Dr. James Riley, University of Pennsylvania, PA) using XbaI and XhoI restriction sites (**Figure 2-12A**). Downstream from the transgene cloning site, vector contains a self-cleaving 2A sequence and a rCD2 marker gene flanked by XhoI and SalI restriction sites to facilitate removal from construct.

Genes to be knocked out were targeted by cloning a gRNA-template oligonucleotide into the 2nd generation lentiviral vector pLentiCRISPR v2[255] (kindly provided by Dr. Feng Zhang) (**Figure 2-12B**)**.** gRNA oligonucleotides were cloned downstream of the U6 RNA polymerase III promoter using the Esp3I restriction site. Vector contains *Streptococcus puogenes* Cas9 gene downstream of the Elongation Factor Short promoter, linked via a 2A self-cleaving sequence to the Puromycin N-acetyltransferase gene conferring Puromycin antibiotic resistance.

Table 2-11. Plasmids used for production of 2nd and 3rd generation lentiviruses.

Purpose	Plasmid name	Plasmid Purpose	Provider
Knock In	pELNS	Transfer plasmid	Dr. James Riley (UPen)
Knock In	pMD2.G	Envelope plasmid	Addgene (plasmid #12259)
Knock In	pMDLg/pRRE	Packaging plasmid	Addgene (plasmid #12251)
Knock In	pRSV-Rev	Packaging plasmid	Addgene (plasmid #12253)
Knock Out	pLentiCRISPR v2	Transfer plasmid	Addgene (plasmid #52961)
Knock Out	pMD2.G	Envelope plasmid	Addgene (plasmid #12259)
Knock Out	psPAX2	Packaging plasmid	Addgene (plasmid #12260)

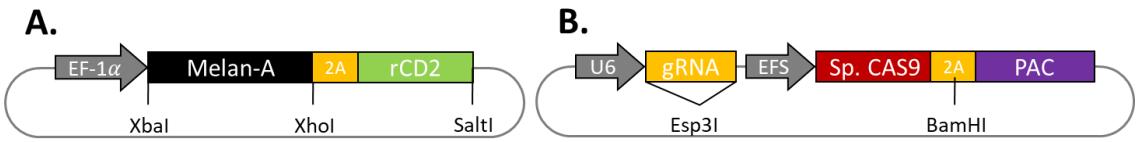

Figure 2-12. **Schematic representation of lentiviral transfer plasmids pELNS (A) and pLentiCRISPR v2 (B).** Promoters are indicated with arrows and transgenes with bars. Restriction sites used for cloning are marked with the name of the restriction enzyme. 2A self-cleaving peptide; EF-1α elongation factor 1α; EFS – short elongation factor; PAC – puromycin N-acetyltransferase.

2.7.2. Expression of gene inserts into pELNS vector

2.7.2.1. Sequences for expression

Nucleotide sequences from genes to be expressed were ordered from Genewiz. Constructs were optimised for *H. sapiens* expression, with *Xba I* and *Xho I* restriction enzyme sequences at the 5' and 3' ends, respectively, and a Kozak sequence to enhance protein translation from the correct start codon[256]. Sequences can be found in **Supplementary figure 1**. The following sequences correspond to the translated DNA for the proteins of interest. Antigenic peptide sequence is indicated in **bold** and coloured according to the colour-code used throughout this thesis. Aminoacid region from IMP-2 isoform 1 region missing in isoform 2 is underlined.

Melan-A/MART1 (UniProtKB code: Q16655)

MPREDAHFIYGYPKKGHGHSYTTAE**EAAGIGILTV**ILGVLLLIGCWYCRRRNGYRALMDKSLHVGTQCALT
RRCPQEGFDHRDSKVSLQEKNCEPVVPNAPPAYEKLSAEQSPPPYSP

BST2/CD317/Tetherin (UniProtKB code: Q10589)

MASTSYDYCRVPMEDGDKRCK**LLLGIGILVL**LIIVILGVPLIIFTIKANSEACRDGLRAVMECRNVTHLLQQEL
TEAQKGFQDVEAQAATCNHTVMALMASLDAEKAQGQKKVEELEGEITTLNHKLQDASAEVERLRRENQV
LSVRIADKKYYPSSQDSSSAAAPQLLIVLLGLSALLQ

IF2B2/IMP-2/VICKZ isoform 1 (UniProtKB code: Q9Y6M1-2)

MMNKLYIGNLSPAVTADDLRQLFGDRKLPLAGQVLLKSGYAFVDYPDQNWAIRAIETLSGKVELHGKIMEV
DYSVSKKLRSRKIQIRNIPPHLQWEVLDGLLAQYGTVENVEQVNTDTETAVVNVTYATREEAKIAMEKLSG
HQFENYSFKISYIPDEEVSSPSPPQRAQRGDHSSREQGHAPGGTSQARQIDFPLRILVPTQFVGAIIGKEGL
TIKNITKQTQSRVDIHRKENSGAAEKPVTIHATPEGTSEACRMILEIMQKEADETKLAEEIPLKILAHNGLVGR
LIGKEGRNLKKIEHETGTKITISSLQDLSIYNPERTITVKGTVEACASAEIEIMKKLREAFENDMLAVNQQANLI
PGL**NLSALGIFST**GLSVLSPPAGPRGAPPAAPYHPFTTHSGYFSSLYPHHQFGPFPHHHSYPEQEIVNLFI
PTQAVGAIIGKKGAHIKQLARFAGASIKIAPAEGPDVSERMVIITGPPEAQFKAQGRIFGKLKEENFFNPKEE
VKLEAHIRVPSSTAGRVIGKGGKTVNELQNLTSAEVIVPRDQTPDENEEVIVRIIGHFFASQTAQRKIREIVQ
QVKQQEQKYPQGVASQRSK

HLA A2*02:01 (UniProtKB code: P01892)

MAVMAPRTLVLLLSGALALTQTWAGSHSMRYFFTSVSRPGRGEPRFIAVGYVDDTQFVRFDSDAASQRM
EPRAPWIEQEGPEYWDGETRKVKAHSQTHRVDLGTLRGYYNQSEAGSHTVQRMYGCDVGSDWRFLRG
YHQYAYDGKDYIALKEDLRSWTAADMAAQTTKHKWEAAHVAEQLRAYLEGTCVEWLRRYLENGKETLQR
TDAPKTHMTHHAVSDHEATLRCWALSFYPAEITLTWQRDGEDQTQDTELVETRPAGDGTFQKWAAVVVP
SGQEQRYTCHVQHEGLPKPLTLRWEPSSQPTIPIVGIIAGLVLFGAVITGAVVAAVMWRRKSSDRKGGSYS
QAASSDSAQGSDVSLTACKV

2.7.2.2. Primers

Table 2-12. Sequences of primers used for PCR and molecular cloning.

Primer name	Sequence (5' → 3')	Application
pELNS F1	GAGTTTGGTVTTGGTTCATTC	. pELNS Colony PCR and pELNS sequencing
pELNS R3	AGAAACTTGCACCGCATATG	pELNS Colony PCR
GeCKO F1	AATGGACTATCTATGCTTACCGTAACT TGAAAGTATTTG	pLentiCRISPR PCR

2.7.2.3. Molecular cloning

Codon optimised inserts for *H. sapiens* expression of antigenic proteins were purchased from GeneArt (ThermoFisher) and delivered in the pUC57 vector backbone, flanked by XbaI and XhoI restriction sites. For cloning of inserts into pELNS vector, both vectors were digested for 1 h at 37°C as indicated below, loaded alongside the 1kb ladder onto a 1% agarose gel and run at 80V for 1 h.

Reagent	Amount
Plasmid DNA (pUC57 or pELNS)	1 µg
10x FastDigest buffer (Thermo Scientific)	2 µl
XbaI (FastDigest, Thermo Scientific)	1 µl
XhoI (FastDigest, Thermo Scientific)	1 µl
Nuclease-free H_2O	to 20 µl

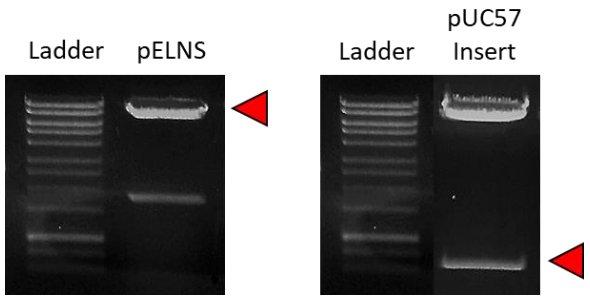

Figure 2-13. Representative agarose gel electrophoresis after XbaI and XhoI enzyme digestion of lentiviral transfer pELNS plasmid and insert-containing pUC57 plasmid. Digested products were run in a 1% agarose gel, visualised and corresponding ~9kb band from pELNS backbone and corresponding band size from insert (Melan-A, ~400bp) were cut out of the gel for purification and ligation (red arrows).

Digested DNA was extracted using Wizard® SV Gel and PCR Clean-up System (Promega), according to manufacturer's instructions. The DNA was eluted in 20 µL nuclease-free water and the concentration of DNA was measured using the NanoDrop™ device (Thermo Scientific). The molar concentration of DNA was calculated according to the following formula:

$$^{ng}/_{\mu l}\ DNA \times \frac{fmol}{660\ fg} \times \frac{10^6 fg}{1\ ng} \times \frac{1}{N} = {}^{fmol}/_{\mu l}\ DNA,$$

where 660 $^{fg}/_{fmol}$ is an average molecular weight of a nucleotide pair, and N is the number of nucleotides. Ligation of insert to pELNS backbone was performed at room temperature for 2 hours as indicated below. As negative control, water was used to substitute insert:

Reagent	**Amount**
pELNS VECTOR	30 fmol *
Insert	150 fmol *
10x T4 DNA Ligase buffer (Thermo Scientific)	2 µL
T4 ligase (Thermo Scientific)	1 µL
Nuclease-free H_2O	to 20 µL

** Combined volumes must never exceed 50% of total reaction volume*

5 µL of ligation reaction was transformed as previously described (see **section 2.5.5**) into 50 µL recombination-deficient XL10-Gold® cells (Agilent Technologies), and grown on Ampicillin-containing (100 µg/mL) LB agar plates at 37°C overnight. Bacterial colonies were screened for the presence of insert by colony PCR. The following mastermix was prepared for n reactions:

Reagent	**Volume per reaction**
pELNS F1 (10µM)	1 µL
pELNS R3 (10µM)	1 µL
GreenTaq 2X MasterMix	12.5 µL
Nuclease-free H_2O	10.5 µL
Bacterial colony on sterile p10 tip	1 colony
Final volume	**25 µL**

The following cycling programme was used:

	Temperature	Time	
Initial denaturation	94°C	10 min	
Denaturation	94°C	20 s	30 cycles
Annealing	60°C	20 s	
Extension	72°C	2 min	
Final extension	72°C	5 min	

PCR reactions were run in a 1% agarose gel as described before (see **section 2.5.5**). Colonies containing an insert were transferred to 5 mL LB media supplemented with 100 µg/ml carbenicillin and grown overnight at 37°C, 220 rpm. Plasmid DNA was then extracted using the PureLink® Quick Miniprep Kit (Invitrogen) following manufacturer's instructions, and sequenced using the Mix2Seq service (Eurofins Genomics). Sequences were confirmed by alignment reference sequence using ApE tool (A plasmid Editor, M. Wayne Davis).

2.7.2.4. Maxiprep

XL10-Gold® colonies containing the verified inserts were used to inoculate 250 mL LB medium supplemented with 100 µg/mL ampicillin, and grown overnight at 37°C, 220 rpm. Bacterial cultures were centrifuged at 4,000 × g for 10 minutes to pellet the cells, and then resuspended in R3 buffer containing RNAse A (PureLink® HiPure Plasmid Filter Maxiprep Kit, Invitrogen). Cells were lysed using the pre-warmed L7 buffer, followed by neutralisation with N4 buffer and transfer to an equilibrated HiPure Filter Column. The column was washed with W8 buffer and the flow through drained by gravity flow. The column-bound plasmid was then eluted into a clean falcon containing isopropanol followed by centrifugation at 4,000 × g for 1h at 4°C. Supernatant was carefully removed and precipitated pellet was washed three times with 70% ethanol. Supernatant was discarded and the purified plasmid pellet was air-dried, resuspended in TE buffer and stored at -20°C after confirmation of correct sequence presence by Sanger sequencing using pELNS F1 primer. DNA concentration was measured using a Nanodrop ND100 (Thermo Scientific).

2.7.3. Gene Knock-Out using CRISPR-CAS9 system

Gene silencing was initially accomplished by cloning of gRNAs into 2nd generation lentiviral transfer vector pLentiCRISPR v2, followed by co-transfection with pMD2.G (envelope) and psPAX2 (packaging) plasmids into HEK 293-T cells to generate lentiviral particles that were later used to infect target cell lines. Further down the line, we published a CRISPR/Cas9 NEON Transfection System[240] to perform genomic engineering of the CRISPR/Cas9 system into multiple cell lines, including primary human T cells. This section describes the procedures for both gene silencing methodologies employed in this thesis.

2.7.3.1. Molecular cloning of oligonucleotides into pLentiCRISPR v2 vector

gRNA sequences consisted of 20 nucleotides (without PAM) targeting the gene of interest. gRNA sequences for *MLANA* gene were designed by Dr. Angharad Lloyd using crispr.mit.edu webtool. Sequences were ordered as a pair of oligonucleotides (Eurofins Genomics) containing Esp3I-compatible ends (in **blue**) as shown below.

Oligo Fw	5’	-	**CACCG**NNNNNNNNNNNNNNNNNNN	-	3’
Oligo Rv	3’	-	CNNNNNNNNNNNNNNNNNNN**CAAA**	-	5’

Where N in Fw oligo indicates nucleotides identical to target sequence without PAM, and N in Rv oligo indicate complementary to nucleotides from Fw oligo.

The following gRNAs targeting *MLANA* gene (Melan-A) were tested:

Table 2-13. gRNAs used to target MLANA gene. Esp3I sequence is indicated in blue

Name	Target exon	Guide sequence (5' → 3')
MLANA_g1	1	**CACCG**GCACGGCCACTCTTACACCA**GTTTT**
MLANA_g2	1	**CACCG**CATCTATGGTTACCCCAAGA**GTTTT**
MLANA_g3	1	**CACCG**GAAGATGCTCACTTCATCTA**GTTTT**
MLANA_g4	1	**CACCG**TCTTACTGCTCATCGGCTGT**GTTTT**

The oligo pair was phosphorylated at 37°C for 30 min, followed by annealing at 95°C for 5 min and ramp down to 25°C at 5°C/min as described below:

Reagent	Volume
Forward oligo (100 µM)	1 µL
Reverse oligo (100 µM)	1 µL
10x T4 ligation buffer (New England Biolabs)	1 µL
T4 polynucleotide kinase (New England Biolabs)	0.5 µL
Nuclease-free H_2O	6.5 µL
Final Volume	10 µL

Transfer vector (pLentiCRISPR v2) was digested and dephosphorylated for 1 h at 37°C as described below:

Reagent	Volume
pLentiCRISPR v2 vector	5 µg
10x FastDigest Buffer (Thermo Scientific)	6 µL
FastDigest Esp3I (Thermo Scientific)	3 µL
FastAP (Thermo Scientific)	3 µL
100 mM DTT	0.6 µL
Nuclease-free H_2O	To 60 µL

The digested plasmid was run on 1% agarose gel, and the band of the corresponding size extracted as described in **Section 2.5.4.** Ligation of the digested plasmid with the inserts was performed for 30 min at room temperature by combining the following reagents:

Reagent	Volume
Digested vector	50 µg
Annealed oligo pair (diluted 1:200)	1 µL
2x Quick Ligase Buffer (New England Biolabs)	5 µL
Quick Ligase	1 µL
Nuclease-free H_2O	To 10 µL

The ligation was then transformed into XL10-Gold® bacteria as described in **Section 2.5.5.** Representative colonies were grown overnight in 5 ml LB media containing 100 µg/mL ampicillin, followed by plasmid purification (PureLink® Quick Miniprep Kit) and sequencing using GeCKO F1 primer (Genewiz). XL10-Gold® colonies containing the verified inserts were used to inoculate 250 mL bacteria cultures and plasmid DNA was extracted using the PureLink® HiPure Plasmid Filter Maxiprep Kit (Invitrogen), as described in **Section 2.7.2.4**.

2.7.4. Lentivirus production

Prior to transfection, $2x10^7$ 293T cells were plated in in a T175 flask in 50 mL transfection medium and incubated until 80% confluent. The following media was prepared and 0.2 µm filtered:

Media	**Composition**
Transfection media (TFM)	DMEM (Life Technologies), 100U/mL Penicillin, 100 µg/mL Streptomycin, 2 mM L-Glutamine, 10% FBS
pH 7.1 medium	DMEM, 25 mL HEPES, pH 7.1
pH 7.9	TFM, 25 mL HEPES, pH 7.9

2nd and 3rd generation lentivirus particles were produced by co-transfection of packaging, envelope and transfer plasmids into HEK 293T cell line. The 2nd generation lentiviral transfer plasmid pLentiCRISPR v2 (12 µg) bearing the corresponding gRNA described in **section 2.7.3.1** was co-transfected with packaging plasmid psPAX2 (10 µg) and envelope plasmid pMD2.G (8 µg). The 3rd generation lentiviral transfer plasmid pELNS (15 µg) carrying the corresponding inserts described in **section 2.7.2.1** was co-transfected with packaging plasmids pRSV-Rev (18 µg) and pMDLg/pRRE (18 µg), and envelope plasmid pMD2.G (7 µg). Co-transfections were performed in pH 7.1 medium in a 15 mL tube. 150 µL of 1 M $CaCl_2$ solution was added to the DNA transfection mix, and then incubated at room temperature for 30 min to allow precipitates to form. The mix was then briefly vortexed and added dropwise to the flask. Transfected 293T cells were incubated overnight and supernatant was replaced 16 hours' post transduction and collected after 48 and 72 hours' incubations, kept at 4°C and filtered through a 0.45 µm filter. The 48 h and 72 h lentivirus particle collections were concentrated as a pool by ultracentrifugation at 140,000xg for 2 h at 4°C (Optima™ L-100 XP with SW28 rotor, Beckman Coulter). After centrifugation, the medium was discarded and the lentiviral pellet was resuspended in 20 mL R10, aliquoted in 1 mL vials and stored at -80°C.

2.7.5. Lentiviral transduction of immortalised cell lines

For adherent cultures, cells were plated a day pre-transduction at 60-80% confluency in a 24-well plate. For suspension cultures, cells were plated at a density of 100,000 cells/well in a 24-well plate on the day of transduction. Cells were transduced with 1 mL of the concentrated lentivirus suspension expressing the sequences described on **section 2.7.2.1** and **2.7.3.1**, then subjected to spinfection at 500xg for 2 hours and incubated at 37°C overnight with 8 µL/mL polybrene. The lentivirus-containing supernatant was replaced with fresh medium 24 h post-transduction, and cells were tested for transgene or marker gene expression 72 h post-transduction.

2.7.5.1. Purification of transduced cell lines

Magnetic bead sorting was used to isolate cell lines positively transduced with a gene of interest. For the expression of a gene co-expressed with rCD2 marker cells were subjected to positive selection based on rCD2 expression following manufacturer´s instructions. In brief, cells were stained with the fluorochrome-conjugated primary antibody of choice for 20 min on ice, washed in pre-chilled MACS buffer as previously described (see **section 2.3.9**), co-incubated with anti-fluorochrome MicroBeads (Miltenyi Biotec) and run through a MACS MS-column. Flow-through was collected and cells were plated at the right density with the appropriate media.

Aria sort or negative magnetic bead sorting was used to isolate cell lines with loss-of-expression (Knock Out) of target through CRISPR/Cas9 transduction, followed by single-cell cloning. Growing clones were validated by antibody staining or Western blot, and efficiently knock out clones pulled as a line to prevent loss of cell heterogeneity derived from single-cell cloning.

2.8. Gene silencing using CRISPR/Cas9 NEON Transfection System

Disruption of target genes in **Table 2-14** was performed by electroporation (Neon® Transfection Device, Life Technologies) of Cas9 protein complexed with an *in vitro* transcribed gRNA according to manufacturer's instructions (GeneArt Precision gRNA Synthesis Kit, Thermo Fisher). gRNA sequences targeting genes of interest were designed using http://guides.sanjanalab.org/#/ webtool[257].

Table 2-14. gRNA sequences for target genes used for gene knockout. gRNA templates were ordered as DNA oligonucleotides and transcribed in vitro.

Target gene	Exon	Guide sequence (5' → 3')	PAM sequence
BST2	4	GGTCTTAAGCGTGAGAATCG	CGG
BST2	2	CCAAGGACAAAAGAAAGTGG	AGG
IMP-2	12	TTGTGTGCCAAGATTTTCAG	AGG
IMP-2	16	GAATCTCTTCATCCCAACCC	AGG

Fusion of the gRNA, or short complementary RNA (crRNA), to guide the Cas9 nuclease to the specified target gene, and a trans-activating crRNA (tracrRNA) necessary for crRNA processing, have been shown to facilitate Cas9-mediated DNA cleavage[258,259]. Fused together they formed the gRNAs described in **Table 2-14**.

Annealing of the crRNAs with tracrRNA was performed as follows:

Reagent	Volume
crRNA (100μM)	10 μL
tracrRNA (100μM)	10 μL
5X Annealing Buffer	10 μL
Nuclease-free H_2O	To 50 μL

The following annealing programme was used:

95ºC	5 minutes
95ºC to 78ºC	-2ºC / second ramp rate
78ºC	10 minutes
78ºC to 25ºC	-0.1ºC / second ramp rate
25ºC	5 minutes
4ºC	∞

For 1.2×10^5 cells, 7.5 pmol of annealed crRNA:tracrRNA duplex was combined with 1.25ng recombinant Cas9 protein (GeneArt Platinum Cas9 Nuclease) in 10 μL and incubated at room temperature for 10 minutes prior to electroporation into pre-washed cells. Electroporation parameters variated with each cell line, and they are described in **Table 2-15**. Electroporated cells were plated into pre-warmed, antibiotic free medium, and the knockout efficiency was determined after 7 days by flow cytometry.

Table 2-15. Neon parameters. Optimisation of Neon electroporation parameters was performed to achieved the best yield of surviving gRNA-transfected cells possible.

Cell line	Pulse (V)	Ms	number
MM909.24	1,200	10	3
C1R	1,300	30	1
MDA-MB-231	1,400	10	4

– Chapter 3 –

Optimised pMHC multimer staining for the identification of low affinity TCR-pMHC interactions

3.1. Introduction

As reviewed in **Chapter 1**, the TCR repertoire encompasses the ability to recognise almost any foreign peptide presented by self MHC. In classically MHC-restricted αβ T cells, TCR recognition of cognate antigenic pMHC complex present at the surface of APCs or target cells is the key event for the mediation of the adaptive immune response. Recognition of pMHC allows T cells to detect and eliminate pathogen-infected cells or cells that have dysregulated their gene expression as consequence of a cancerous transformation.

The development of soluble fluorochrome-conjugated pMHC multimers in 1996[260] enabled the direct visualisation, phenotyping and TCR characterisation of antigen-specific T cells without the pre-requisite of cellular activation. Peptide-MHC multimer staining has become the gold standard for the detection of antigen-specific T cells in *ex vivo* samples. The original platform for pMHC multimers consisted of four biotinylated pMHC molecules bound to fluorochrome-conjugated streptavidin (**Figure 3-1A**). Ever since the development of the resulting pMHC tetramers, many alternative multimerization platforms encompassing a higher number of pMHC molecules have been developed to extend their capacity and allow high-throughput epitope discovery[261–264] (**Figure 3-1B** and **C**). However, pMHC multimer staining has been shown to be critically dependant on the affinity and/or half-life of the TCR-pMHC interaction[85]. Indeed, the affinity threshold required for regular pMHC tetramer staining is considerably higher than the required for T cell triggering[85]. As a consequence, conventional pMHC tetramer staining may have disregarded many fully functional T cells. This problem manifests particularly in the staining of autoimmune and anti-tumour cells T cells, which usually express lower affinity TCRs compared to anti-pathogen T cells[82,265–268]. Moreover, unlike the CD8 co-receptor, the CD4 co-receptor does not cooperate in the binding of pMHC multimers, which makes staining with pMHCII multimers even more challenging[249,269].

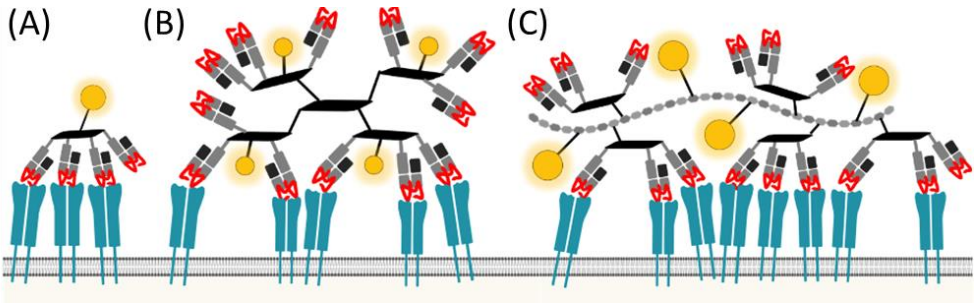

Figure 3-1. Several platforms are available for pMHC multimerization. Tetramers (4 pMHC molecules per reagent) **(A)**, Dodecamers (12 pMHC molecules per reagent) **(B)** and Dextramers (>10 pMHC molecules per reagent on a dextran backbone) **(C)** are some of the many multimerization platforms developed to detect antigen-specific T cells.

A considerable amount of data suggests a direct relationship between TCR-pMHC binding affinity and T cell functionality[135,270], implicating that higher affinity TCRs correlate with better pMHC multimer staining and superior sensitivity to cognate antigen. However, more recent studies have demonstrated that pMHC multimers can fail to detect fully functional T cells[265,268,271,272],

suggesting that data collected with the use of standard pMHC multimer technology might have underestimated the size and diversity of antigen-specific T cell responses. In accordance, studies conducted by *Derby and colleagues*[273] showed that T cell sensitivity correlated with TCR-mediated signalling but not with TCR affinity of pMHCI tetramer binding. Furthermore, *Ploegh and colleagues*[274] demonstrated that equivalent anti-tumour activity can be mediated by $CD8^+$ T cells expressing either high or low affinity TCRs, and *Evavold and colleagues*[275] observed that T cells with low affinity receptors can perform as major responders in primary $CD4^+$ T cell responses.

Although the reasons underlying why fully functional T cells fail to stain with conventional pMHC technology are not completely understood, some features of the T cell response are known to impact on pMHC multimer binding. For instance, TCR and CD8 co-receptor surface expression levels play a key role in the stabilisation of the TCR-pMHC complex. Thus, chronic stimulation of T cells during active disease can induce TCR and CD8 downregulation, thereby hindering staining with pMHC multimers[276]. Indeed, in studies with persistent Cytomegalovirus (CMV) infections known generate functional T cell populations representing >5% of $CD8^+$ T cells, *Khan and colleagues*[277] showed that standard pMHCI tetramer staining fails to detect an HLA-A*0201 restricted CMV response.

Multiple strategies have been employed to optimise pMHC multimer staining so that these reagents capture all functional T cells. The strategies still in common use are detailed below.

3.1.1. Anti-coreceptor antibody stabilisation of pMHC multimers

It has long been acknowledged that the CD8 glycoprotein is required for the stabilisation of the TCR/pMHCI complex at the cell surface, by binding to an invariant region of the MHCI molecule independent of the TCR-binding site[278]. This effect was subsequently shown to be related to a delay in the TCR/pMHCI dissociation rates, which are dependent on the affinity of the TCR/pMHCI interaction[81]. In flow cytometric analysis, anti-CD8 antibodies are commonly used for the identification of CTLs, however, certain anti-CD8 antibodies have been shown to impact on the binding of pMHCI tetramers[279]. Subsequent studies by my own laboratory showed that, while some anti-CD8 antibodies could block pMHCI tetramer binding, other antibody clones, that bound to different epitopes, could act to increase tetramer binding[280]. The effects of these antibodies on pMHCI multimer staining were paralleled in T cell activation assays and occurred in the absence of interaction between MHCI and CD8[280]. Consequently, all subsequent studies with pMHC multimers have avoided anti-coreceptor antibody clones that impede staining. The choice of anti-CD4 antibody for co-staining has also been shown to impact on pMHC-II multimer staining[281]. In summary, pMHC multimers are best used in conjunction with anti-coreceptor antibodies that enhance staining intensity.

My laboratory also developed CD8-enhanced pMHCI tetramers using a mutation that increased the affinity of the CD8-MHCI interaction[249]. These reagents exhibit improved detection of antigen-specific T cell populations with weak TCRs[282] but they can also result in increased background staining so this approach has not been widely adopted.

3.1.2. Higher order multimers

Peptide-MHC multimers stably stain cells due to the “avidity effect” of multiple TCR-pMHC interactions. The term avidity is used to describe the combined binding “strength” of a molecule with multiple binding sites, such as pMHC multimers[266]. Therefore, a higher number of TCR-pMHC interactions with each multimer is likely to stabilize the interaction. Consequently, higher order pMHC multimerization platforms have been developed in order to improve off-rates. These higher order multimers have been shown to result in increased T cell detection of antigen-specific T cells when compared to the conventional tetramer platforms. This difference is especially noticeable where TCR affinity is low. Thus, when detecting autoimmune or anti-cancer T cells, multimerization of pMHC complexes on a dextran backbone (dextramers, **Figure 3-1C**) often give better results than conventional pMHC tetramers[267]. Similarly, *Davis and colleagues*[271] showed that pMHC dodecamers (**Figure 3-1B**) displayed a better sensitivity, stronger signal strength, higher binding avidity and a slower dissociation rate when compared to pMHC tetramers. Other studies conducted by Guilleaume et. al.[283] showed that in pMHC octamers CD8 contribution to the binding was less relevant than with pMHC tetramers, however pMHC octamers still failed to detect $CD8^+$ T cells expressing exceptionally low affinity TCRs. It’s important to note that variations in the manufacturing quality of these reagents can influence the efficiency of antigen-specific T cell detection.

3.1.3. Inclusion of a Protein Kinase Inhibitor

Studies in my laboratory examining the protein kinase inhibitor (PKI) *Dasatinib* discovered that incubating primary human T cells in this PKI increased surface expression of TCR and CD3 coreceptor[284]. As these receptors are critical for the engagement of pMHC multimers, it was hypothesised that inclusion of PKI during pMHC multimer staining might enhance staining intensity. The testing of this hypothesis showed remarkable results that could not be explained by the modest increases in TCR expression induced by PKIs[250]. Indeed, the effects could be observed within 30 seconds of PKI addition suggesting that there was another mechanism at play[250]. Microscopic analyses showed that Dasatinib and other PKIs that inhibit Lck, the proximal kinase in TCR triggering, prevent TCR down-regulation[250]. It was hypothesised that by preventing TCR down-regulation, inclusion of PKI during staining could prevent TCR internalisation following non-productive pMHC engagement (an engagement that fails to capture pMHC multimer from solution) and keeps these TCRs that would have been internalised without pMHC (and associated fluorochrome) at the cell surface where they can undertake subsequent *productive* engagements. This affect was shown to enhance pMHC multimer staining with very weak TCR ligands by >50-fold and was applicable to both pMHCI and pMHCII in human and mouse[250]. Dasatinib is now produced cheaply for research purposes and it is recommended that it be included in all pMHC multimer stains.

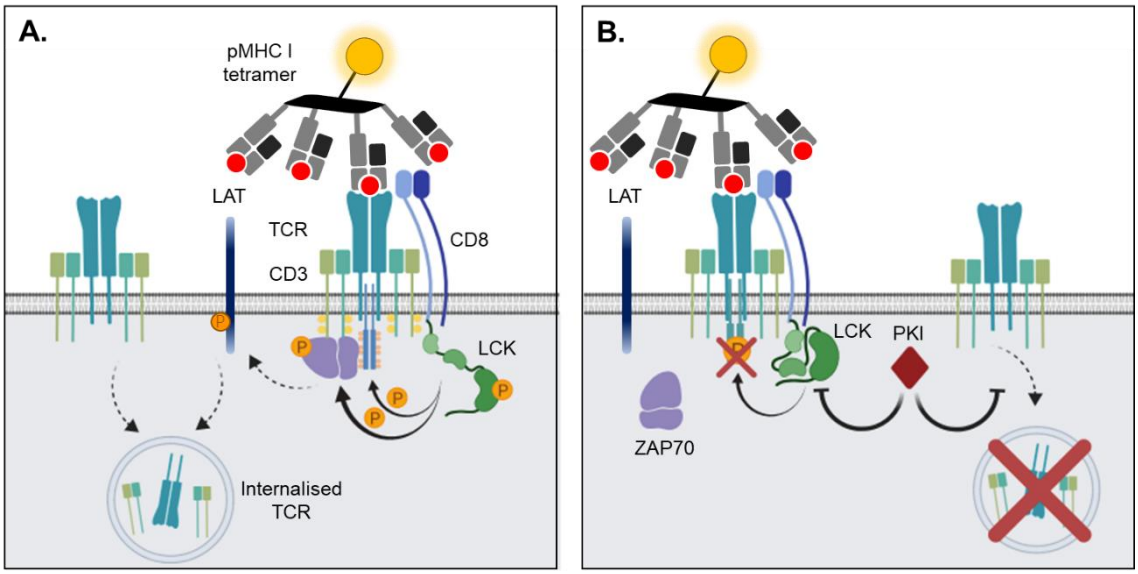

Figure 3-2. **PKI-mediated inhibition of TCR downregulation. (A)** Upon engagement of a cognate pMHC, TCR/CD3-mediated signal transduces into activation of CD8 co-receptor-associated LCK tyrosine kinase, followed by phosphorylation of ITAM motifs in the CD3 ζ chains, which in turn constitutes a docking site for the ZAP70 kinase activated by LCK. ZAP70 phosphorylates LAT to generate secondary responses of T cell activation and proliferation. TCR triggering results in the downregulation of the TCR through internalisation and degradation. Inhibition of LCK through the use of Protein Kinase Inhibitors can prevent TCR downregulation **(B)**. PKI also prevents recycling of TCRs that have not been captured by a pMHC multimer. Discontinuous arrows indicate that other enzymes are implicated but are not described for simplicity.

3.1.4. Antibody crosslinking of pMHC multimers

Since the use of PKI reagents maintained pMHC multimers at the T cell surface cell surface, my laboratory hypothesised that further signal amplification might be attainable using fluorochrome-conjugated antibodies against pMHC multimer components to enhance intensity via sandwich staining. Since most of the pMHC multimers are linked to fluorochromes, we tested the advantages of including an anti-fluorochrome primary (1^{ary}) Ab and a fluorochrome-conjugated secondary (2^{ary}) Ab to enhance the fluorescence signal detection by flow cytometry[268]. The application of this sandwich technology gave surprisingly good results that could not be accounted for by the additional fluorochrome. Instead, it was shown that most of the increase in staining could be achieved by simply using the 1^{ary} Ab alone as cross-linking of pMHC multimer reduced the off-rate during cell washing[268]. My laboratory now routinely uses an anti-fluorochrome antibody to cross link pMHC multimers during staining as this technique is simple and inexpensive. While the addition of a fluorochrome-conjugated 2^{ary} Ab further enhances staining the increase is more modest and can result in enhanced background staining.

The adoption of PKI staining, higher order multimers and antibody cross-linking as described above has been used by my laboratory to develop an optimised staining protocol that can result in up to 50-fold improvement in the staining of weak TCR-pMHC multimer binding compared to standard pMHC tetramer staining[244,250,265–268,285]. Combination of PKI and anti-fluorochrome antibodies has previously enabled the detection of tumour-specific T cells in the tumour Infiltrating Lymphocyte (TIL) population that failed to stain with pMHCI tetramers[268]. In the present study, I expanded these findings to samples from diverse clinical settings and included TCR profiling of antigen-specific T cells isolated with pMHCI multimers. The pMHC multimer staining strategies outlined in **Figure 3-3** have been employed throughout the study.

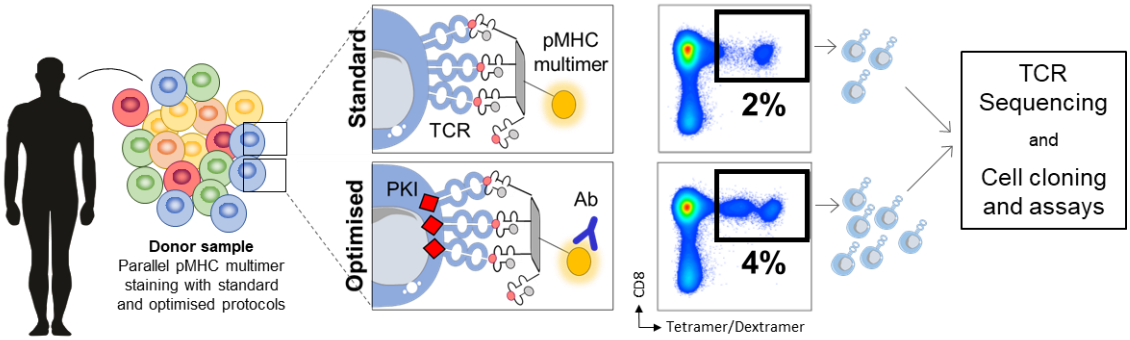

Figure 3-3. **Study approach.** Cell samples obtained from healthy donors and cancer patients were stained in parallel using standard and optimised pMHC multimer protocols. Standard approaches used pMHC tetramer or dextramer, while optimised approaches included incubation with PKI Dasatinib and anti-fluorochrome antibody (Ab). Viable multimer$^+$ CD8$^+$ T cells were sorted by flow cytometry and handled accordingly to downstream applications.

3.1.5. Aims

My overall aim at the start of my project was to dissect successful tumour-infiltrating lymphocyte (TIL) therapy by examining tumour-specific TCRs in TIL infusion product and in peripheral blood following complete remission. Previously, Dr V. Bianchi had partially characterised the T cell response mediated via HLA A2 in an HLA-A 02:01 stage IV melanoma patient who underwent complete remission following TIL therapy. This patient was known to make a substantial response to the Melan-A protein[286] (also called MART-1[287]) via the HLA A2-restricted Melan-A_{25-35} (sequence: EAAGIGILTV). Indeed, >10% of the TIL sample from this patient stained with HLA A2-Melan-A_{25-35} tetramer. During the course of these studies, it became apparent that many functional Melan-A_{25-35} -specific clonotypes were failing to stain with pMHC multimers and that these reagents were considerably underestimating the size of the antigen-specific T cell population. I therefore set out to test whether the cells that were being missed expressed different TCRs. In order to demonstrate that the failure of tetramers to detect relevant T cell clonotypes was a more general problem, I extended my studies to incorporate CD8 responses towards immunodominant epitopes from Influenza, Cytomegalovirus (CMV), Epstein Barr virus (EBV), Yellow Fever (YF) and insulin-like growth factor 2 mRNA- binding protein 2 (IMP-2)-specific T cells in the blood of HLA $A2^+$ healthy donors. I was particularly interested in the shortfalls of standard pMHC multimer for capturing fully functional antigen-specific T cells and the impact of using optimised staining on TCR profiling. The results of this Chapter formed the basis of a paper published at **Journal of Immunology** in 2018 entitled "***Peptide-MHC Class I tetramers can fail to detect relevant functional T cell clonotypes and underestimate antigen-reactive T cell populations***"[244].

3.2. Results

3.2.1. Failure to detect tumour-specific T cell clones in TILs using standard pMHC tetramer staining

Adoptive cell transfer of TILs is the most promising therapeutic approach for metastatic melanoma (MM) patients that have shown refractory responses to other forms of treatment, closely followed by successes in treatment with immune checkpoint inhibitors. In 2015, our collaborators at the CCIT and Herlev Hospital (Copenhagen, Denmark) successfully completed a phase I/II clinical trial (NCT00937625) with 31 participants (age 18-71 years) diagnosed with stage IV malignant melanoma and treated with Young TIL therapy.

Briefly, admitted participants received a lymphodepleting chemotherapy regime consisting of Cyclophosphamide and Fludarabine Phosphate. Excised tumour were surgically resected from subcutaneous nodules or lymph nodes, then cut into 1-2 mm fragments and placed in culture to allow bulk growth of tumour-infiltrating lymphocytes (TILs)[288,289]. Cultures with >90% viability and $>20 \times 10^6$ TILs were further expanded making use of a Wave bioreactor[290]. After 2 weeks, the expansion rate had increased by >1,000-fold, and cells were harvested and administered to the corresponding lymphodepleted patient intravenously. An outline of TIL therapy is illustrated in **Figure 1-13**. The trial was approved by the by the Scientific Ethics Committee for the Capital Region of Denmark and conducted in accordance with the Helsinki declaration and good clinical practice as described by Danish law. Objective response rates (OR) of >40% and complete remission rates (CR) of 22% were achieved[289].

The dissection of anti-cancer reactivity of the infused αβ TIL products in three complete remission patients was the focus of a PhD project undertaken by Dr V.Bianchi in my laboratory prior to my arrival[291]. During these studies, Dr. Bianchi described a *HLA-A*0201* (HLA A2 hereon) restricted Melan-A specific anti-tumour response in one of the patients (MM909.24, see **Table 3-1** for details). Observations derived from my colleague's work concluded that standard pMHC multimer staining underestimates the extent of the Melan-A specific response in this patient[268]. I set out to formally test this conclusion and to determine whether the functional T cells that were missed by standard pMHC tetramer staining possessed different TCRs.

Table 3-1. **Patient treatment details and clinical outcome.** Patient MM909.24 had metastases to skin, subcutaneous, or distant lymph nodes (M1a) as defined by the American Joint Committee on Cancer (AJCC) before receiving therapeutic TIL infusion. After TIL infusion, patient was categorised as Complete Remission (CR), as defined by the RECIST guidelines[292] and remains tumour-free over 5-years after treatment.

Patient ID	AJCC stage	Clinical response	HLA class I	Treatment composition			
MM909.24	M1a	CR (>5years)	A*02 A*30 B*40 B*40 C*03 C*03	$11x10^{10}$ infused cells	67% αβ $CD8^+$	20% αβ $CD4^+$	0.1% $γδ^+$

As discussed above, standard pMHC tetramer staining can fail to detect all functional T cells. This deficiency is especially marked when low-affinity TCRs predominate such as with anti-cancer T cells. Following the strategy outlined in **Figure 3-3**, I stained the TIL product of patient MM909.24. Consistent with previous observations[268], more HLA A2-restricted Melan-A_{25-35} (E**L**AGIGILTV, heteroclitic residue in bold) tetramer$^+$ T cells were detected when using the optimised protocol (13.5% of CD3$^+$) when compared to standard protocol (11% of CD3$^+$) (**Figure 3-4A**). Isolation of CD8$^+$ Melan-A tetramer$^+$ populations using standard or optimised protocols resulted in the processing of >54,000 and >79,000 cells, respectively, for high throughput sequencing. TCR sequencing results can be found in **Supplementary table 1**.

TCRβ analysis of sorted T cell populations showed a narrower repertoire of Melan-A-specific T cells isolated with standard tetramer-based isolation compared to optimised tetramer-based sorting. Optimised staining revealed 19 unique clonotypes when compared to only 1 for the standard protocol. Four TCRβ clonotypes were shared between protocols; accounting for >95% of the TCRs sequenced with the standard protocol. Consistent with previous reports, gene usage for Melan-A specific TCRs was dominated by TRBV27[293] paired with TRBJ2-3 (>60% of total reads) (**Figure 3-4B**). The dominant CDR3β conserved motif "Glycine-Leucine-Glycine" (GLG) was rearranged with members of the TRBJ1 cluster as previously described[26]. Interestingly, optimised sort of Melan-A specific TCRs also showed the usage of the public "GLG" motif by TRBJ2-7 clonotypes. Moreover, the recurrent motif was restricted to TRBV30, TRBV6-3 in the standard tetramer sort, whereas optimised tetramer sort extended the motif usage to TRBV28 and TRBV20-1 (**Supplementary table 1**).

Next, I set out to isolate, grow Melan-A-reactive monoclonal T cell populations from the TIL infusion product used to treat patient MM909.24. TCRβ profiling of bulk Melan-A tetramer$^+$ sorted cells from these TIL described above enabled me to find the TCRs associated with these T cell clones. Amongst the clonotypes, the TCRβ corresponding to the T cell clone CR24 was detected in the Melan-A tetramer$^+$ population sorted using both standard and optimised procedures. In contrast, the TCRβ-chains of the CD8$^+$ T cell clones CR31 and VB6G4.24 were only detected when cells were sorted using the optimised staining protocol. (**Figure 3-4A**). I next sought to examine how the corresponding T cell clones stained with each protocol. The CR24 clone could be stained with the standard and optimised protocol whereas clone VB6G4.24 could only be stained using the optimised procedure (**Figure 3-4C**). Thus, pMHC tetramer staining of Melan-A T cells within the TIL infusion product matched those with monoclonal T cell populations.

I next examined T cell activation in response to Melan-A Wild Type (EAAGIGILTV) peptide or the commonly used heteroclitic version of this peptide where a leucine was substituted at position 2 to enhance binding to HLA A2 (E**L**AGIGILTV) using MIP-1β production as a readout (**Figure 3-4D**). Both CR24 and VB6G4.24 clones responded to MOLT3 cells transduced with the Melan-A protein (**Figure 3-4E**). Noticeably, although both clones exhibited lysis of the autologous melanoma, the VB6G4.24 clone, that could only be stained using the optimised protocol, exhibited stronger cytotoxicity at all effector to target (E:T) ratios tested (**Figure 3-4F**).

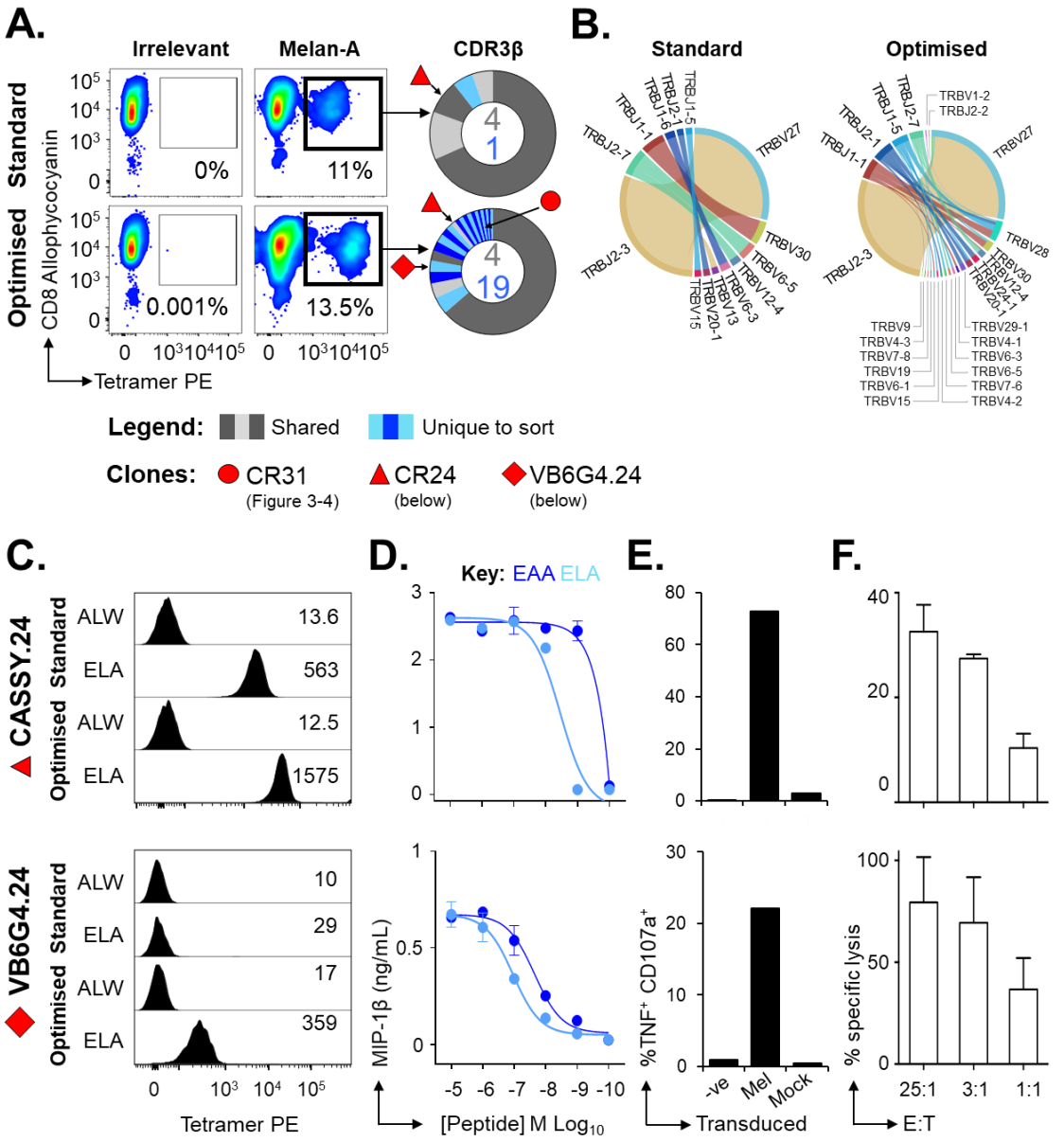

Figure 3-4. Clonotypic analysis of TILs using optimized pMHC staining reveals functional T cells missed by standard approaches. (A) Melan-A specific T cells were sorted from the TIL infusion product from complete remission metastatic melanoma patient MM909.24 with HLA A2–restricted Melan-A_{25-35} (ELAGILGILTV) tetramer using standard or optimised staining protocols. The percentage of $CD8^+$ $tetramer^+$ cells is displayed. Gates were set on single lymphocytes and live $CD3^+$ $CD14^{neg}$ $CD19^{neg}$ cells. Irrelevant HLA A2–restricted pre-proinsulin antigen (ALWGPDPAAA)^{294} was used to set the gates for sorting. TCR sequencing and CDR3 analysis of β chains are displayed as sort-shared (grey) or sort unique (blue) section of a pie, with each section for each sort corresponding to a different CDR3β relative to its frequency in the sort. Geometrical red figures correspond to identified TCRβ chains pertaining to a $CD8^+$ T cell clone derived from the same patient. **(B)** TCRβ Variable (arc on the right) and Joining (arc on the left) gene rearrangements enriched in $CD8^+$ $tetramer^+$ sorted cells. Segments represent frequency in sort. Links represent how commonly genes rearrange. Plots were generated using *VDJViz*[252]. **(C)** $CD8^+$ T cell clones from patient MM909.24: **CR24** and **VB6G4.24**, were stained with standard and optimised protocols using HLA A2–ELAGIGILTV and irrelevant HLA A2– ALWGPDPAAA tetramers, with Mean Fluorescence Intensities (MFI) shown. **(D)** Overnight activation against the Melan-A_{25-35} wild type (EAA, in light blue) and heteroclitic (ELA, in blue) peptides in presence of T2 cell line, as measured by MIP-1β release. EC_{50} values of peptide sensitivity are shown. **(E)** Intracellular cytokine staining of the T cell clones following 4h co-incubation with MOLT3 cell line un-transduced (-ve), transduced with Melan-A (Mel) or with irrelevant Collagen (Mock) protein. % of TNF^+ and $CD107a^+$ $CD8^+$ viable cells is shown. **(F)** T cell cytotoxicity measured by ^{51}Cr release after 8 hours co-incubation with autologous tumour at the indicated E:T ratios. Representative data of two experiments, mean and SEM are shown.

Collectively, these data showed that the low-affinity TCR-bearing T cell clone, VB6G4.24, that could not be detected with standard tetramer was fully functional. I therefore conclude that standard pMHC multimer staining misses fully functional T cell clonotypes, thus underestimating the size and diversity of the antigen-specific response to Melan-A within patient derived TIL.

3.2.2. Fully functional T cell clonotypes can be overlooked by standard tetramer staining

To further validate the above findings that standard pMHC tetramer staining missed fully functional T cells, a total of n=62 (n=13 with Standard staining; n= 49 with Optimised staining) Melan-A tetramer$^+$ CD8$^+$ T cell clones from MM909.24 TILs were grown using the strategy outlined in **Figure 3-3**. Isolation using standard tetramer staining resulted in n=1 Melan-A tetramer^{neg} and n=12 Melan-A tetramer$^+$ clones (**Figure 3-5A**); whereas isolation using optimised tetramer staining resulted in n=43 Melan-A tetramer$^+$ T cell clones that stained sufficiently with the standard protocol, but n=6 that only stained in combination with PKI and anti-fluorochrome antibody (**Figure 3-5B**).

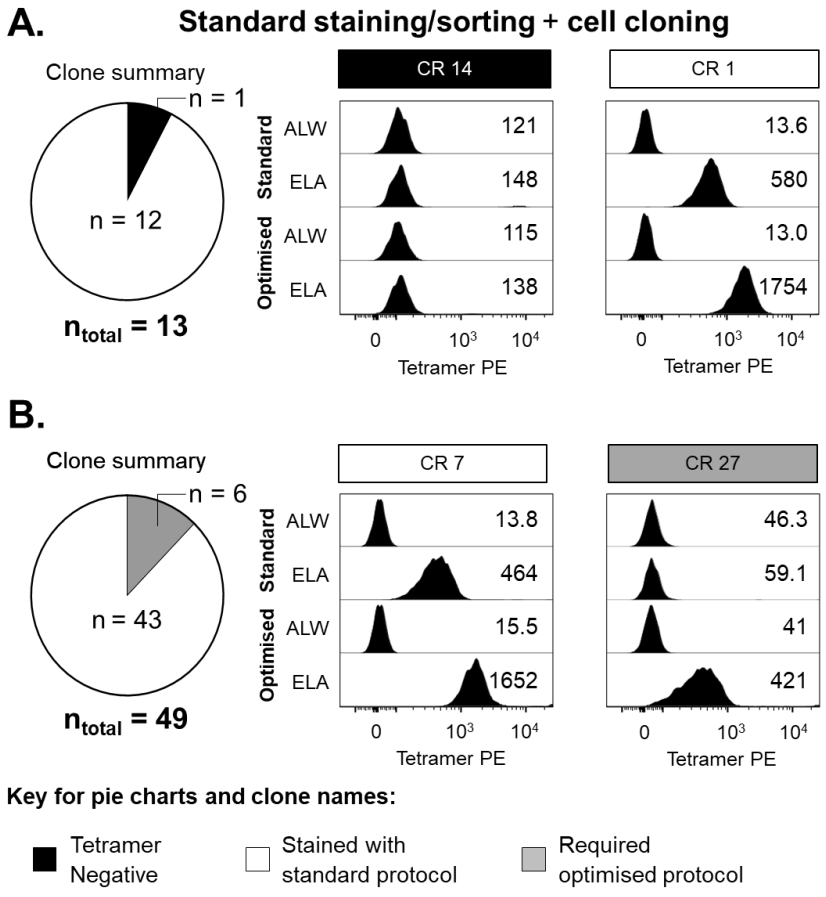

Figure 3-5. Clones grown from optimally stained and sorted TILs stain with tetramer *in vitro*. Melan-A tetramer$^+$ CD8$^+$ T cells sorted from the TILs of patient MM909.24 using standard **(A)** or optimised **(B)** staining protocols were cloned by limiting dilution (see **material and methods**). Growing clones were stained with HLA A2–ELAGILGILTV and irrelevant HLA A2–ALWGPDPAAA tetramers using standard (open) or optimised (filled) staining protocols. A summary of the number of clones grown and stained from each sort is shown in the respective pie (left panel). Representative CD8$^+$ T cell clones encompassing all staining patterns seen is shown (middle and right panels).

TCR sequencing revealed that T cell clone CR31 expressed a TRBV30 TRBJ5-1 TCRβ chain with CDR3β amino acid sequence CAWSSQGLGQPQHF. Similar to VB6G4.24, this TCRβ was recovered from the TIL product with optimised but not with standard staining protocol, (red circle, **Figure 3-4**). The ability of CR31 clone to bind the Melan-A tetramer was re-assessed by performing parallel staining of the T cell clone with both protocols, confirming that CR31 failed to stain with standard pMHC tetramer staining **Figure 3-6A**, left panel). However, the low affinity threshold for pMHC tetramer binding did not impair the clone's recognition of both the wild type and the heteroclitic versions of Melan-A peptide (**Figure 3-6A**, middle panel), nor activation when challenged with autologous melanoma as measured by MIP-1β secretion (**Figure 3-6A**, right panel).

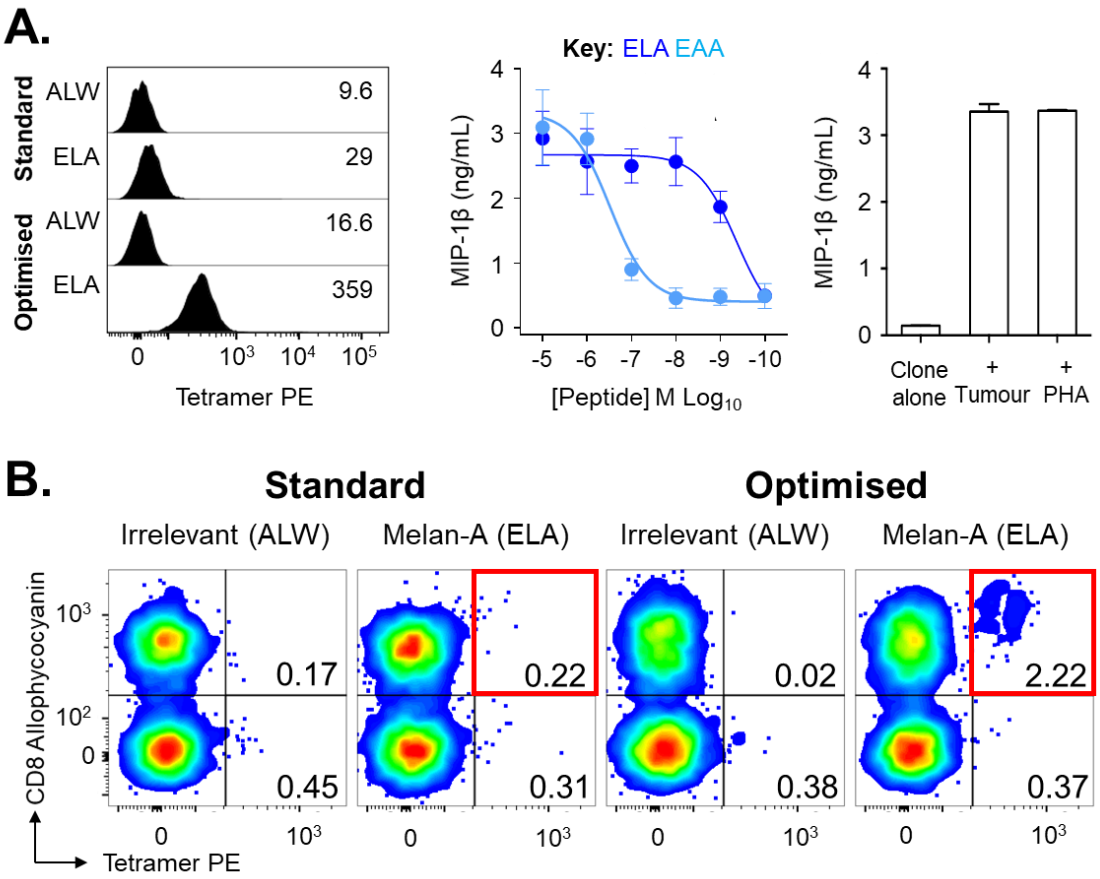

Figure 3-6. Standard tetramer staining protocol does not recover low-affinity Melan-A specific T cells (A) Patient MM909.24 derived CD8⁺ T cell clone CR31 grown from the optimised pMHC tetramer sorted TILs was stained with standard (open) and optimised (filled) with HLA A2–ELAGILGILTV (blue) and irrelevant HLA A2–ALWGPDPAAA (grey) tetramer, with MFI values displayed (left panel). Overnight activation against the Melan-A_{25-35} wild type (EAA) and heteroclitic (ELA) peptides as measured by MIP-1β release (middle panel). Overnight activation after co-incubation with autologous tumour at 2:1 ratio (right panel). T cell alone and PHA as negative and positive controls, respectively, are shown. Representative data of two experiments, mean and SEM are shown. **(B)** Recovery of CD8⁺ T cell clone CR31 spiked at ~2% of CD3⁺ cells into HLA $A2^{neg}$ PBMC using standard and optimised HLA A2–ELAGILGILTV tetramer staining. Irrelevant HLA A2–ALWGPDPAAA tetramer was used as negative control. % of tetramer-bound background is displayed for CD8⁺ and $CD8^{neg}$ cells. % of CD8⁺ Melan-A tetramer⁺ cells is highlighted in the red box.

I next sought to examine the recovery of fully functional antigen-specific T cells from PBMC by spiking the CR31 clone into HLA A2^{neg} PBMC at ~2% of CD3^{+} cells, followed by parallel staining with standard and optimised pMHC tetramer staining protocols (**Figure 3-6B**). Conveniently, the CD8^{high} nature of cultured T cell clones relative to those from fresh PBMC allowed tracking of the clone within the PBMC sample. Standard tetramer staining failed to recover functionally relevant CR31 T cell clone, but this clone stained well with optimised tetramer staining. I extended these results with three more Melan-A specific T cell clones, increasing the spiking to ~5% of CD3^{+} cells. As shown in **Figure 3-7A**, MEL5 and CR29 T cell clones stained efficiently with standard pMHC tetramer staining, and could be neatly recovered with both standard and optimised protocols (**Figure 3-7B**, middle and lower panels). In contrast and like the CR31 clone, the low affinity VB6G4.24 clone described in the previous sections could not be recovered by standard pMHC tetramer staining protocols (**Figure 3-7B**, upper panel), despite having proved to be efficient at recognising the autologous melanoma.

Overall, these experiments demonstrate that clones bearing a low affinity TCR and that can only be revealed by optimised pMHC staining, can be functionally relevant.

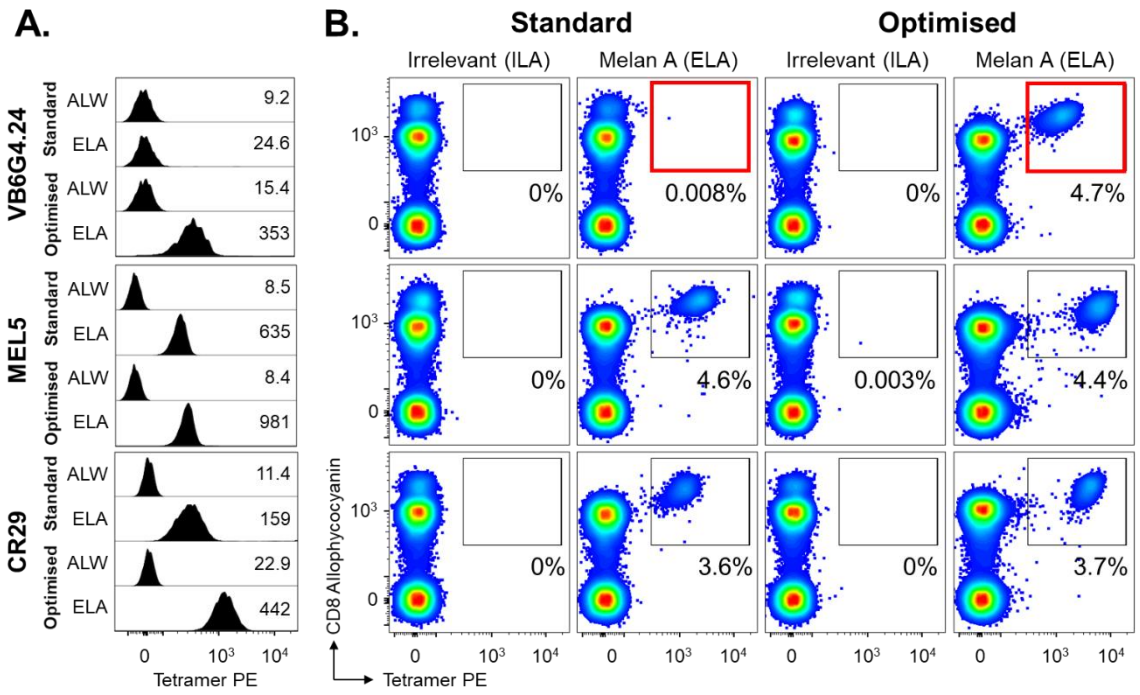

Figure 3-7. **Standard tetramer staining protocol fails to detect low-affinity Melan-A -specific T cell clones from PBMC. (A)** Parallel tetramer staining using standard (open) and optimised (filled) protocols of the Melan-A specific T cell clone VB6G4.24 (upper panel) bearing low affinity TCR, and two high affinity TCR clones MEL5 (middle panel) and CR29 (lower panel). Irrelevant HLA A2-restricted hTERT$_{540-548}$ (ILAKFLHWL)^{295} was used as control. MFI values are displayed. **(B)** Recovery of the Melan-A specific T cell clones spiked into HLA A2^{neg} PBMC at ~5% of CD3^{+} cells using standard and optimised protocols with HLA A2–ELAGILGILTV and irrelevant HLA A2-ILAKFLHWL. Cells were gated on lymphocytes, then viable CD3^{+} CD14^{neg} CD19^{neg}. Percentages are shown for the respective gates.

3.2.3. Dominant persistent Melan-A T cell clonotypes require an optimal tetramer staining protocol

Previous research conducted by my colleagues demonstrated that tumour-reactive TCRβ clonotypes present in the TIL infusion product (cryopreserved and without further in vitro manipulation) used to treat patient MM909.24, persisted in the blood (PBMC) taken after the patient was diagnosed with complete remission (~6 months post-treatment), potentially protecting against cancer recurrence[296]. Briefly, the TIL infusion product and the blood post-infusion were stimulated with autologous melanoma in a TAPI-0 assay, followed by sorting of tumour-reactive T cells based on TNF and CD107a markers and TCRβ clonotypic analysis using HTS. Persistence of tumour-reactive infused T cells in peripheral blood has been correlated with tumour regression in melanoma patients[289], indicating their potential role in orchestrating a successful response to treatment and in the prevention of tumour recurrence.

37.6% of TILs and 4.13% of the T cells in patient blood after complete remission responded to the autologous tumour cell line by upregulation of CD107a and/or TNF (**Figure 3-8A**), with n=91 and n=59 TCRβ clonotypes detected at frequencies ranging from 0.003-28.7% and 0.019-23.4%, respectively (**Figure 3-8B**). From the tumour-reactive TCRβ clonotypes that persisted in the blood, 33.9% were also observed in the infused TIL product (**Figure 3-8B**, indicated in **grey** and **Supplementary table 2**). Interestingly, three persistent CDR3β found both in the TILs and blood (CASTLGGGTEAFF, CASSNGFNTLYF and CATSDRGQGANWDEQFF) corresponded to previously described Melan-A specific clonotypes that required the optimised pMHC staining protocol to be detected (**Figure 3-8B** marked in **red**). Moreover, CATSDRGQGANWDEQFF CDR3β was the fifth most frequent clonotype found in the blood, and is expressed by the Melan-A specific VB6G4.24 T cell clone bearing a low affinity TCR but capable of effective cytotoxic activity against autologous tumour, despite not staining with standard pMHC protocols (**Figure 3-4**). Remarkably, these three clonotypes underwent substantial enrichment from the TIL infusion product (0.12%, 0.14%, 0.34%, respectively) in the blood, where they accounted for a total of 44% of the response (22.4%, 14.3% and 7.3%, respectively) of all tumour-reactive CDR3β present in the PBMC of the patient after complete remission (**Figure 3-8B)**. Although at a lower frequency, the CDR3β of the previously described Melan-A specific T cell clone CR24 (CASSYSFTEATYEQYF) (**Figure 3-4C**) was also observed in both TIL product and blood post-infusion (0.003% and 0.9%, respectively) (**Figure 3-8B**, marked in **black**). Of note, CR24 shows cytotoxicity against autologous tumour and stains with standard pMHC multimer protocol (**Figure 3-4C**). In summary, tumour-reactive T cells directed towards the Melan-A antigen that could only be visualised *in vitro* using optimal pMHC multimer staining were shown to be fully functional *in vitro* and *ex vivo*. Moreover, the TCRβ clonotypes associated to these T cells were shown to be dominant in the blood of the complete durable remission patient MM909.24, indicating their potential importance in tumour clearance. Importantly, data from CR24 and VB6G4.24 T cell clones, demonstrates that *in vitro* TCR-pMHC multimer staining does not correlate with superior sensitivity to cognate antigen or with T cell cytotoxicity.

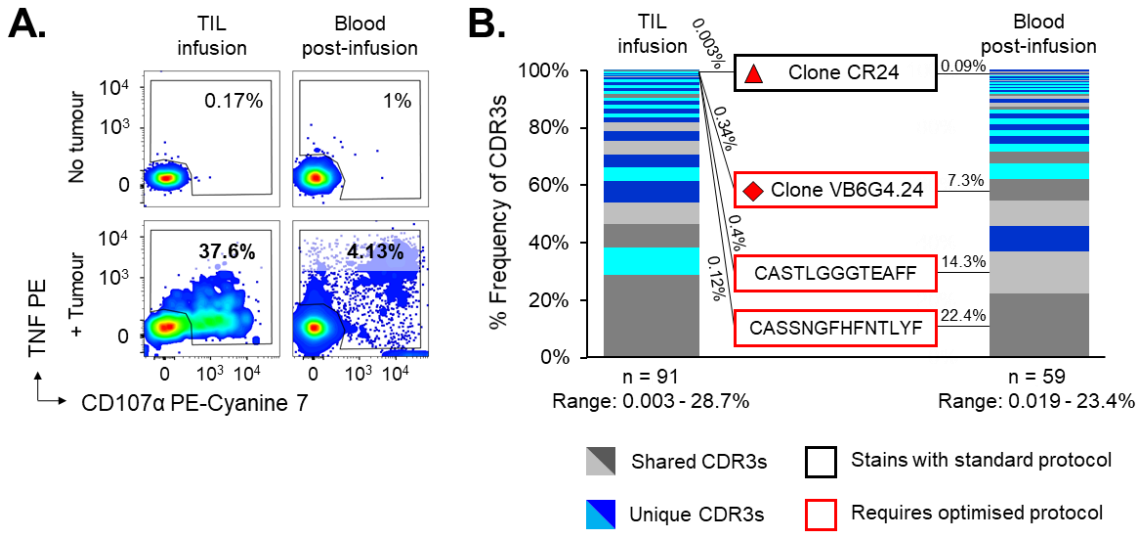

Figure 3-8. Melanoma-reactive T cells in the blood of a patient cured of cancer are dominated by clonotypes that require an optimal protocol to stain with Melan-A tetramer. (A) Intracellular cytokine staining of the original TIL infusion product and post-infusion PBMCs (6 months), following 5h co-incubation with autologous tumour (gated on Vivid^{neg} CD3^{+} CD8^{+}). Reactive T cells were viable cell sorted for TCR clonotyping. **(B)** Tumour-reactive TCRβ clonotypes in TIL infusion product or post-infusion PBMC are displayed as sort-shared (grey) or sort-unique (blue) vertical slices. The number of total CDR3β for the respective sorts are shown at the bottom of each chart, with the range of CDR3β frequencies from the respective sort below. Persistent clonotypes corresponding to in vitro grown CD8^{+} clones CR24 and VB6G4.24, and the Melan-A reactive CDR3β sequences previously described in donor MM909.24 are indicated. CDR3β clonotypes detected with standard or optimised Melan-A tetramer are shown in **black** and red, respectively. Data courtesy of Dr. V Bianchi

3.2.4. Differences in staining efficacy between standard and optimised pMHC tetramer staining protocols are independent of staining temperature

Due to the particularities of the Optimised pMHC multimer staining protocol, it could be envisaged that the proposed modifications in the protocol could introduce a bias independent to the synergetic effects of PKI and anti-fluorochrome antibody in the detection of antigen-specific T cells bearing a low affinity TCR. For instance, for this study tetramer staining was performed on ice, whereas many studies perform staining at room temperature or 37°C. Membrane fluidity and lipid raft fluidity are temperature sensitive factors that have proven crucial for tetramer staining[77,297]. It could be therefore argued that the low temperatures employed during the staining, rather than the use of PKI and anti-fluorochrome antibody, reduces the efficacy of Standard tetramer staining and magnifies the improvement observed when Optimised tetramer staining is performed.

In order to address this point, I compared the staining of the TIL infusion product from patient MM909.24 with HLA A2-EAAGIGILTV and HLA A2-ELAGIGILTV tetramers at 4°C, room temperature (~22°C) and 37°C by parallel staining with standard and optimised protocols. Staining at higher temperatures increased the overall % of CD8^{+} Tetramer^{+} cells slightly, but the differences observed in the staining efficacy between standard and optimised protocols were independent of temperature (**Figure 3-9A**). Consistent with previous findings[271], staining of PBMC

from HLA A2⁺ Type I diabetes patients with Preproinsulin (PPI_{15-24}) dextramers at higher temperatures showed an increase in non-specific background (**Figure 3-9B**), and a reduction of the signal/noise ratio compared to staining at 4°C; hence I resolved to perform all pMHC multimer staining on ice. Moreover, it's been previously reported that T cells rapidly internalise pMHC multimers when stained at room temperature or 37°C[297,298].

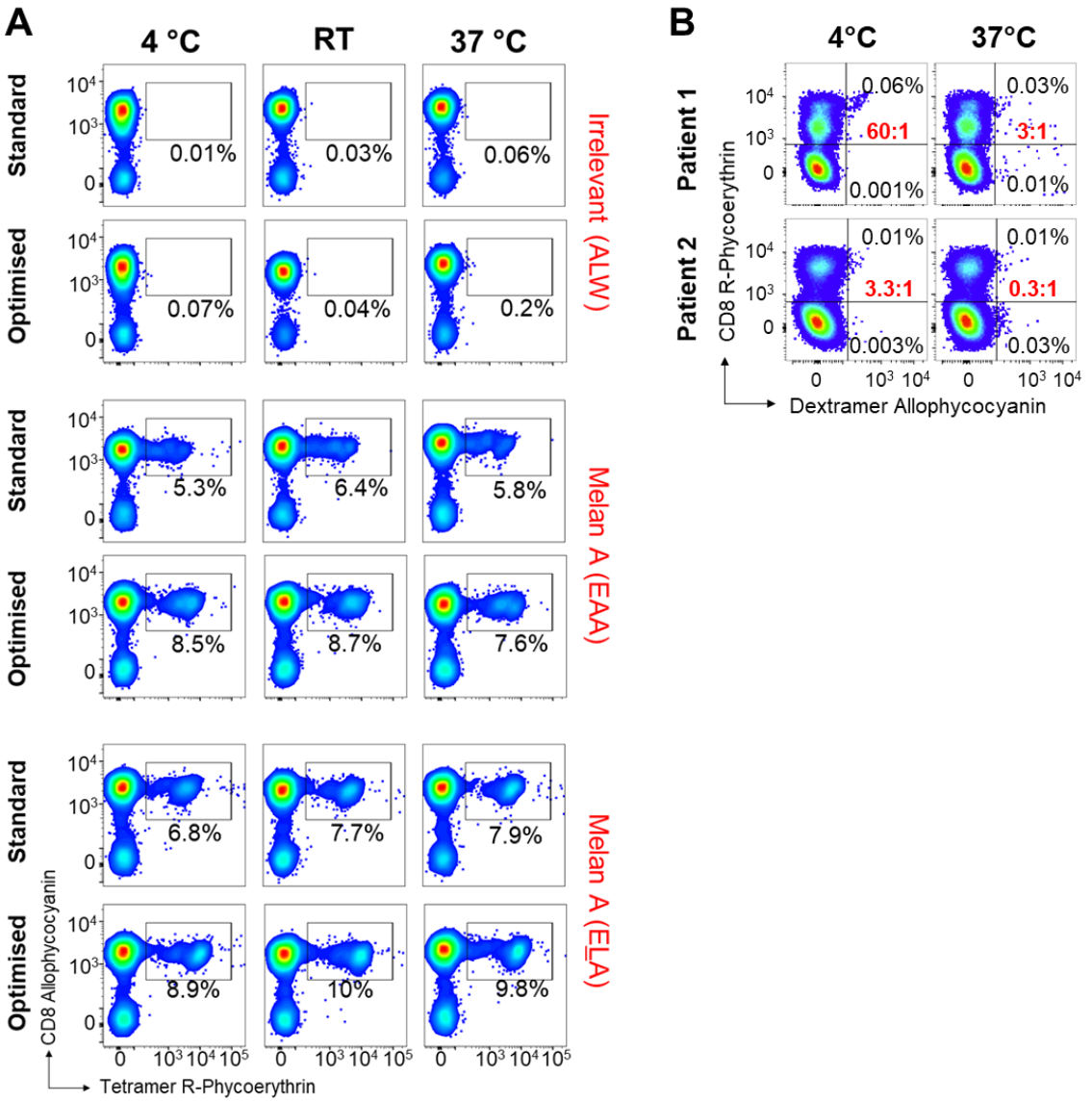

Figure 3-9. **Improved recovery of antigen-specific cells observed with optimised pMHC protocols is independent of staining temperature.** **(A)** Melan-A specific TILs from donor MM909.24 were stained using HLA A2-EAAGILGILTV and HLA A2-ELAGILGILTV standard or optimized tetramer staining at 4°C, room temperature (~22 °C) or 37°C. The % of CD8⁺ Tetramer⁺ cells is displayed. Gates were set on single lymphocytes and live $CD3^{+}$ $CD14^{neg}$ $CD19^{neg}$ cells. Irrelevant HLA A2-ALWGPDPAAA tetramer was used to set the gates. **(B)** Peripheral blood monocular cells from HLA A2⁺ donors with type I diabetes were thawed and stained with HLA A2-ALWGPDPAAA allophycocyanin conjugated dextramer. Staining was performed at 4°C or 37°C. The percentage of viable CD3 cells is shown for the $CD8^{+}$ dextramer⁺ (upper right) and $CD8^{neg}$ control (lower left) gate, with the signal to noise ratio in red.

3.2.5. Standard pMHC tetramer staining fails to detect functional tumour-specific T cell clonotypes in direct *ex vivo* PBMC samples

The most common use of pMHC multimers is the detection of antigen-specific T cells in *ex vivo* PBMC. Because the previous data was generated from minimally cultured TILs, I extended my observations to the T cell response for a different self-epitope in direct *ex vivo* PBMC samples. For this study, the insulin-like growth factor-2 mRNA-binding protein 2 (IMP-2) was selected. IMP-2 is a member of three oncofoetal antigens known to be overexpressed between the zygote and the embryo stages, but more recent reports have documented overexpression of IMP-2 in some cancers correlated with poor survival[299–303]. Some studies have suggested that IMP-2 function may be implicated in the regulation of cancer cell metabolism and promoting metastasis[301] by stabilisation of oncogenic mRNAs encoding HMGA1, thus preventing Let-7 target gene silencing[304,305]. From the studies described in **Chapter 4,** I have determined that residues 366-376 of IMP-2 (sequence NLSALGIFST) are presented at the surface of HLA A2$^+$ IMP-2 expressing cells and represents a novel immunogenic HLA A2-restricted epitope.

In order to determine whether optimised pMHC staining protocol could identify tumour-specific T cells from *ex vivo* samples that failed to stain with the standard pMHC tetramer protocol, *ex vivo* PBMCs from the HLA A2$^+$ healthy donor 0439 were stained and sorted using standard and optimised tetramer protocols bearing the IMP-2$_{366\text{-}376}$ antigen. As shown in **Figure 3-10A**, standard protocol revealed significantly less CD8$^+$ tetramer$^+$ T cells in comparison with the optimised protocol (0.002% versus 0.05% of total CD3$^+$). As previously, TCRβ analysis by HTS of tetramer-based isolation revealed a reduced diversity in the TCRβ repertoire of standard tetramer-based sort when compared to the optimised sort. TCR sequencing of CD8$^+$ Tetramer$^+$ cells revealed 13 CDR3β (n=69 sorted cells) for the standard and 31 CDR3β (n=324 sorted cells) for the optimised Tetramer, with 10 CDR3β sequences shared between protocols. Gene usage for IMP-2 specific TCRs in standard tetramer stained cells was dominated by TRBV7-2 paired with TRBJ1-5 (>30% of total reads) (**Figure 3-10B**, left). However, VJ-gene usage in optimised tetramer stained cells showed further diversity, resulting in a shared incidence of TRBV7-9 and TRBV29-1 paired with TRBJ2-7, but with no strong VJ-gene dominance for any of the sorts (**Figure 3-10B**, right). TCR sequencing results can be found in **Supplementary table 3.**

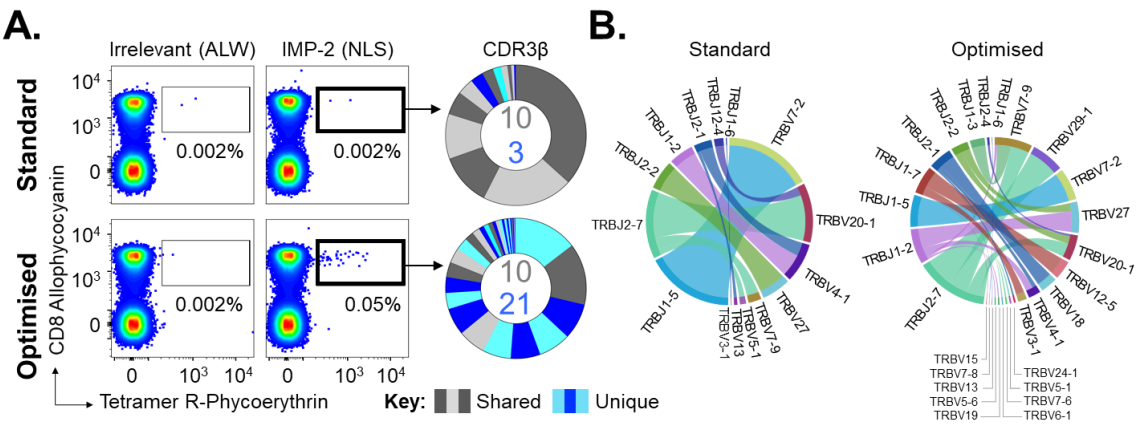

Figure 3-10. **Optimised pMHC multimer staining reveals low affinity antigen-specific T cells. (A)** IMP-2-specific T cells were sorted from the PBMC of donor 0439 with HLA A2–restricted IMP-$2_{366-376}$ (NLSALGIFSTG) tetramer using standard or optimised staining protocols. The percentage of $CD8^+$ $tetramer^+$ cells is displayed. Gates were set on single lymphocytes and live $CD3^+$ $CD14^{neg}$ $CD19^{neg}$ cells. Irrelevant HLA A2–restricted pre-proinsulin antigen (ALWGPDPAAA)^{294} was used to set the gates for sorting. TCR sequencing and CDR3 analysis of β chains for both sorts are displayed as sort-shared (grey) or sort unique (blue) section of a pie, with each section for each sort corresponding to a different CDR3β relative to its frequency in the sort. **(B)** TCRβ Variable (arc on the right) and Joining (arc on the left) gene rearrangements enriched in $CD8^+$ $tetramer^+$ sorted cells using standard and optimised tetramer staining protocols from the two sorts. Segments represent frequency in sort. Links represent how commonly genes rearrange. Plots were generated using *VDJViz*[252].

To formally prove that standard pMHC multimer staining fails to detect functional TCRs, I generated a NLSALGIFST-specific $CD8^+$ T cell clone from the PBMC of donor 0439. The clone CR0439.NLS (TRAV40 TRAJ53 CDR3α: CLTPSGGSNYKLTLF; TRBV11-3 TRBJ2-5 CDR3β: CASAAYGETQYF) failed to stain with standard pMHC tetramer protocol, but staining with optimised protocol increased MFI by >30 fold (**Figure 3-12A**). The T cell clone showed sensitivity towards cognate NLSALGIFST peptide (**Figure 3-12B**) and IMP-2 transduced HLA $A2^+$ LCL line MOLT3 (**Figure 3-12C**) when MIP-1β secretion was measured after overnight incubation with target. Moreover, CR0439.NLS clone was capable of exhibiting cytotoxicity against the HLA $A2^+$ melanoma cell line MM909.24 expressing IMP-2 (**Figure 3-12D** and **Figure 3-11**). Furthermore, CR0439.NLS clone could be recovered using optimised pMHC staining protocol, but not using the standard protocol, when spiked into HLA $A2^{neg}$ PBMC at ~1% (**Figure 3-12E**) of $CD3^+$ cells. These data were consistent with my data with low affinity Melan-A specific T cell clones, further emphasizing the shortcomings of standard pMHC staining protocols.

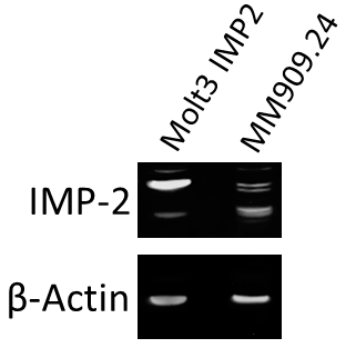

Figure 3-11. IMP-2 Western Blotting of MM909.24 melanoma line. The lymphoblastoid cell line MOLT3 lentivirus-transduced with whole length IMP-2 protein was used as positive control. β-Actin blotting was used as loading control.

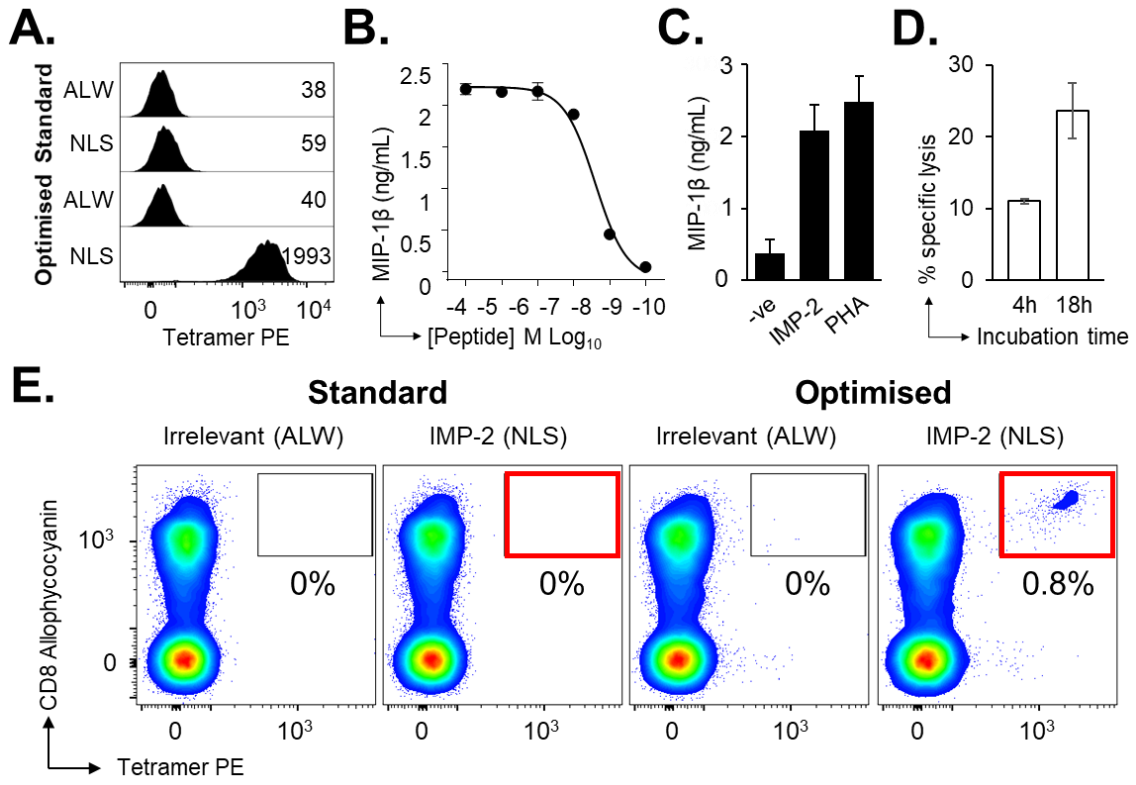

Figure 3-12. Standard pMHC multimer staining fails to detect the low affinity CR0439.NLS T cell clone. (A) CR0439.NLS CD8$^+$ T cell clone grown from the PBMC of donor 0439 was stained with HLA A2–restricted IMP-2$_{366-376}$ (NLSALGIFSTG) tetramer using standard or optimised staining protocols. HLA A2-ALWGPDPAAA irrelevant tetramer was used as control. MFI values are displayed. **(B)** Overnight activation against the IMP-2$_{366-376}$ peptide as measured by MIP-1β release. EC_{50} values of peptide sensitivity are shown. **(C)** Overnight activation against HLA A2$^+$ LCL cell line MOLT3 transduced with IMP-2 as measured by MIP-1β release. Responses to non-transduced LCL (-ve) and PHA as negative and positive controls, respectively, are shown. Mean and SEM of two independent experiments are shown. **(D)** Anti-tumour cytotoxicity as assessed in a chromium release assay (^{51}Cr) after co-incubation with IMP-2 expressing melanoma cells (MM909.24) at 2:1 after 4 and 18h. Mean and SEM are shown. **(E)** Recovery of the IMP-2 specific T cell clones spiked into HLA A2^{neg} PBMC at ~1% of CD3$^+$ cells using standard and optimised protocols with HLA A2–NLSALGIFSTG and irrelevant HLA A2-ALWGPDPAAA. Cells were gated on lymphocytes, then viable CD3$^+$ CD14^{neg} CD19^{neg}. Percentages are shown for the respective gates.

3.2.6. Optimised pMHC tetramer staining can improve recovery of virus-specific T cell populations

In contrast to anti-tumour TCRs, TCRs responding to viral antigens are known to bind to cognate pMHC with relatively high affinity[80,82] and, standard pMHC tetramer staining is commonly assumed to recover all viral antigen-specific T cells of required specificity. My studies showing that standard pMHC tetramer staining can fail to detect fully functional cancer-specific T cells led me to re-examine whether these reagents captured T cells capable of responding to a viral epitope. Following the strategy outlined in **Figure 3-3**, I stained the PBMCs from three HLA $A2^+$ donors with pMHC multimers carrying previously described immunodominant epitopes from the common viruses Influenza $M1_{58-66}$ (GILGFVFTL), Epstein-Bar virus (EBV) $LMP2A_{426-434}$ (CLGGLLTMV) and Cytomegalovirus (CMV) $pp65_{495-503}$ (NLVPMVATV). Similar sized populations of $CD8^+$ $Tetramer^+$ cells were observed in all three donors regardless of the staining protocol used, although the increased MFI values exhibited by the optimised pMHC staining protocol facilitated the separation from the background $CD8^+$ $Tetramer^{neg}$ cells (**Figure 3-13A**).

Next, I examined the TCR repertoire in the responses of two further donors using the immunodominant EBV antigens $LMP2A_{426-434}$ and $BMLF1_{280-288}$ (GLCTLVAML). Parallel staining of donors 4 and 5 with tetramers bearing the $BMLF1_{280-288}$ or $LMP2A_{426-434}$ antigens, respectively, showed a similar % $CD8^+$ $Tetramer^+$ recovery with standard and optimised protocols (**Figure 3-13B** and **D**). TCRβ sequencing of donor 4 sorted $CD8^+$ $Tetramer^+$ cells with each protocol consistently showed a very skewed repertoire comprising two TCRβ chains, where TRBV29-1 TRBJ1-4 CDR3β: CSVGTGGTNEKLFF accounted for >99% and TRBV27 TRBJ2-7 CDR3β: CASTKTREKLYF accounted for <0.1% of the total frequency reads **Figure 3-13B** and **C**). The dominant TRBV29-1 TRBJ1-4 CDR3β: CSVGTGGTNEKLFF TCRβ clonotype has been previously described as a "public" TCR observed in other EBV-infected HLA $A2^+$ individuals[253,306]. Similarly, staining of donor 5 PBMCs with standard and optimised protocols revealed 0.18% of $CD3^+$ to be $CD8^+$ T cells responding to the CLG-antigen. TCRβ sequencing sorted $CD8^+$ $Tetramer^+$ cells revealed 4 shared CDR3β between protocols. However, sorting with standard pMHC staining displayed TCRβ dominance of TRBV10-2 TRBJ1-1 CDR3β: CASSEDGMNTEAFF shared clonotype accounting for ~99% of the total frequency reads, whereas optimised pMHC staining displayed a more even distribution with no acute dominance of a TCRβ clonotype (**Figure 3-13D** and **E**). TCR sequencing results can be found in **Supplementary table 4** and **Supplementary table 5**.

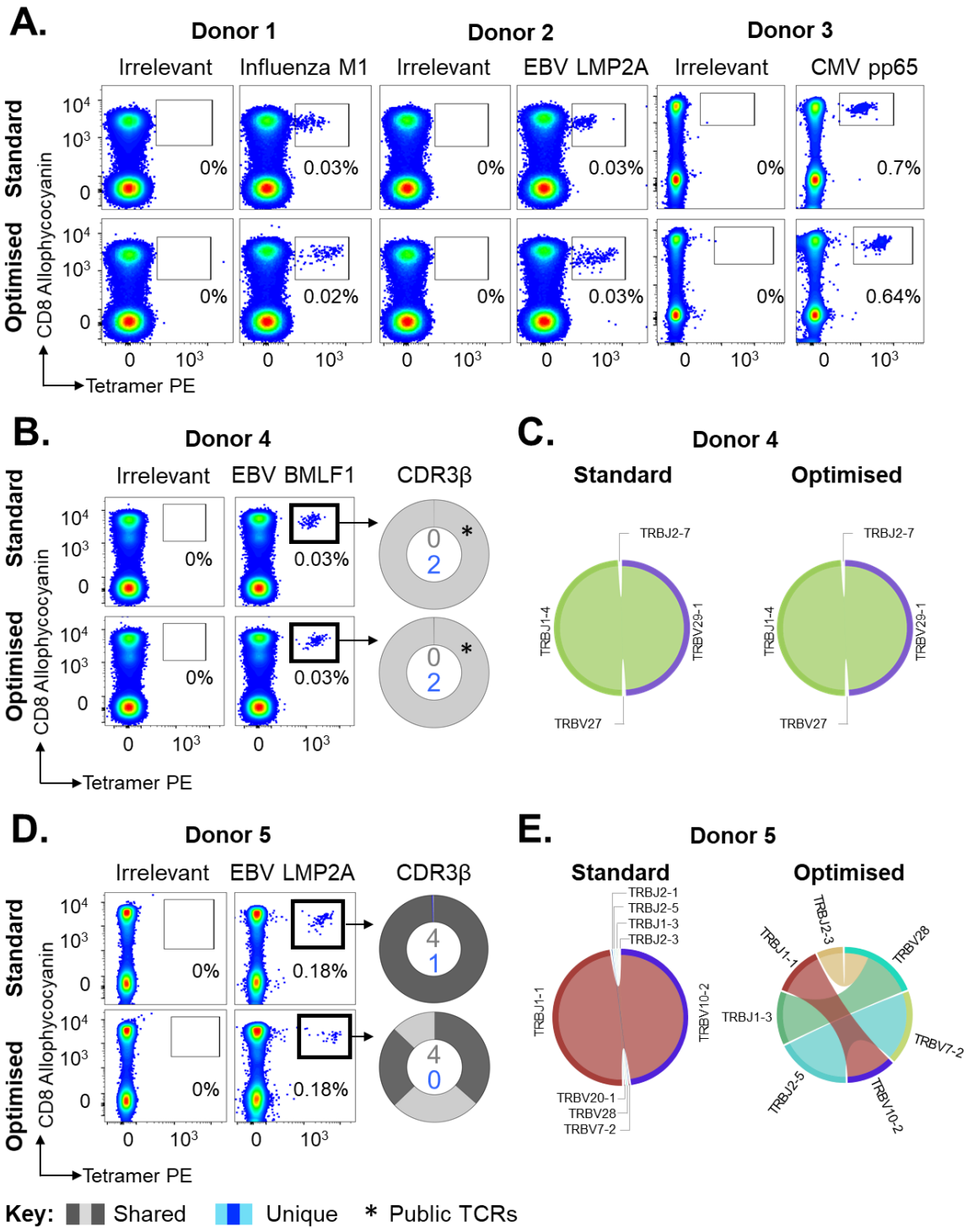

Figure 3-13. Ex vivo detection of virus antigen-specific CD8⁺ T cells using standard pMHC multimer staining technology. Parallel tetramer staining using standard or optimised protocols of the PBMC's from five HLA A2⁺ healthy donors. Tetramers were loaded with Influenza M1$_{58\text{-}66}$ peptide (GILGFVFTL, left), Epstein-Bar virus (EBV) LMP2A$_{426\text{-}434}$ peptide (CLGGLLTMV, middle), Cytomegalovirus (CMV) pp65$_{495\text{-}503}$ peptide (NLVPMVATV, right) **(A)**, EBV LMP2A$_{426\text{-}434}$ **(B)** or EBV BMLF1$_{280\text{-}288}$ (GLCTLVAML) **(D)**. Gates were set on lymphocytes and live CD3⁺CD14^{neg}CD19^{neg} cells. Irrelevant HLA A2–restricted PPI$_{15\text{-}24}$ was used to set the gates. % of CD8⁺ Tetramer⁺ T cells is shown for each gate. TCRβ sequencing and CDR3β analysis of sorted CD8⁺ Tetramer⁺ T cells from donor 4 **(B)** and donor 5 **(D)** are displayed as sections of a donut pie, with each section corresponding to a CDR3β relative to its frequency in the sort. The number of sort-shared (grey) or sort unique (blue) CDR3β for the respective sorts is shown at the centre of each pie. (**C** and **E**) TCRβ Variable (arc on the right) and Joining (arc on the left) gene rearrangement in CD8⁺ tetramer⁺ sorted cells from donor 4 **(C)** and donor 5 **(E)**. Segments represent frequency in sort. Links represent how commonly genes rearrange. Plots were generated using *VDJViz*[252].

The results shown in **Figure 3-13** indicated that standard pMHC tetramer staining with the BMLF1$_{280-288}$ EBV epitope might underestimate the size of the relevant T cell population. This potential deficiency warranted further investigation; therefore, five further HLA A2^{+} donors were stained with BMLF1$_{280-288}$ tetramer. A sizeable population of BMLF1$_{280-288}$-specific T cells could be detected using the optimised staining protocol in all five donors (**Figure 3-14A**). Surprisingly, standard pMHC tetramer staining failed to detect these populations.

TCRβ clonotyping of GLC-specific responses in donor 3205 revealed 2 unique TCRβ sequences with similar dominance using standard pMHC staining protocol, with no shared clonotypes between standard and optimised protocols. In contrast, 17 unique TCRβ sequences were revealed when the optimised protocol was used, where 65% of the response was dominated by the TRBV29-1 TRBJ1-4 CDR3β CSVGGYGTNEKLFF clonotype. Moreover, three public clonotypes were identified: TRBV29-1 TRBJ1-4 CDR3β CSVGTGGTNEKLFF[306] (3.34%), TRBV20-1 TRBJ1-2 CDR3β CSARDRVGNGYTF[307] (1.65%) and TRBV20-1 TRBJ1-3 CDR3β CSARDRVGNTIYF[308] (0.33%) (**Figure 3-14B** and **C**), assuring the efficacy of the optimised pMHC staining in detecting antigen-specific T cells. TCR sequencing results can be found in **Supplementary table 6**.

Donor 0439 was of particular interest, as multiple attempts to stain donor's PBMC with HLA A2-GLCTLVAML tetramer using standard staining protocols over 15 years ago failed to detect a response, resulting in this donor being excluded from the study as a non-responder[309]. The ELISPOT conducted to screen potential responding donors showed that the PBMC from donor 0439 responded to both EBV dominant epitopes LMP2A$_{426-434}$ and BMLF1$_{280-288}$ (**Supplementary figure 2**), however standard pMHC staining with the BMLF1$_{280-288}$ epitope did not elicit a response. The level of response observed by ELISPOT in Donor 0439's PBMCs against the GLCTLVAML peptide translated to ~0.1% of CD3^{+} cells, which was consistent with the 0.15% CD8^{+} Tetramer^{+} cells staining with HLA A2-GLCTLVAML tetramer when optimised protocol was employed, and did not correspond to the lack of pMHC tetramer staining previously observed in this individual using standard tetramer staining. These studies showed that the level of staining observed with the standard protocol was very poor in comparison to the optimised protocol, explaining why it had been previously assumed that this donor did respond to BMLF1$_{280-288}$ peptide (**Figure 3-14D**). TCRβ sequencing of the CD8^{+} Tetramer^{+} populations revealed >100 clonotypes, 10 of which were only detectable with standard pMHC staining protocol, and 119 only detected with optimised staining (**Supplementary table 7**). Only the TRBV7-9 TRBJ1-1 CDR3β CASTFKESIVNTEAFF clonotype was shared between staining protocols but at very different frequencies (29.04% of reads with standard staining and 0.05% of the reads with optimised staining). These results also suggested that the GLC-specific TCRβ repertoire in this donor is very large, showing minimal overlap between replicate samples. However, given the poor mean fluorescence intensity (MFI) values of the staining in the standard pMHC sorted cells, the possible capture of background CD8^{+} Tetramer^{neg} clonotypes that do not respond to the GLCTLVAML peptide cannot be disregarded. Overall, these results indicate once more that standard pMHC staining fails to detect functional T cell clonotypes even with some in viral epitopes previously thought to elicit high affinity TCR responses.

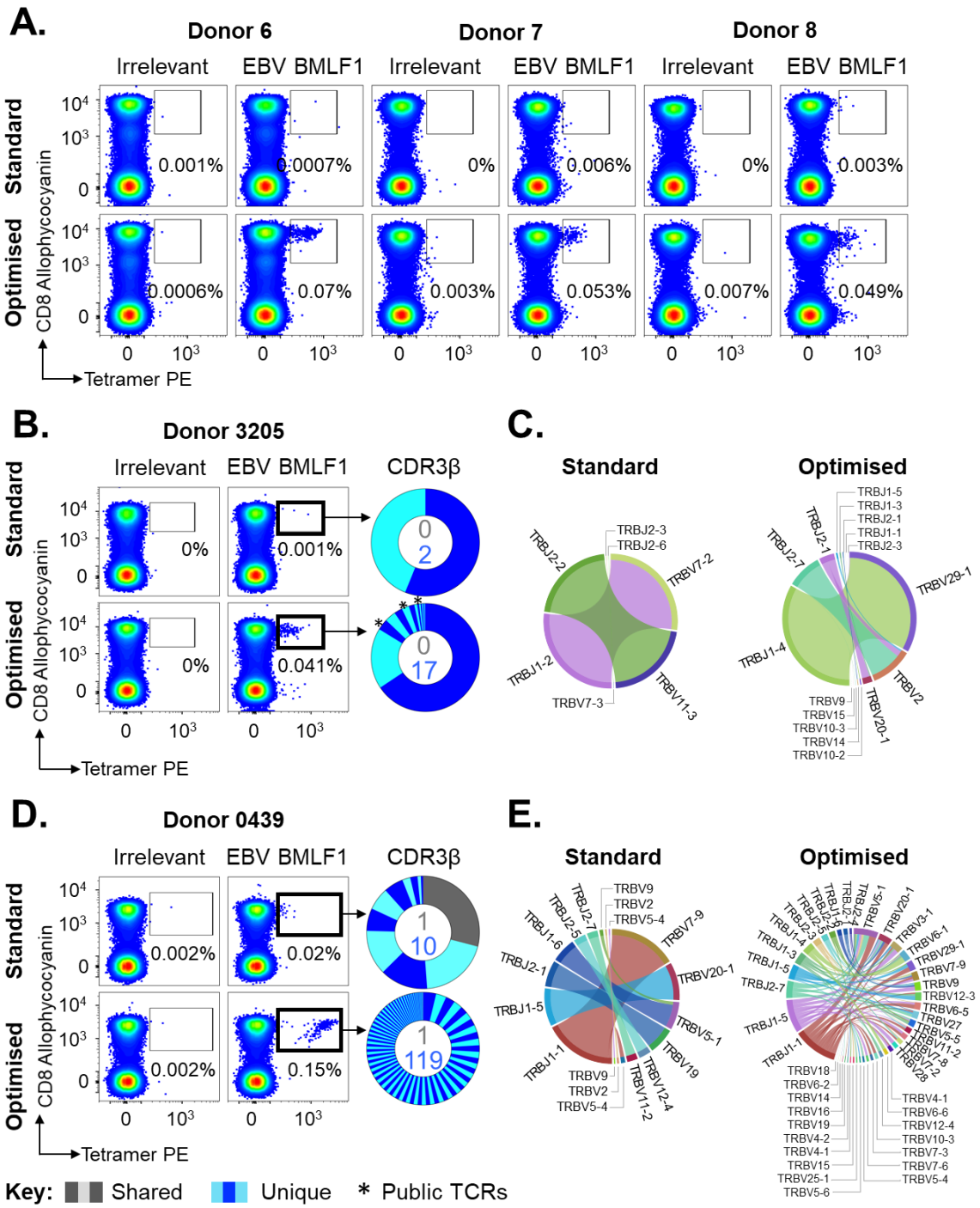

Figure 3-14. **Standard pMHC multimer staining fails to detect EBV-specific CD8⁺ T cells *ex vivo*. (A)** *Ex vivo* staining of PBMC's from three HLA A2⁺ healthy donors using standard or optimised tetramer staining loaded with EBV BMLF1$_{280-288}$ peptide (GLCTLVAML). Gates were set on lymphocytes and live CD3⁺CD14^{neg}CD19^{neg} cells. Irrelevant HLA A2–restricted PPI$_{15-24}$ was used to set the gates. % of CD8⁺ Tetramer⁺ T cells is shown for each gate. CD8⁺ tetramer⁺ T cells from donor 3205 **(B)** and donor 0439 **(C)** were sorted using BMLF1$_{280-288}$ standard or optimised tetramer staining protocols, followed by TCRβ chain sequencing. CDR3β are displayed as sections of a donut pie, with each section corresponding to a CDR3β relative to its frequency in the sort. The number of sort-shared (grey) or sort unique (blue) CDR3β for the respective sorts is shown at the centre of each pie. Public TCRβ clonotypes are indicated with an asterisk. **(C** and **E)** TCRβ Variable (arc on the right) and Joining (arc on the left) gene rearrangement in CD8⁺ tetramer⁺ sorted cells from donor 3205 **(C)** and donor 0439 **(E)**. Segments represent frequency in sort. Links represent how commonly genes rearrange. Plots were generated using *VDJViz*[252]

To formally prove that functional GLC-specific clonotypes failed to stain with standard pMHC staining, I grew monoclonal T cells from the $CD8^+$ $Tetramer^+$ optimised pMHC sorted population from donor 0439. Single cell cloning was performed from a total of 755 $CD8^+$ $Tetramer^+$ cells sorted in the presence of irradiated allogenic PBMC and PHA as described in **Materials and Methods (sections 2.2.4** and **2.2.5)**, followed by screening for functionality. Only 4 clones grew to a sufficient level for experimentation. TCR sequencing showed that all four clones expressed the same TCR made from pairing TRAV5 TRAJ15 CDR3α CAEKGAGTALIF and TRBV29-1 TRBJ1-5 chain CDR3β CSVAGTGDLNQPQHF. This clone was named CR0439.GLC and, although not observed in the TCRβ repertoire from the first sort, it showed a preferential bias towards *in vitro* expansion. My laboratory has observed similar culture bias on numerous occasions. The reasons underlying preferential adaptability of some T cell clones to *in vitro* culture remain unknown, but the ability of only some clones to expand to large numbers *in vitro* may reflect a specific mutation or some aspect of the phenotype at the time of culturing.

The $CD8^+$ CR0439.GLC T cell clone failed to stain with standard protocol but stained efficiently with optimised protocol, suggesting that this clone is a representative of the TCRβ clonotypes identified only with the optimised protocol in the PBMC of donor 0439 (**Figure 3-15A**, left). In contrast, a clone generated from the PBMC of another donor using standard pMHC tetramer staining, GD.GLC17, expressing the public TCR: TRAV5 TRAJ31 CDR3α CAEDNNARLMF and TRBV20-1 TRBJ1-3 CDR3β CSARVGVGNTIYF, effectively stained with both standard and optimized protocols (**Figure 3-15A**, right). Overnight activation of clone CR0439.GLC with titrated GLCTLVAML peptide showed sensitivity to cognate antigen even at concentrations <1nM (**Figure 3-15B**) and recognition of autologous EBV-infected LCL (**Figure 3-15C**). These data confirm that standard pMHC tetramer staining misses fully functional anti-viral T cell clonotypes.

To further emphasize the relevance of using optimised pMHC staining as a routine, both CR0439.GLC and GD.GLC17 $CD8^+$ T cell clones were spiked into HLA $A2^{neg}$ PBMCs at ~1% of total cells, followed by HLA A2-GLCTLVAML tetramer staining using standard and optimised protocols. As expected, the high affinity TCR expressed by clone GD.GLC17 allowed the recovery of the cells with both protocols, although the optimised protocol showed increased MFI. In contrast, the CR0439.GLC T cell clone bearing a low affinity TCR could only be recovered with optimised pMHC tetramer staining (**Figure 3-15D**). Conveniently, the previously described $CD8^{high}$ nature of cultured T cell clones[267] allowed visualization of the clone within the PBMCs without the need for tetramer staining.

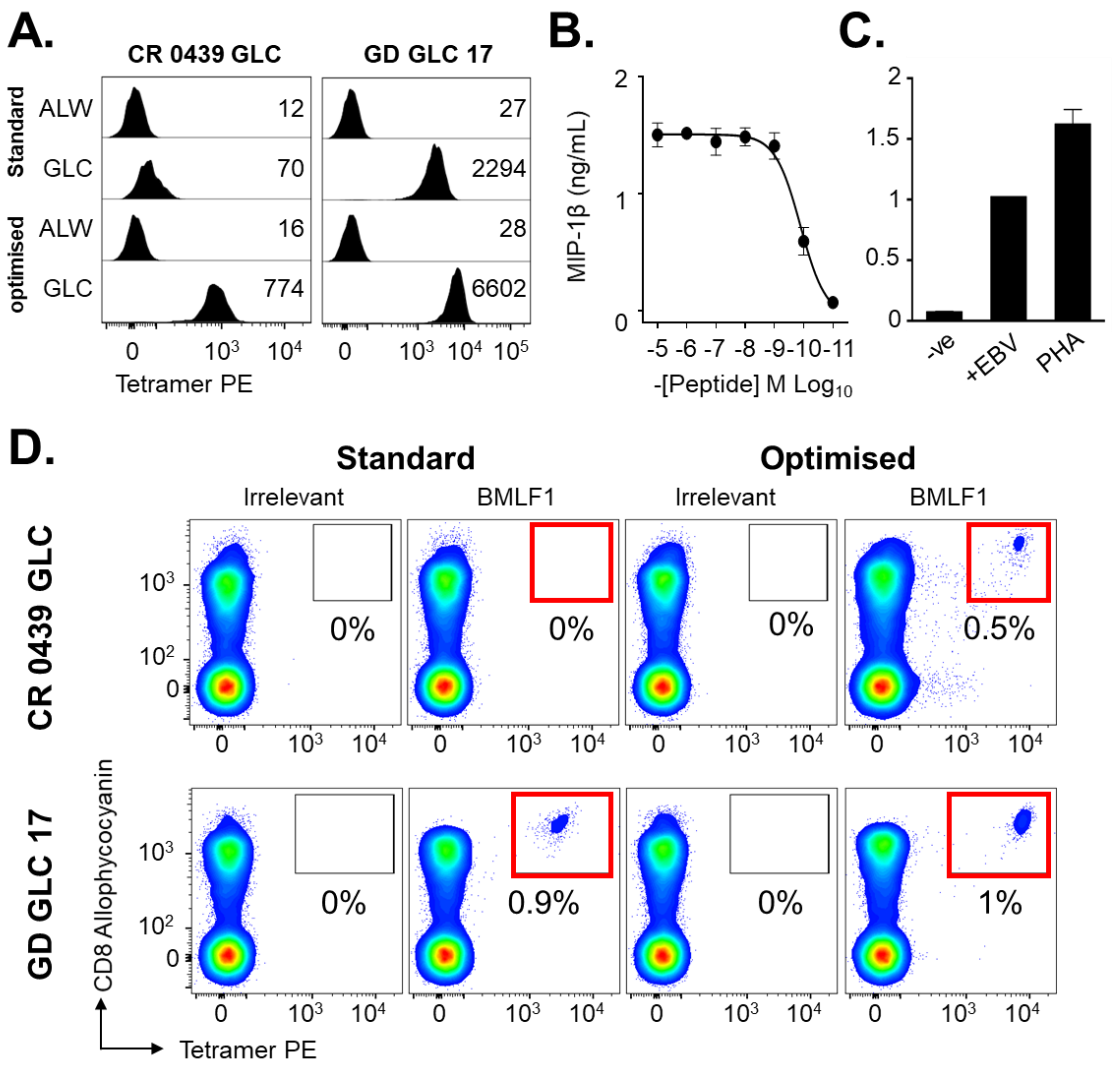

Figure 3-15. **EBV-specific CD8+ T cell clones bearing a low affinity TCR show anti-viral effector functions. (A)** The BMLF1$_{280-288}$-specific CR0439.GLC CD8$^+$ clone (left) and GD17.GLC public CD8$^+$ clone (right) were stained with HLA A2–GLCTLVAML tetramer using standard or optimised staining protocols. HLA A2-ALWGPDPAAA irrelevant tetramer was used as control. MFI values are displayed. **(B)** CR0439.GLC CD8$^+$ clone overnight activation against the BMLF1$_{280-288}$ peptide at different concentrations as measured by MIP-1β release. . EC$_{50}$ values of peptide sensitivity are shown. **(C)** CR0439.GLC CD8$^+$ clone overnight activation against HLA A2$^+$ EBV-infected autologous cells measured by MIP-1β release. Responses to uninfected autologous LCLs (-ve) and PHA as negative and positive controls, respectively, are shown. **(D)** Recovery of the EBV BMLF1$_{280-288}$-specific CR0439.GLC (top panel) and GD17.GLC (bottom panel) T cell clones spiked into HLA A2^{neg} PBMC at ~1% of CD3$^+$ cells using standard and optimised protocols with HLA A2–GLCTLVAML and irrelevant HLA A2-ALWGPDPAAA. Cells were gated on lymphocytes, then viable CD3$^+$ CD14^{neg} CD19^{neg}. Percentages are shown for the respective gates.

I next examined whether optimised pMHC multimer staining could be of benefit when detecting other anti-viral responses by extending my findings to Yellow Fever virus.

3.2.7. Staining with Optimised pMHC dextramer protocol reveals a more heterogeneous Yellow Fever-specific response

Yellow Fever (YF) virus prevention is currently accomplished by immunisation with the live attenuated YF-17D vaccine, which generates an immunodominant HLA A2-restricted CD8+ T cell response towards the residues 214-222 of the Non-structural protein 4b epitope (NS4B, LLWNGPMAV) [310–312]. Some studies have aimed to characterise the size of T cell responses in vaccinated patients using tetramers loaded with the $NS4B_{214-222}$ epitope[310,313,314]; however, due to the evidence presented above, it is possible that previously published studies underestimated the LLW-specific response. Therefore, I sought to determine if the immunodominant responses towards the YF $NS4B_{214-222}$ epitope could benefit from the use of optimised pMHC multimer technology.

Because directly *ex vivo* detection of LLW-specific T cells was challenging due to the low number of antigen-specific T cells, PBMCs of a vaccinated donor (0345) and two unvaccinated donors (9 and 10) were cultured with 10^{-5}M LLWNGPMAV peptide for 14 days to expand a cell population for analysis. The resultant cultured lines were stained with tetramers bearing the immunodominant $NS4B_{214-222}$ epitope using standard and optimised pMHC protocols. Consistent with previous observations with EBV $BMLF1_{280-288}$-specific $CD8^+$ T cells, optimised pMHC tetramer staining revealed higher numbers of $CD8^+$ $Tetramer^+$ T cells accompanied by increased MFI values that facilitated separation from the $CD8^+$ $Tetramer^{neg}$ population. Interestingly, unvaccinated donors 9 and 10 stained with the optimised protocol exhibited large LLW-specific populations (0.08% and 0.5%, respectively) that could be the result of potential cross-reactive responses to either Yellow Fever virus or other closely related viruses[315–317] (**Figure 3-16A**).

To further examine the characteristics of TCR repertoire used by YF $NS4B_{214-222}$ T cells, I sequenced the TCRs from 0345 vaccinated donor $CD8^+$ cells stained with YF $NS4B_{214-222}$ tetramer by standard and optimised procedures (**Figure 3-16B**). Previous studies conducted by my group have shown that higher-order multimers are better at staining T cells bearing low affinity TCRs[265], thus allowing the maximal recovery of T cells from PBMC for TCR repertoire analysis. Optimised dextramer staining of donor 0345 cells doubled the population of $CD8^+$ $Tetramer^+$ T cells identified with optimised staining protocol (0.08% in **Figure 3-16A** versus 0.17% in **Figure 3-16B** of total $CD3^+$ cells). TCR repertoire analysis of sorted cells using HTS revealed 9 CDR3α and 9 CDR3β sequences for the standard dextramer-stained cells (n=750 cells sorted), in contrast to the 27 CDR3α and 18 CDR3β sequences revealed for the optimised dextramer-stained cells (n=2,066 cells sorted). Sorts shared 8 CDR3α and 6 CDR3β sequences, leaving 19 CDR3α and 12 CDR3β unique sequences being exclusively revealed with optimised dextramer staining protocol, from which four public TCRα chains were identified: TRAV12-2 TRAJ30 CDR3α CAVIGDKIIF, TRAV12-2 TRAJ30 CDR3α CATGDDKIIF, TRAV12-2 TRAJ27 CDR3α CAVIAGKSTF and TRAV12-2 TRAJ31 CDR3α CAVNNARLMF (**Figure 3-16B** and **Supplementary table 8**).

Moreover, standard pMHC dextramer sorting revealed a V-gene dominance shared by TRAV16 (~51% in sort, dominated by TRAJ37 pairing) and TRAV12-2 (~44.6% in sort, paired with several J-gene usages) and TRBV20-1/TRBJ2-7 (~52%). Consistent with previous characterisation of the LLW-specific response[318], optimised sort revealed an acute TRAV12 usage bias (~79% of total TRAV gene usage) paired with a more diverse TRAJ usage. Vβ-gene and Jβ-gene usage dominance in the optimised sort was shared between clonotypes expressing TRBV15/TRBV20-1, and TRBJ2-7/TRBJ2-1, respectively, although no Vβ-gene bias has been previously described for LLW-specific T cell responses (**Figure 3-16C** and **Supplementary table 9**).

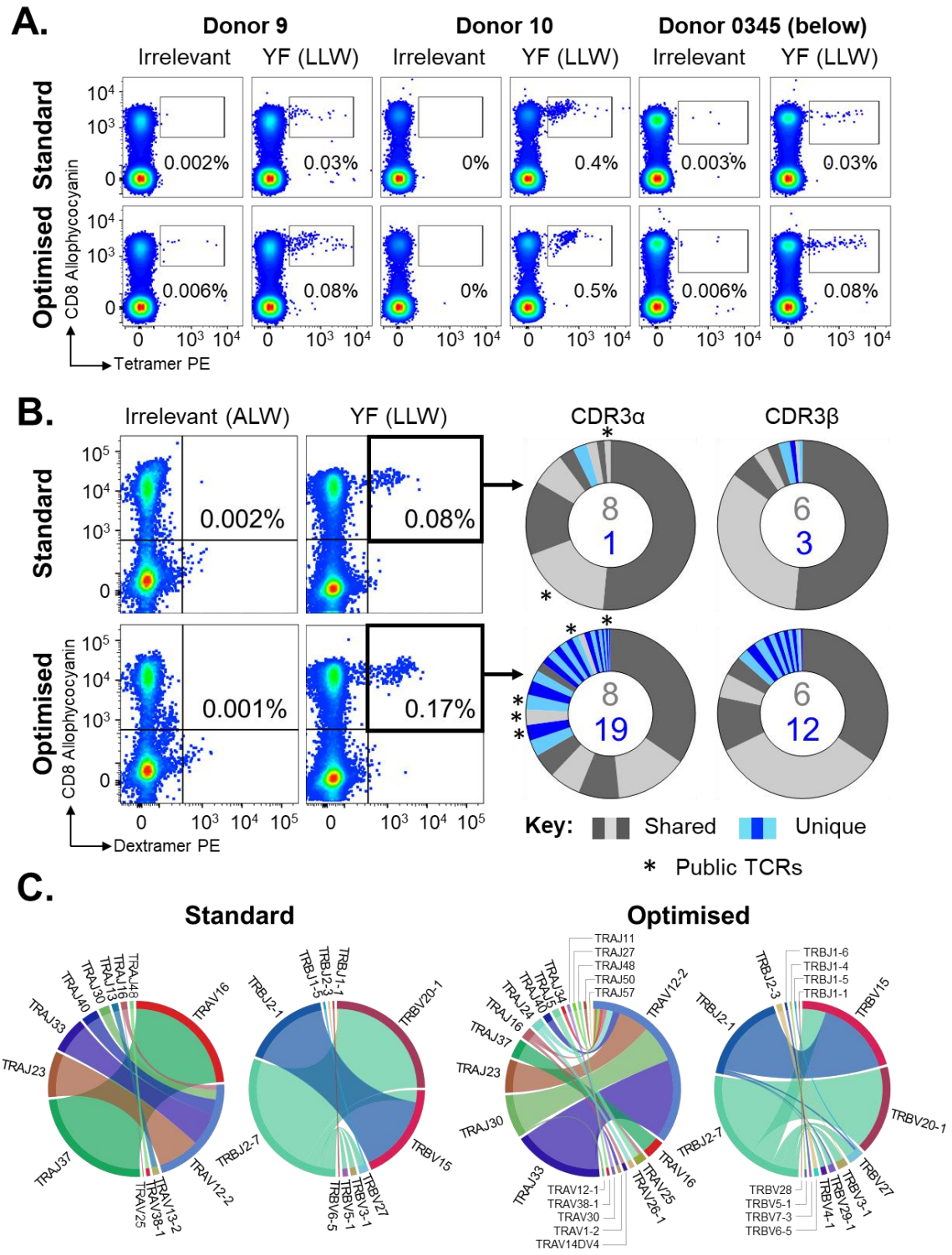

Figure 3-16. Optimised pMHC tetramer and dextramer staining reveals greater diversity in Yellow Fever-specific TCR repertoire. **(A)** Staining of T cell lines from three HLA A2⁺ donors using standard or optimised tetramer staining loaded with the $NS4B_{214-222}$ peptide (LLWNGPMAV). Gates were set on lymphocytes and live $CD3^{+}CD14^{neg}CD19^{neg}$ cells. Irrelevant HLA A2-restricted PPI_{15-24} was used to set the gates. % of $CD8^{+}$ $Tetramer^{+}$ T cells is shown for each gate. **(B)** T cell line from the HLA A2⁺ YF-vaccinated donor 0345 was sorted using $NS4B_{214-222}$ standard or optimised dextramer staining protocols (**left**) followed by TCRα and β chain sequencing (**right**). CDR3s are displayed as sections of a donut pie, with each section corresponding to a CDR3s relative to its frequency in the sort. The number of sort-shared (grey) or sort unique (**blue**) CDR3s for the respective sorts is shown at the centre of each pie. Public TCR clonotypes are indicated with an asterisk. **(C)** TCRα and TCRβ Variable (arc on the right) and Joining (arc on the left) gene rearrangement in $CD8^{+}$ $tetramer^{+}$ sorted cells from donor 0345. Segments represent frequency in sort. Links represent how commonly genes rearrange. Plots were generated using *VDJViz*[252].

3.3. Discussion

The incorporation of pMHC multimers to the immunology toolbox has revolutionised the study of antigen-specific T cell populations by enabling their direct analysis in *ex vivo* samples without the prior need for activation or concomitant alteration of phenotype. Several recent reports indicate that standard pMHC multimer staining might fail to detect a significant fraction of functional antigen-specific T cells[268,271,272], thus introducing a bias that underestimates the lower affinity component of antigen-specific polyclonal responses[86]. The results presented in this Chapter support this statement and formally document that fully functional T cell clonotypes can fail to stain with standard procedures. Furthermore, the inherent diversity of the TCR genetic footprint provides a unique barcode that enables the tracking of T cell responses throughout the development of the immune response. A combination of pMHC multimer staining and HTS of antigen-specific cells forms an attractive platform for the characterisation of antigen-specific TCR repertoires in any clinical setting.

I initiated my studies by staining the TIL infusion product that was used to induce complete remission of patient MM909.24 with stage IV melanoma with pMHC tetramers bearing the heteroclitic version of the HLA A2-restricted peptide Melan-$A_{25\text{-}35}$. It became clear that standard pMHC tetramer staining missed T cell clonotypes that could respond well to autologous tumour. Due to the potential importance of this finding, I next extended my studies to a further novel cancer-associated epitope IMP-$2_{366\text{-}376}$ (described in **Chapter 4**). The optimal pMHC multimer staining protocol, that included PKI and cross-linking Ab, was able to detect functional T cell clonotypes that could not be detected using standard procedures in parallel. Some of the optimally-recovered clonotypes in the TIL product were enriched in the blood of patient MM909.24 after complete melanoma remission. Indeed, three persistent TCR clonotypes that could not be detected with standard pMHC tetramer staining accounted for ~44% of the entire anti-tumour response in the patient's blood, suggesting their significant contribution to tumour clearance. The significance of these results further underlines how weak TCR-pMHC multimer affinities observed *in vitro* may not mimic *in vivo* TCR-pMHC affinity.

I next extended my studies to anti-viral responses. Anti-viral TCRs are known to bind cognate pMHC with relative high affinity, and the general assumption is that standard pMHC staining efficiently recovers the antigen-specific response. I found that these assumptions were upheld during staining of healthy PBMCs with pMHC tetramers specific for HLA A2–restricted epitope from Influenza $M1_{58\text{-}66}$, CMV $pp65_{495\text{-}503}$ and EBV $LMP2A_{426\text{-}434}$, across multiple donors, although staining with optimal pMHC tetramer protocol showed a considerable increase in the intensity of the staining without an adverse signal/noise effect. In contrast, staining of healthy PBMCs with pMHC tetramers specific for HLA A2–restricted epitope from EBV $BMLF1_{280\text{-}288}$ and staining for Yellow Fever Virus $NS4B_{214\text{-}222}$–specific cells in HLA $A2^+$ healthy and vaccinated donors, revealed that the incorporation of Protein Kinase Inhibitor (PKI) and anti-fluorochrome cross-linking antibody could improve the identification of these anti-viral responses.

Collectively, I have demonstrated that standard pMHC multimer staining of antigen-specific T cells can fail to detect fully functional T cells across multiple systems. I therefore conclude that standard pMHC tetramer staining, as used in numerous previous studies, can substantially underestimate the size of antigen-specific T cell populations. My findings are consistent with other reports that were published during my experimentation. For instance, *Davis and colleagues*[271] showed that pMHC dodecamers provided a significant advantage over tetramers for the detection of antigen-specific $CD4^+$ and $CD8^+$ T cells. These results confirmed earlier studies undertaken by my own laboratory comparing parallel staining with pMHC tetramers and dextramers[265]. However, *Davis and colleagues* did not incorporate the use of PKI to prevent TCR downregulation or antibody cross-linking to stabilise the TCR-pMHC complex, so it is possible that further integration of these reagents could potentially reveal larger antigen-specific T cell populations as we detected in some samples using pMHC dextramers.

Evavold and colleagues[272] described a discordance in the detection Lymphocyte choriomeningitis Virus (LCMV) and myelin oligodendrocyte glycoprotein (MOG)–specific murine CD4+ T cell populations using pMHCII tetramers and 2D analysis[319], indicating the presence of an heterogeneity in the TCR affinity in functional polyclonal responses that might have been overlooked due to the avidity limitations inherent to pMHCII reagents. Subsequent studies performed by my group further demonstrated the benefits of incorporating PKI treatment and anti-fluorochrome antibody cross-linking during pMHCII tetramer and dextramer isolation of auto-reactive T cells in patients with Type 1 Diabetes and Ankylosing Spondylitis[285].

Overall, I have confirmed that optimal pMHC multimer isolation of antigen-specific T cells can detect fully functional T cells that are missed by standard procedures. It has been suggested that the extensive use of pMHC multimer staining over the last twenty years may have introduced a bias that has continually underestimated the lower-affinity, but functional, components within diverse Ag-specific TCR repertoires[86]. Accumulating evidence suggests that T cells with very low–affinity TCRs can make important contributions to immunity *in vivo*[272–275,320,321]. Further work will be required to determine whether the optimal staining procedure as used here is capable of revealing all functional clonotypes.

In summary, all pMHC multimer staining described in this thesis was performed following the optimised pMHC tetramer protocol, unless otherwise stated. Of note, incubation with PKI was observed to be as effective when incubation time was reduced from 30 to 5 minutes, and anti-fluorochrome antibody could be added in conjunction with surface antibody staining, resulting in an effective, rapid staining protocol that I made use of for examining antigen-specific T cell responses in TIL in **Chapter 4**.

– Chapter 4 –

Dissection of successful TIL therapy for melanoma

4.1. Introduction

Cytotoxic $CD8^+$ T cells play an important role in tumour clearance, as demonstrated by the remarkable success of T cell checkpoint inhibitors for some cancers[180,185,186,322]. T cells have also successfully cleared late stage cancer during numerous ACT studies where *in vitro* reactivated and expanded TILs induced cancer regression when transferred back into the patient (reviewed in [193]). Tolerogenic mechanisms can be overcome with adoptive cell transfer therapies, as it enables the selection and activation of highly reactive T cell populations and manipulation of the host environment. However, aside from highly immunogenic cancers like melanoma, renal cell carcinoma, ovarian and lung cancer, the *in vitro* expansion of sufficiently high numbers of TILs to exert anti-cancer activity has proven challenging. Development of successful $CD8^+$ T cell therapies directed at the targeting of a comprehensive number of malignancies has the potential of revolutionising the field of cancer immunotherapy. However, clinical translation has been limited due to challenges in the identification of suitable target antigens as well as TCRs that are both safe and effective. Effective T cell targeting of cancer requires that three main challenges are overcome. First, the targeted antigenic ligands must be expressed in cancer but not healthy cells. Second, peptide ligands must be presented by class I molecules at the surface of cancer cells; and thirdly, selected ligands must be recognised by the TCRs with sufficient affinity to generate an immunogenic response. Dissection of persistent tumour-specific T cell clones associated with complete tumour regression after adoptive transfer of TILs may encompass the key to overcome all these hurdles. *Robbins and colleagues*[323] demonstrated that persistence of adoptively transferred lymphocyte clonotypes correlated with metastatic melanoma regression in patients receiving T cell transfer therapy. Posterior analysis of the antigen specificity these highly persistent T cell clonotypes in the blood of melanoma patients revealed that Melan-A-specific T cells were present in those patients achieving almost complete responses[324]. Closer examination of a tumour-specific TIL-derived T cell clones persistent in the blood of one patient 5 months after therapy revealed recognition of a novel mutated HLA class I molecule expressed on autologous tumour cells[325]. The antigen specificity of very few persistent T cell clones after adoptive transfer of TILs has ever been determined. The antigens recognised by such T cell clones might provide an illuminating signpost towards the types of response that are able to clear cancer. The main goal of my project was to dissect the responses in the TIL infusion product used to successfully treat HLA $A2^+$ Stage IV melanoma patient MM909.24 studies in **Chapter 3**. I was especially interested in the responses that were mediated through HLA A2 as this is the most common HLA-I allele in the population. I reasoned that the TIL of patient MM909.24 might respond to new peptide epitopes that could potentially be successfully utilised for downstream immunotherapy approaches.

4.1.1. Dissection of tumour-specific persistent TCRs

Tumour regression following adoptive T cell transfer in some patients has led to attempts to understand the nature of these responses by identifying novel immunogenic antigens. As activated T cells are generally transferred to patients in large number during TIL therapy, the responses seen in complete remission patients without side effects should have a high chance of being safe to use in other patients. Thus, dissection of the persistent anti-cancer T cell responses following successful TIL therapy has potential to reveal responses that are both safe and effective. I was particularly interested in establishing whether any of the antigens targeted during successful TIL therapy might also be effective for targeting other 'cold' tumours that do not have large $CD3^+$ cell infiltrates that can be studied.

Optimal broadly cancer-specific T cell antigens should, *a priori*, be expressed on multiple cancers, but not on essential healthy tissue. Ideally, such targets should also be crucial for cancer survival, proliferation and/or metastasis so as to prevent immunoevasion through downregulation of target[326]. However, the characterisation of ligands involved in tumour clearance has historically been challenging.

Several different classes of tumour antigens are currently being exploited in cancer immunotherapy. For instance, TSAs generally result from tumour-specific mutations, which translates into the expression of neoantigens that are exclusively expressed by tumour cells. Evidence of $CD8^+$ T cell neoantigen targeting was initially provided by *Robbins and colleagues*[327]. Persistent T cell clonotypes that achieved complete tumour regression in a melanoma patient after adoptive transfer of TILs, were shown to recognise two neoantigens derived from GAS7 (growth arrest-specific gene 7, residues 281-290) and GAPDH (glyceraldehyde-3-phospate dehydrogenase, residues 169-178). The authors used a strategy based on the phage display developed by *Parmley* and *Smith*[328] to identify ligands, where pools of autologous tumour cDNA libraries of phage expressing 10^7-10^9 different tumour peptides were used to screen for their ability to stimulate IFNγ release from bulk TIL populations, followed by sequencing, computational HLA A2 binding prediction of candidate peptide, and target validation (**Figure 4-1A**).

Another approach for selecting the optimal cancer-associated target is based on whole-exome sequencing (WES) to identify non-synonymous mutations in tumours, followed by *in silico* analysis for prediction of epitope binding to MHC and confirmation of recognition by autologous T cells[329–331] (**Figure 4-1B**). Several authors have employed WES to determine the mutational load of patients with pancreatic cancer[223], melanoma[332], non-small cell lung cancer[333] and classical Hodgins lymphoma[334]. Thus, the discovery of enhanced T cell immunity to tumour point mutations resulted in a major shift in the field towards the utilization of personalised immunotherapies to selectively target neoantigens. However, the vast majority of non-synonymous mutations lead to non-immunogenic neoantigens which are generally patient unique[332], thus making the treatment highly individualised and complex. Neoantigen therapy can also lead to loss-of-function mutations, for example in β2m, that result in unresponsiveness to therapy[335]. Moreover, several

authors have now reported the existence of fewer than expected neoantigen-specific TILs that mediate tumour rejection[168,336,337]. Although the identification of unique neoantigens has the potential to develop into highly effective personalized immunotherapeutic interventions, shared TAAs constitute an ideal group of antigens for the future development of broadly applicable cancer immunotherapies.

A very versatile approach was developed by *Bentzen and colleagues*[261] using DNA-labelled multimers. The utility of pMHC multimers to detect antigen-specific T cells has been discussed in **Chapter 3**. In their approach, *Bentzen and colleagues* incorporated short DNA barcodes to the fluorescently-labelled pMHC scaffold, allowing the identification of $>10^{10}$ potential different pMHC complexes in a single sample. Thus, testing peptides for T cell recognition could be sourced from WES, RNAseq or single-aminoacid substitutions from cognate peptide (if known). pMHC-bound cells are then sorted based on fluorescent label and the composition of the DNA-labelled multimer is sequenced (**Figure 4-1C**). The greatest advantage presented by this approach is the capacity to use the relative DNA barcode reads to determine the frequency composition of antigen-responsive T cells in a polyclonal sample based on the number of interactions detected. However, several factors such as efficient production and peptide synthesis capabilities can limit library sizes.

An alternative method for the identification of T cell ligands was presented by *Patel and colleagues*[338] by demonstrating the robustness of using whole genome Genome-scale CRISPR/Cas9 Knock-out (GeCKO) libraries in the identification of CD58 and members of the JAK/STAT signalling pathway as targets of the clinically tested NY-ESO αβ TCR. Briefly, the GeCKO screen is based on the interaction of two cell types: the target and the T cells. Targets are engineered with a CRISPR/Cas9 library targeting a single gene per cell, and T cells used as selecting factor to determine which disrupted genes confer resistance to T cell-mediated lysis of target; thus allowing the identification of genes important in T cell immunity (**Figure 4-1D**). Similar conclusions were reached in my laboratory by Dr Legut[326], Dr Wheeler[339] and Dr Crowther[340], by using GeCKO libraries for the discovery of antigens recognised by non-HLA restricted T cells. However, αβTCR degenerate recognition of multiple antigens can achieve recognition of the GeCKO engineered tumours regardless of the CRISPR/Cas9-mediated loss of target; and thus, this approach was considered suboptimal for the purpose of my investigations.

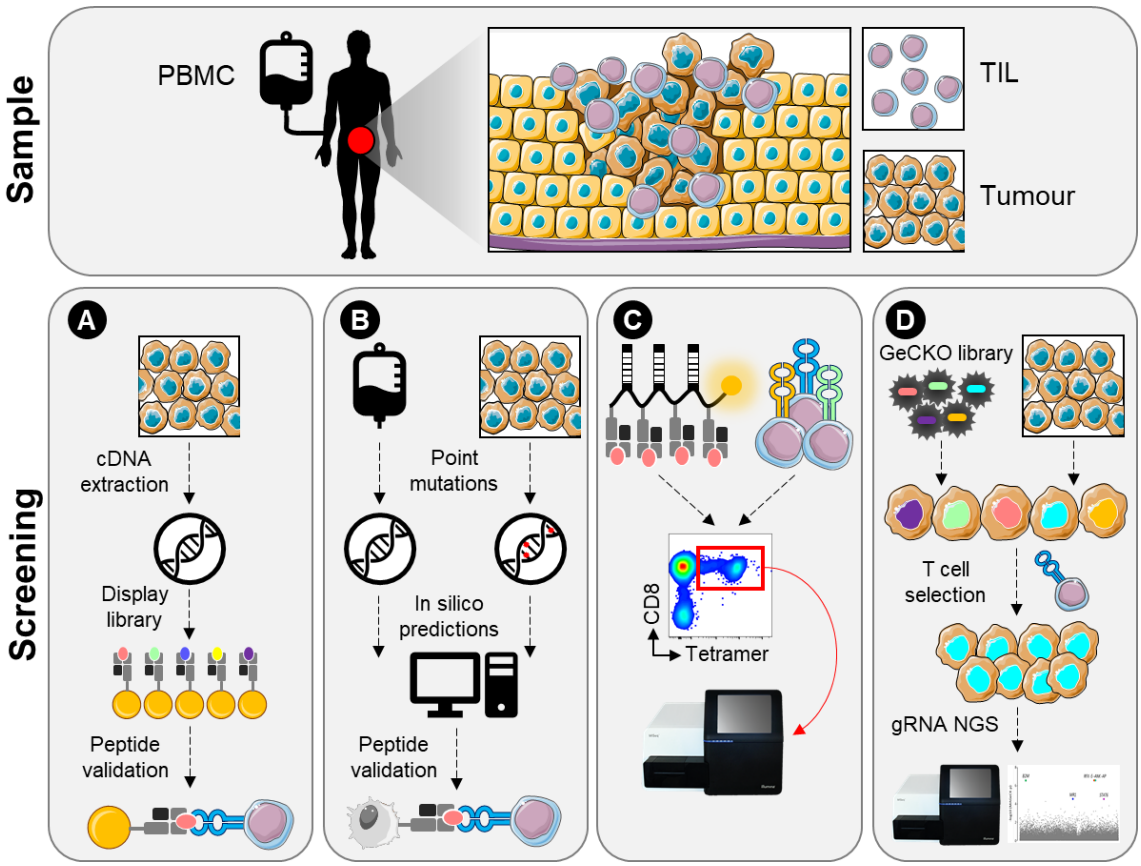

Figure 4-1. **Methods for antigen identification of orphan TCRs present in TILs. (A)** Surface display libraries. Libraries encoding fragmented cDNA derived from a patient's tumour sample and the HLA of choice are cloned into yeast[341] or phage to stably transfect into target cells for surface display[327]. T cell response-inducing libraries can be sequenced and peptides validated based on the capacity to induce a functional T cell response. **(B)** The tumour mutational load can be determined by WES and RNAseq. Parallel sequencing of tumour biopsies and normal cells allows for a comprehensive identification of somatic protein-coding mutations. *In silico* algorithms enable the prediction of HLA binding of candidate peptides[342]. Peptide are synthetized and validated based on the capacity to induce a T cell functional response. **(C)** DNA-labelled pHLA multimers can be loaded with peptides of choice. Peptides can be derived from any of the aforementioned approaches. Monoclonal or polyclonal populations of TILs can be assayed in a "one pot" strategy. **(D)** GeCKO libraries encoding for a CRISPR/Cas9 targeting a single gene per cell are transduced into target tumours. T cells are used as selecting factor, so that CRISPR/Cas9 encoding for antigenic target will be resistant to killing. gRNAs transduced into outgrowing tumour cells are then sequenced and target genes identified. Antigenic peptide sequence must then be investigated.

4.1.2. PS-CPL-based cancer antigen discovery

Positional Scan Combinatorial Peptide Libraries (PS-CPLs) for *n-mer* peptides are characterised by a fixed amino acid residue position and randomised amino acid residues in all other positions (see **section 2.3.8**). PS-CPLs were introduced as an approach to allow identification of unknown epitopes and binding motifs[343]. With the rise of cancer peptide vaccines, PS-CPLs have been employed to optimise cognate sequences based on the amino acid preference observed at a certain backbone position[344]. A recent study from my laboratory showed the potential of PS-CPLs to generate super-agonist altered peptide ligands (APL) from a T cell clone recognising the Melan-A_{26-35} peptide[178]. In our study, we showed that Melan-A specific T cells that recognise the super-agonist peptide MTSAIGILPV demonstrated improved killing of melanoma tumour *in vitro*[178].

PS-CPLs allow for an assessment of peptide specificity that is applicable to all TCRs, irrespective of their specificity or MHC restriction. Since this approach is based on the screening of highly convoluted peptide mixtures, the large body of data generated usually requires computational analytic tools. An algorithm for predicting peptides from PS-CPL data was designed by Zhao and coleagues[345]. In their model, potential peptides were constructed based on the sum of individual recorded responses of T cells to a specific fixed position. Results were then used to search for predicted stimulatory peptides in public protein databases. However, such analyses did not account for peptide-HLA binding, and thus many predicted peptides failed to elicit T cell responses.

Previous data from my group has shown how T cell interrogation of peptide backbone preferences using PS-CPLs allows for the identification of antigenic targets in viral and self-protein databases[99,177,346]. Dr G. Dolton and Dr. B. Szomolay have further expanded the scope of the database by including tumour-associated antigens from across the published literature, including TANTIGEN[347], NCBI (National Center for Biotechnology Information), UniProt (Universal Protein Resource), and PDB (Protein Data Bank) (Dolton, Szomolay *et al*. manuscript in preparation). Once accepted for publication, this CPL-based database search will been integrated into the current WSBC framework webtool (http://nero.wsbc.warwick.ac.uk/tools/user_cases.php). In brief, this database was built from various mathematical algorithms that allow the identification of HLA-binding antigenic peptides present in the sequences of previously published cancer-associated proteins. The algorithm assigns a ranking score that relates to likelihood of TCR recognition to each peptide. The predictive value of the algorithm is then validated by measuring functional sensitivity of the T cell clone under investigation for a selection of peptides from the predicted agonist list.

In this chapter I developed a strategy to identify immunogenic ligands for *in vitro* grown αβ T cell clones using a combination of PS-CPL screening, validation of predicted cancer peptide recognition and validation of HLA-presentation by CRISPR/Cas9 technology.

4.1.3. Aims and hypothesis

The aim of my studies was to dissect successful TIL therapy by examining cancer-specific T cell responses in the *in vitro* expanded TIL infusion product from the stage IV melanoma patient (MM909.24) presented in **Chapter 3**. I hypothesised that examination of cancer-specific TCRs and their antigen-specificities could identify clinically relevant therapeutic agents. Previous characterisation by Dr V. Bianchi of MM909.24 T cell responses via HLA A2 showed that substantial responses were made towards the Melan-A protein[286], and to a lesser degree towards other well characterised HLA A2-restricted melanoma-associated antigens described by *Andersen and colleagues*[348]. I hypothesised that antigens eliciting an anti-tumour response in the TILs of patient MM909.24 may not be restricted to melanoma cells, thus constituting a source of broadly cancer-reactive TCRs that could be explored as immunotherapeutic agents available for the treatment of a wider range of malignancies. Since re-infusion of TILs did not elicit therapy-associated off-target side effects in terms of T cell-mediated autoimmunity in patient MM909.24, I contemplated the possibility that such anti-tumour TCRs could be safe for TCR-based therapies.

I therefore aimed to elicit TCR clonotypes from the MM909.24 TIL that mediated HLA A2-restricted cytotoxicity of a broad tumour panel arising from different tissues. I was particularly interested in those clonotypes that persisted in the PBMC of patient MM909.24 after therapy and exhibited broad recognition of cancer malignancies, such as CR24 and VB6G4.24 T cell clones presented in **Chapter 3**. I set out to identify the antigen(s) eliciting TCR broad tumour recognition. In order to identify such targets, an “epitope discovery pipeline” was designed encompassing PS-CPL screens, *in silico* examination of candidate TAAs and validation of targets using lentiviral transduction and CRISPR/Cas9 technology.

4.2. Results

4.2.1. The majority of tumour-specific T cells in the TIL from patient MM909.24 are HLA A2-restricted

Previous characterisation of T cell responses in patient MM909.24 by Dr V. Bianchi[291] showed strong reactivity of the TIL infusion product used to treat this patient towards the Melan-A_{26-35} (HLA A2-EAAGIGILTV) antigen, and to a lesser degree towards other well characterised HLA A2-restricted melanoma-associated antigens described by *Andersen and colleagues*[348], including $gp100_{476-485}$ (MLGTHTMEV), $MG50_{1243-1251}$ (RLGPTLMCL), $p53_{187-197}$ (GLAPPQHLIRV), and TRAG-3_{58-66} (ILLRDAGLV). For my studies, I set out to further dissect TIL responses that elicited tumour regression in patient MM909.24. In **Chapter 3**, I demonstrated that >13% of MM909.24 TILs stained with a tetramer loaded with the heteroclitic Melan-A_{26-35} peptide (ELAGIGILTV)[171] (**Figure 3-4**). A slightly smaller population stained with tetramers made with the natural Melan-A_{26-35} peptide (EAAGIGILTV) (**Figure 4-2A**). However, a much larger population (~40%) of MM909.24 TIL responded to the autologous tumour line (**Figure 4-2B**). Collectively, these results indicate that most of the melanoma-reactive TIL from patient MM909.24 do not recognise Melan-A_{26-35} or the other known HLA A2-restricted peptides tested, and suggest that most cancer-specific T cells in these TIL must recognise another epitope. The HLA class I type of patient MM909.24 is HLA A*0201, A*3001, B*4002, C*0304. At this point, it was not possible to determine which HLA-I(s) acted as the restricting element for the majority of the T cell response to autologous tumour in MM909.24 TIL.

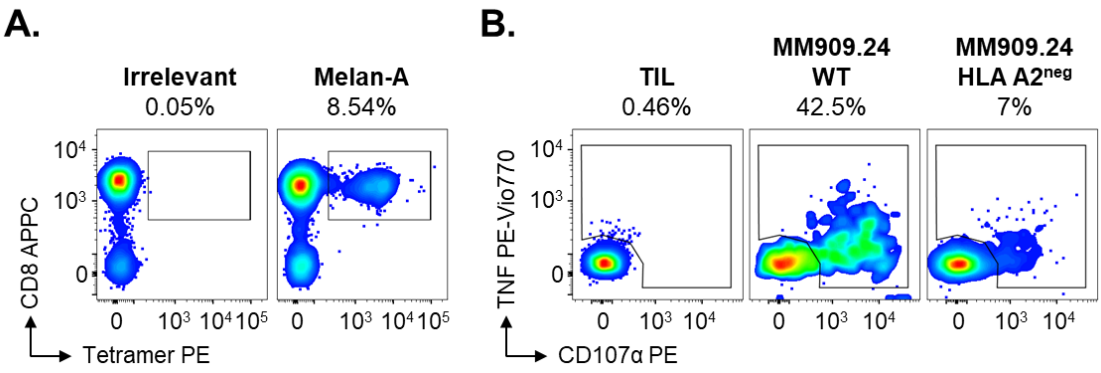

Figure 4-2. **The majority of the tumour-specific T cell response in patient MM909.24 TIL is HLA A2-restricted. (A)** HLA-A2 Melan-A_{26-35} (EAAGIGILTV) tetramer staining of TIL infusion product from patient MM909.24. Gates were set on single lymphocytes and live $CD3^+$ cells. The percentage of $CD8^+Tet^+$ T cells is shown for each gate. Irrelevant tetramer made with human telomerase reverse transcriptase ($hTERT_{540-548}$, ILAKFLHWL) was used to set the gates. **(B)** TAPI-0 staining of tumour reactive T cells from heterologous TIL population co-incubated for 5 hours with the indicated tumour lines followed by viable sorting based on expression of CD107a and TNF on live $CD8^+CD3^+$ cells. Percentage of tumour-reactive cells found within the population is indicated above each panel.

The very high frequency of HLA A2 in the human population makes it the most attractive classical HLA candidate for T cell-based therapies. I therefore wanted to establish whether any of the non-Melan-A response in the TIL of this patient operated via HLA A2. To this end, I made an HLA A2 deficient version of the autologous tumour line from this patient by transduction with a lentivirus encoding Cas9 and a guide (g)RNA targeting the HLA A2 gene, followed by single cell cloning and validation of abrogation of HLA A2 expression by flow cytometric analysis. Removal of HLA A2 from the MM909.24 tumour line (MM909.24 $A2^{neg}$) reduced the reactivity of the TIL towards this line by 6-fold (**Figure 4-2B**). Remarkably, these results indicate that most of the tumour-specific response in this patient operates through HLA A2 and is neither Melan-A-specific or operating via known melanoma epitopes from gp100, MG50, p53 or TRAG3.

4.2.2. M909.24 TIL responds to multiple HLA $A2^{+}$ cancer types

My colleague, Sarah Theaker, previously generated preliminary data showing that the TIL used to treat patient MM909.24 responded to a panel of HLA $A2^{+}$ cancer lines, including those from breast tumours[349]. These results suggested that the TIL from patient MM909.24 might respond to multiple different antigens and warranted further detailed investigation. As the tumour lines the MM909.24 TIL responded to only shared HLA A2, it was therefore hypothesised that T cells were recognising the different cancer lines in the context of HLA A2. To formally prove this hypothesis, I knocked out this HLA from each tumour cell line by transduction with the aforementioned lentivirus encoding Cas9 and a gRNA targeting the HLA A2 gene, followed by single cell cloning and validation of abrogation of HLA A2 expression (hereon HLA $A2^{neg}$) by flow cytometric analysis (**Figure 4-3A**). All successfully grown HLA $A2^{neg}$ clonal cells from a tumour line were pooled together for experimentation. In addition, naturally HLA $A2^{neg}$ tumour lines were transduced with a HLA A2 transgene and purified to a minimum of 70% HLA $A2^{+}$ expression by magnetic cell sort-based isolation (**Figure 4-3B**). Recognition of each target was examined by co-incubation with *in vitro* cultured TIL product from patient MM909.24 for 5 h (**Figure 4-3C**). MM909.24 TIL showed effective recognition of the ovarian-derived A2780 cell line (~40% reactivity), whereas more moderate responses (~10% reactivity) were observed towards the EBV-transformed B lymphoblast C1R, colorectal-derived COLO205 adenocarcinoma and the cervix-derived SIHA carcinoma. Allorecognition of non-melanoma tumours was considered to be unlikely as no shared HLAs were present across these lines (**Figure 4-3A** and **B**).

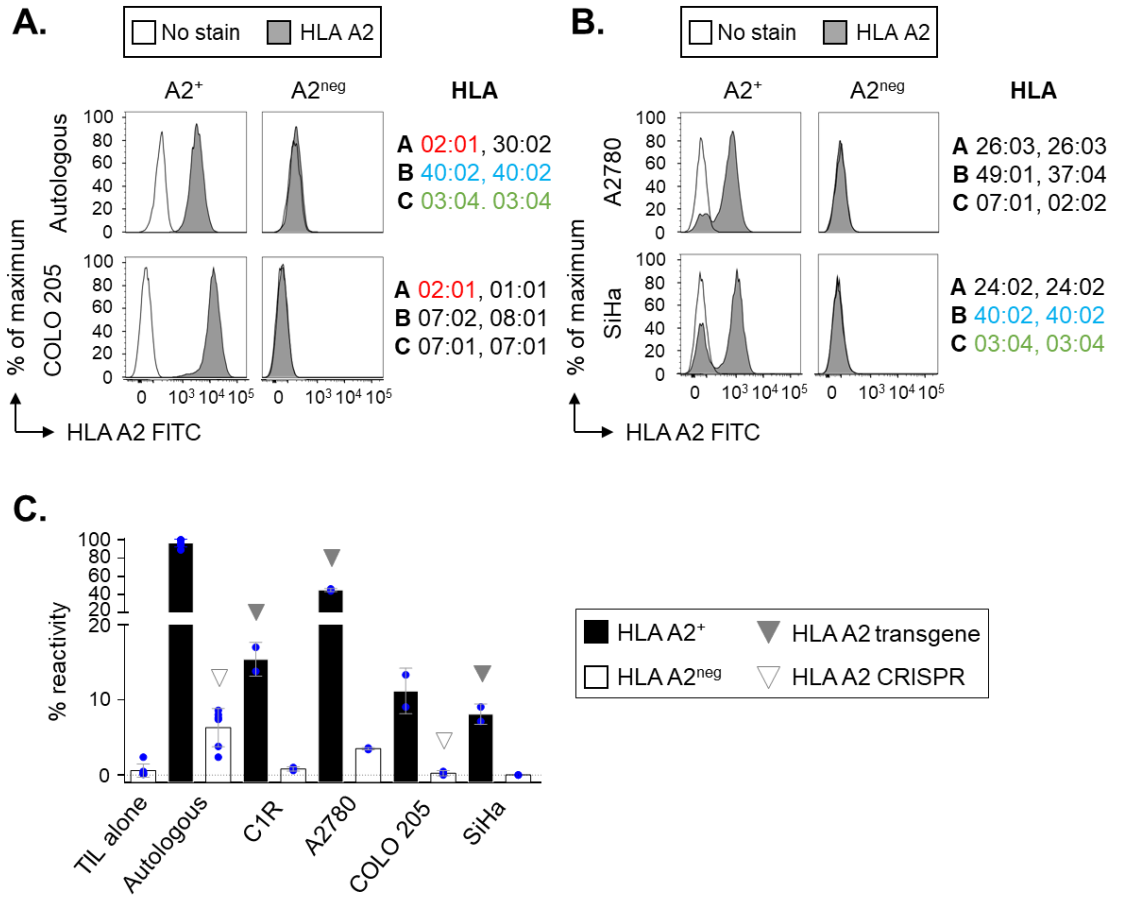

Figure 4-3. Patient MM909.24 TIL infusion product recognises non-melanoma tumours through HLA A2. Naturally HLA A2^{+} tumour cell lines were transduced with CRISPR/Cas9 targeting HLA A2 **(A)**, whereas naturally HLA A2^{neg} tumour cell lines were transduced with a construct expressing the HLA A2 transgene **(B)**, thus generating HLA A2^{neg} and HLA A2^{+} lines, respectively. Both HLA A2^{+}and HLA A2^{neg} tumour lines were surface antibody stained to confirm HLA A2 expression. Unstained cells (negative control) are indicated in white (□), HLA A2 stained cells are indicated in grey (■). HLA typing of each tumour line is indicated at the right of the panel. Matching HLAs to MM909.24 are indicated in colour. **(C)** TAPI assay of TIL24 co-incubated for 5h with a panel of HLA A2^{+} and HLA A2^{neg} matched tumour lines. Data represent mean ±SD. Each blue spot represents a repeat. Open (□) and coloured (■) triangles indicate tumour line has been transduced with a HLA A2 sgRNA or HLA A2 transgene, respectively. C1R cells (naturally HLA A2^{neg}) were previously transduced with HLA A2 using pCDNA3[350]. Data courtesy of Dr. Garry Dolton.

4.2.3. Clonotyping of broadly tumour-reactive TCRs in M909.24 TIL

I next set out to establish which TCRs in MM909.24 TIL responded to each tumour line. Tumour-reactive T cells were stained with TNF and CD107a markers and sorted as live cells prior to α and β TCR bulk sequencing analysis. Reactivity towards the different cancer cell lines varied depending on the tissue of origin, showing the highest reactivity towards autologous tumour and those cells with a breast-cancer origin (**Figure 4-4A**). The following number of viable CD8^{+} tumour-reactive T cells were sorted for each cancer line: MM909.24 (autologous melanoma): 14,339 events; MDA-MB-231 (breast, adenocarcinoma): 18,878 events; MCF-7 (breast, carcinoma): 4,484 events; MS 751 (cervix, carcinoma): 5,965 events; LnCap (prostate, carcinoma): 3,903 events; SaOS (bone, osteosarcoma): 2,565 events; H69 (lung, carcinoma): 385 events; COLO 205 (colon, adenocarcinoma): 4,287 events; RCC17 (renal, carcinoma): 771 events.

The oligoclonal expansion that occurs upon T cell encounter with their antigenic counterpart, leads to the presence of predominant TCR clonotypes within the population. Thus, high frequency of specific clonotypes within the TIL repertoire may indicate that these clonotypes respond to tumour[330]. Clonotypic analysis of bulk α and β chains of TCRs identified 32 TCRα and 23 TCRβ that responded to the autologous melanoma line and one other tumour cell line (**Figure 4-4B** and **Supplementary figure 5A**). At the outset of my studies, the available sequencing methodologies did not provide with information regarding αβTCR chain pairing; thus, the disparity in the number of α and β TCR chains observed is likely due to the inherent caveats of bulk chain sequencing. Assuming that an observed α chain could be paired with more than one β TCR chain, and vice versa, a further layer of dimensionality in TCR repertoire sequencing could be achieved with more recent advances in the field of single cell repertoire analysis such as DropSeq[351] and 10X Genomics[352] but I did not have access to such techniques when this work was undertaken.

I next examined if the TCRs that responded to the autologous melanoma were present in a patient PBMC sample taken at 6-months post TIL infusion. Importantly, 8 out of 23 TCRβ chains found to respond to the patient autologous melanoma line in TIL were also identified in patient PBMC following complete remission (**Figure 4-4B**, **red** arrow). These *persistent* clonotypes are of special interest as they may have been responsible for cancer clearance in this patient and are capable of responding to many different cancer types. Unsurprisingly, Melan-A specific clonotypes were well represented within the TCRs that reacted to the autologous tumour in both TIL and PBMC. Three of the eight persistent clonotypes identified were previously shown to respond to Melan-A, as I had either isolated the T cell clone or the TCRs were identified in Melan-A tetramer sorts in **Chapter 3**. The three persistent Melan-A-reactive clonotypes were TRB24-1 TRBJ2-1 CDR3β: **CATSDRGQGANWDEQFF** corresponding to VB6G4.24 T cell clone; TRB12-4 TRBJ1-1 CDR3β: **CASTLGGGTEAFF** and TRB27 TRBJ2-3 CDR3β: **CASSNGFHFNTLYF**. Five non-persistent TCRβ chains were also present in the HLA A2-ELAGIGILTV tetramer^{+} sorts of MM909.24 TIL presented in **Chapter 3** (TRB29-1 TRBJ2-1 CDR3β: **CSVEGSLGRALRANEQFF**, TRB6-3 TRBJ1-6 CDR3β **CASSYVGLGSPLHF**:, TRB20-1 TRBJ2-1 CDR3β: **CSEGSPYNEQFF**:, TRB27 TRBJ2-3 CDR3β: **CASSFAGTDTQYF**, TRB12-4 TRBJ2-7 CDR3β: **CASSWAGPVEQYF**). The antigenic specificity of the other 5 persistent clonotypes found in both the TIL used to treat patient MM909.24 and PBMC following tumour remission (TRB20-1 TRBJ2-1 CDR3β: **CSARDLLAETYEQYF**, TRB12-4 TRBJ1-2 CDR3β: **CASSPTTGLKTRSGYTF**, TRB7-8 TRBJ2-2 CDR3β: **CASSLGEGSPGELFF,** TRB20-1 TRBJ2-7 CDR3β: **CSAREDGGQTYEQYF** and TRB12-4 TRBJ2-3 CDR3β: **CASSNTGGYTQYF**) was unknown, making these clonotypes of particular interest (for graphic representation refer to **Supplementary figure 3**).

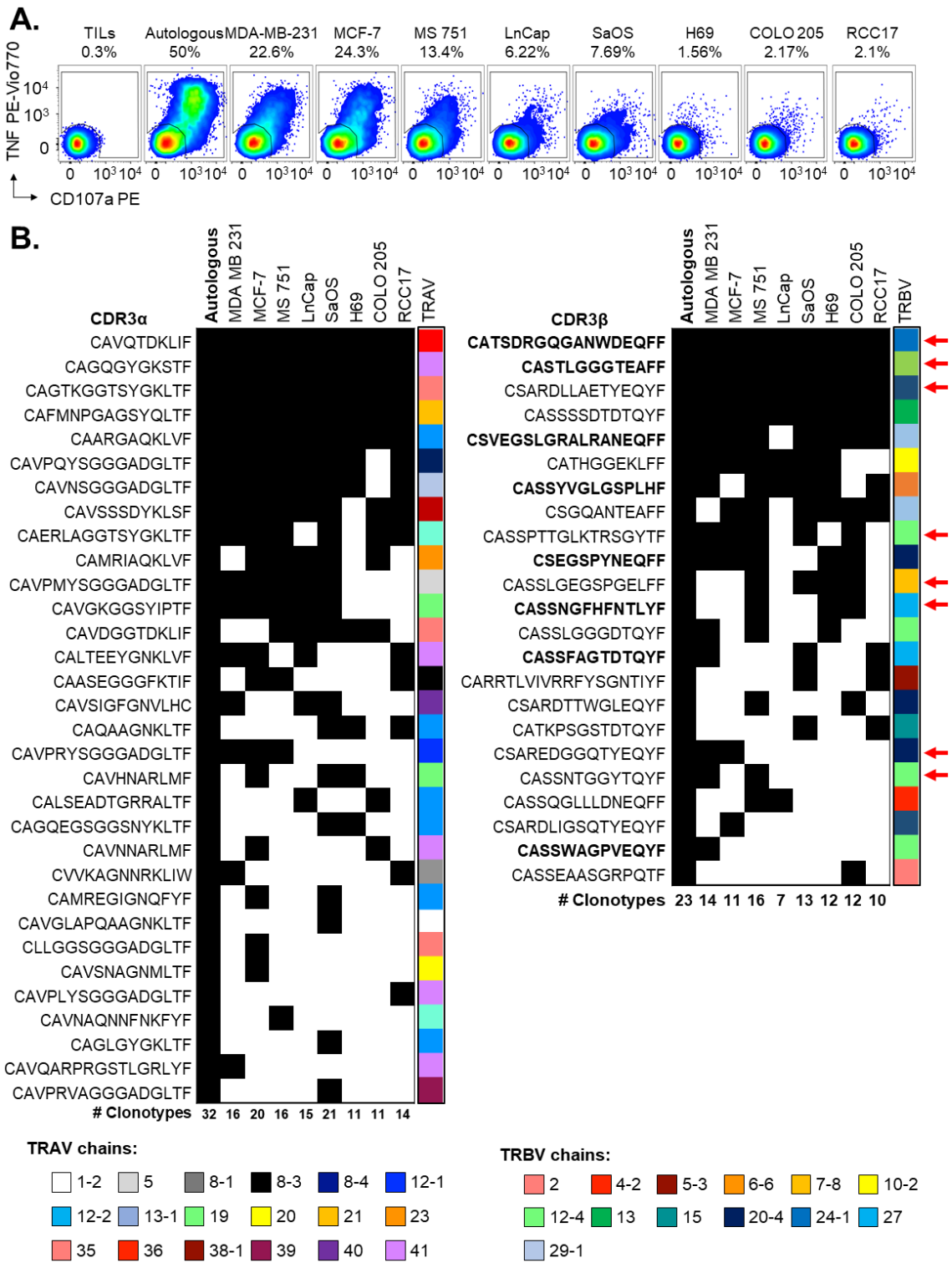

Figure 4-4. Several TIL clonotypes recognise multiple tumour lines. (A) TAPI-0 assay and staining of tumour reactive T cells from heterologous TIL population co-incubated for 5 hours with the indicated tumour lines followed by viable sorting based on expression of CD107a and TNF on live $CD8^{+}CD3^{+}CD14^{neg}CD19^{neg}$ cells. Percentage of tumour-reactive cells found within the population is indicated above each panel. **(B)** CDR3 alpha (left) and beta (right) of tumour-reactive clonotypes found in each sorted population. Autologous tumour (MM909.24)-reactive clonotypes found in the corresponding tumour sample are indicated in black. TRAV and TRBV gene usage is displayed colour-coded on the right side of the map. Indicated in **Bold**, CDR3β clonotypes corresponding to the HLA A2-ELAGIGILTV tetramer^{+} sorts presented in **Chapter 3**. Red arrow indicates persistent clonotypes described in **Chapter 3**. Distribution of TRAV/TRAJ and TRBV/TRBJ gene usage in tumour-reactive clonotypes is enclosed in **Supplementary figure 5**. HLA typing for each cancer cell line is enclosed in **Supplementary table 10.**

I also sequenced the TCRs that responded to the other 8 cancer lines tested in **Figure 4-4**. Remarkably, 5 TCRα and 4 TCRβ were found to respond to all these tumours in addition to the autologous melanoma line. This finding was especially interesting as there is no known shared tumour-associated antigen expressed by all these tumour lines. The ability of T cell clonotypes to respond to all tumour lines tested therefore suggests that they maybe recognising new epitopes. Noticeably, both the TCRα and TCRβ chains of the previously characterised persistent T cell clone VB6G4.24 were found as the most enriched TCR sequences in all tumour-reactive sorts. VB6G4.24 was previously shown to stain with tetramers loaded with the HLA A2-restricted Melan-A peptide EAAGIGILTV (**Figure 3-4**). As Melan-A is only expressed in melanoma and melanocytes, the occurrence of this clonotype in responses to other tumours suggests that this clonotype might also recognise another tumour-associated antigen in addition to the Melan-A-derived peptide EAAGIGILTV. The recognition of more than one tumour-associated antigen on the same target by a single TCR is unprecedented. I therefore set out to test whether T cell clone VB6G4.24 really could respond to tumour lines that did not express Melan-A.

Remarkably, the VB6G4.24 T cell clone was observed to respond to four other HLA $A2^+$ tumour cell lines (LnCap, MDA-MB-231, RCC17 and SaOS; **Figure 4-5**). This result prompted me to examine whether other TIL-derived Melan-A-specific T cell clones might also respond to cancer cell lines that do not express Melan-A.

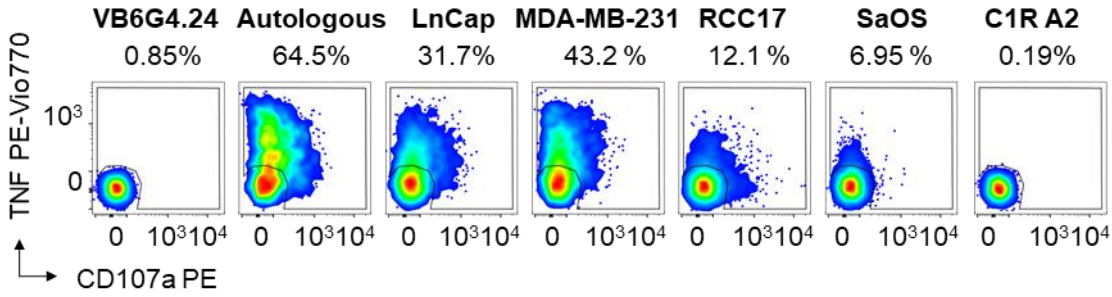

Figure 4-5. **Patient MM909.24 derived $CD8^+$ T cell clone VB6G4.24 shows broad recognition of HLA-A2 cancer lines. (A)** TAPI assay following 5-hour co-incubation with a panel of HLA-$A2^+$ tumours from diverse tissue origin. Gates were set on single lymphocytes and live $CD8^+CD3^+$ cells. Percentage of tumour-reactive cells based on TNF and CD107a outputs is indicated above each panel.

4.2.4. TIL-derived Melan-A-specific T cells respond to multiple HLA A2$^+$ tumour cell lines

I next examined whether Melan-A-specific CD8$^+$ T cell clones CR24, CR124 and CR324 (**Figure 4-6A**) grown from the TIL used to treat patient MM909.24 could recognise other tumour types that did not express Melan-A. Surprisingly, all these Melan-A-specific clonotypes also responded to other HLA A2$^+$ cancer lines suggesting that, in accordance with observations made with the VB6G4.24 T cell clone, they might also be recognising a further epitope (**Figure 4-6B**). Moreover, each T cell clone gave different recognition patterns across the various tumour types, suggesting that they might have different antigenic specificities in addition to Melan-A.

This exciting result prompted me to confirm that individual T cell clones really could respond to multiple different tumours and to search for the peptide epitopes that made such recognition possible. I chose CR24 for my initial experiments as this MM909.24 TIL-derived T cell clone persists in patient PBMC post complete remission and this clonotype exhibited strong reactivity to Melan-A negative tumour types, including C1R-A2 cells unlike VB6G4.24, suggesting that these clones had a different specificity (**Figure 4-6B**).

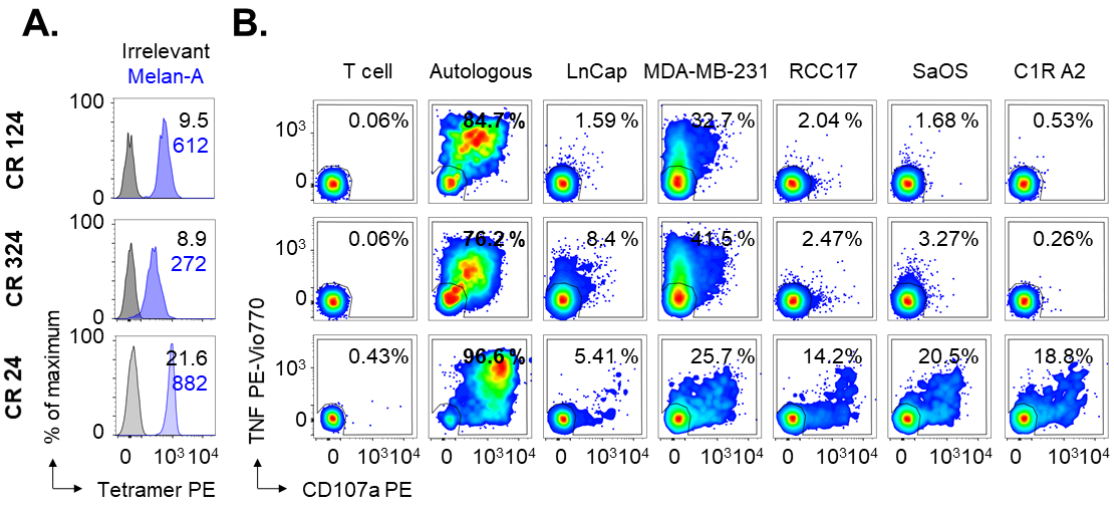

Figure 4-6. **Patient MM909.24 derived CD8$^+$ T cell clones show broad recognition of HLA-A2 cancer lines. (A)** T cell clones staining with HLA A2-restricted Melan-A$_{25\text{-}35}$ (EAAGILGILTV, in blue) and Irrelevant HLA A2-restricted hTERT$_{540\text{-}548}$ (ILAKFLHWL, in grey) tetramers. MFI values are displayed. **(B)** TAPI assay following 5-hour co-incubation with a panel of HLA-A2$^+$ tumours from diverse tissue origin. Gates were set on single lymphocytes and live CD8$^+$CD3$^+$ cells. Percentage of tumour-reactive cells based on TNF and CD107a outputs is indicated in each panel.

4.2.5. CR24 exhibits broad HLA A2-restricted anti-tumour response

As mentioned above, the Melan-A_{26-35} specific $CD8^+$ T cell clone, CR24, generated from the TIL infusion product of donor MM909.24 showed persistence in blood post-cure (**Figure 3-8**). This T cell clone also responded to cancer cell lines that do not express Melan-A (**Supplementary figure 4**), suggesting that it must also see a further tumour epitope. The presence of T cell clones in the TIL infusion product that was used to induce complete remission in a Stage IV cancer patient, that persisted in patient blood after cure, and that might recognise multiple different epitopes, is exciting as such T cells have not been described previously. It is possible that T cells that recognise cancer via more than one epitope might correlate with a positive outcome.

To formally prove that CR24 T cell was capable of recognising different cancer lines in the context of HLA A2, I abrogated the expression of this HLA from each HLA $A2^+$ tumour cell line as previously described (**section 4.2.1**) using CRISPR/Cas9 technology, (**Figure 4-7A**), and transduced naturally HLA $A2^{neg}$ tumour lines with an HLA A2 transgene (**Figure 4-7B**).

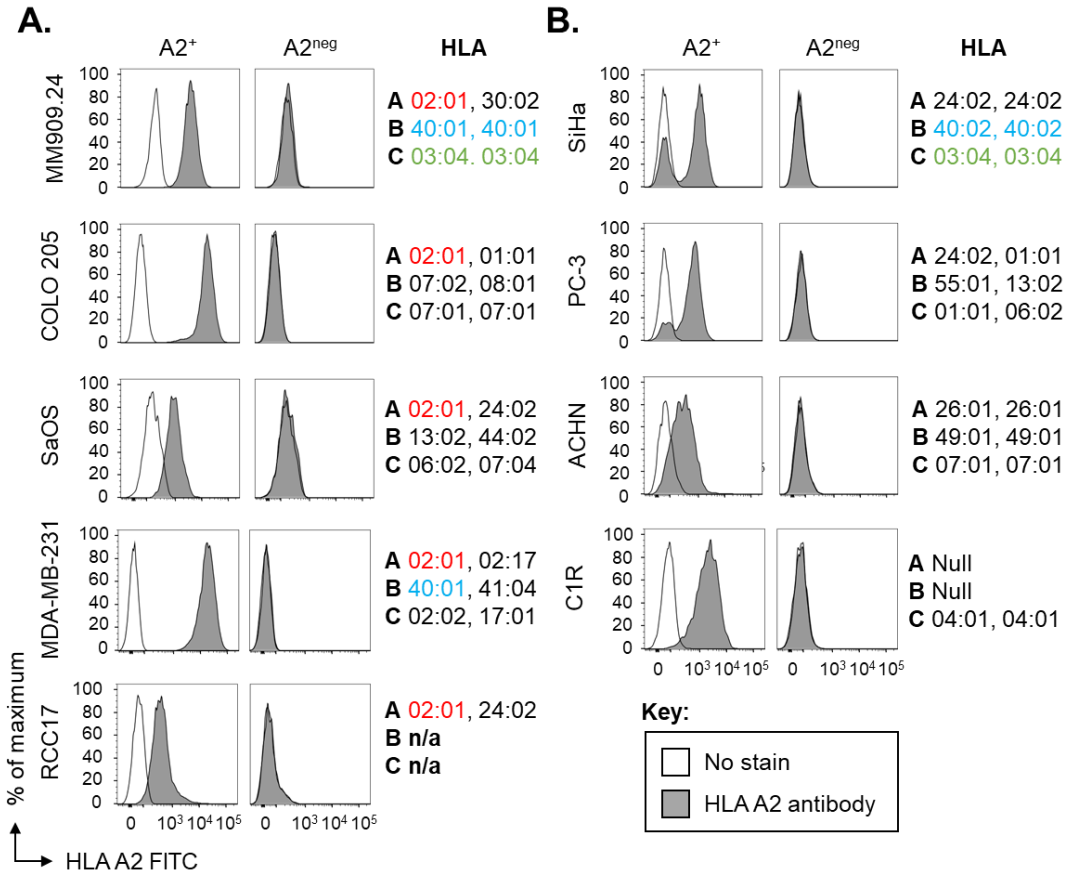

Figure 4-7. **HLA A2 antibody characterisation of tumour cell lines.** Naturally HLA $A2^+$ tumour cell lines were transduced with CRISPR/Cas9 targeting HLA A2 **(A)**, whereas naturally HLA $A2^{neg}$ tumour cell lines were transduced with a construct expressing the HLA A2 transgene **(B)**, thus generating HLA $A2^{neg}$ and HLA $A2^+$ lines, respectively. Both HLA $A2^+$and HLA $A2^{neg}$ tumour lines were surface antibody stained to confirm HLA A2 expression. Unstained cells (negative control) are indicated in white (□), HLA A2 stained cells are indicated in grey (■). HLA typing of each tumour line is indicated at the right of the panel. Matching HLAs to MM909.24 are indicated in colour. As indicated earlier, C1R cells were transduced with HLA A2 using pCDNA3 vector prior to my arrival[350]. n/a indicates HLA typing not available.

As shown, CR24 was highly cytotoxic against the autologous tumour and naturally Melan-A^{neg} EBV-transformed B lymphoblast C1R cells when they expressed HLA A2 (90% lysis; **Figure 4-8A**). CR24 also exhibited strong secretion of IFNγ in response to non-autologous HLA A2^{+} melanoma lines (**Figure 4-8B**) and produced TNF in response to tumour lines from a wide range of origins (**Figure 4-8C**). Noticeably, the non-melanoma MDA-MB-231, SaOS, SiHa and PC-3 tumour lines induced a stronger TNF secretion than the autologous tumour suggesting that these cell lines might be abundant in the alternative antigen. Importantly, recognition of cancer cell lines was irrespective of tissue source and HLA-allotype. CR24 did not respond to the healthy HLA A2^{+} hepatocyte cell line Hep2 or healthy the lung fibroblast HLA A2^{+} cell line MRC5 (**Figure 4-8D**). CR24 responded to these healthy cell lines when they were pulsed with the Melan-A$_{26-35}$ (EAAGIGILTV) peptide, thus confirming that these cell lines could be targeted when loaded with exogenous antigen. Collectively, these data show that CR24 can target non-melanoma cell lines through a target other than Melan-A and that this target is not present on the healthy cell lines tested. These results suggest that CR24 can recognise more than one tumour-associated antigen. I next set out to try and determine what this other tumour-associated antigen was.

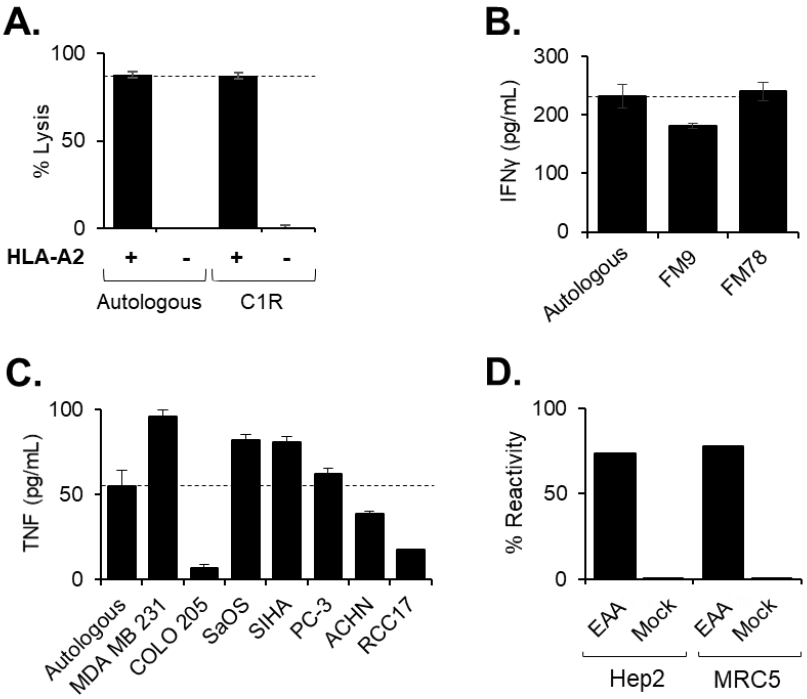

Figure 4-8. **CR24 responses to multiple cancer cell lines. (A)** Cytotoxicity of CR24 clone following 2-day co-incubation with HLA-A2^{+} or HLA-A2^{neg} autologous tumour or C1R cell line at 1:1 ratio as measured in a long term killing assay. Gates were set on dead CD3^{neg} and %reactivity normalised to "no T cells" sample where T cells were omitted. Samples were run in triplicate and standard deviation from the mean is shown. T cell reactivity towards a panel of HLA-A2^{+} melanomas **(B)** and non-melanoma cancer cell lines **(C)** was determined by IFNγ and TNF cytokine release (in pg/mL), respectively, measured by ELISA after overnight co-incubation. Reactivity towards the HLA-A2^{neg} matched tumour line was subtracted. Standard error of the mean is shown. Autologous MM909.24 tumour was used as reference. Dotted line indicates maximum reactivity towards autologous tumour. **(D)** HLA-A2^{+} non-cancerous lines Hep2 (hepatocyte) and MRC5 (lung fibroblast) were pulsed with 10^{-7}mM EAAGIGILTV or irrelevant (mock) peptide (GILGFVFTL, from Influenza M1) for an hour at 37°C under rotation, followed by extensive washing prior to 4-hour co-incubation with CR24 T cell clone. TAPI assay and staining with TNF and CD107α Ab was then performed. Gates were set on single lymphocytes and live CD8^{+}CD3^{+} cells. Background reactivity is subtracted from %reactivity. Percentage of reactive cells (%TNF^{+} CD107a^{+}) is shown as a bar graph.

4.2.6. T cell target identification

The TCR-pMHC interaction can be highly degenerate, allowing a TCR to recognise many peptides in the context of a single[353] or several[354,355] MHCs. Previous work from my lab has reported the use of Positional Scanning Combinatorial Peptide Libraries (PS-CPLs) to quantify the number of peptides of a certain length that can be recognised by a single TCR[99]. As described in the introduction of this chapter, *Szomolay and colleagues*[346] developed a webtool to search large viral protein-derived ligand databases and produce a list of potential peptide agonists ranked in order of likelihood of recognition by an orphan TCR. This webtool has since been complemented with a bespoke cancer proteomics database (Dolton, Szomolay *et al*. manuscript in preparation). The addition of this proteomic database to this webtool has allowed for the design of the "*epitope discovery pipeline*" for cancer epitopes as described in **Figure 4-9**. This approach has vastly expedited epitope prediction and revolutionizes *in silico* agonist peptide prediction and design.

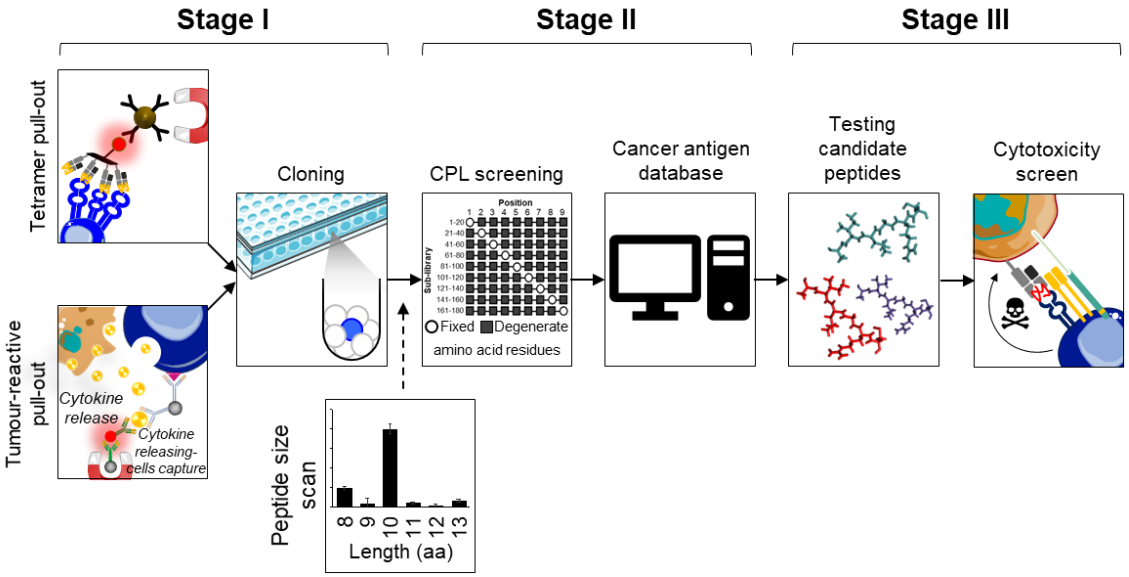

Figure 4-9. T cell epitope identification pipeline. Initially, T cells from patients or donors are pulled out by magnetic sorting using peptide-loaded tetramers and anti-fluorochrome magnetic beads, or by co-incubation with desired target in the presence of TNF and IFNγ secretion kits (Miltenyi). Enriched cells are then cloned by limiting dilution and expanded as required (**Stage I**). Alternatively, single T cells can be Aria sorted into individual 96U wells, although cell viability might be compromised. In **Stage II**, growing clones are screened by Positional Scanning Combinatorial Peptide Library (PS-CPL) and the output is run through a cancer proteomics database using general-purpose computing on graphics processing units (GP-GPU) (Dolton G, Szomolay B *et al*. manuscript in preparation). When unknown, peptide length preference can be determined prior to PS-CPL using custom-built "peptide size scan" libraries. In **Stage III**, predicted peptides are tested in peptide titration assays and targets are further validated using gene transfer and/or CRISPR/Cas9 knockout approaches.

My laboratory has previously shown that $CD8^+$ T cells exhibit a peptide length preference[248]. To determine the peptide length preference of CR24 $CD8^+$ T cell I used a custom-built sizing scan, comprising a mixture of random peptides of different lengths (**Figure 4-10A**). CR24 T cell clone exhibited a preferential recognition of peptides of 10 amino acids length (decamer) in the context of HLA A2. Next, I sought to determine the TCR recognition footprint of the CR24 T cell clone using a decamer PS-CPL. This approach allowed determination of the amino acid preferences of CR24 across the antigenic peptide backbone, and revealed that the EAAGIGILTV sequence was suboptimal for this T cell clone at some positions (**Figure 4-10B**). Consistent with previous structural analyses of Melan-A specific TCR binding to HLA A2-EAAGIGILTV[356], the TCR degeneracy was more restricted in the central region (from Position 4 to Position 6), suggesting that the TCR might make the majority of its peptide contacts with these residues. In contrast, recognition was highly degenerate at the remaining positions at the N- and C- terminal regions of the peptide backbone; suggesting that CR24 could potentially recognise a vast array of different decamer amino acid combinations in addition to the cognate EAAGIGILTV peptide. Raw peptide length-matched data from the PS-CPL screen was analysed using the novel cancer proteomics database and webtool described above, allowing the identification of potential peptide agonists from a large tumour-associated-protein database. The output of the top peptides predicted using this approach is shown in **Table 4-1**. During her studies, Dr V. Bianchi also performed PS-CPL examination of the CR24 sister clone, ST8.24. Sister clones ST8.24 and CR24 exhibited similar patterns of TCR degeneracy. I did not realise that CR24 and ST8.24 have an identical TCR until the antigen receptors from these clones were sequenced.

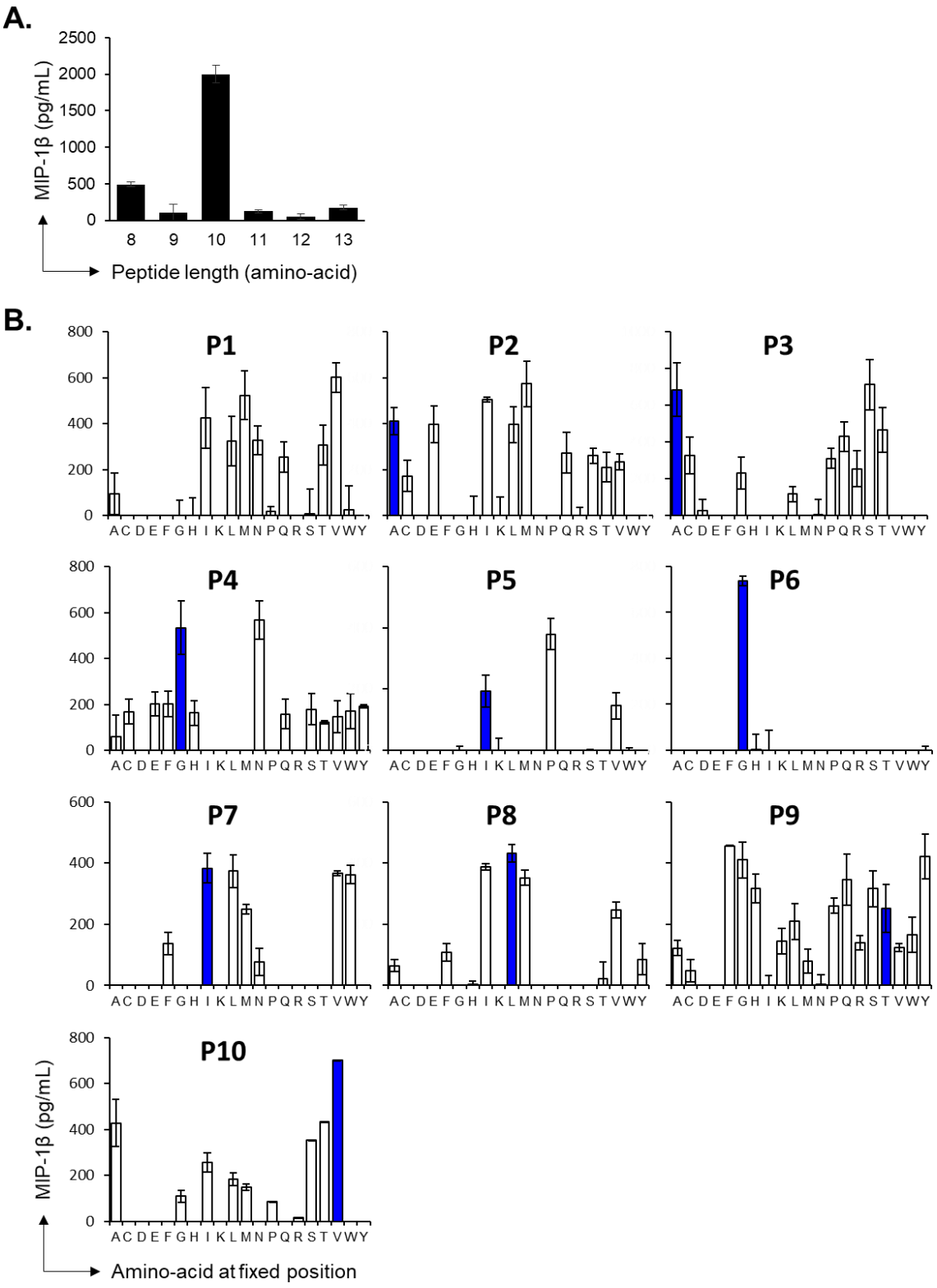

Figure 4-10. Decamer CPL-screening of Melan-A-specific T cell clone CR24. (A) Peptide size-scan using MIP-1β (pg/mL) output measured using ELISA following overnight co-incubation of T cells with peptide-pulsed T2 shows a strong preference for decamer peptides. **(B)** Decamer PS-CPL library (10^{-4}M) using MIP-1β ELISA as a readout. Results are displayed as histogram plots of the L-amino acid residue landscape (shown in single-letter code format) and SD from the mean of two replicates is shown. The index Melan-A peptide sequence (EAAGIGILTV) is shown in blue. Y axis marks indicate increments of 200 pg/mL.

Table 4-1. Candidate peptide sequences from CR24 CPL scan ranked in order of recognition likelihood[291]. Data obtained in collaboration with Dr. Bianchi.

Sequence	Protein	Abreviation	UniProt code
E**L**AGIGILTV	Melanoma antigen recognized by T cells 1 (analogue)	Melan-A	-
NLAAVGLFPA	Insulin-like growth factor 2 mRNA-binding protein 1	IF2B2	*Q9NZI8*
EAAGIGILTV	Melanoma antigen recognized by T cells 1	Melan-A	*Q16655*
LLLGIGILVL	Bone marrow stromal antigen 2	BST2	*Q10589*
NLSALGIFST	Insulin-like growth factor 2 mRNA-binding protein 2	IF2B2	*Q9Y6M1*
VYAALGILQG	Canalicular multispecific organic anion transporter 2	MRP3	*O15438*
LILNIAIFFV	Dermatan-sulfate epimerase	DSE	*Q9UL01*
ATSAMGTISI	Mucin-16	MUC16	*Q8WXI7*
ISAVVGILLV	Receptor tyrosine-protein kinase erbB-2	ERBB2	*P04626*
TSSAIPIMTV	Mucin-16	MUC16	*Q8WXI7*
TYSCVGVFQH	Heat shock 70 kDa 1A	HS71A	*P08107*
LRLALGLLQL	G-protein coupled receptor 143	GP143	*P51810*
MVSCIIFFFV	ATP-binding cassette sub-family C member 11	ABCC11	*Q96J66*
QLLAEGVLSA	Anoctamin-7	ANO7	*Q6IWH7*
TTLAICLLYV	Canalicular multispecific organic anion transporter 2	MRP3	*O15438*
GVSGIGVTLF	Tyrosine-protein kinase Fgr	FGR	*P09769*
LIAARGIFYG	Canalicular multispecific organic anion transporter 2	MRP3	*O15438*
TSSAIPTLPV	Mucin-16	MUG16	*Q8WXI7*
TIPSMGITSA	Mucin-16	MUG16	*Q8WXI7*
TTQSLGVMSS	Mucin-16	MUG16	*Q8WXI7*
VLNAVGVYAG	Melanoma-associated antigen C2	MAGE-C2	*Q9UBF1*
MISAIPTLAV	Mucin-16	MUG16	*Q8WXI7*
AVAAIWVASV	Melanocyte-stimulating hormone receptor	MC1R	*Q01726*
SVTWIGAAPL	Prostate-specific antigen	KLK3	*P07288*
LTSSKGQLQK	Perilipin-2	PLIN2	*Q99541*
AASAIKVIPT	Indoleamine 2,3-dioxygenase 1	IDO1	*P14902*
MVLGIGPVLG	Solute carrier family 45 member 3	SLC45A3	*Q96JT2*
SAAGLGLVAI	Solute carrier family 45 member 3	SLC45A3	*Q96JT2*
QTQAVPLLMA	P protein	P protein	*Q04671-2*
STLNIDLFPA	Peroxidasin homolog	PXDN	*Q92626*
ILNGIKVLKL	Multidrug resistance-associated protein 1	MRP1	*P33527-9*
VLTAMGLIGI	Calcium-activated chloride channel regulator 2	CLCA2	*Q9UQC9*

The top 5 predicted cancer epitopes for CR24 were: (1) the Melan-A heteroclitic analogue peptide ELAGIGILTV (bold lettering signifies the difference from the natural Melan-A sequence); (2) **NLAAV**G**LFPA** from the Insulin-like Growth Factor-2 mRNA-Binding Protein 1 ($IMP1_{369-378}$); (3) The natural Melan-A peptide sequence EAAGIGILTV; (4) **LLL**GIGIL**VL** from the Bone marrow stromal antigen 2 protein ($BST2_{22-31}$) and (5) **NLSAL**GI**FST** from the Insulin-like Growth Factor-2 mRNA-Binding Protein 2 ($IMP\text{-}2_{367-376}$, previously introduced in **Chapter 3**). Of these top 5 predicted agonists, only the IMP-1 peptide was not well recognised by CR24 (**Figure 4-11**).

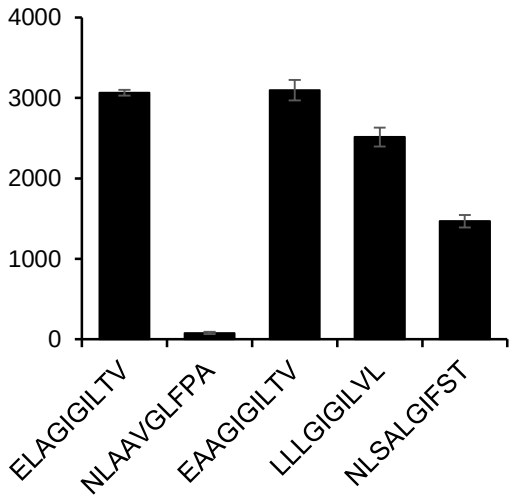

Figure 4-11. TOP5 candidate peptides from CR24 PS-CPL screen data. Activation to peptide was assessed by MIP-1β (pg/mL) release measured by ELISA after overnight co-incubation with 10^{-6} M candidate peptides at >40% manufacturing purity, obtained from the informatic processing of PS-CPL data. Mean and standard experimental error from duplicate samples is shown. *Data courtesy of Dr V. Bianchi*.

The IMP-$2_{367-376}$ (**NLSAL**GI**FST**) and $BST2_{22-31}$ (**LLL**GIGIL**VL**) epitopes described in **Table 4-2** have never been previously described so it was important to determine whether these sequences were genuinely processed and presented at the cancer cell surface. The 9mer version of the peptide **LLL**GIGIL**VL** (**LL**GIGIL**VL)** has already been described as an HLA A2 binding epitope, although it remains unknown whether this sequence is actually processed and presented[357,358]. BST2, also called Tetherin, CD317 or HM1.24 antigen, is a type II transmembrane glycoprotein of 180 amino acids found to be overexpressed in multiple myeloma and various cancer cells isolated from lung, kidney, endometrium, breast and skin[359–363]. This broad cancer-specific expression fits with the fact that CR24 recognises many non-Melan-A-expressing cancer cell lines (**Figure 4-8**). There is no known HLA A2-restricted IMP-2 epitope.

Table 4-2. Candidate new cancer epitopes recognised by the CR24 T cell clone. Amino acid residues that differ from the EAAGIGILTV peptide sequence are underlined. Assigned colour (colour ID) will be used throughout this thesis to reference each antigen.

Colour ID	Peptide	Protein	Names	Residues	UniProt ID
🔴	**LLL**GIGIL**VL**	Bone marrow stromal antigen 2	BST2 HM1.24 CD317 Tetherin	22-30	Q10589
🟢	**NLSAL**GI**FST**	Insulin-like growth factor 2 mRNA-binding protein 2	IF2B2 IMP-2 VICKZ-2	367-376	Q9Y6M1

4.2.7. The Melan-A-specific T cell clone CR24 recognises multiple different Tumour Associated Antigens

CR24 cross-recognition of Melan-A_{26-35}, $BST2_{22-31}$ and IMP-$2_{367-376}$ was validated by pMHC tetramer staining (**Figure 4-12A**) and peptide sensitivity measured by MIP-1β secretion (**Figure 4-12B**). Based on EC_{50} values, the LLLGIGILVL peptide showed a similar sensitivity to the cognate EAAGIGILTV peptide, whereas NLSALGIFST peptide was only recognised at the highest concentrations (10^{-5} M and 10^{-6} M). Recognition of exogenously supplied peptide and staining with cognate pMHC tetramers confirmed the CR24 TCR was capable of binding these peptide-HLA but did not prove that the epitopes were processed and presented at the surface of cancer cells. In order to demonstrate that the new IMP-2 epitope was real, I co-transduced the naturally HLA $A2^{neg}$ lymphoblastoid line MOLT3 with 3rd generation lentiviral particles encoding the HLA A2 transgene and Melan-A, IMP-2 or Collagen (as negative control) transgenes co-expressed with the rat-CD2 (rCD2) surface marker. Transduced cells were purified and >60% transgene incorporation was confirmed by flow cytometry prior to assay (**Supplementary figure 6**). CR24 T cell activation was assessed by MIP-1β release after overnight co-incubation with transgenic targets (**Figure 4-12C**), and the percentage of reactive $CD8^+$ cells was measured using TNF (TAPI-0 assay) and surrogate marker of lytic granule release CD107a (**Figure 4-12D**).

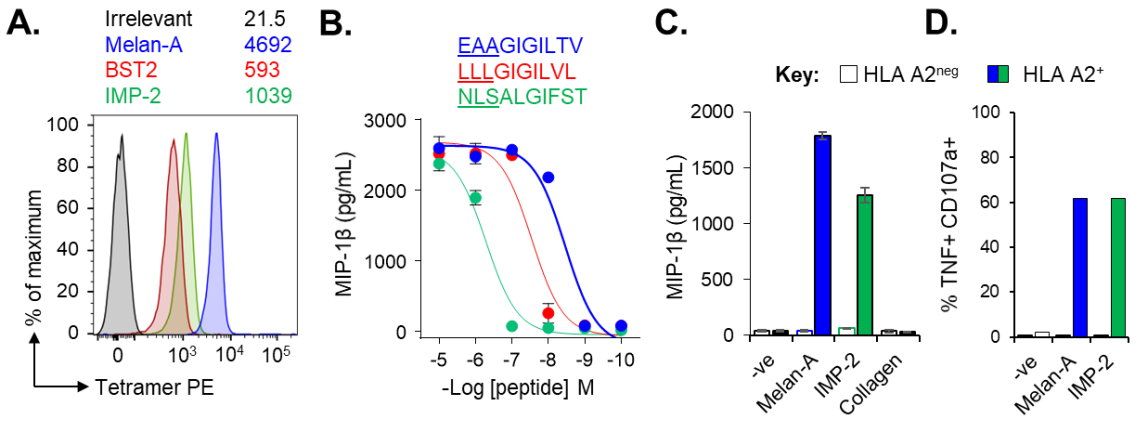

Figure 4-12. **Validation of CR24 cross-reactivity. (A)** The CR24 T cell clone was stained with HLA A2 Melan-A_{26-35} (blue), $BST2_{22-31}$ (red) or IMP-$2_{367-376}$ (green) tetramers. Gates were set on single lymphocytes and live $CD3^+$ $CD8^+$ cells. Mean Fluorescence Intensities (MFIs) are shown for each stain. Irrelevant tetramer made with human telomerase reverse transcriptase (in grey, $hTERT_{540-548}$) was used as negative control. **(B)** EC_{50} values of peptide sensitivity was assessed by MIP-1β (pg/mL) release measured by ELISA after overnight co-incubation with cognate Melan-A_{26-35} peptide (blue) and potentially new epitopes $BST2_{22-31}$ (red) and IMP-$2_{367-376}$ (green). Mean and standard experimental error from duplicate samples is shown. **(C)** Recognition of HLA $A2^{neg}$ MOLT3 cell line transduced with Melan-A and IMP-2 with or without the HLA A2 transgene was assessed by MIP-1β (pg/mL) release measured by ELISA after overnight co-incubation with target. Non-transduced (-ve) cells were used as negative control for background reactivity towards the MOLT3 cell line. Collagen transduction was used as negative control for background reactivity towards the transgene backbone. Mean and standard experimental error from duplicate samples is shown. **(D)** TAPI assay following 4-hour co-incubation with MOLT3 cell line transduced with Melan-A and IMP-2 with or without the HLA A2 transgene. Gates were set on single lymphocytes and live $CD8^+CD3^+$ cells. Percentage of tumour-reactive cells is shown as a bar graph based on % TNF^+ $CD107a^+$.

Overall, peptide recognition and efficient polyfunctional HLA A2-restricted responses confirmed the validity of the epitope identification pipeline described in **Figure 4-9** for the prediction of agonist peptides by identifying the IMP-$2_{367-376}$ as a novel immunogenic target. I next sought to use the HLA A2-IMP-$2_{367-376}$ and HLA A2-BST2_{22-31} tetramers I had made to examine whether the TIL infusion product used to treat patient MM909.24 contained T cells with these specificities.

4.2.8. BST2_{22-31} and IMP-$2_{367-376}$ -reactive TCRs are present within the TIL infusion product used for therapy

The discovery that a T cell clonotype CR24 from the TIL used to successfully treat patient MM909.24 could recognise three different peptides from three different cancer-specific antigens, could be highly significant as it would be extremely difficult for a melanoma cell to escape from such a 'multipronged' attack. Consequently, the presence of such *multipronged T cells* in the TIL infusion product used for treatment might benefit prognosis. I therefore sought to characterise if the TIL infusion product used to treat patient MM909.24 contained T cells capable of recognising the new BST2 and IMP-2 epitopes I identified. As shown in **Figure 4-13A**, 0.5% $CD3^+$ TILs stained with BST2 Tetramer whereas 1.2% stained with IMP-2 Tetramer. As this patient received 11×10^{10} infused TILs in total[289], these fractions both add up to the patient having received 550×10^6 and 1.3×10^9 T cells with these new specificities, respectively. Unfortunately, limited sample meant that the TIL infusion product stained in these experiments was on the 3rd passage (P3), so it is possible that the TCR repertoire frequencies might differ from that transfused into the patient as the result of further *in vitro* culturing. Nevertheless, IMP-2- and BST2-specific T cells were almost certainly transfused into patient MM909.24 in large numbers prior to complete remission.

I next examined functionality by incubating the TIL overnight with HLA $A2^{neg}$ MOLT3 cell line transduced with Melan-A and IMP-2 transgenes with or without HLA A2. I also made a further MOLT3 line that was transduced with the BST2 transgene. Consistent with the staining, TILs in P3 could mount an HLA A2-restricted response to both IMP-2 and BST2 transduced cells (**Figure 4-13B)** further confirming that these antigens are genuinely processed and presented on HLA A2 and that T cells that could respond to each target resided within the TIL used to treat patient MM909.24.

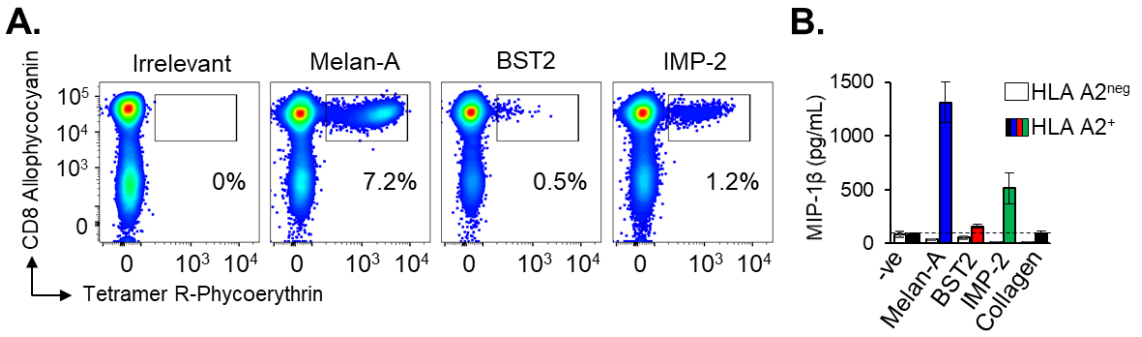

Figure 4-13. Patient MM909.24 TIL infusion product shows responses towards Melan-A, BST2 and IMP-2 antigens. (A) TIL from patient MM909.24 were stained with HLA A2 Melan-A_{26-35} (EAAGIGILTV), $BST2_{22-31}$ (LLLGIGILVL) and IMP-$2_{367-376}$ (NLSALGIFST) tetramers. Gates were set on single lymphocytes and live $CD3^{+}CD14^{neg}CD19^{neg}$ cells. The percentage of $CD8^{+}Tet^{+}$ T cells is shown for each gate. Irrelevant tetramer made with human telomerase reverse transcriptase ($hTERT_{540-548}$, ILAKFLHWL) was used to set the gates. **(B)** Recognition of HLA $A2^{neg}$ MOLT3 cell line transduced with Melan-A, BST2 and IMP-2, with or without the HLA A2 transgene, assessed by MIP-1β (pg/mL) release measured by ELISA after overnight co-incubation with target. Non-transduced (-ve) cells were used as negative control for background reactivity towards the MOLT3 cell line. Collagen transduction was used as negative control for background reactivity towards the transgene backbone. Mean and standard experimental error from duplicate samples is shown.

Next, I sought to identify the clonotypic architecture of the TCRs recognising the HLA A2-resticted responses to Melan-A_{26-35}, $BST2_{22-31}$ and IMP-$2_{367-376}$ epitopes. MM909.24 TILs (P3) were sorted by flow cytometry based on $CD8^{+}$ $Tetramer^{+}$ staining as shown in **Figure 4-13A**. The following number of viable $CD8^{+}$ $tetramer^{+}$ T cells were sorted: 38,711 EAAGIGILTV $tetramer^{+}$ cells; 2,090 LLLGIGILVL $tetramer^{+}$ cells; 5,081 NLSALGIFST $tetramer^{+}$ cells.

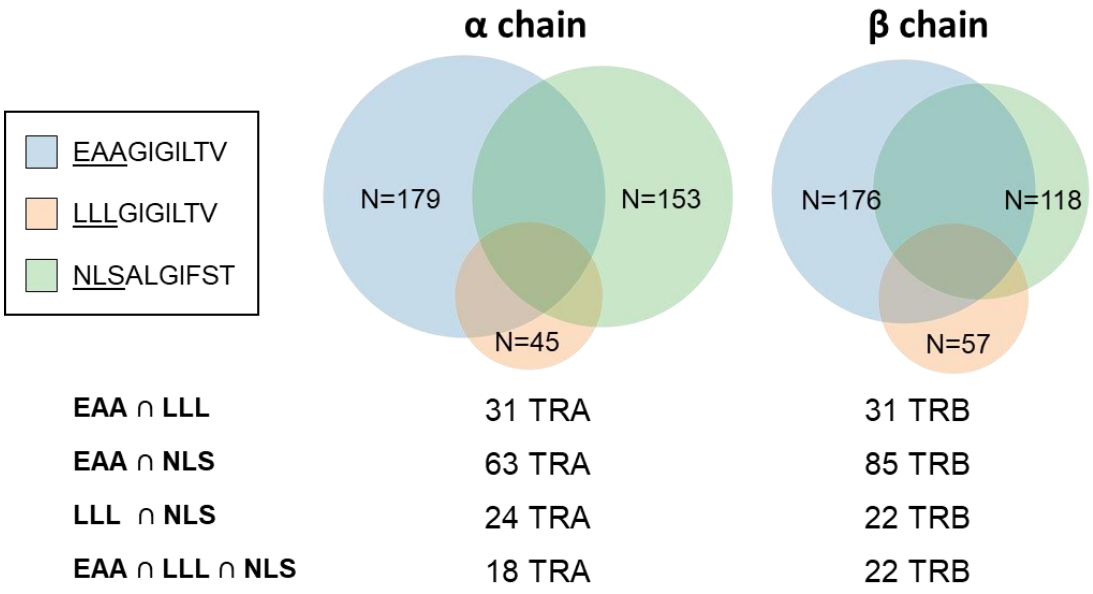

Figure 4-14. TCRα and TCRβ clonotypes from $CD8^{+}$ $tetramer^{+}$ sorted TIL populations. TILs from patient MM909.24 were stained with HLA A2 Melan-A_{26-35} (EAAGIGILTV), $BST2_{22-31}$ (LLLGIGILVL) and IMP-$2_{367-376}$ (NLSALGIFST) tetramers, followed by NGS sequencing of bulk α- and β- chains. Clonotypic analysis of overlapping α- (left) and β- (right) chains between tetramer sorts is displayed as a Venn Diagram, with number of overlapping CDR3 sequences annotated below. The number of isolated CDR3 sequences are displayed for each data set. " ∩ " indicates intersection of datasets.

A.

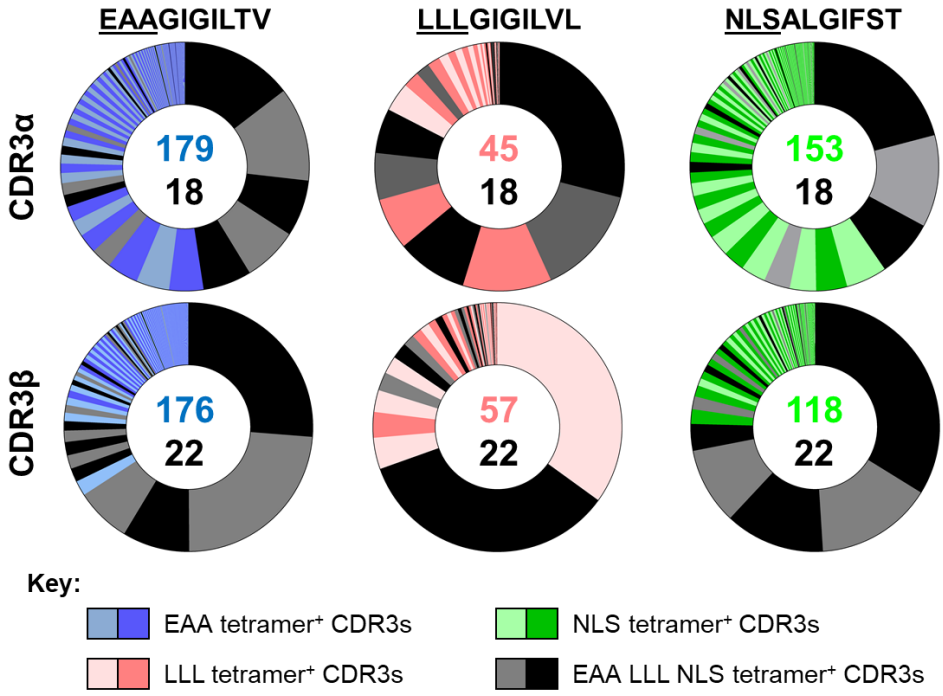

B.

	% frequency in sort				% frequency in sort		
CDR3α	**EAA**	**LLL**	**NLS**	**CDR3β**	**EAA**	**LLL**	**NLS**
CAMSVGFGNVLHC	14.57	0.01	0.44	**CATSDRGQGANWDEQFF**	26.24	0.99	33.80
CAARGAQKLVF	12.21	0.05	0.15	CASSPYSGSGETQYF	23.64	0.47	0.48
CAVNSGGGADGLTF	7.34	0.06	0.75	CSGQANTEAFF	8.73	1.50	0.97
CAVGLAPQAAGNKLTF	7.12	0.10	0.37	CSVEGSLGRALRANEQFF	7.21	0.37	15.19
CALGFGNVLHC	6.31	0.06	7.53	CASSFVPTEQFF	1.78	0.21	1.67
CAAAGGGADGLTF	2.70	14.24	0.98	**CASSWAGPVEQYF**	1.75	0.21	0.20
CAVNIGARLMF	1.57	29.02	0.34	CSEGSPYNEQFF	1.74	0.16	12.96
CAVNNARLMF	1.54	6.10	0.40	CSATGLAGLGEQFF	1.48	34.57	0.24
CAVQTDKLIF	1.14	0.21	20.93	CSVELGENIQYF	1.23	0.13	0.69
CAGLPWAGNMLTF	0.84	5.81	11.97	CASTLGGGTEAFF	1.01	0.17	0.10
CAVNQFYF	0.39	1.82	0.02	CSVEESSGIYEQYF	0.67	2.12	0.10
CAVPRGAQKLVF	0.33	0.18	0.07	CASSSSDTDTQYF	0.53	0.05	0.87
CAVKNNDMRF	0.29	0.09	0.02	CASSSPLDGGAYEQYF	0.51	0.07	0.07
CAANNARLMF	0.26	0.94	0.03	CATSDLLLAGGRSSYNEQFF	0.30	0.06	0.01
CAGTKGGTSYGKLTF	0.13	0.04	3.40	CASVPGGTYGYTF	0.29	0.07	9.97
CAERLAGGTSYGKLTF	0.09	0.10	0.29	CASSLGAGTANRQFF	0.27	2.39	0.02
CAVYGGSQGNLIF	0.05	9.20	0.05	CASSLGLAGNEQYF	0.27	0.06	0.38
CAENSGGGADGLTF	0.04	0.11	0.43	CASSLGSSGEQYF	0.26	0.04	3.48
CAVRDLRDNYQLIW	0.03	0.08	0.36	CARRTLVIVRRFYSGNTIYF	0.24	0.46	0.20
				CASSQGLAGSNEQFF	0.24	0.28	0.06
				CASSQYNEQFF	0.13	0.07	0.05
				CASTRQGRNEQYF	0.07	0.07	0.05

Figure 4-15. TCRα and TCRβ clonotype frequency distribution from CD8+ tetramer+ sorted MM909.24 TIL populations. (A) CDR3α (top) and CDR3β (bottom) clonotypes from HLA A2-EAAGIGILTV, HLA A2-LLLGIGILVL and HLA A2-NLSALGIFST tetramer+ sorted TILs are displayed as sections of a pie, with each section for each sort corresponding to a different CDR3. Shared clonotypes between the three sorts are indicated in grey/black. The number of total and shared CDR3s for the respective sorts are shown in the centre of each pie. **(B)** List of MM909.24 TIL clonotypes that bound to all three HLA A2-EAAGIGILTV, LLLGIGILVL and NLSALGIFST tetramers. Frequency (%) of each clonotype in the sort is indicated for each tetramer-sorted population. TCR chains corresponding to VB6G4.24 and B17.24 T cell clones are shown in **bold** text.

Clonotypic analysis of bulk α and β TCR chains revealed individual clonotypes capable of binding to more than one tetramer (**Figure 4-14**). Remarkably, 18 CDR3α and 22 CDR3β were found capable of binding to tetramers loaded with all three antigens. The frequency distribution of these TCRs sequences is displayed in **Figure 4-15A**. Shared CDR3s were found at different frequencies amongst the dominant clonotypes in the tetramer$^+$ sorts. Interestingly, both α and β TCR chains corresponding to the MM909.24 TIL-derived T cell clone, B17.24 (TRAV12-2 TRAJ54 CDR3α: **CAVPRGAQKLVF**, TRBV12-4 TRBJ2-7 CDR3β: **CASSWAGPVEQYF**) and the persistent VB6G4.24 T cell clone (TRAV36DV7 TRAJ34 CDR3α: **CAVQTDKLIF**, TRB24-1 TRBJ2-1 CDR3β: **CATSDRGQGANWDEQFF**), were found in EAAGIGILTV, LLLGIGILVL and NLSALGIFST tetramer$^+$ sorts (**Figure 4-15B**), however the discrepancy in the %frequency of each VB6G4.24 TCR chain may indicate they do not dimerise for the binding of such antigens.

Unfortunately, the TCR of CR24 T cell clone and other Melan-A-specific clonotypes described in previous sections, were not found in any of the tetramer sorts. This event reflects inherent caveats of NGS MiSeq platform sequencing observed in my laboratory, whereby samples containing a high diversity are not exhaustively sequenced, thus requiring repeated rounds of sampling and sequencing (*Attaf et al, unpublished*). In hindsight, I should have used a higher throughout platform such as HiSeq for this work, but we did not anticipate that there would be such a widespread diversity of TCRs within a single TIL infusion product when I undertook these studies.

An enrichment of TRAV12-2 gene in shared EAAGIGILTV, LLLGIGILVL and NLSALGIFST tetramer$^+$ TCR clonotypes was observed (**Figure 4-16A**). Previous data published by *Cole et al.*[364] examined the structural and thermodynamic properties of the TRAV12-2 encoded TCR MEL5 in complex with HLA A2-ELAGIGILTV. This study revealed the dominance of the CDR1α loop in peptide binding, indicating an unusual and important role for the TRAV12-2 gene in peptide recognition. This TRAV12-2 gene bias has been reported for other HLA A2-restricted responses from a variety of human diseases[318]. It could therefore be envisaged that TRAV12-2 might exert an acute impact on allowing the degenerate recognition of EAAGIGILTV, LLLGIGILVL and NLSALGIFST peptides. Corroboration of this hypothesis would require structural studies of the CR24 TCR in complex with the cognate antigens. These studies are currently being undertaken by my colleague, Aaron Wall. No significant Vβ gene dominance was found (**Figure 4-16B**).

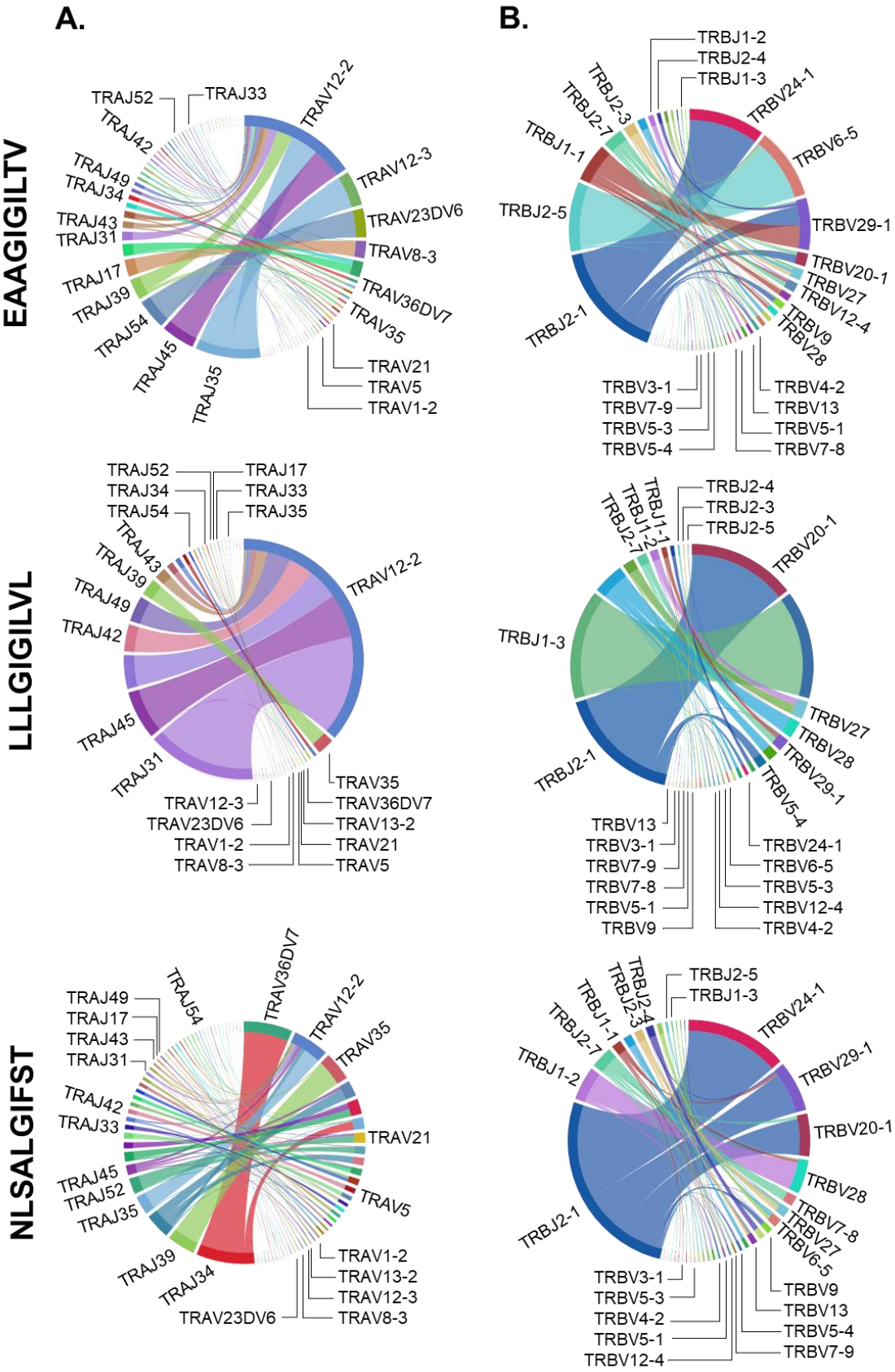

Figure 4-16. **VJ gene usage of shared CDR3 sequences of tetramer-sorted MM909.24 TIL.** TCRα **(A)** and TCRβ **(B)** Variable (arc on the right) and Joining (arc on the left) gene rearrangement from HLA A2- Melan-A_{26-35} (EAAGIGILTV), $BST2_{22-31}$ (LLLGIGILVL) and $IMP\text{-}2_{367-376}$ (NLSALGIFST) $CD8^+$ $tetramer^+$ sorted cells from donor MM909.24 TIL. Only gene usage for overlapping clonotypes is annotated in the graphical display for simplification.

I next examined if the TCRs that showed recognition of autologous tumour in **Figure 4-4B** were capable of binding the tetramers loaded with the candidate cross-reactive antigens. As shown in **Figure 4-17**, 8 out of 35 TCRα and 11 out of 32 TCRβ chains that were found to respond to the autologous tumour also bound to HLA A2-EAAGIGILTV, HLA A2-LLLGIGILVL and HLA A2-NLSALGIFST tetramers. Importantly, 4 persistent TCRβ clonotypes were present in all three tetramer$^+$ sorts: TRB24-1 TRBJ2-1 CDR3β: **CATSDRGQGANWDEQFF** corresponding to VB6G4.24 T cell clone; TRB12-4 TRBJ1-1 CDR3β: **CASTLGGGTEAFF,** TRB5-3 TRBJ1-3 CDR3β**:** **CARRTLVIVRRFYSGNTIYF** and TRB24-1 TRBJ2-1 CDR3β: **CATSDLLLAGGRSSYNEQFF** (**Figure 4-17**, **red** arrow). Interestingly, 13 TCRα and 15 TCRβ clonotypes that bound to more than one tetramer also showed broad recognition of non-melanoma tumours in **Figure 4-4B** (**Figure 4-17**, in **bold**). TCR clonotypic analysis also revealed the presence of clonotypes that only bound to the HLA A2-EAAGIGILTV tetramer, but had been observed to exert broad recognition of tumours lacking the expression of Melan-A. These clonotypes are of special interest as they may possess different 'multipronged' cross-reactivities to the Melan-A/BST2/IMP-2 example described here.

Sequencing of the tetramer$^+$ populations within MM909.24 TIL also provided information on the antigenic specificity of the broadly tumour-reactive TCRs shown in **Figure 4-4B** and **Figure 4-17**. Two broadly tumour reactive clonotypes (TRB20-1 TRBJ2-1 CDR3β: **CSARDLLAETYEQYF,** TRB12-4 TRBJ1-2 CDR3β: **CASSPTTGLKTRSGYTF** and TRB7-8 TRBJ2-2 CDR3β: **CASSLGEGSPGELFF)** were capable of binding both EAAGIGILTV and NLSALGIFST tetramers. A further clonotype **(**TRB12-4 TRBJ2-3 CDR3β: **CASSNTGGYTQYF**) that reacted to most tumour types bound to only the NLSALGIFST tetramer (**Figure 4-17**).

Together this data suggests that TCR cross-recognition of Melan-A$_{26-35}$, BST2$_{22-31}$ and IMP-2$_{367-376}$ peptides is a shared feature of several T cell clonotypes present in the therapeutic TIL of patient MM909.24. I next set out to explore if such cross-reactivity might be beneficial for recognition of tumour.

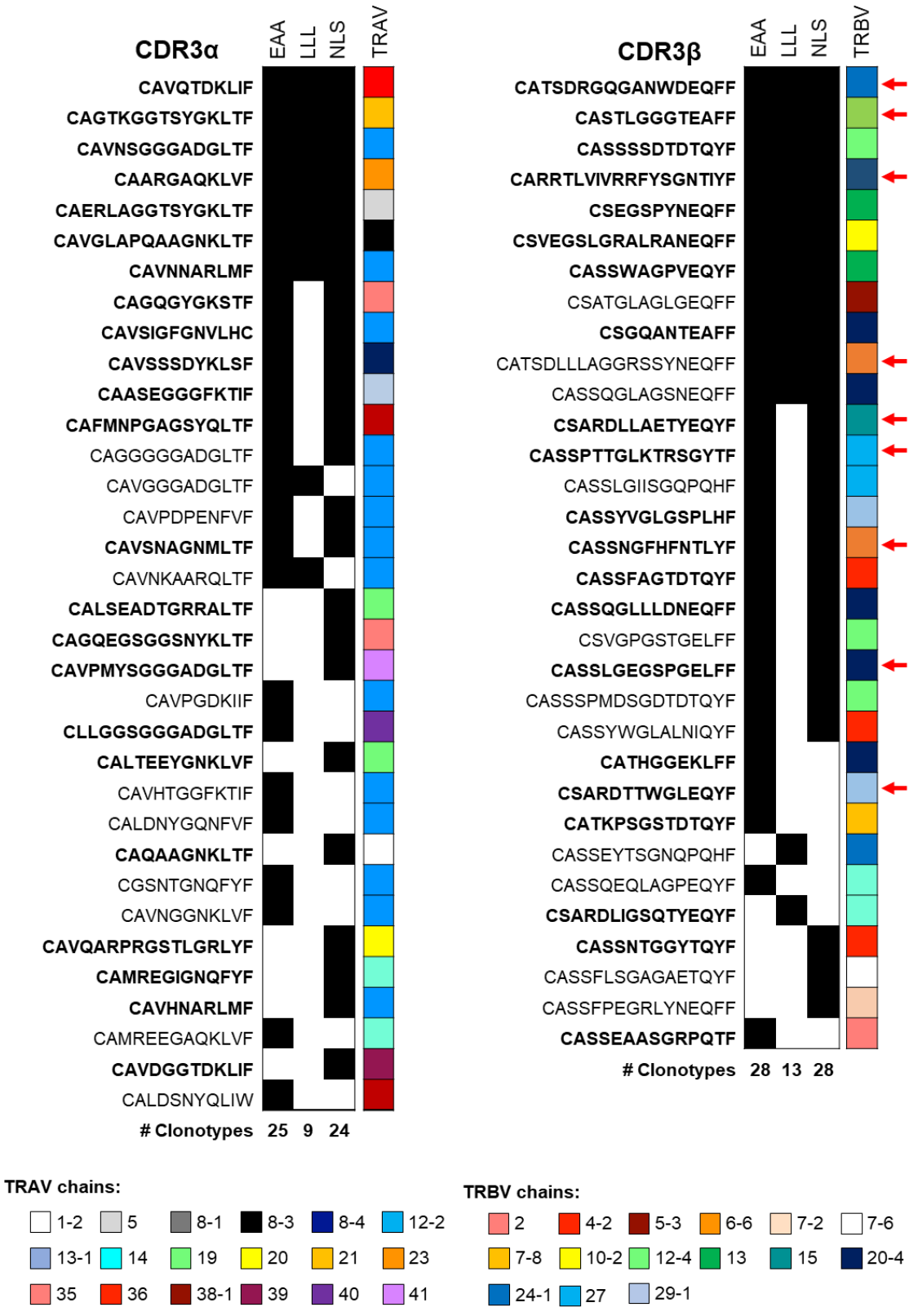

Figure 4-17. **Cross-reactive TCRs respond to autologous tumour.** CDR3 alpha (left) and beta (right) of tumour-reactive clonotypes found in each tetramer sorted population. TRAV and TRBV gene usage is displayed colour-coded on the right side of the map. Indicated in **Bold**, CDR3β clonotypes found to exert broad recognition of tumours in Figure 4-4. Red arrow indicates persistent clonotypes described in **Chapter 3**. Clonotypes are ordered based on the number of different tetramers bound (3 tetramers at the top then 2 and then just a single tetramer). Frequencies of clonotypes in sort are shown in Supplementary table 11.

4.2.9. Synergistic effect of Melan-A, BST2 and IMP-2 antigens in tumour clearance

Recognition of multiple antigens presented at the surface of a target cell may confer multipronged TCRs with enhanced sensitivity due to an increased overall density of cognate antigen presented at the cancer cell surface. I hypothesised that antigens recognised by multipronged TCRs have a synergetic effect on T cell activation when more than one antigen is expressed by the tumour. I tested for potentially additive effects of Melan-A, BST2 and IMP-2 on recognition by the CR24 'multipronged' T cell clone. Highly synergistic effects were observed when the three peptides were combined at a low exogenous concentrations (10^{-8} M; **Figure 4-18**). Synergistic CR24 activation was comparable to the levels of MIP-1β release observed when T cell was incubated with higher concentrations of single peptides, thus suggesting that TCR recognition of multiple targets induces more effective T cell activation. This property could be highly relevant as tumours downregulate the MHC machinery to avoid an immune-attack. Thus, it seems likely that T cells with multipronged TCRs that can recognise more than one tumour-associated antigen will be more likely eliminate tumour *in vivo*.

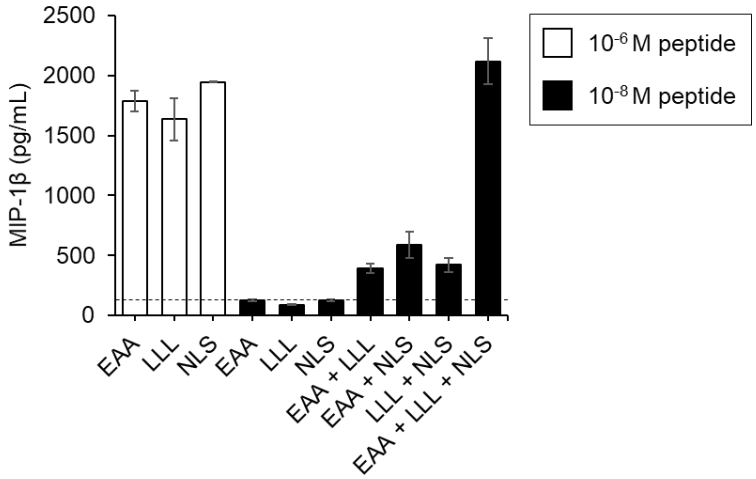

Figure 4-18. **Peptide agonists of a multipronged TCR have an additive effect.** Overnight activation of CR24 T cell clone co-incubated with peptide-pulsed T2 was assessed by MIP-1β ELISA. Melan-A_{26-35} (EAAGIGILTV). $BST2_{22-31}$ (LLLGIGILVL) and IMP-$2_{367-376}$ (NLSALGIFST) peptides were used alone or combined at the indicated concentrations. Mean and standard experimental error from duplicate samples is shown.

4.2.10. Loss of Melan-A expression does not impair CR24 recognition

One of the Darwinian mechanisms developed by tumour cells to achieve immunoevasion is the loss of immunogenic target antigens[146] (see **section 1.4.2**). Multipronged TCRs may limit the possibility for tumour immunoevasion, as escape from any single antigen might not confer the tumour with a selective advantage. To formerly prove that a multipronged TCRs could target tumour cells in the absence of one of the cognate antigens, I set out to investigate whether the loss of Melan-A expression in the autologous tumour impaired the recognition of CR24 T cell clone. For this purpose, five gRNAs targeting different exons on the Melan-A gene (MLANA) were designed. As shown below, the use of CRISPR/Cas9 system allows a rapid and efficient generation of cells deficient in the desired target gene, resulting in more robust phenotypes than those achieved with other gene editing methods, such as siRNA-mediated gene knockdown[326,365]. The alignments of gRNAs with natural MLANA sequences are shown in **Figure 4-19A**. I then transduced the melanoma line from patient MM909.24 with a lentivirus encoding for Cas9, a gRNA specific for Melan-A and a puromycin resistance gene as described in **materials and methods (section 2.7.3)**. Tumours were selected in 1 μg/mL puromycin for up to 2 weeks after infection to allow selection for cells that had effectively incorporated the lentivirus. I then performed single cell cloning to grow a monoclonal population of cells for further testing. Growing Melan-A deficient tumour clones were validated based on and intracellular antibody staining (**Supplementary figure 7**). Due to the heterogeneity within tumour cell lines, it was hypothesised that single cell cloning could result in the selection of cells that were differentially susceptible to T cell-mediated recognition, thus introducing a bias in the results. Therefore, validated Melan-A-deficient clones were combined into a MM909.24 Melan-A^{CRISPR} line (**Figure 4-19B**) for examining T cell reactivity.

I next examined whether the multipronged CR24 and the Melan-A-specific CR124 and CR324 T cell clones (**Figure 4-6A**) grown from the TIL used to treat patient MM909.24 could recognise the Melan-A deficient autologous tumour **Figure 4-19C**). Abrogation of Melan-A expression did not impair CR24 multipronged recognition of autologous tumour, based on TNF and CD107a secretion. In contrast, tumour recognition by both CR124 and CR324 T cell clones was decreased from ~80% (-ve) to ~20% (Melan-A^{CRISPR}) in the absence of Melan-A expression. Notably, CR124 and CR324 only exhibited cross-recognition of tumours from breast origin (**Figure 4-6B**), suggesting that they recognised different antigens than CR24.

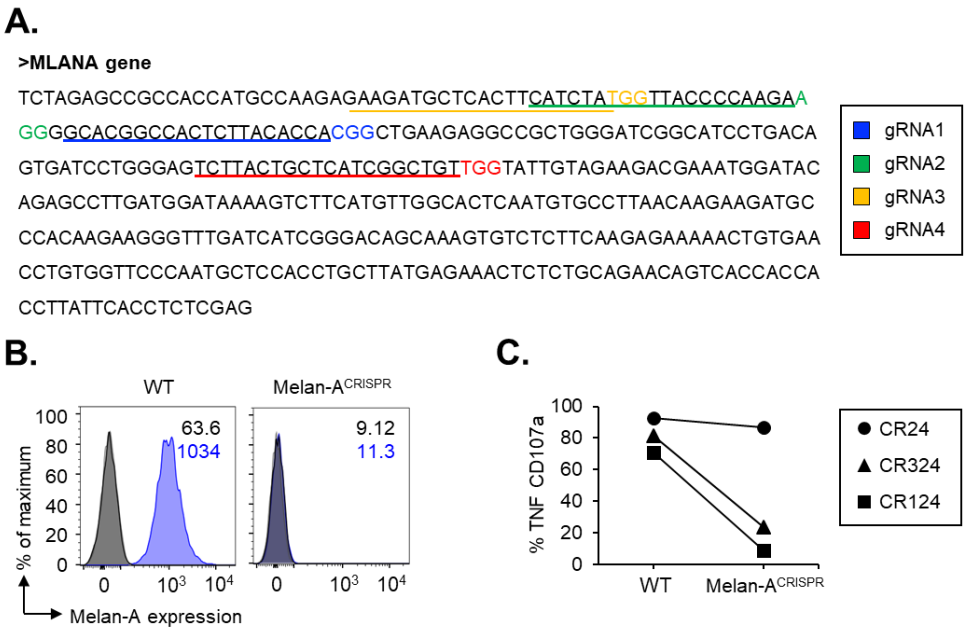

Figure 4-19. MM909.24 TIL-derived T cell clones recognise autologous melanoma regardless of Melan-A expression. **(A)** Five different gRNAs were designed to match the Melan-A gene (*MLANA*). Nucleotide matches are underlined. Protospacer Adjacent Motif (PAM) sequences are shown with the correspondent colour code. **(B)** Melan-A expression in patient MM909.24 autologous melanoma measured by intracellular antibody staining in Wild Type (WT) and CRISPR transduced patient-autologous tumour (Melan-A^{CRISPR}). Mean Fluorescence Intensities (MFI) for Isotype (**black**) and Melan-A (**blue**) are shown. **(C)** T cell clones CR24 (●), CR324 (▲) and CR124 (■) were subjected to a TAPI assay following 4-hour co-incubation with Wild Type (WT) or CRISPR transduced (Melan-A^{CRISPR}) autologous melanoma. Gates were set on single lymphocytes and live CD8$^+$CD3$^+$ cells. Percentage of reactive cells (%TNF$^+$ CD107a$^+$) is shown.

Next, I further corroborated the findings above by testing if CR24 could recognise melanoma targets that were naturally Melan-A low but with high expression of BST2 and/or IMP-2. Tumour lines were sourced from the MM909 patient cohort as RNAseq data was available for all these lines (*data provided by the CCIT*). Transcriptomic analyses revealed that tumours from the HLA A2^{neg} patients MM909.11, MM909.22, and MM909.45 expressed low levels of Melan-A (**Figure 4-20A**). Since CR24 is HLA A2-restricted, I first transduced melanoma lines MM909.11, MM909.22 and MM909.45 with a lentivirus encoding HLA A2 (**Figure 4-20B**). Recognition of these Melan-A^{low} BST2$^+$ IMP-2$^+$ melanoma lines by CR24 was assessed by TNF and CD107a upregulation after 4 h co-incubation with HLA A2$^+$ and HLA A2^{neg} matched melanomas. Incorporation of HLA A2 transgene in the melanomas resulted in T cell recognition (**Figure 4-20C**). Moreover, similar cytotoxicity was observed towards autologous MM909.24 Melan-A^{CRISPR} melanoma, MM909.11 and MM909.22, indicating that recognition was likely mediated through BST2 and IMP-2. The best recognised melanoma line was MM909.45 despite this line expressing relatively low levels of Melan-A and IMP-2. The MM909.45 line expressed a high level of BST2. Thus, it is possible that most the recognition of the MM909.45 melanoma line was via the new BST2 epitope LLLGIGILVL known to act as an agonist for CR24. Further experiments where BST2 was knocked out of melanoma line MM909.45 would be required to formally confirm that BST2 acts as the dominant antigen for CR24 recognition of these cells. Overall, my data confirmed the ability of multipronged TCR CR24 to maintain recognition of tumour when one of the cognate antigens was knocked out or when two were expressed at naturally low levels.

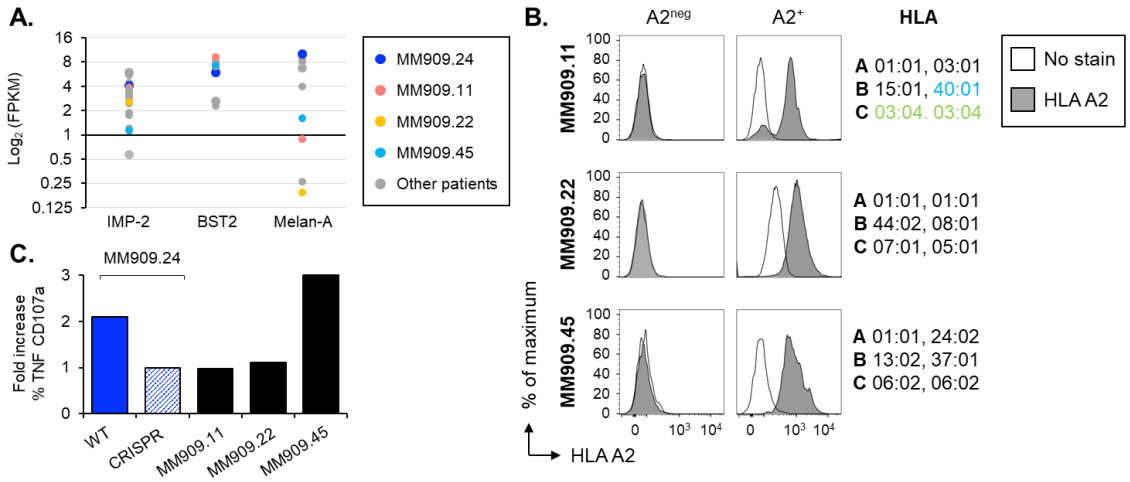

Figure 4-20. **CR24 recognises melanoma tumours that express low levels of Melan-A. (A)** Normalised and log_2 transformed gene transcript levels of IMP-2, BST2 and Melan-A genes expressed in FPKM units (Fragments per kilobase of exon per million reads mapped) in melanoma lines from other malignant melanoma patient samples. The selected Melan-A^{low} $BST2^{high}$ IMP-2^{high} expressing tumours MM909.11 (•), MM909.22 (•), MM909.45 (•) are shown as coloured. MM909.24 (•) autologous melanoma is used as reference and is shown in blue. Data were collected by the CCIT and processed by *Thomas Walley* **(B)** Naturally HLA $A2^{neg}$ tumour cell lines from donors MM909.11, MM909.22 and MM909.45 were transduced with a construct expressing the HLA A2 transgene, thus generating HLA $A2^+$ lines. Both HLA $A2^+$ and HLA $A2^{neg}$ tumour lines were surface antibody stained to confirm HLA A2 expression. Unstained cells (negative control) are indicated in white, HLA A2 stained cells are indicated in grey. HLA typing of each tumour line is shown on the right of the panel. Matching HLAs to MM909.24 are indicated in colour. **(C)** TAPI assay following 4-hour co-incubation of CR24 T cell clone with HLA $A2^+$ and HLA $A2^{neg}$ matched autologous (in **blue**) and allogenic (in **black**) melanomas. Results are shown as fold increase of % TNF^+ $CD107a^+$ secretion relative to MM909.24 Melan-A^{CRISPR}. Gates were set on single lymphocytes and live $CD8^+CD3^+$ cells. Basal % TNF^+ $CD107a^+$ T cell secretion and reactivity towards the HLA $A2^{neg}$ matching line were subtracted from results.

4.2.11. BST2 and IMP-2 are expressed by most tumour cell lines

Next, I sought to investigate the expression patterns of BST2 and IMP-2 in the tumour cell lines recognised by the CR24 T cell clone. This was especially easy for BST2 as it is expressed at the cell surface and there are commercially available antibodies. BST2 expression was high in the MM909.24 autologous melanoma, the B lymphoblast cell line C1R, and the cervix carcinoma line SIHA (**Figure 4-21A, top panel**). Lower levels of BST2 were detected on the breast adenocarcinoma MDA-MB-231, the osteosarcoma SaOS and the colorectal adenocarcinoma COLO 205 cell lines (**Figure 4-21A, middle panel**). The renal cell adenocarcinomas ACHN and RCC17, or the prostate adenocarcinoma PC-3 cell lines did not stain with a BST2-specific antibody (**Figure 4-21A, lower panel**). As IMP-2 is not expressed at the cancer cell surface, examination was performed using a Western Blot of whole cell protein. This staining showed that IMP-2 was expressed by every assayed tumour cell line, with exception of MDA-MB-231 (**Figure 4-21B**). The lack of IMP-2 expression by MDA-MB-231 is in line with a previous study[300]. The antibody used for western blot analysis also stained a lower molecular weight species. This is believed to be IMP-2 isoform 2 (missing amino acids 358-400, including antigenic NLSALGIFST sequence) in samples MM909.24, SaOs, COLO 205, ACHN and PC-3. The lack of Melan-A antigen expression in cancer cell lines from a non-melanoma origin was confirmed using *Genevestigator*[366] (**Supplementary figure 4**).

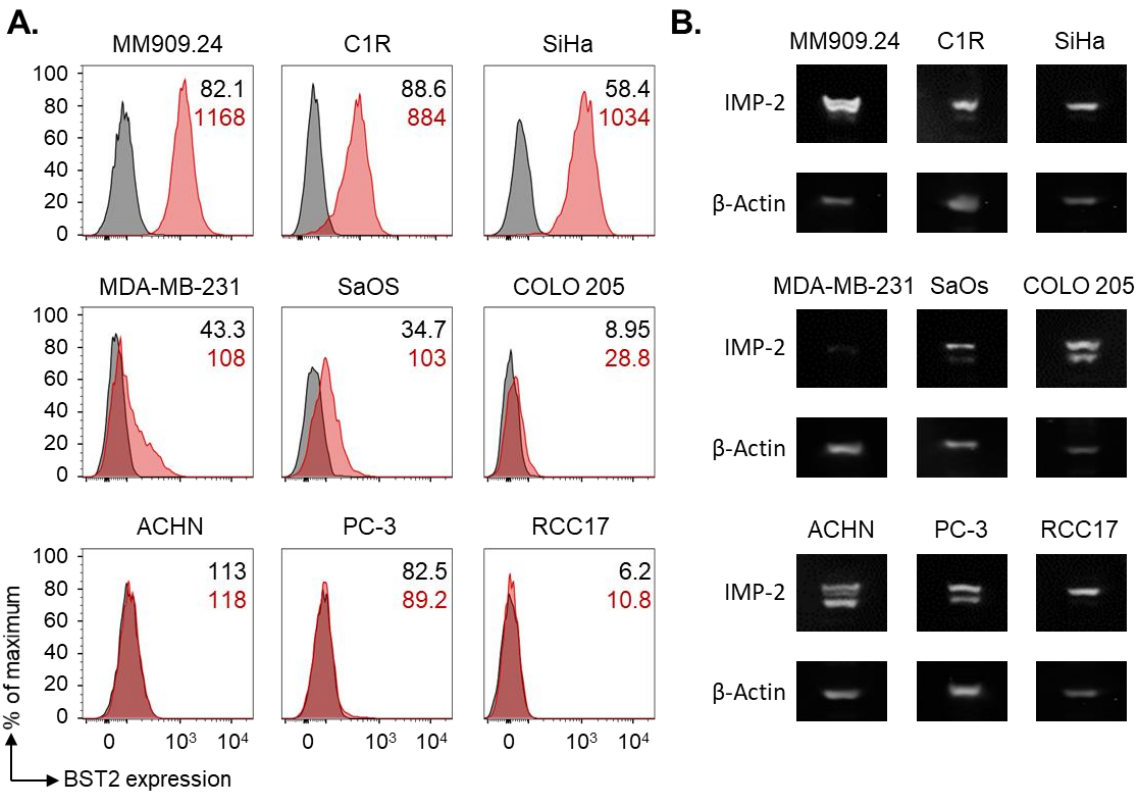

Figure 4-21. **BST2 and/or IMP-2 proteins are naturally expressed by tumour cells. (A)** Surface anti-BST2 antibody staining on tumour cell lines. Fluorescence minus one negative control (FMO) is indicated in grey. BST2 staining is indicated in red. Mean Fluorescence Intensities (MFIs) are shown for each stain. **(B)** Whole tumour cell lysates were blotted for IMP-2 expression. Blotting against β-Actin was used as loading control. MM909.24 cell line was shown to express IMP-2 by WB in Figure 3-11 and was here used as positive control.

Interestingly, of all the cancer lines tested, the strongest targets for CR24 were the BST2^{+} IMP-2^{neg} cell line MDA-MB-231, and the BST2^{+} IMP-2^{+} cell lines C1R, SaOS and SiHa. Further assays directed towards ablation of BST2 expression in these cell lines using CRISPR/Cas9 technology could elucidate if CR24 cytotoxicity is indeed BST2-mediated, or whether an alternative antigen is responsible for CR24 targeting of MDA-MB-231. To test this hypothesis, I started by designing two gRNAs targeting exons 2 and 6 on the BST2 gene. These were applied using the new CRISPR/Cas9 delivery system Neon® developed by Thermo Fisher during my studies. The Neon transfection system uses electroporation to deliver both the gRNA and the Cas9 enzyme, accomplishing higher transfection efficiency and cell viability. I successfully generated BST2 deficient MM909.24, C1R and MDA-MB-231 (BST2^{CRISPR}) lines, as confirmed by BST2 surface antibody staining (**Supplementary figure 8**). Unfortunately, I did not have the time to finish these studies off prior to submission of my PhD thesis as the CR24 T cell clone became difficult to culture. We hope to make the CR24 T cell using TCR replacement technology[240] so that this work can be completed.

4.2.12. Multiple Melan-A$_{26-35}$-specific TCRs derived from patient MM909.24 also recognise BST2$_{22-31}$ and/or IMP-2$_{367-376}$

Since I had established that Melan-A-specific T cells from the TIL used to induced complete durable remission in melanoma patient MM909.24 could respond to multiple cancer lines that do not express Melan-A (**Figure 4-8** and **Supplementary figure 4**), I next investigated whether a panel of 11 further Melan-A-specific clones grown from the TIL infusion product used to treat patient MM909.24, could also recognise BST2$_{22-31}$ and/or IMP-2$_{367-376}$. First, I examined how each clone bound to HLA A2 Melan-A$_{26-35}$, BST2$_{22-31}$ or IMP-2$_{367-376}$ tetramers. Remarkably, 8/11 clones stained with all three tetramers (**Figure 4-22**). Three other clones, including the dominant persistent clonotype, VB6G4.24, only stained with the Melan-A tetramer. Clone VB6G4.24 was previously shown to respond to multiple different tumour lines that do not express Melan-A (**Figure 4-5**). These results suggest that VB6G4.24 must recognise a second epitope in addition to the Melan-A peptide EAAGIGILTV and that this second epitope is neither BST2$_{22-31}$ or IMP-2$_{367-376}$.

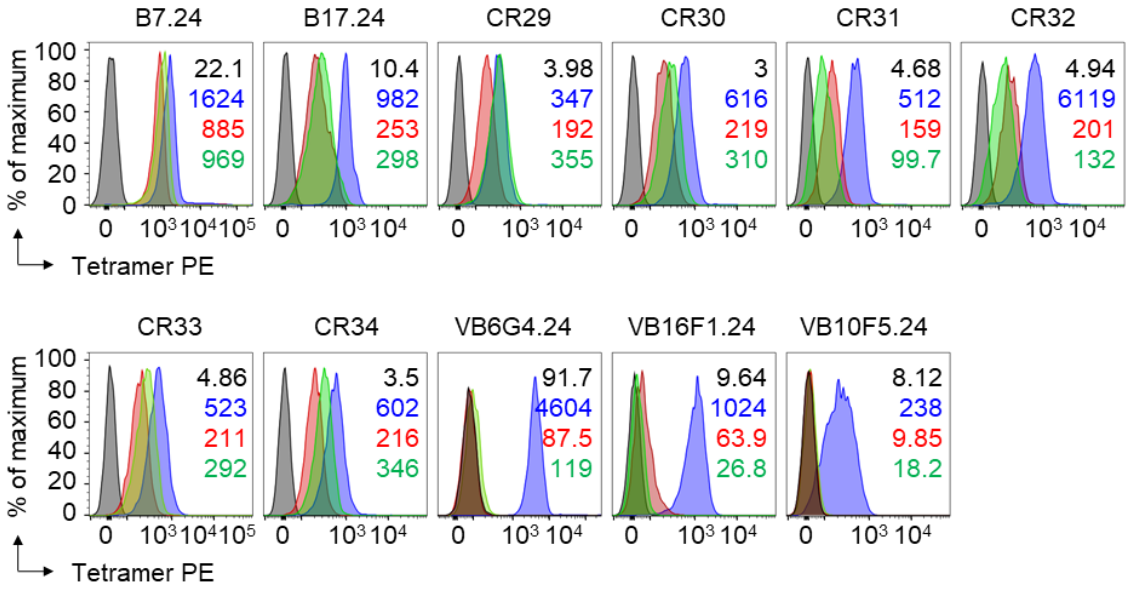

Figure 4-22. **Some TIL24-derived CD8⁺ T cell clones share cross-reactive pattern with CR24.** T cell clones grown from the TIL infusion product of patient MM909.24 were stained with HLA-A2 Melan-A$_{26-35}$ (blue), BST2$_{22-31}$ (red) or IMP-2$_{367-376}$ (green) tetramers. Gates were set on single lymphocytes and live CD3⁺ CD8⁺ cells. Mean Fluorescence Intensities (MFIs) are shown for each stain. Irrelevant tetramer made with human telomerase reverse transcriptase (in grey, hTERT$_{540-548}$) was used as negative control.

The broad cytotoxicity towards tumours observed by dominant persistent clonotype VB6G4.24 called for a closer examination of degenerate peptide recognition by this T cell clone. Unfortunately, sufficient numbers of VB6G4.24 T cells could not be generated for a PS-CPL scan. An approach to bypass this hurdle involving TCR replacement in primary T cells[240] has been developed by my laboratory, and is further discussed in **section 4.3.3.** PS-CPL analysis of the VB6G4.24 TCR is currently in progress.

4.2.13. Effective Melan-A-specific TCRs from healthy donors have capacity to recognise multiple different peptide antigens.

My laboratory has previously compared multiple Melan-A-specific CD8$^+$ T cells from various sources, including the DMF4 and DMF5 TCRs isolated from melanoma patients by the Rosenberg group at NIH[367]. The most effective TCR we have analysed, in terms of mediating recognition of melanoma cells, is MEL5. As this TCR was the most effective, we have previously studied it extensively including using it to generate the second ever TCR in complex with its cognate tumour–associated antigen[170]. Our discovery that some Melan-A-specific TCRs could recognise multiple different tumour-associated peptide antigens – especially those T cells that were most effective at exerting tumour cytotoxicity – prompted me to take a closer look at whether the MEL5 TCR could also recognise other antigens. Indeed, the MEL5 T cell clone bound to HLA A2 tetramer loaded with EAAGIGILTV, LLLGIGILVT and NLSAGIFST peptides confirming that the MEL5 TCR could also recognise these targets (**Figure 4-23A**). MEL5 also showed effective T cell activation, as measured by TNF secretion, after overnight co-incubation with MOLT3 targets transduced with the Melan-A, BST2 or IMP-2 transgene, co-transduced with the HLA A2 transgene (**Figure 4-23B**). These results provide a mechanism for why the MEL5 T cell clone was previously shown to be so effective at recognising HLA A2$^+$ melanomas in comparison to other, presumed to be monospecific, T cell clones and TCRs.

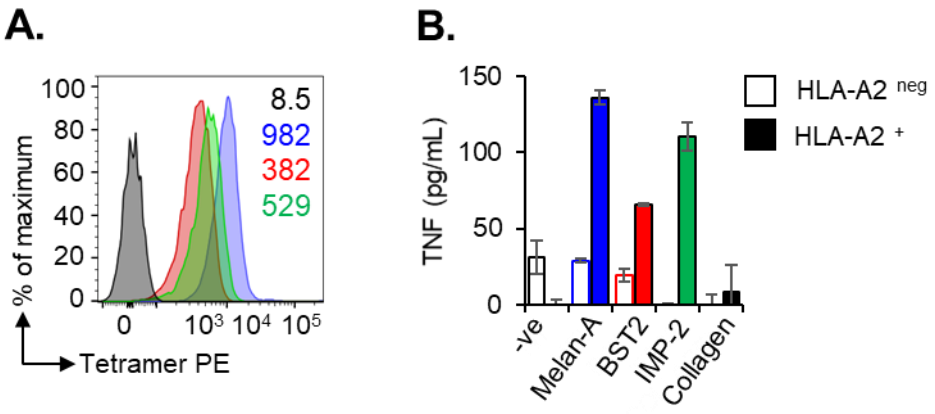

Figure 4-23. **MEL5 CD8+ T cell shows multipronged recognition of Melan-A, BST2 and IMP-2 epitopes. (A)** CD8$^+$ T cell clone MEL5 was stained with HLA A2 Melan-A$_{26-35}$ (blue), BST2$_{22-31}$ (red) or IMP-2$_{367-376}$ (green) tetramers. Gates were set on single lymphocytes and live CD3$^+$ CD8$^+$ cells. Mean Fluorescence Intensities (MFIs) are shown for each stain with the respective colour-code. Irrelevant tetramer made with hTERT$_{540–548}$ (in grey) was used as negative control. **(B)** Recognition of HLA A2^{neg} MOLT3 cell line transduced with Melan-A, BST2 and IMP-2 with or without the HLA A2 transgene was assessed by TNF (pg/mL) release measured by ELISA after overnight co-incubation with target. Non-transduced cells (-ve) were used as negative control for background reactivity towards the MOLT3 cell line. Collagen transduction was used as negative control for background reactivity towards the transgene backbone. Mean and standard experimental error from duplicate samples is shown.

4.2.14. Anti-tumour T cell responses induced from healthy subjects can exhibit multipronged TCRs

So far, my studies had demonstrated that multiple TCRs derived from patient MM909.24 TIL could recognise Melan-$A_{26-35,}$ $BST2_{22-31}$ and IMP-$2_{367-376}$ antigens. I also demonstrated that the effective Melan-A-specific T cell clonotype MEL5, generated from a healthy donor, could also recognise all these antigens. The dominant persistent clonotype in patient MM909.24, VB6G4.24 recognised Melan-A_{26-35} and showed strong recognition of multiple cancer cells lines that did not express Melan-A; however, VB6G4.24 did not respond to $BST2_{22-31}$ or IMP-$2_{367-376}$, suggesting it must recognise other cancer lines by a different epitope. Unfortunately, I was unable to grow sufficient VB6G4.24 for PS-CPL analysis. Collectively, the above results suggest that Melan-A-specific TCRs can exhibit different multipronged specificities and that multipronged, effective T cell clones can be grown from healthy donors.

I next decided to examine whether Melan-A-specific T cells from healthy donors could exhibit different multipronged cross-reactivities. To examine this possibility, I sought to determine if peptide stimulation could prime Melan-$A_{26-35,}$ $BST2_{22-31}$ and IMP-$2_{367-376}$ cross-reactive TCRs. Briefly, $CD8^+$ T cells isolated from the PBMC of HLA $A2^+$ healthy donors were primed with Mock (1% DMSO in PBS, as negative control), Melan-A (EAAGIGILTV), BST2 (LLLGIGILVL) or IMP-2 (NLSALGIFST) peptides and irradiated autologous PBMC for 2 weeks as described in **section 2.3.2**, followed by tetramer staining with each candidate cross-reactive agonist (approach outlined in **Figure 4-24A**). Priming with EAAGIGILTV peptide elicited a greater magnitude of BST2 (0.44% and 2.92% for donor A and B, respectively) and IMP-2 (0.95% and 6.66%) $tetramer^+$ cells than priming with LLLGIGILVL or NLSALGIFST in both donors (**Figure 4-24B**).

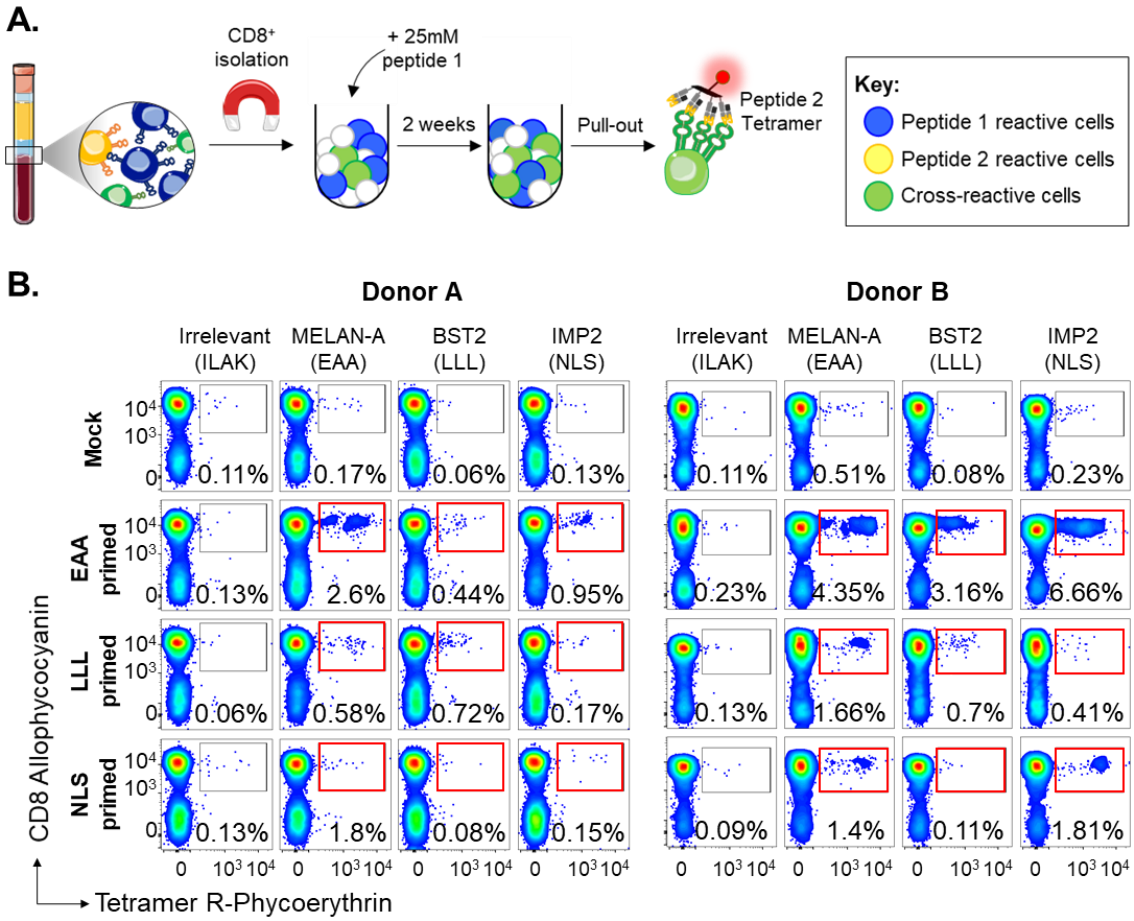

Figure 4-24. Priming of healthy HLA-A2 PBMC with peptide results expands Melan-A, BST2 and IMP-2 tetramer+ cells. **(A)** $CD8^+$ T cells were magnetically isolated from the PBMC of a healthy HLA $A2^+$ donor, followed by priming with autologous irradiated $CD8^{neg}$ cells (1:2 ratio) and 10^{-6} M peptide of choice for 2 weeks. Primed T cells are then magnetically isolated using pMHC tetramers bearing the second peptide of choice. Isolated cross-reactive cells are further validated using functional assays. **(B)** $CD8^+$ T cells from two donors were primed with HLA-A2-restricted Melan-A_{26-35} (EAAGIGILTV), $BST2_{22-31}$ (LLLGIGILVL) or IMP-$2_{367-376}$ (NLSALGIFST) peptides, followed by tetramer staining with each epitope after 2 weeks in culture. Mock priming was performed with 1% DMSO in media to stablish background antigen-specific T cells present in the donor. Irrelevant tetramer made with $hTERT_{540-548}$ was used to set the gates. Gates were set on single lymphocytes and live $CD3^+CD14^{neg}CD19^{neg}$ cells. The percentage of $CD8^+Tet^+$ T cells is shown for each gate.

I focused on the characterisation of cross-reactive responses between Melan-A_{26-35} and IMP-$2_{367-376}$ at the clonal level. The two clones CACTUS and LIMÓN were generated from the Donor B EAAGIGILTV-primed line, whereas the clone MANUELA was generated from the NLSALGIFST-primed line. αβTCR sequencing confirmed that the three clones expressed different TCRs, but shared TRAV12-2 gene segment usage. The Melan-A-derived T cell clones CACTUS and LIMÓN showed similar affinity for the HLA A2-EAAGIGILTV and HLA A2-NLSAGIFST tetramers, whereas the IMP-2-derived T cell clone MANUELA bound the HLA A2-EAAGIGILTV at lower affinity in comparison to the binding to the HLA A2-NLSAGIFST tetramer, as indicated by the MFI values (**Figure 4-25A**).

Peptide sensitivity as measured by MIP-1β secretion after overnight incubation with peptides further corroborated these observations (**Figure 4-25B**). Of the three clones that recognised Melan-A and IMP-2, LIMÓN showed highest sensitivity towards both EAAGIGILTV and

NLSAGIFST peptides at the lowest concentrations (10^{-8} M and 10^{-9} M, respectively), whereas MANUELA showed high sensitivity towards the NLSAGIFST peptides at the lowest concentration (10^{-10} M), but only recognised the EAAGIGILTV peptide at higher concentrations (10^{-6} M). Similarly, CACTUS showed higher sensitivity towards the EAAGIGILTV peptide than towards the NLSAGIFST peptide.

Next, CACTUS, LIMÓN and MANUELA were tested for recognition of a panel of HLA $A2^{+}$ tumour lines, and their correspondent HLA $A2^{neg}$ counterparts by MIP-1β ELISA (**Figure 4-25C**). All three T cell clones lysed a diverse panel of cancer cell lines, spanning melanoma, breast cancer, cervical cancer, bone osteosarcoma and renal cell carcinoma that shared no common HLA other than HLA A2. Although different patterns of tumour pan-recognition were observed between CACTUS, LIMÓN and MANUELA, preferential HLA A2-restricted recognition of the ovarian cancer cell line SiHa and the renal cell carcinoma cell line RCC17 was observed.

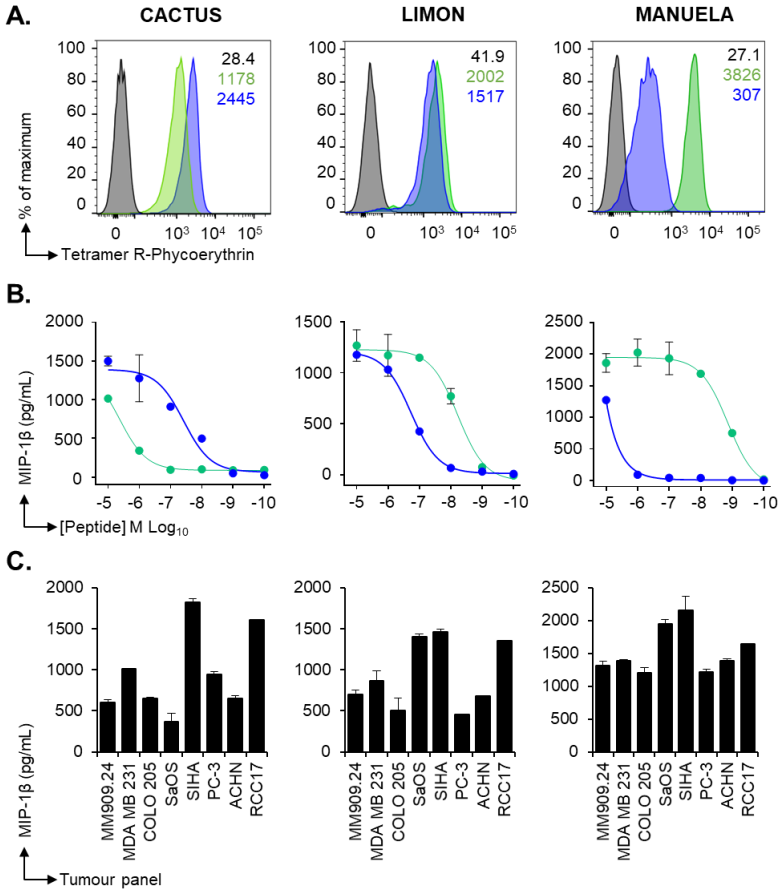

Figure 4-25. Generation of CD8⁺ IMP-2 and Melan-A cross-reactive T cell clones after priming of healthy HLA-A2 donor's PBMC. (A) CD8⁺ T cell clones were stained with HLA-A2 Melan-A_{26-35} (blue) or IMP-$2_{366-376}$ (green) tetramers. Gates were set on single lymphocytes and live $CD3^{+}$ $CD8^{+}$ cells. Mean Fluorescence Intensities (MFIs) are shown for each stain with the respective colour-code. Irrelevant tetramer made with $hTERT_{540-548}$ (in grey) was used to set the gates. **(B)** T cell clone overnight activation with cognate Melan-A_{26-35} peptide (in blue) or IMP-$2_{367-376}$ (green) peptides and assessed by MIP-1β (pg/mL) release measured by ELISA. Mean and standard experimental error from duplicate samples is shown. **(C)** T cell reactivity towards a panel of HLA-$A2^{+}$ cancer cell lines determined by MIP-1β cytokine release (in pg/mL) measured by ELISA after overnight co-incubation. Reactivity towards the HLA-$A2^{neg}$ matched tumour line was subtracted and standard error of the mean is shown.

Two more CD8⁺ T cell clones, MARIA and TESLA, were grown from Donor B PBMC by priming with EAAGIGILTV and NLSALGIFST peptides, respectively. Clones MARIA and TESLA only recognise either the Melan-A_{26-35} or IMP-$2_{367-376}$ peptide (**Figure 4-26A**), yet both clones showed effective recognition of tumour cell lines that did not express these antigens (**Figure 4-26B**). These results suggest that MARIA and TESLA must be recognising a further TAA.

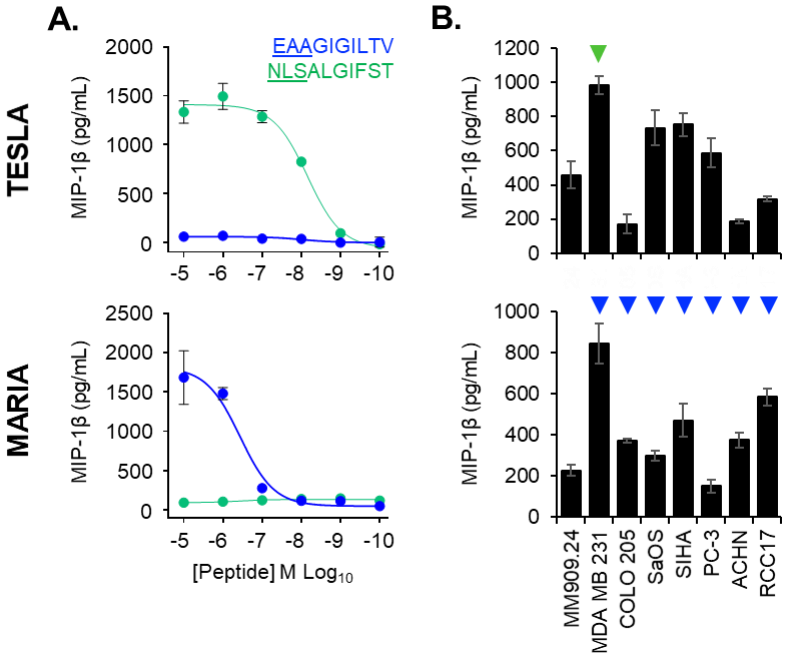

Figure 4-26. **MARIA and TESLA T cell clones exhibit multipronged recognition of IMP-2⁺ and IMP-2^{neg} tumour cell lines. (A)** T cell clone overnight activation with cognate Melan-A_{26-35} peptide (in blue) or IMP-$2_{367-376}$ (green) peptides and assessed by MIP-1β ELISA. Mean and standard experimental error from duplicate samples is shown. **(B)** T cell reactivity towards a panel of HLA-A2⁺ cancer cell lines determined by MIP-1β ELISA after overnight co-incubation. Reactivity towards the tumour cell lines lacking the cognate antigen is indicated with an arrow (▼for IMP-2, ▼for Melan-A). Reactivity towards the HLA-A2^{neg} matched tumour line is subtracted for plotting. Standard error of the mean is shown.

I next decided to try and identify the potential cross-reactive ligands using the proven CPL-based ligand identification described (see **section 4.2.6**) as I could expand T cell clones MARIA and TESLA to sufficient number for PS-CPL screening. The PS-CPL screen of TESLA showed that TCR recognition was highly conserved at residues 6 and 8, but far more degenerate at the remaining positions at the N- and C- terminal regions of the peptide backbone (**Figure 4-27A**). These results suggested that TESLA could potentially recognise a vast array of different decamer amino acid combinations in addition to the cognate NLSALGIFST peptide. Tumour associated peptides predicted with the epitope discovery pipeline (**Figure 4-9**) are shown in **Table 4-3**. Candidate cancer peptides (60% purity) were initially tested at 10^{-6} M in an overnight activation assay followed by MIP-1β cytokine release. From the top ranked candidate peptides, TESLA showed activation towards three peptides: (1) **LA**S**Q**LG**VYRA** from the Breakpoint cluster region protein (BCR, residues 584-593), (2) **VL**S**GI**G**VRAG** from the Melanoma-associated antigen C1 (MAGE-C1, residues 1022-1031) and (3) **SAAG**LG**LVAI** from the Solute carrier family 45 member 3 (SLC45A3, residues 526-535) (differing amino acid residues from the index NLSALGIFST peptide are indicated in bold) (**Figure 4-27B** and **Table 4-3**).

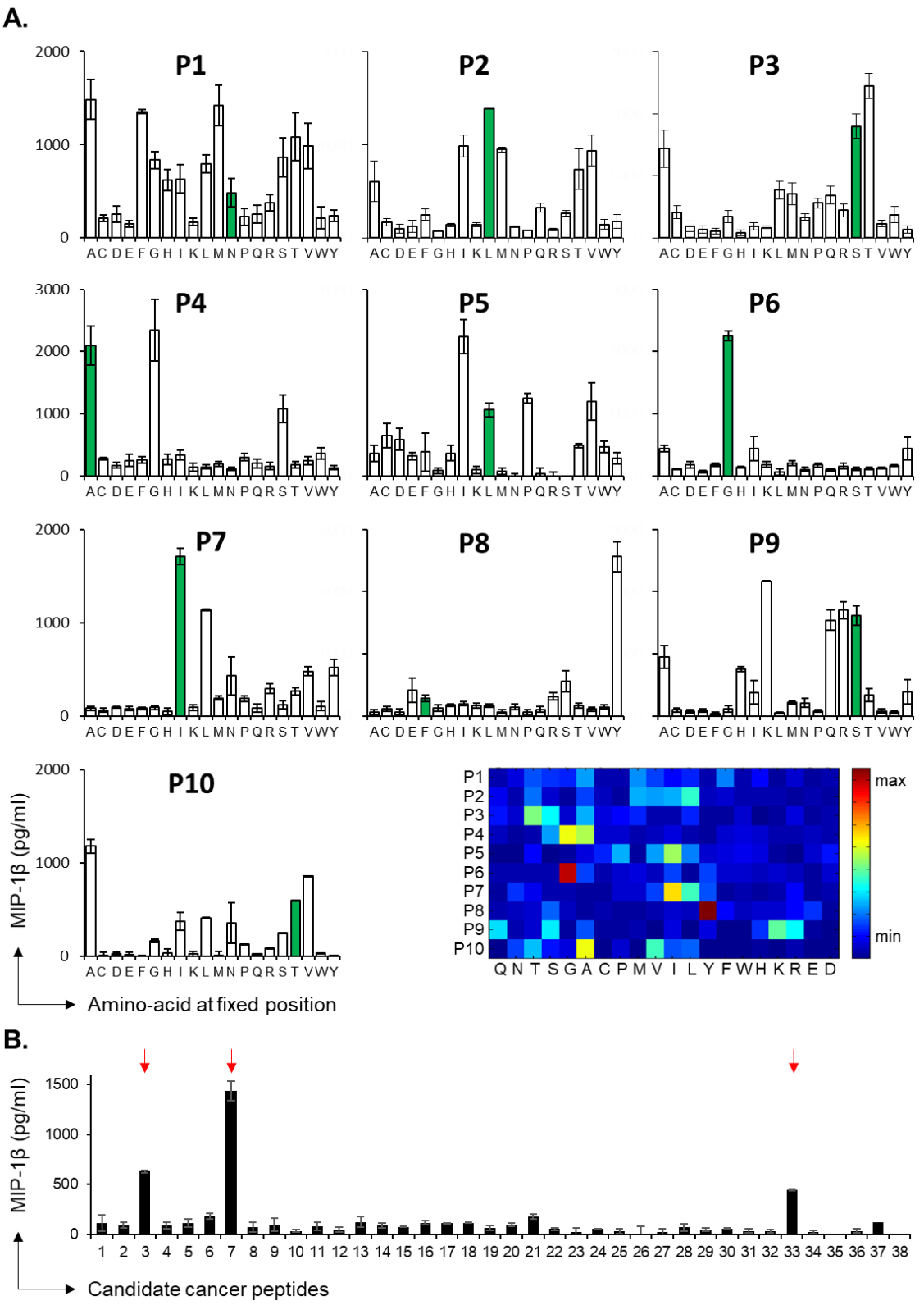

Figure 4-27. Decamer CPL-screening of the IMP-2-specific T cell clone TESLA. (A) Following overnight incubation with a decamer CPL library (10^{-4}M), MIP-1β (pg/mL) output was measured using ELISA to determine the preferred L-amino acid residue landscape (shown in single-letter code format) of TESLA's TCR. Results are displayed as histogram plots and SD from the mean of two replicates is shown. Each tick in the Y axis indicates an increment of 1000 pg/mL. The index IMP-2 peptide sequence (NLSALGIFST) is shown in green. A heatmap summarising PS-CPL scan data for TESLA is shown. **(B)** Activation to candidate cancer peptides was assessed by MIP-1β (pg/mL) release measured by ELISA after overnight co-incubation with 10^{-6}M peptide at 60% manufacturing purity, obtained from the informatic processing of PS-CPL data. Potentially recognised peptides are indicated with a red arrow. Mean and standard experimental error from duplicate samples is shown.

Table 4-3. Candidate peptide sequences from TESLA CPL scan ranked in order of recognition likelihood.

#	Sequence	Protein	Abreviation	UniProt
1	LLSSPYYYSA	Isoform 3 of Paired box protein	Pax-2 OS	Q02962-3
-	NLSALGIFST	Insulin-like growth factor 2 mRNA-binding protein	IGF2BP2	Q9Y6M1
2	HMAAAGISST	Sarcoma antigen 1	SAGE	Q9NXZ1
3	LASQLGVYRA	Breakpoint cluster region protein	BCR PE	P11274
4	RILGPGLNKA	60S ribosomal protein L10a	RPL10A	P62906
5	SVAGWGLGSA	Isoform 2 of Cancer/testis antigen 1	CTAG1A	P78358-2
6	NITSLGLRSL	Epidermal growth factor receptor	EGFR	P00533
7	VLSGIGVRAG	Melanoma-associated antigen C1	MAGEC1	O60732
8	AAPAPGIFSS	Apoptosis regulator Bcl-2	BCL2 PE	P10415
9	LLGSPYYYSA	Breakpoint cluster region	BCR	P11274
10	GTSGLGNRSL	Leukocyte tyrosine kinase receptor isoform 3 precursor	LTK	P29376
11	AAAAAGVSST	Melanoma-associated antigen B2	MAGEB2	O15479
12	VLNAVGVYAG	Melanoma-associated antigen C2	MAGEC2	Q9UBF1
13	GMEEVGIYRV	Paired box protein 5	PAX5	Q02548
14	TLAALGASKL	Transient receptor potential cation channel subfamily M member 8	TRPM8	Q7Z2W7
15	CLVSIILYRA	Anoctamin-7	ANO7	Q6IWH7
16	FLPEFGISSA	Lengsin	LGSN	Q5TDP6
17	GLSADALERL	Poly [ADP-ribose] polymerase 12	PARP12	Q9H0J9
18	GISWLGLRSL	Receptor tyrosine-protein kinase erbB-2	ERBB2	P04626
19	GIMGVIYRKA	Canalicular multispecific organic anion transporter 2	ABCC3	O15438
20	SAAGYGLGSA	Transcription factor SOX-10	SOX10	P56693
21	ALSSVGLHMT	Squamous cell carcinoma antigen recognized by T cells	SART3	Q15020
22	GITRLGPYSL	Mucin-16	MUC-16	Q8WXI7
23	ALLAVGATKV	Isoform 4 of Melanocyte protein PMEL	PMEL	P40967-4
24	ALLSLGYSHS	DNA-binding protein SATB1	SATB1	Q01826
25	NITELGPYSL	Mucin-16	MUC-16	Q8WXI7
26	AIAGAKLRKV	Isoform 2 of Protein enabled homolog	ENAH	Q8N8S7-2
27	SMTGLPLSAL	Zinc finger protein 395	ZN395	Q9H8N7
28	AVAGIRVESL	Tyrosine-protein kinase STYK1	STYK1	Q6J9G0
29	ITSGPDINSA	Mucin-16	MUC-16	Q8WXI7
30	LVSGWGLLAN	Kallikrein-4	KLK4	Q9Y5K2
31	AMTSPPVSST	Mucin-16	MUC-16	Q8WXI7
32	AITSPGPEAS	Mucin-16	MUC-16	Q8WXI7
33	SAAGLGLVAI	Solute carrier family 45 member 3	S45A3	Q96JT2
34	TTSSPGTSTV	Mucin-16	MUC-16	Q8WXI7
35	MLTSLVISSG	Mucin-16	MUC-16	Q8WXI7
36	VVAGIVVLVI	Epithelial cell adhesion molecule	EPCAM	916422
37	ILQGFLVMLA	Isoform 2 of Canalicular multi-specific organic anion transporter 2	MRP3	O15438-2
38	SAAGYGLGSA	Transcription factor SOX-10	SOX10	P56693

Table 4-4. **Candidate cancer-related peptides recognised by TESLA T cell clone.** Amino acid residues that differ from the cognate NLSALGIFST peptide sequence are indicated in bold and underlined.

#	Peptide	Protein	Names	Residues	UniProt ID
3	**LASQ**LG**VYRA**	Breakpoint cluster region protein	BCR NY-REN-26	584-593	P11274
7	**V**LS**GIGVRAG**	Melanoma-associated antigen C1	MAGE-C1 CT7.1	1022-1031	O60732
33	**SAAG**LG**LVAI**	Solute carrier family 45 member 3	SLC45A3 Prostein	526-535	Q96JT2

As shown in **Figure 4-27B**, the strongest response of TESLA to exogenously supplied peptide was observed towards the cancer testis antigen MAGE-C1$_{1022-1031}$ (VLSGIGVRAG). MAGE-C1 is consistently expressed by malignant plasma cells in multiple myeloma patients, and does not appear to be downregulated during the course of the disease[368]. Lower activation levels of TESLA were observed towards the Prostein-derived peptide SAAGLGLVAI. Prostein has been described as a prostate tissue-specific protein that is uniquely and abundantly expressed in normal and cancerous prostate tissues[369]; and loss of expression has been correlated with loss of cell migration and invasion *in vitro*[370]**.** Interestingly, a study conducted by *Pin and colleagues*[371] looking at serological markers for patients with prostate cancer identified autoantibodies for both Prostein and IMP-2 proteins. Finally, TESLA T cell clone showed activation towards a NY-REN-26-derived peptide (LASQLGVYRA), a renal carcinoma antigen encoded by the BCR gene. BCR is one of the two genes of the BCR-ABL complex known to translocate and fuse, causing a genetic abnormality in chromosome 22 known as the Philadelphia translocation[372]. This genetic abnormality is observed in leukaemia cancer cells. Importantly, BCR-ABL-specific T lymphocytes have been identified in Philadelphia$^+$ ALL patients[373].

HLA A2-restricted T cell responses have been described towards MAGE-C1 for the treatment of multiple myeloma[374]. Similarly, HLA A2-restricted peptides derived from Prostein have been described by *Friedman and colleagues*[369], and *Kiessling and colleagues*[375]; and BCR-ABL-specific T lymphocytes have been identified in Philadelphia$^+$ ALL patients[373]. Yet, no reports have described immunogenicity of the VLSGIGVRAG, SAAGLGLVAI or LASQLGVYRA peptides. Validation of the predicted epitopes MAGE-C1$_{1022-1031}$, BCR$_{584-594}$ and Prostein$_{526-535}$ antigen immunogenicity would involve examining TESLA recognition of endogenously expressed antigen and staining with cognate pMHC tetramers. Unfortunately, I did not have time to complete the validation of these epitopes before the completion of my PhD thesis.

The PS-CPL screen of MARIA showed that TCR recognition degeneracy was consistent with previous structural analyses of Melan-A specific TCR binding to HLA A2-EAAGIGILTV[356] (**Figure 4-28**). Indeed, the number of amino acids recognised by MARIA was restricted in the central region of the peptide (residues 4 to 6); whereas most degenerate peptide backbone residue recognition was observed at the N and C terminal regions, showing hotspots for amino acid preference in the N terminal positions and extreme positional degeneracy at C terminal regions. Predicted tumour-associated peptides are shown in **Supplementary table 12**. Unfortunately, I did not have time to explore MARIA's recognition of candidate peptides before the completion of my studies. Current efforts are dedicated to the expansion of sufficient numbers of MARIA to perform a screen of >50 candidate cancer peptides to proceed to stage III of the epitope discovery pipeline described in **Figure 4-9**.

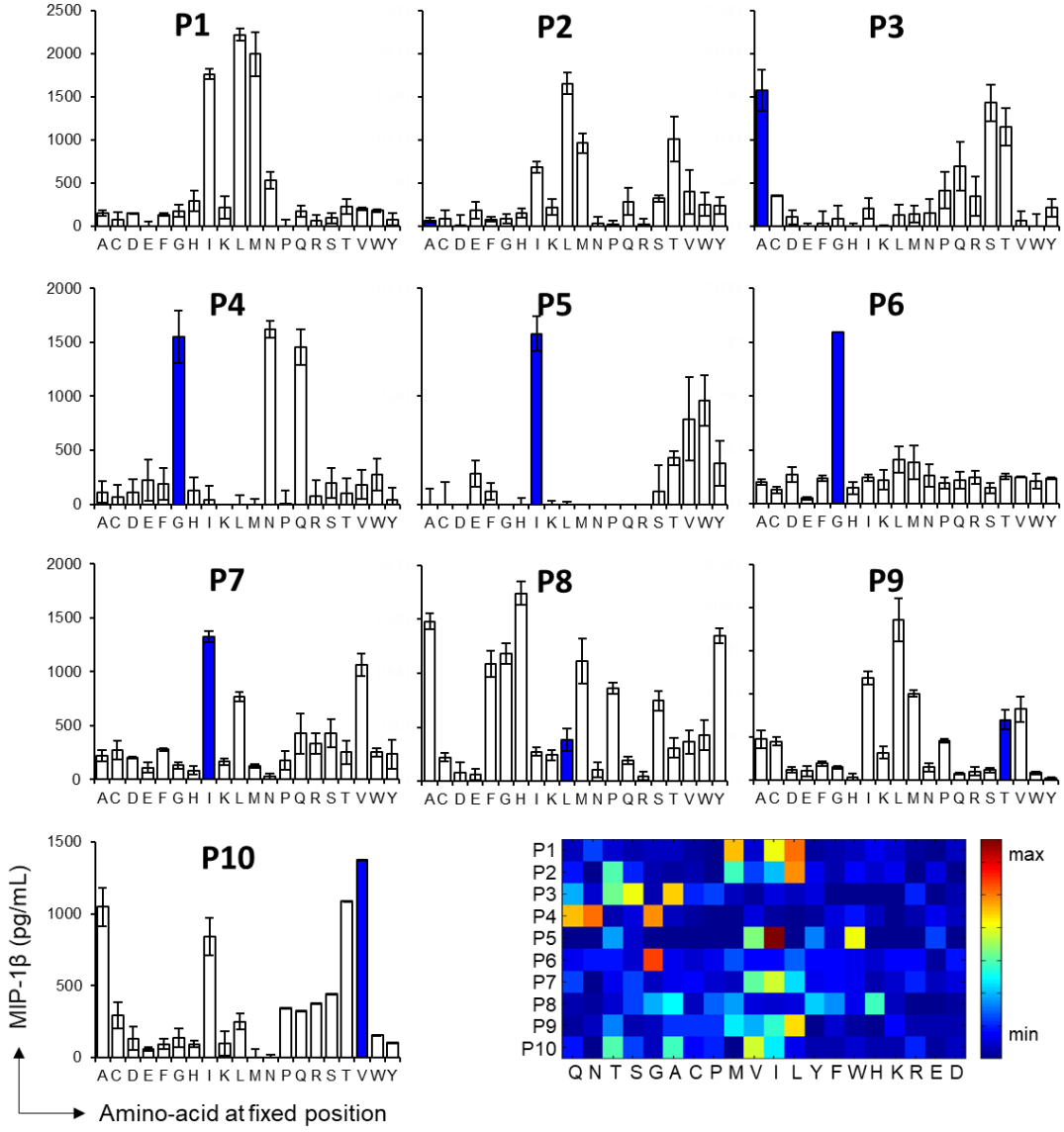

Figure 4-28. **Decamer CPL-screening of the Melan-A-specific T cell clone MARIA.** Following overnight incubation with a decamer CPL library (10^{-4}M), MIP-1β (pg/mL) output was measured using ELISA to determine the preferred L-amino acid residue landscape (shown in single-letter code format) of MARIA's TCR. Results are displayed as histogram plots and SD from the mean of two replicates is shown. The index Melan-A peptide sequence (EAAGIGILTV) is shown in blue. Each tick in the Y axis represents an increment of 500 units. A heatmap summarising PS-CPL scan data for TESLA is shown.

4.3. Discussion

4.3.1. Summary of findings in this chapter

Development of immunotherapies that are effective, safe and applicable to multiple cancer types represents a major challenge in the field. Re-infusion of *ex vivo* expanded TILs has shown great promise for the treatment of patients with metastatic cancer[217,289,376–379]. The proven feasibility and safety of recently developed genetic engineering tools constitute a promising approach for cancer immunotherapy by facilitating the introduction of genetically modified T cells with well characterised αβTCR chains of known specificity[134]. However, the selection of the antigenic target is still a major hurdle in the field. At the outset of my work, I hypothesised that the dominant clonotypes that persisted in patient blood following successful TIL therapy for melanoma might provide a guide as to the best antigens to target and provide effective TCRs that could be used for treatment of other patients via TCR gene transfer (TCR-T therapy). The fact that activated T cells with such TCRs had been transfused into patients in large number without adverse secondary effects provided a strong indication that these receptors would be safe for therapy.

In this chapter, I dissected the cancer-specific T cell response in the TIL used to successfully treat stage IV melanoma patient MM909.24. Following with the work presented in **Chapter 3**, I confirmed that some T cell clones in the TIL used to treat this patient persisted in patient blood after complete durable tumour remission. These *persistent* clonotypes and the antigens they recognised were of particular interest as they might have been responsible for tumour clearance in this patient. Amongst all the tumour-cleared patients in the MM909 cohort, patient MM909.24 was selected for their HLA Class I allotype, as they were HLA $A2^+$ and expresses only a single HLA B and HLA C allele. It was therefore hoped that much of the anti-tumour response observed in this patient was directed through HLA A2. HLA A2 is the most frequent HLA in the human population, occurring in ~45% of individuals worldwide[380]. The frequency of HLA A2 in the population makes it the most attractive HLA-I molecule for immunotherapy approaches.

Staining of the TIL used to treat patient MM909.24 with tetramers of the common HLA A2-restricted melanoma antigen, Melan-A_{26-35} (EAAGIGILTV), showed that ~8.5% of the TCRs in these TIL were specific for this antigen (**Figure 4-2**). However, over 40% of these TIL responded to autologous tumour, suggesting that only a minority of the tumour-specific T cells in MM909.24 TIL targeted Melan-A_{26-35}. In order to determine whether any of the non-Melan-A_{26-35} response in MM909.24 TIL was HLA A2-restricted, I abrogated HLA A2 expression from the autologous tumour line, observing a reduction in the number of responding T cells from 42.5% to 7%. This data suggested that the majority of the response within MM909.24 TIL was HLA A2-restricted but not Melan-A_{26-35}-reactive, thus indicating that MM909.24 TIL might recognise new HLA A2-restricted cancer-specific epitopes.

Work by previous PhD students in my laboratory had shown that MM909.24 TIL could respond to non-melanoma cancer cell lines, suggesting that some T cells in these TIL might target broadly expressed tumour antigens. Indeed, MM909.24 TIL showed HLA A2-restricted recognition of the ovarian-derived A2780 cell line, EBV-transformed B lymphoblast C1R, colorectal-derived COLO205 adenocarcinoma and the cervix-derived SIHA carcinoma (**Figure 4-3**), thus confirming that these broadly tumoricidal T cells operated through the common HLA A2 molecule. Allorecognition of non-melanoma tumours was unlikely as no shared HLAs were present across these lines. There are no known HLA A2-restricted epitopes shared by all these tumour lines suggesting that MM909.24 TIL must recognise novel HLA A2-restricted epitopes.

Sequencing of broadly tumour-reactive TCRs in patient MM909.24 TILs identified that 8/23 TCRβ chains in patient PBMC following complete remission (**Figure 4-4**). These *persistent* clonotypes are of special interest as they may have been responsible for cancer clearance in this patient. Three of the eight persistent clonotypes identified were previously shown to be present in sorts with Melan-A_{26-35} tetramer (**Chapter 3**) indicating that they were specific for this common antigen. The target for the remaining five HLA A2-restricted persistent clonotypes was unknown. The identity of these epitopes and TCRs that recognise them could prove to be very valuable to the field of cancer immunotherapy. Examination of the TCR clonotypes responding to each tumour revealed 5 TCRα and 4 TCRβ capable of responding to all these tumours in addition to the autologous melanoma line (**Figure 4-4**). The ability of T cell clonotypes to respond to all tumour lines tested suggested that they might be recognising important new epitopes. Notably, both the TCRα and TCRβ chains of the formerly characterised persistent T cell clone VB6G4.24, previously shown to stain with tetramer loaded with the HLA A2-restricted Melan-A peptide EAAGIGILTV, was the most enriched TCR sequence in all tumour-reactive sorts. None of the non-melanoma cancer cell lines express Melan-A suggesting that the VB6G4.24 T cell clone must be capable of recognising cancer targets via another epitope. Dual recognition of two different cancer-specific epitopes via a single TCR is unprecedented and warranted further investigation.

In vitro confirmation of VB6G4.24 response to HLA $A2^+$ prostate carcinoma, breast adenocarcinoma, renal cell carcinoma and bone osteosarcoma cell lines (**Figure 4-5**) prompted me to examine whether other Melan-A-specific $CD8^+$ T cell clones could also recognise HLA $A2^+$ cancer cell lines that did not express Melan-A. Similar to observations made with the VB6G4.24 T cell clone, MM909.24 TIL derived T cell clones CR24, CR124 and CR324 (**Figure 4-6**) also responded to other HLA $A2^+$ cancer lines, suggesting that they might also be recognising a further epitope. As each T cell clone gave different recognition patterns across the various tumour types, it was considered possible that each clone might exhibit different antigenic specificities in addition to Melan-A.

I next set out to determine which further antigens were being targeted by these Melan-A-specific T cells. I chose CR24 for my initial experiments because it: (i) could be expanded to sufficient number for PS-CPL screening; (ii) showed the best reactivity to non-melanoma cancer cell lines of the clones tested; and, (iii) persisted in the blood of patient MM909.24 after complete durable

remission suggesting that this clonotype may have played an important role in cancer remission. The T cell epitope identification pipeline described in **Figure 4-9** was applied to CR24. A sizing scan indicated that CR24 exhibited a preference for peptides of ten amino acids in length and a decamer PS-CPL screen was applied. In common with other known Melan-A-specific T cells, this screen suggested reduced degeneracy in the middle of the peptide (residues 4-6) whereas many amino acids could be substituted outside of this core 'footprint'. Application of GP-GPU-based prediction algorithm in conjunction with a bespoke cancer proteomics database to the PS-CPL data generated a ranked list of potential epitopes recognised by CR24. Four of the top five predicted epitopes were recognised by CR24 when tested, thereby showing the validity of this new approach to cancer epitope identification. In addition to the natural Melan-A sequence and its commonly used heteroclitic variant, two potential new epitopes were identified. These two new putative epitopes were **LLL**GIGIL**VL** from the Bone marrow stromal antigen 2 protein ($BST2_{22\text{-}31}$) and **NLS**AL**G**I**FST** from the Insulin-like Growth Factor-2 mRNA-Binding Protein 2 (IMP-$2_{367\text{-}376}$). CR24 cross-recognition of Melan-$A_{26\text{-}35}$, $BST2_{22\text{-}31}$ and IMP-$2_{367\text{-}376}$ was validated by pMHC tetramer staining and activation assay (**Figure 4-12**). While these results proved that these antigens bound to the CR24 TCR and that the T cell clone could respond to these peptides, they did not prove that the peptides could be genuinely processed and presented at the tumour cell surface. In order to validate these new putative epitopes, I expressed them +/- HLA A2 in MOLT3 cells. Recognition of MOLT3 targets by CR24 and by another multipronged T cell clone, MEL5, required that MOLT3 expressed HLA A2 in conjunction with either Melan-A, BST2 or IMP-2 (**Figure 4-12** and **Figure 4-23**); confirming the discovery of two novel *bona fide* HLA A2-restricted cancer epitopes.

Hundemer and colleagues[357] previously suggested that a nonamer BST2 peptide (LLLGIGILV, residues 22-30) might be an HLA A2-restricted T cell target for multiple myeloma, however presentation of this nonamer peptide was never formally tested. Interestingly, high levels of BST2 expression have been reported in ovarian cancer[361], neoplastic B cells[381], bladder cancer[382], breast cancer[363], endometrial cancer[383] lung cancer[384] and oesophageal, gastric and colorectal cancer[385], supporting my finding that this epitope might be expressed at the cell surface of many HLA $A2^+$ cancers. IMP-2 is also expressed by many cancer types and has been associated with poor prognosis in AML[303], ovarian[299], breast[301], and hepatocellular carcinoma[386]. Notably, all the tumour lines tested during my work expressed at least one of the candidate targets. **Figure 4-29** summarises the proposed biological roles of BST2 and IMP-2.

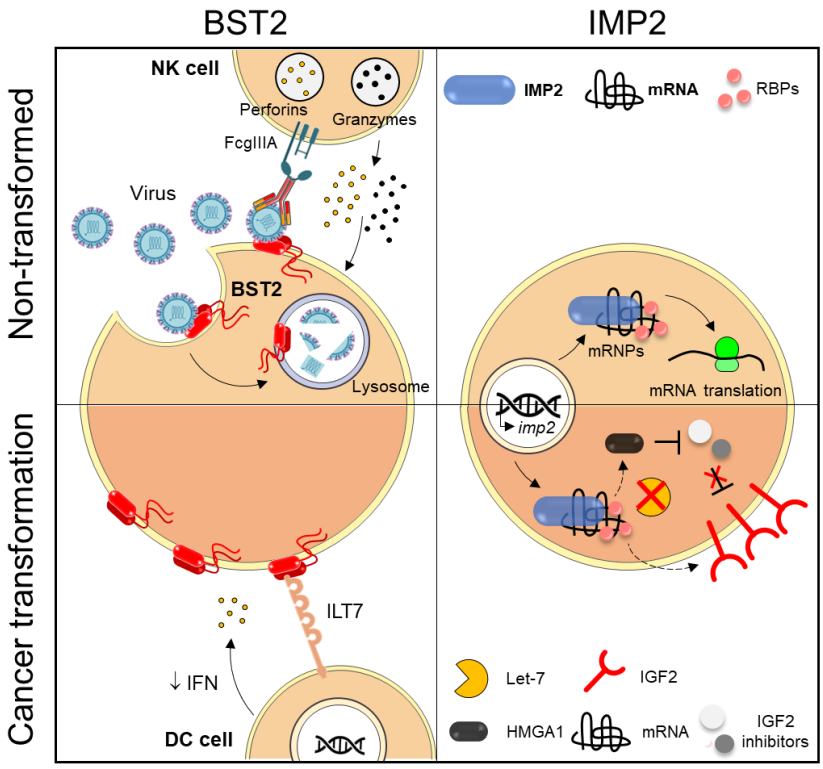

Figure 4-29. **BST2 and IMP-2 in health and disease. (A)** In non-transformed cells, BST2 has an antiviral activity. BST2 considerably reduces the release of enveloped viruses by physically trapping de novo formed mature viral particles at the surface of infected cells[387]. BST2 also inhibits cell-to-cell viral spread by eliciting antibody-dependent cellular cytotoxicity via FCγIIIA receptors in NK cells[388]. In cancer cells however, overexpression of BST2 enhances migration, invasion, proliferation and anchorage-independent growth[363,389,390]. Although the mechanistic insights have not yet been discovered, it is believed that in the TME where BST2 is constitutively overexpressed, the interaction with cognate ILT7 suppresses IFN response by DCs, thus contributing to tumour tolerance and progression[391]. **(B)** In healthy cells, IMP-2 associates with specific target mRNAs and other RNA-binding proteins (RBPs), forming a stable ribonucleoprotein complexes (RNPs) that allow mRNA transport to ribosomes for translation[392]. Some studies have also suggested that IMP-2 function may be implicated in the regulation of cancer cell metabolism and promoting metastasis[301] by stabilisation of oncogenic mRNAs encoding HMGA1, thus preventing Let-7 target gene silencing. HMGA1 in turn suppresses inhibitors of IGF2 action, which promotes cancer cell growth[304,305].

The discovery that a T cell clonotype CR24 from the TIL used to successfully treat patient MM909.24 could cross-recognise three different peptides from three different cancer-specific antigens was considered to be highly significant, as it might be very challenging for a cancer cell expressing more than one cognate target to escape from such a multipronged T cell attack (as discussed below). I next sought to determine whether there were further T cells specific for BST2 and IMP-2 antigens in the TIL used to successfully treat patient MM909.24. 0.5% $CD3^+$ TILs stained with BST2 tetramer whereas 1.2% stained with IMP-2 tetramer indicating that the patient received huge numbers of activated T cells that could respond to these epitopes. TCR profiling of $tetramer^+$ TIL's revealed the presence of 18 TCRα and 22 TCRβ Melan-A/BST2/IMP-2 cross-reactive clonotypes in the TIL infusion product of patient MM909.24 (**Figure 4-17**). Importantly, 8 out of 22 TCRβ cross-reactive to all three epitopes were found to exert broad tumour recognition, four of which were found to persist in the PBMC of patient MM909.24 6 months' post treatment.

Driven by these results, I investigated whether a panel of 11 further Melan-A-specific clones grown *in vitro* from the TIL infusion product used to treat patient MM909.24, could also recognise BST2$_{22-31}$ and/or IMP-2$_{367-376}$. Remarkably, 8/11 clones stained with HLA A2 Melan-A$_{26-35}$, BST2$_{22-31}$ and IMP-2$_{367-376}$ tetramers (**Figure 4-22**). The remaining three clones, including the dominant persistent clonotype, VB6G4.24, only stained with the Melan-A tetramer. Clone VB6G4.24 was previously shown to respond to multiple different tumour lines that do not express Melan-A (**Figure 4-5**) suggesting that VB6G4.24 must recognise a second epitope in addition to the Melan-A peptide EAAGIGILTV, and that this second epitope is neither BST2$_{22-31}$ or IMP-2$_{367-376}$. Surprisingly, the α- and β- TCR chains of this T cell clone were present in the EAAGIGILTV, LLLGIGILVL and NLSALGIFST tetramer sorts, suggesting that both chains can pair with alternative α- and β- counterparts. Implementation of single-cell sequencing technologies to TCR repertoire analysis to highlight chain pairing of TCRs would add further useful dimensionality to these data.

These unexpected results indicate that the dominant persistent clonotypes following successful TIL therapy in patient MM909.24 can recognise multiple different combinations of HLA A2-restricted epitopes via a single TCR. Such multipronged T cells might be the key to cancer clearance as described below. Unfortunately, I was unable to expand the VB6G4.24 T cell clone to sufficient number for PS-CPL analysis as successfully applied to CR24. The new TCR replacement technology developed by my laboratory[240] now makes it possible to build primary T cell clones in almost unlimited number. This technology only recently became available and has not yet been applied to the other dominant persistent clonotypes in patient MM909.24. As I had shown that the persistent Melan-A-reactive clonotypes CR24 and VB6G4.24 from patient MM909.24 could both recognise further, different non-Melan-A specific epitopes, I hypothesised that other Melan-A-specific T cell clones could also exhibit multipronged recognition. Indeed, testing of the most effective Melan-A clonotype studied in our laboratory to date, MEL5, showed that it also recognised BST2$_{22-31}$ and IMP-2$_{367-376}$ epitopes (**Figure 4-23**). I therefore extended my observations to include Melan-A and IMP-2 T cells derived from healthy donors where I could generate sufficient numbers of individual clones for further analyses and epitope characterisation.

Healthy donor-derived IMP-2-reactive T cell clones LIMÓN, CACTUS and MANUELA could recognise COLO 205, SIHA, PC-3, ACHN and RCC17 via HLA A2 suggesting that the different TCRs from these clones can mediate effective targeting of common epithelial human cancers. Notably, common epithelial cancers such as those arising in colon, liver, stomach, pancreas prostate, ovary *etc*. rarely respond to current immunotherapies so these TCRs and the epitopes that they recognise might be useful for developing future therapies for these cancers. T cell clone TESLA, raised with IMP-2$_{367-376}$ peptide, responded to multiple HLA A2$^+$ cancer lines of differing origin but did not bind to Melan-A$_{26-35}$ or BST2$_{22-31}$ tetramer. The cancer epitope prediction pipeline successfully applied to CR24 was applied to TESLA and predicted that this clone could recognise peptides derived from the NY-REN-26 (LASQLGVYRA, residues 584-593), MAGE-C1 (VLSGIGVRAG, residues 1022-1031) and Prostein (SAAGLGLVAI, residues 526-535). Further investigation encompassing peptide testing, validation of expression on target and cytotoxic

screens with engineered tumour lines would be required to further validate these observations. Nevertheless, my results indicate that individual T cell clones and TCRs can recognise cancer cells via multiple different HLA-A2-restricted, cancer-specific epitopes. Such recognition is unprecedented. My finding that the dominant persistent clonotypes in a patient cured of Stage IV melanoma following TIL therapy possess this new property raises the intriguing question of whether such multipronged T cells hold the key to cancer eradication.

4.3.2. Multipronged TCRs exhibit improved recognition of tumour

The broadly tumoricidal T cell clone, CR24, recognised autologous melanoma even when Melan-A expression was ablated by CRISPR/Cas9 lentiviral transduction (**Figure 4-19**) indicating that loss of an individual target antigen did not allow tumour escape from this T cell. Indeed, recognition of HLA A2-EAAGIGILTV, HLA A2-LLLGIGILVL and HLA A2-NLSALGIFST was shown to exhibit additive effects (**Figure 4-18**) suggesting that in the absence of the Melan-A antigen, synergistic recognition of BST2 and IMP-2 was sufficient to mediate CR24 cytotoxicity. Similarly, it could be envisaged that reactivity towards the non-melanoma cell lines tested during my studies is a result of the synergetic effects of BST2 and IMP-2 targeting. The advantages of simultaneous Melan-A, BST2 and IMP-2 targeting by the same T cell could be highly significant in preventing tumour escape. In addition, such multipronged recognition of tumour cells could allow a highly effective TCR to circumvent the rigours of central tolerance and populate the periphery (assuming that such a TCR only ever encountered the cognate antigens individually in the thymus).

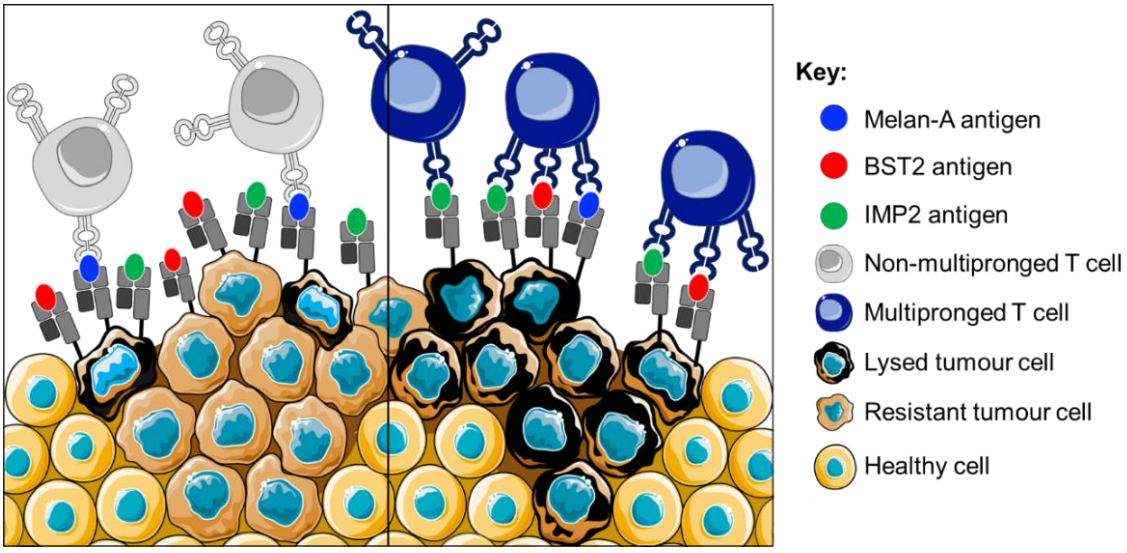

Figure 4-30. **Advantages of multipronged responses to cancer.** Recognition of multiple tumour antigens by individual T cells likely prevents tumour escape by loss of antigen while effectively increasing the antigen density at the cancer cell surface.

During my studies, I attempted to abrogate the expression of BST2 and IMP-2 in the MM909.24 autologous tumour line using CRISPR/Cas9 transfection using a Neon® device (Life Technologies) in addition to knocking out Melan-A. However, whereas BST2 expression impairment proved successful, cells incorporating the IMP-2 gRNA died 2-3 days post-transfection. Other authors have attempted abrogation of the expression of IMP-2; however, only transient downregulation reports were found. For instance, *He and colleagues*[303] attempted targeting of IMP-2 with shRNA lentivirus in AML cell lines, showing that IMP-2 downregulation impairs AML cell growth, adding blood malignancies to previous studies reporting that IMP-2 can drive cancer cell proliferation in various solid tumours[305]. Another study from *Boudoukha and colleagues*[393] attempted targeting IMP-2 with transient transfection of siRNA, revealing that IMP-2 controls cell motility and invasive capacity. Despite the set-backs encountered at IMP-2 knock out, I set out to develop a strategy that would allow effective IMP-2 depletion in tumours. My IMP-2 knock out strategy consisted of transduction of target cells with lentivirus encoding IMP-2 isoform 2, prior to CRISPR/Cas9 transfection targeting IMP-2 isoform 1. Isoform 2 lacks amino acids from position 358 to 400, which includes the immunogenic NLSALGIFST peptide (see **section 2.7.2.1**), while maintaining functions *in vitro*. Unfortunately, I did not have time during my PhD to complete this work. The inability to knock IMP-2 out from tumour cell lines could be highly significant if it were also true in primary cancers, as it would mean that tumours could not escape from IMP-2-specific T cells by losing IMP-2 expression, as to do so would lower tumour fitness. Interestingly, tetramer staining of the TIL used to unsuccessfully treat HLA $A2^+$ patient MM909.37 showed that, while there was a response to Melan-A_{26-35}, there was no response to IMP-$2_{367-376}$ (**Supplementary figure 9**). These results suggest that progressing HLA $A2^+$ patient MM909.37 did not possess Melan-A/BST2/IMP-2 multipronged T cells as seen in the TIL used to successfully treat patient MM909.24.

4.3.3. Safety profile of CR24 TCR for immunotherapy

The presence of BST2 and IMP-2-reactive T cells in the TIL infusion product used for treatment of patient MM909.24 without therapy-related secondary effects, and the presence of IMP-2 reactive T cells in the blood of AML and CLL patients (**Supplementary figure 10**), strongly suggest the safety of targeting these epitopes in immunotherapy approaches. Furthermore, similar to Melan-A-specific T cells, BST2- and IMP-2-specific TCRs can be found in the PBMC of healthy individuals without presenting signs of autoimmune responses (**Figure 4-24** and **Supplementary figure 11**).

Recently, two clinical trials for the treatment of a oesophageal cancer (NCT00681330) and non-small cell lung cancer (NCT00674258) based on a multiple vaccine therapy using peptides restricted to HLA A*24:02 have shown to induce potent and specific CTL immune responses[394]. This peptide vaccine cocktail contains an IMP-3 peptide (KTVNELQNL, residues 508-516), which is also present in the sequence of IMP-2 (residues 530-538), and thus corroborating the safety profile of IMP-targeting for immunotherapy. Moreover, a clinical trial using vaccination with autologous DCs pulsed with several Tumour Associated Peptide Antigens (TAPAs), including

BST2, is available for patients with progressive and/or refractory solid malignancies expressing one or more of these TAPAs (NCT02224599). Unfortunately, no information regarding the clinical results is has yet been made public.

Once a desirable cancer antigen has been validated the challenge is finding an optimal, safe receptor specific for this antigen that could be applied in TCR-T immunotherapy approaches. My works suggests CR24 multipronged TCR (TRAV12-2 TRAJ8 CDR3α: CAVQKLVF, TRBV6-5 TRBD2 TRBJ2-7 CDR3β: CASSYSFTEATYEQYF), and those like it could represent a good potential therapeutic TCR. During my studies, I've started assessing the safety of CR24 by exploring cytotoxicity towards the two HLA $A2^+$ healthy cell lines MRC5 and Hep5, however future exploitation of the CR24 TCR will require the generation of a full safety profile. Nevertheless, the fact that the CR24 clonotype was transfused into patient MM909.24 in large number and persisted after complete durable remission without causing toxicity strongly suggests that it does not recognise any healthy tissue *in vivo*. Indeed, the *in vivo* safety testing that comes with TIL therapy makes successful infusion products an attractive source of effective safe TCRs for TCR-T approaches as being applied by *Adaptimmune* and others.

In summary, I have made significant advances by characterising and validating two new HLA A2-restricted cancer-specific epitopes from BST2 and IMP-2 proteins. I have further shown that individual clonotypes can recognise multiple different tumour-associated epitopes, a property here termed 'multipronged' recognition. I have shown that multipronged TCRs recognising Melan-A, BST2 and IMP-2 in the context of HLA A2 can mediate tumour clearance without off-target toxicities. Further studies will be required to assess whether further antigens are also recognised by CR24 TCR and to elucidate which antigens are targeted by other multipronged TCRs within MM909.24 TIL.

– Chapter 5 –

General discussion and concluding remarks

5.1. Summary of work and relevance of findings

Since the isolation of αβ $CD8^+$ T cells (cytotoxic T cells, CTLs) from PBMC and tumour tissue of patients suffering from different malignancies[395–398], their pivotal role tumour-clearance has been broadly acknowledged. Moreover, the identification of TAAs and TAA-specific CTLs in regressing tumours, aid the establishment of a correlation between tumour regression and $CD8^+$ T cell infiltration[399]. Remarkable results have been achieved with the advent of recent approaches; such that, in 2013, cancer immunotherapy was awarded "Breakthrough of the year" by the magazine *Science*[148]. The increasing number of treatment modalities being approved by the FDA further underlines the relevance, and success, of immunotherapy for treating cancer. Nevertheless, the poor immunogenicity of tumours and the T cell-suppressive microenvironment within solid tumours both play against successful CTL function. Improving T cell responses in cancer immunotherapy is a current "hot topic" in the field.

The architecture of the cancer-specific αβ $CD8^+$ TCR repertoire is likely to be a key determinant for the successful clearance of malignancies by allowing the recognition of cancer-derived peptide antigens, presented by major histocompatibility complexes while sparing healthy cells. High Throughput Sequencing (HTS) of tumour-reactive repertoires in patients has given an insight into the extensive diversity of αβ TCR repertoires in cancer responses. The work outlined in this thesis is integrated by the common goal of dissecting successful αβ $CD8^+$ T cell responses in cancer patients in terms of clonotypic TCR characterisation and tumour-specific antigenic target identification. Collectively, the research projects described in this thesis demonstrate the outstanding role of tumour-specific T cells and highlight the importance of understanding the correlates of favourable immunotherapy outcome so that these successes can be replicated in other patients and with other cancer types.

I started my research by improving current antigen-specific T cell detection technology using pMHC multimers and observed that the standardised tetramer protocols fail to detect functionally relevant T cells with anti-tumour specificity involved in tumour clearance of a stage IV melanoma (**Chapter 3**). These observations were initially made from the tetramer staining and TCR clonotypic analysis of the TIL infusion product of a stage IV melanoma patient (MM909.24) in complete remission after receiving adoptive TIL transfer, but were later extended to T cells with viral- and self-specificities to demonstrate the widespread implications of my findings. *In vitro* grown T cell clones from patient MM909.24 exhibited effective cytotoxicity towards autologous tumour; however, some T cell clones failed to stain with pMHC tetramers loaded with the cognate Melan-A peptide (EAAGIGILTV), unless an optimised tetramer protocol was used. This optimised tetramer protocol incorporated two simple extra steps in the staining procedure: (1) addition of PKI *Dasatinib* to prevent TCR downregulation upon tetramer binding, and (2) inclusion of unconjugated anti-fluorochrome antibody to stabilise the TCR-pMHC complex. The importance of using my optimised procedure was further demonstrated with the TAA described later in **Chapter 4**, IMP-2, and anti-viral TCRs specific for EBV $BMLF1_{280\text{-}288}$, EBV $LMP2A_{426\text{-}434}$ and Yellow Fever Virus $NS4B_{214\text{-}222}$. I concluded that the incorporation of PKI and unconjugated anti-fluorochrome

antibody maximises T cell recovery at a very negligible extra cost (~£0.30 per sample). These reagents are now routinely applied during pMHC tetramer staining in my laboratory and were used throughout my thesis.

The TCR repertoire provides a mirror of successful T cell responses[21]. In my studies, analysis of TCR diversity was considered crucial for the understanding of molecular mechanisms of successful T cell immunity in cancer. The rapid development of High Throughput Sequencing (HTS) platforms, the reducing costs of sequencing and the development of bioinformatics analyses tools[252,253,400] has allowed a more thorough examination of TCR repertoires than previously possible. HTS examination of the tumour-reactive TCRβ repertoire in the TIL infusion product of patient MM909.24 revealed T cells that only stained with the HLA A2-EAAGIGILTV optimised pMHC tetramer protocol, such as VB6G4.24, and T cells staining sufficiently with standard pMHC tetramer protocol, such as CR24, both persisted in the tumour-reactive PBMC extracted from blood 6 months after therapy. Such T cell clonotypes were considered to be involved in the clearance of melanoma in patient MM909.24.

The preliminary results of another student in my group found that MM909.24 TIL could recognise cancer lines of breast cancer origin[349]. In **Chapter 4,** I extended my investigations to TCR profiling of broadly tumour-reactive T cells within successful TIL in the hope that such TCRs could elicit recognition of tumour-antigen(s) widely expressed by cancers arising from diverse tissues. The optimal antigenic target(s) should be broadly cancer-specific, and should also be crucial for cancer survival, proliferation and/or metastasis in order to prevent immunoevasion through downregulation of target[134]. During my work, I confirmed that cancer-reactive MM909.24 TIL were predominantly HLA A2-restricted and successfully identified VB6G4.24 and CR24 persistent clonotypes from **Chapter 3** as being broadly tumour-reactive via HLA A2. Since VB6G4.24 proved difficult to grow *in vitro*, my observations in this chapter focused primarily on CR24. In **Chapter 3**, the CR24 T cell clone was shown to be Melan-A (EAAGIGILTV)-specific, but showed cytotoxic recognition of non-Melan-A-expressing cancer cell lines through HLA A2, suggesting that it might possess the hitherto unknown property of recognising more than one cancer-specific HLA A2-restricted antigen. Application of a novel cancer-epitope prediction platform developed by my colleagues identified that CR24 responded to two novel immunogenic targets: IMP-2 (NLSALGIFST) and BST2 (LLLGIGILVL). CR24 T cells were shown to bind pMHC tetramers loaded with both of these peptides in addition to those presenting the EAAGIGILTV peptide. I then proceeded to show that these new peptide antigens were genuinely presented at the tumour cell surface such that they could act in unison to enhance recognition of tumour while preventing tumour escape. The “epitope identification pipeline” developed during my studies was later used to characterise TCR degenerate recognition of cancer antigens by other T cell clones.

My finding that CR24 could recognise EAAGIGILTV, LLLGIGILVL and NLSALGIFST led me to examine whether other [thought-to-be Melan-A-specific] T cells might also demonstrate this triple recognition profile. Staining of MM909.24 TIL and PBMC post successful treatment with HLA A2-EAAGIGILTV, -LLLGIGILVL and -NLSALGIFST tetramers followed by TCR clonotyping revealed

the presence of other cross-reactive TCRs capable of recognising tumours of diverse origin and that persisted in the blood of patient MM909.24 post-therapy. To my knowledge, these results are the first to describe cross-reactive TCR responses synergistically targeting multiple cancer antigens expressed by the same cancer cell. This novel concept was here referred to as being "*multipronged*" to distinguish it from conventional (*monospecific* and *monopronged*) T cell recognition. Simultaneous Melan-A, BST2 and IMP-2 targeting by the same T cell was considered to be highly significant in preventing tumour escape as described below.

5.1.1. The importance of cross-reactive TCR responses

During my studies, I have shown that ACT therapy with TILs that exhibit cross-reactive recognition of TAAs, such as Melan-A, BST2 and IMP-2, might have been key in mediating the complete response in the stage IV melanoma patient MM909.24 as such T cells were not present in an HLA A2 patient who progressed following TIL therapy. Since the recognition of multiple peptides by a single TCR turned out to be so important to my findings it is appropriate that I discuss this crucial property in detail. TCR cross-recognition of multiple pMHC complexes was initially described in 1977 by Matzinger and Bevan[401], but it wasn't until two decades later that the concept of "one clonotype-one specificity" presented by N. K. Jerne[402] was formally challenged[96]. Since then, numerous reports have provided evidence of T cell cross-reactivity. Because the degeneracy of TCR cross-recognition encompasses an intrinsic challenge to the utilisation of TCRs – especially *in vitro* enhanced TCRs that have not passed through thymic selection – in clinical therapy, the mechanisms by which a TCR can cross-react with multiple antigens have become a hot topic of current research.

Initially, it was believed that the capacity of a TCR to exploit the similarities between key structural and chemical features of two molecules ("mimicry") underlined cross-reactive responses[354,403]. Advances in structural biology have provided a better understanding of the mechanisms for αβ TCR recognition of the antigenic pMHC[404]. Generally, the CDR1 and CDR2 loops make the majority of their contacts with the MHC in a roughly conserved diagonal docking mode, whereas the CDR3 loops engage the peptide[405]. The intrinsic conformational plasticity of the CDR3 loops has been often highlighted as the underlying contributor to TCR cross-reactivity[39,102,406]. However, these general rules have been shown not to fit all TCR-pMHC structures generated to date[407], and many studies have now shown that TCR-pMHC interactions allow a certain flexibility to change its conformation following binding (reviewed in [60]). In addition, T cell cross-reactivity is TCR dependent and the number of peptides to which a single T cell can respond varies widely[408]. According to *Chao and colleagues*[101], the affinity of a TCR for a MHC will influence its cross-reactivity. Thus, high TCR-MHC affinity would require minimum binding energy from the peptide, allowing TCR recognition of a much larger set of peptides than those TCRs that bind poorly to MHC. However, a high TCR-MHC affinity would echo in a highly degenerate peptide binding that could potentially lead T cells to react to self-peptides. Examples for the several mechanisms exploited by T cells to achieve degenerate pMHC binding are summarised in **Figure 5-1**.

A. Molecular mimicry

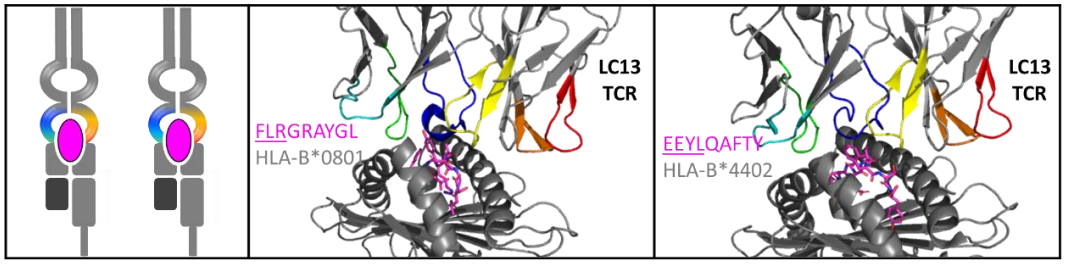

B. Differential TCR docking

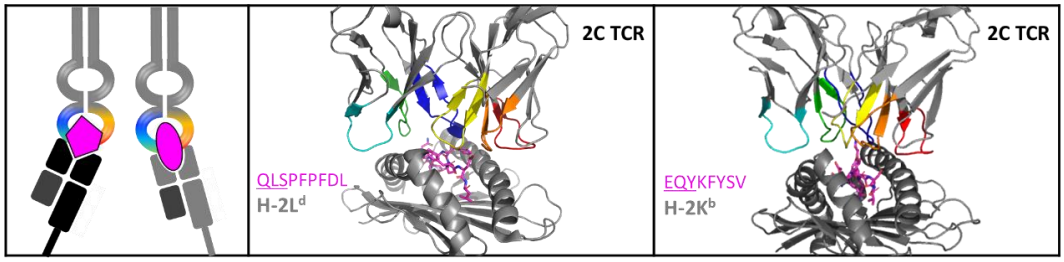

C. Induced fit

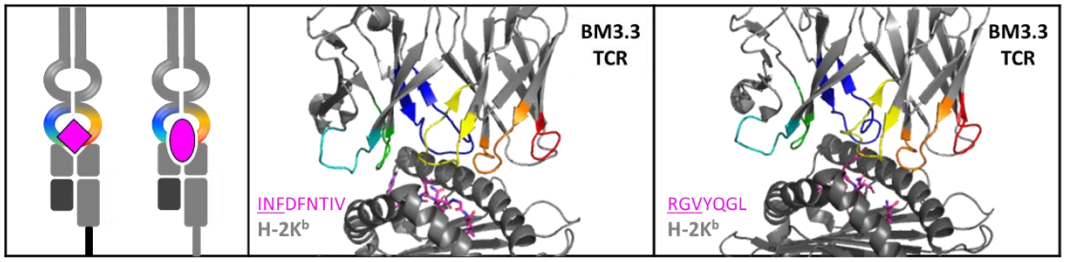

D. Tuning of pMHC flexibility

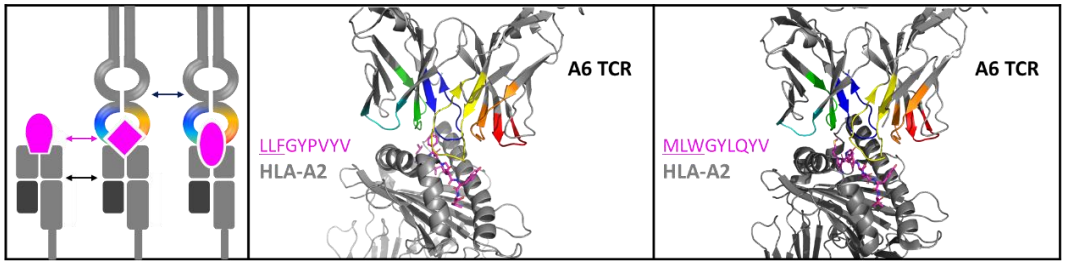

Figure 5-1. Mechanisms of TCR Cross-reactivity (A) Ligands sharing key structural and chemical features can underly TCR cross-reactivity through *molecular mimicry*. LC13 TCR recognises the immunodominant EBV epitope from EBNA 3A (FLRGRAYGL) restricted by self HLA-B*0801 (middle panel, PDB ID:**1MI5**), but also cross-reacts with an alloreactive peptide (allopeptide) derived from an ATP binding cassette protein ABCD3 (EEYLQAFTY) bound to the allogenic HLA-B*4405 (right, PDB ID: **3KPS**) via molecular mimicry[354]. **(B)** TCR binding of two different pMHC complexes using different docking orientations has been observed to contribute to cross-reactivity the binding of the murine 2C TCR to the self-ligand QL9-HV (QLSPFPFDL) bound to H-2K^{d} (middle panel. PDB ID: **2OI9**)[409] or allorecognition of the foreign ligand dEV8-H (EQYKFYSV) bound to H-2L^{d} (right panel. PDB ID: **2CKB**)[410]. **(C)** Structural adjustments in the TCR binding site upon pMHC engaging while maintaining the same overall docking orientation are observed in the murine BM3.3 TCR in complex with recognises pBM1 (INFDFNTI) endogenous peptide[409] (middle, PDB ID: **2OL3**) and VSV8 (RGVYQGL)[102] viral peptide (right, PDB ID: **1NAM**) bound to H-2K^{b}. **(D)** Different peptides can affect the dynamics of the MHC peptide-binding groove facilitating TCR engagement. This phenomenon was observed in the disparate A6 TCR recognition of the Tax antigen (LLFGYPVYV. Middle panel. PDB ID: **4FTV**) and the Tel1p antigen (MLWGYLQYV. Right panel. PDB ID: **3H9S**)[411]. Schematic representation for each model is depicted on the left panel. Colour coding of CDR regions in the TCR goes as follows: CDR1α, CDR2α, CDR3α, CDR1β, CDR2β, CDR3β. Peptide is indicated in pink. *Adapted from Yin et al* [406].

There is no simple answer to how TCRs achieve specificity and cross-reactivity; instead, the vast chemical and structural variability in each TCR-pMHC interface means that each TCR might be capable of multiple binding strategies. Some interactions on the pMHC surface seem more important than others to trigger recognition by a particular TCR, confirming what have been denominated as "hot spots" for TCR cross-reactivity[404,412]. Unfortunately, during my studies I did not have the opportunity to see completed crystallographic analysis of the persistent multipronged CR24 TCR (TRAV12-2 TRAJ8 CDR3α: CAVQKLVF, TRBV6-5 TRBD2 TRBJ2-7 CDR3β: CASSYSFTEATYEQYF) bound to HLA A2-EAAGIGILTV, LLLGIGILVL and NLSALGIFST. These experiments are currently being conducted by PhD student Aaron Wall. The molecular structure of CR24, and other multipronged TCRs with their varied cognate antigens would allow an understanding of the molecular mechanisms by which these TCRs achieve their degenerate recognition profile(s). Two recent studies have extended what is possible in terms of plasticity at the TCR-pMHC interface. My own group recently described an 'induced fit' mechanism by which a cancer-specific TCR could alter the anchoring of a peptide within the HLA A2 binding groove[413]. A similar 'frame shift' can occur to generate T cell cross-reactivity without molecular mimicry[414] so it is important to be aware that there may be new mechanisms by which a single TCR can bind pMHC, that have yet to emerge, when examining TCR cross-reactivity.

5.1.2. Implications of T cell cross-reactivity in health and disease

The concept that immunoprotection is achieved through limited numbers of highly cross-reactive T cells has many implications. The TCR repertoire is heavily influenced by the array of previously encountered pathogens and the establishment of the immunological memory (see **section 1.1.3.1**). An increasing body of evidence suggests that previous exposure to related or unrelated antigens could alter host's response to an infection or malignancy, leading to protective immunity or immunopathology[415]. This concept of "original antigenic sin" was first described for antibody responses[416] but is also believed to occur with antiviral $CD8^+$ T cells[417]. It is well established that the antigen-responding TCR repertoire becomes fixed at the point of antigen clearance, maintaining the distribution of dominant T cells in the interactive memory pool while altering distributions of memory T cells deposited from previous responses[418]. After the memory pool for a given antigen has been established, some of these relatively highly frequent memory T cells could encounter a cross-reactive pMHC, potentially eliciting a strong T cell response towards an otherwise weak cross-reactive epitope, resulting in either immunoprotection or immunopathology depending on the specific circumstances[98].

The existence of populations of foreign antigen-specific polyclonal cross-reactive T cells is likely to be highly beneficial for preventing immune escape and is temporally and spatially favourable for ensuring rapid antigen-encounter. Events of heterologous cross-reactivity between related pathogens were first described in the early 1980s with the discovery of Nucleo Protein (NP)-specific T cells that cross-reacted between the two H1N1 and H3N2 Influenza A strains[419]. This early recognition of T cell cross-reactivity was further expanded to unrelated pathogens in the early 1990s with the observation of immunodominant cross-reactive $CD8^+$ T cells in hosts with

immunity towards *Lymphocytic Choriomeningitis Virus (LCMV)* when challenged with heterologous *Pichinde Virus* (PV)[420]. However, despite all the evidence accumulated regarding viral cross-reactivity, translation into other fields of immunological health has been limited, reflecting the complexity of the mechanisms involved. Nevertheless, the paradigm "one clonotype one specificity" has now been successfully challenged as theorised by Mason[96]. My own group have described how an individual autoimmune T cell clone can recognise well over a million different peptides of 10 amino acids in length in the context of HLA A2[99]. The potential consequences of T cell cross-reactivity are summarised in **Figure 5-2** with known examples from the literature listed in **Table 5-1**.

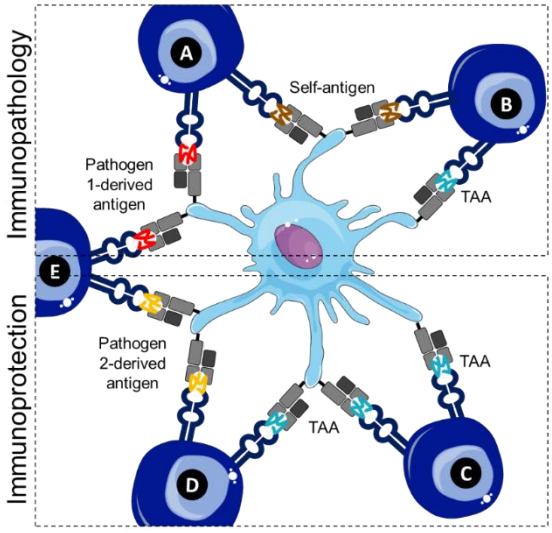

Figure 5-2. The many consequences of T cell cross-reactivity. Graphical summary of TCR cross-reactivity interactions leading to immunoprotection or immunopathology. Cross-recognition of self-antigens and **(A)** pathogen-derived determinants or **(B)** TAAs results in autoimmune responses. Degenerate recognition of multiple TAAs **(C)** and pathogen-derived antigens **(D)** can drive an anti-cancer immunoprotective response. **(E)** Heterologous recognition of microbial-derived determinants can result in both immunoprotective or immunopathological responses by influencing cross-reactive memory cells that have been exposed to past heterologous infections.

Table 5-1. Examples of cross-reactivity through molecular mimicry in human's health and disease. **DENV**: Dengue Virus; **HCV**: Hepatitis C Virus; **IAV**: Influenza Virus A; **EBV**: Epstein Barr Virus; **HIV**: Human Immunodeficiency Virus, **NS**: non-structural; **HHV**: Human Herpes Virus; **RVE**: Rubella Virus; **MBP**: Myelin Basic Protein; **SFV**: Semliki Forest Virus; **MOG**: Myelin Oligodendrocyte Glycoprotein; **GAD**: Glutamic acid decarboxylase; **T1D**: Type 1 Diabetes;

Type	Cross-reactive targets$_{(peptide\ residues)}$	HLA	Ref
Protective Heterologous immunity	DENV-1 serotype DENV-3 serotype	A*1101 A*1101	421
	HCV NS3 HCV NS4	A*0201 A*0201	422
	EBV BMLF1$_{280-288}$ EBV BRLF1$_{190-198}$	A*0201 A*0201	423
	EBV BMLF1$_{280-288}$ EBV LMP2$_{329-338}$	A*0201 A*0201	423
	EBV BMLF1$_{280-288}$ IAV-M1$_{58-66}$	A*0201 A*0201	423
	EBV BMLF1$_{280-288}$ IAV-NP$_{85-94}$	A*0201 A*0201	424
	HIV-Gag$_{76-84}$ HCN-NS5b$_{2594-2602}$	A*0201 A*0201	425
	IAV-M1$_{58-66}$ HIV p17 GAG$_{77-85}$	A*0201 A*0201	426
	HCV NS5B$_{2816-2825}$ HHV1 UL55$_{29-39}$	A*0201 A*0201	427
Pathologic Heterologous immunity	Influenza A M1$_{58-66}$ EBV BMFL1$_{280-288}$	A*0201 A*0201	424
	IAV-NA$_{231-239}$ HCV NS3$_{1073-1081}$	A*0201 A*0201	428
Autoimmunity (T1D)	GAD-65$_{261-269}$ CVB4 P2C$_{1137-1145}$	A*0201 A*0201	429
	GAD-65$_{339-352}$ CMV pUL57$_{674-687}$	DRB1*0301 DRB1*0301	430
	GAD-65$_{274-286}$ RVE1$_{157-176}$	DRB1*04 DRB1*04	431
	GAD65$_{555-567}$ IA-M1$_{61-71}$	DRB1*04 DRB1*04	432
Autoimmunity (Multiple Sclerosis)	MBP$_{85-99}$ EBV DNA Polymerase $_{627-641}$	DRB1*1501 DRB5*0101	433
Autoimmune psoriasis	*Epidermal keratin K14$_{168-181}$* *Streptococcus pyrogenes (M6 protein)*	Cw*0602	434
Cancer protective	Melan-A$_{26-35}$ *Mycobacterium tuberculosis*	A*0201 A*0201	435
Cancer immunotherapy (lethal)	MAGE- A3$_{168-176}$ Titin$_{394-403}$	A*01:01 A*01:01	241

5.1.3. Implications of T cell cross-reactivity for TCR-based cancer immunotherapy

Several TCR-based immunotherapy trials are currently in progress and aimed at treating a variety of different tumour types. Such trials focus on the targeting of TAAs that are expressed by multiple tumour types but not by healthy tissue[436]; however, as discussed in **section 1.3**, the footprint of rigorous thymic selection against T cells for TCRs specific for self-derived antigens manifests itself in tumour-specific T cells expressing TCRs with lower affinity for TAAs than pathogen-derived antigens[46,48]. Affinity-enhanced TCRs have been developed, however, the implicit high level of TCR degeneracy in recognition of pMHC complexes means that engineered TCRs may exhibit unknown and unintended specificity for self peptides processed and presented by MHC molecules on healthy tissues[241,437].

In 2006 the first human TCR gene therapy clinical trial was successfully conducted using T cells modified with the Melan-A-specific TCR DMF4, however only a small fraction of patients (4%) experienced an objective response[438]. Trials using the higher affinity Melan-A-specific TCR DMF5 resulted in 30% objective tumour responses, however >80% of treated patients exhibited grade 3 adverse effects due to "on-target, off organ" responses due to expression of Melan-A in melanocytes in the skin and other organs such as the eye[367,439]. Further cases of fatal adverse events were more recently reported following adoptive transfer of affinity-enhanced TCR targeting HLA-A*0201-restricted MAGE-A3$_{168-176}$ antigen for the treatment of patients with myeloma and melanoma[241]. *Post-mortem* analysis of the *in vivo* enriched engineered T cells in patients, revealed that unpredicted cross-recognition of an unrelated peptide derived from the striated muscle-specific protein Titin (residues 394-403) was achieved through molecular mimicry[440]. Studies conducted by *Rosenberg and colleagues*[437] also described neurological toxicity in cancer patients after adoptive cell therapy of autologous TCR-engineered T cells targeting MAGE-A3 due to cross-recognition of MAGE-A12 expressed in human brain. Therefore, potential cross-recognition of self-epitopes is a serious risk factor that must be taken into consideration when designing any TCR-based immunotherapy.

TCR cross-reactivity is not a random event but rather driven by a structural and energetic alignment with the peptide[441]; however, the true nature and extent of TCR cross-reactivity has not yet been deciphered. Hence, characterisation of the structural features that trigger a TCR-specific recognition of a pMHC complex is of high relevance to guide large-scale *in silico* screenings that could predict TCR cross-reactivity. *Mendes and colleagues*[442,443] have developed a webtool for prediction of TCR cross-recognition of viral epitopes. The algorithm was based on the electrostatic potential of the conserved contacts that are shared by all TCR-pMHC structures available; yet, despite the increasing number of crystallographic structures being deposited in the Protein Data Bank (PDB), there are many TCR-pMHC complexes that fail to form structures (specially for low affinity interactions), and could potentially bias the prediction outcomes in the algorithms being developed.

Further *in silico* tools for antigenic TCR recognition have been developed by *Dash*[444], *Glanville*[445] *and colleagues*. These approaches analyse the underlying features of the CDR3 in antigen-specific repertoires and could be in turn used to predict if a given TCR could react towards an array of candidate antigens. If the database became a comprehensive study of epitope-specific TCR repertoires, it could be envisaged that candidate therapeutic TCRs could be evaluated within the database to screen for potential cross-recognition of further antigens based on conserved CDR3 motifs.

Other approaches for in-depth characterisation of TCR cross-recognition patterns could complement *in silico* structure-based prediction methodologies. For instance, *Bentzen and colleagues*[261,446] showed that the fingerprints of each TCR cross-recognition profile could be explored with DNA barcode-labelled MHC multimer-based by substituting every single amino acid of the cargo peptide with all naturally occurring amino acids. Furthermore, *Garcia and colleagues*[404] developed a system for individual TCR screening of pMHC ligands using yeast display libraries paired with deep sequencing. Both studies concluded that conserved features of a peptide, such as charge and hydrophobicity, are targeted by cross-reactive TCRs. On that note, our group has made significant contributions to the exploration of TCR cross-reactivity using Combinatorial Positional Screening libraries (PS-CPLs) (see **section 2.3.8**)[72,99,178,346,447]. In my thesis, PS-CPL technology was used to dissect broadly expressed cancer-specific targets that could be safely targeted for a T cell-based therapy in HLA-A2 patients. I successfully identified BST2 and IMP-2 novel antigens, and started exploring targeting of new epitopes from BCR, MAGE-C1 and Prostein by T cell clone TESLA.

5.2. Future work

Dissection of antigen specificities of other persistent T cell clones that do not share CR24 multipronged pattern of recognition but that clearly recognise multiple, different tumour-specific antigens will allow further assessment of how such T cells might contribute to successful clearance of cancer. By way of example, the α and β TCR chains of the Melan-A-specific T cell clone VB6G4.24 were found to respond to a wide variety of non-melanoma tumours, thus indicating that recognition must be mediated through an antigen-specificity other than Melan-A. Unfortunately, my failure to grow VB6G4.24 *in vitro* to the number required for PS-CPL and subsequent analyses put a halt into any further investigations with this interesting T cell clone. This obstacle could now be bypassed by employing the "TCR replacement protocol" designed in our laboratory by Dr Legut[240], where an αβTCR of choice can be transduced together with CRISPR/Cas9 targeting the C' region on the TCRβ chain of recipient cells. More recently, a novel method for TCR replacement with near-physiological T cell function has been developed by *Schober and colleagues*[448], consisting of simultaneous editing of α and β chains by introducing a transgenic TCR into the endogenous TCRα locus and CRISPR/Cas9 targeting the C' region on the TCRβ chain. These strategies allow for construction of huge numbers of a T cell clone for analyses and mean that the limitations of *in vitro* culturing need not inhibit future studies.

Besides the *in vitro* grown CR24 and VB6G4.24 T cell clones, the TCRβ chains of seven other persistent clonotypes were found to also recognise non-melanoma tumours, two of which were described as Melan-A-specific in **Chapter 3**. Unfortunately, bulk TCR α and β chain sequencing does not allow for the identification of TCR chain pairs; and thus, exploration of TCR reactivity relies on *in vitro* growth of a clone. In future, therapeutically relevant TCRs could be derived directly from single-cells in emulsion technologies such as DropSeq[449] or 10x Genomics microfluidics. In short, hydrogel coated beads carrying barcoded DNA oligonucleotides are encapsulated with T cells through an oil-based microfluidics system. Each captured cell is lysed within the formed droplets, and mRNA binds to the primers carried by the bead, followed by RT-PCR amplification and sequencing. Application of nucleic acid barcoding then allows direct pairing of the TCRα and TCRβ expressed by each individual T cell. Application of such new technologies will be highly enabling for future dissection of TCR specificities as described in **Figure 5-3**.

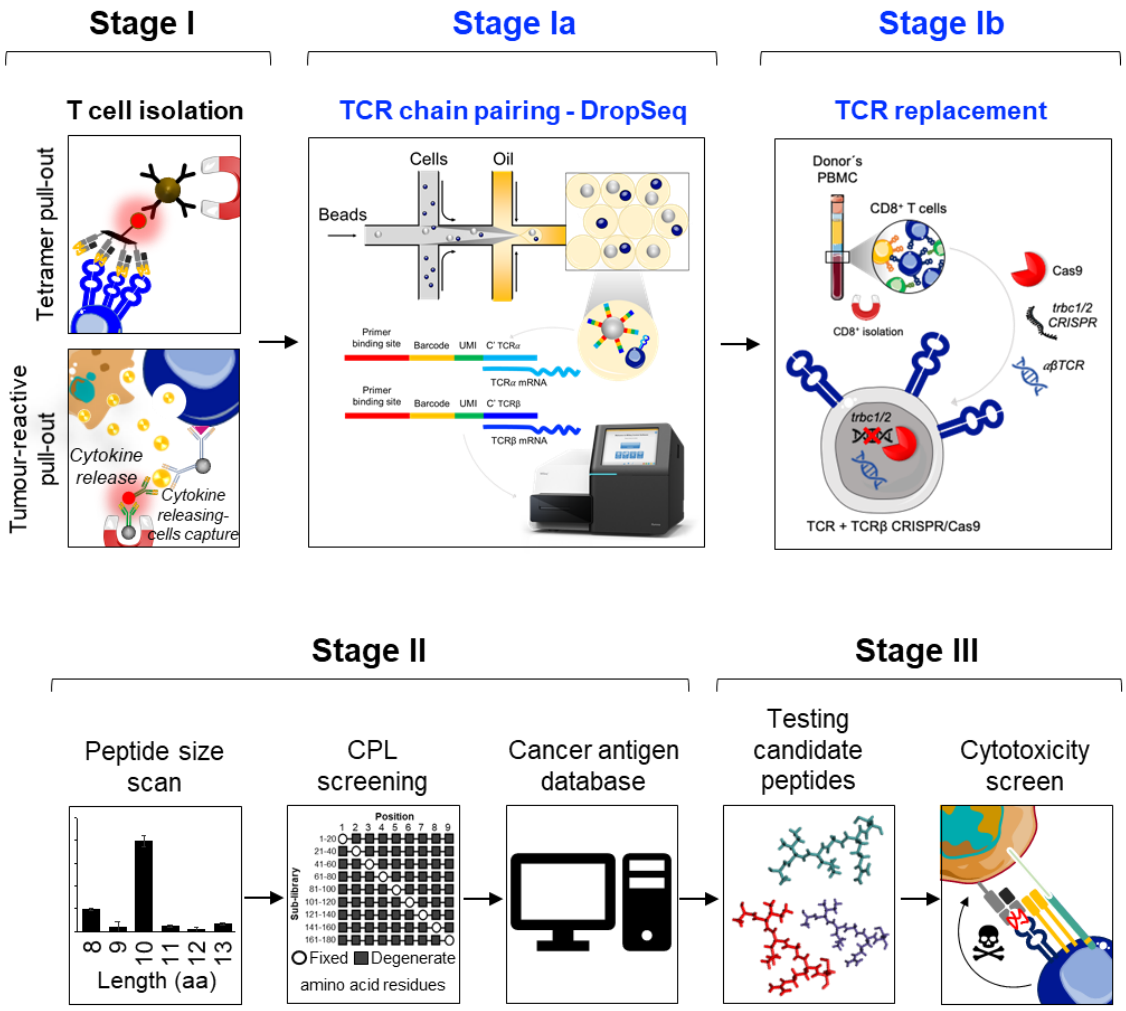

Figure 5-3. Improvement of the "T cell epitope identification pipeline" described in Figure 4-7. Following T cell isolation (stage I), single-cells can be encapsulated using a microfluidics devise with a bead containing a primer binding site for downstream PCR and sequencing, a "cell barcode" that is identical across all the primers on the surface of the one bead, a Unique Molecular Identifier (UMI) that is different on each primer and used to identify PCR duplicates, and a TCR capture sequence (1:1 TRAC and TRBC) (stage Ia). Captured cells are lysed in the droplet, then RNA captured by the T cell-specific capture oligos, followed by reverse transcription and PCR amplification of αβTCR transcripts. Once the identity of the desired αβTCR has been stablished, transcripts can be cloned into a lentiviral vector and co-delivered with CRISP/Cas9 targeting endogenous TRBC of recipient T cells derived from healthy PBMC (stage Ib). Stages II and III remain the same as in the original protocol. Modifications to the "T cell epitope identification pipeline" presented in this thesis are indicated in blue.

5.3. Future perspectives in cancer immunotherapy

Adoptive transfer of autologous cancer-reactive T cells has achieved remarkable recent clinical successes. ACT initially involved re-infusion of *ex vivo* expanded TILs[216], but has been now expanded to include engineered T cells expressing an antigen receptor of choice. Such genetic re-direction of T cells can be achieved by expression of a CAR or a TCR. While CAR-T can be highly successful for the targeting of surface molecules, TCR-T therapies have the advantage of the inherent ability of the TCR to scan the entire cellular proteome through its interaction with pMHC; thereby accessing a much greater range of potential targets, including those proteins responsible for cellular transformation.

Potential success and patient eligibility for a specific cell-based immunotherapeutic agent is dependent on a multitude of criteria that limit treatment to only a small subset of cancer patients. For example, CAR-T therapy is only successful for *soluble* tumour and effective treatments are currently limited to patients with B cell malignancies expressing specific surface markers, such as CD19[450,451]. This situation contrasts with the αβTCR where both TIL and CPI therapy show that manipulation of $CD8^+$ T cells can result in clearance of solid tumours. Consequently, T cells expressing a tumour-specific αβTCR are now being widely explored as treatments for many cancer types and an effective broadly cancer-specific TCR-T therapy that is readily available in large numbers at a sensible scale, has the potential to revolutionise the field of cancer immunotherapy. From the research conducted during my PhD, I believe that cancer-specific multipronged CR24 TCR could be used to genetically engineer patient's autologous T cells to target cancer as described below.

5.3.1. CR24 TCR translation to the clinic

The persistent T cell clone CR24 was identified from the dissection of successful anti-tumour responses in a stage IV melanoma patient following successful TIL therapy. The TAAs recognised by this broadly cancer-reactive TCR were revealed using the "epitope discovery pipeline" developed as part of my thesis studies. Engineering therapeutic T cells with the desired TCRs specific for antigens of interest, such as CR24, has become a reality. Many clinical trials have embraced this form of immunotherapy (see **Table 1-4**). Recent studies conducted by my group have demonstrated that redirection of primary $CD8^+$ and $CD4^+$ T cells with pan-cancer reactive natural TCRs is substantially improved when CRISPR/Cas9 gene editing is used to disrupt the endogenous TCR chains[240]. Such "TCR replacement" has multiple benefits as in addition to removing the capacity for TCR chain mispairing it also ensures that more of the transduced TCR is expressed at the T cell surface. More recently, *Schober and colleagues*[448] showed a CRISPR/Cas9-based method for simultaneous editing of α and β chains by targeted TCR insertion into endogenous TCRα constant (TRAC) gene locus combined with targeted disruption of endogenous TCRβ chain, leading to accurate αβ pairing and TCR regulation similar to that of physiological T cells. This technology could overcome the regulatory and safety considerations of lentiviral gene transfer.

An affinity-enhanced version of CR24 could be considered for clinical use in order to induce stronger anti-cancer responses; however, engineering a TCR to exhibit improved binding to multiple TAA-derived peptides would encompass the inherent possibility of unintended cross-recognition of a peptide expressed by healthy cells. As T cells with the natural CR24 TCR were adoptively transferred to patient MM909.24 in large number and persisted in this patient without any obvious signs of autoimmunity disease, this TCR, unlike others used in ACT, has been effectively tested *in vivo* (in one patient).

The adverse effects associated with the infusion of genetically engineered lymphocytes observed in past clinical trials due to unforeseen "on-target off-tumour" or "off-target off-tumour" reactivities, demands that caution is used when considering new therapies. Numerous genetic engineering strategies have been designed to improve the safety of TCR-T adoptive transfer, including "SynNotch" receptors[452,453] and druggable suicide switches[454,455] that can dampen the T cell activity at the onset adverse effects. Strategies for enhancing the safety profile of gene engineered T cells have recently been reviewed by Lim and June[456] and will not be considered in detail here. Briefly, a "suicide switch", called iCasp9, has been clinically validated in limiting graft versus host disease in patients undergoing hematopoietic stem cell transplants[455]. Another approach involves transducing TCR-T cells with a gene for CYP4B1 enzyme that leads to T cell death through the activation of protoxin 4-ipomenaol[457]. Alternatively, methods for transient expression of TCRs using mRNA electroporation of T cells have been described by *Mensali and colleagues*[458]. Clinical trials for first human testing of transient TCR therapy (NCT03431311) will determine safety and effectiveness of this approach.

5.3.2. Beyond the TCR: the need for combination immunotherapies

The optimal therapeutic TCR-based product should: (1) efficiently traffic to tumour site, (2) overcome immunosuppressive tumour microenvironment, (3) eliminate all tumour cells, and (4) be inert to healthy tissues[134]. In this thesis, CR24 multipronged TCR has been shown to effectively eliminate all tested tumour cells and be inert to healthy cells *in vitro*. To further optimise the benefits of a therapy encompassing CR24 TCR-transduced T cells, the considerations stated below should be examined (summarised in **Figure 5-4**).

The immunosupressive tumour microenvironment has the ability to limit the effectiveness of all T cell immunotherapy approaches and represents a substantial hurdle to expanding the success to greater numbers of patients. The microenvironment favours tumour and impairs T cells in several ways. Firstly, the hypoxic tumour microenvironment impairs T cell proliferation due to glucose deprivation. Hypoxia promotes the reprogramming of fibroblast progenitor cells into CAFs, thus creating physical barriers, and contributes to aberrant vasculatures to inhibit T cell trafficking towards transformed tissue, by downregulating adhesion molecules, co-stimulatory ligands or inhibiting the expression of chemo-attractants[224,459,460] (**Figure 1-10**). Several therapeutic strategies have been developed to normalise tumour vasculature, including VEGF-targeted

inhibitory agents[461,462] and direct peptide-mediated targeting of cytokines to the tumour vasculature[463]. Both these approaches have demonstrated enhanced T cell infiltration of tumour.

Regimens of lymphodepletion and IL-2 infusion delivered with ACT have also been shown to counteract the immunosuppressive *milieu*[225]. Furthermore, gene modification of infused lymphocytes to express chemokine receptors have been shown to improve T cell trafficking[464,465]. Beyond genetic engineering, advanced biomaterials and drug delivery systems are being developed (reviewed by *Riley et al*[466] and *Mi et al*[467]). For instance, restoration of T cell function in a colorectal mouse model has been achieved with nanoparticles encapsulating a TGFβR1 inhibitor, made of the FDA-approved polymer PEG[468]. Secondly, defects in the antigen-presenting machinery are common features of many cancers as a mechanism of escape[66,143–145]. *Benavente and colleagues*[142] described downregulation of HLA-I was mediated through the epidermal growth factor receptor (EGFR). Targeted antibody therapy with anti-EGFR agents have showed an increase in HLA-I expression in tumour cells[469], so it is plausible that combination therapy of CR24 TCR-T transfer with anti-EGFR antibodies, such as the FDA-approved *Nimotuzumab*[470], could provide improved results.

T cell exhaustion is a major concern during T cell-based immunotherapies. Due to chronic antigen exposure and inflammation in the tumour microenvironment, TILs often become exhausted and undergo senescence, thus becoming functionally incapable of performing cytotoxic activities[471] or of proliferating[472]. Transition from early to late effector stage is marked by downregulation of CD28, and analysis of persisting TIL clones indicate a preferential survival of clonotypes expressing highest levels of CD28[327]. Accumulation of senescent $CD8^{+}$ $CD28^{neg}$ T cells has been observed in solid tumours[473]. Senescence and exhaustion can be overcome by selecting the adequate subsets of T cells, by inducing gene expression of CD28, or by CRISPR/Cas9-based abolition of senescence-related genes in TCR gene-recipient cells. *In vivo* persistence can also be accomplished by infusion of cytokines inducing proliferative effects on T cells such as IL-2 and IL-15[207,474,475].

Finally, TILs are characterised by high expression levels of inhibitory receptors, such as PD-1 and CTLA-4[330]. Tumours upregulate ligands for these T cell checkpoints to minimise T cell attack[146]. Combination therapy of ACT with checkpoint inhibitors has been shown beneficial in patients with melanoma[476]. As an alternative to antibody therapies, CRISPR/Cas9 interruption of PD-1 expression in neoantigen-targeted TCR-T cells has been approved for clinical trial (NCT03970382). Nevertheless, engineered T cells for solid tumours that are resistant to checkpoint inhibition will require precision targeting and control mechanisms to avoid off-tumour effects while retaining on-target effects.

Milestones in fields of immunology, genetic engineering and biotechnology have contributed to the successful development of immunotherapies, such as TCR-T, CAR-T cell therapy and immune-checkpoint inhibitors. Overall, these are exciting times for immunotherapy treatments, as many therapies are now under active investigation in the clinical setting. Cellular therapies remain

complicated and expensive. The cells from one patient can vary widely from the cells of another. Reduction in cost and production of a uniformly effective product may require the development of “off-the-shelf” allogenic clinical products that can be stored in large number and given to patients when required. Cellular and genomic editing is moving apace so such products may become available within the next 5 years. The other key aspect in future approaches will be knowing which antigens to target and which TCRs to use. I believe that the discoveries that can be made by dissecting successful cancer immunotherapy, as applied in my work, will play a part in illuminating the path for the next phase of cellular immunotherapy.

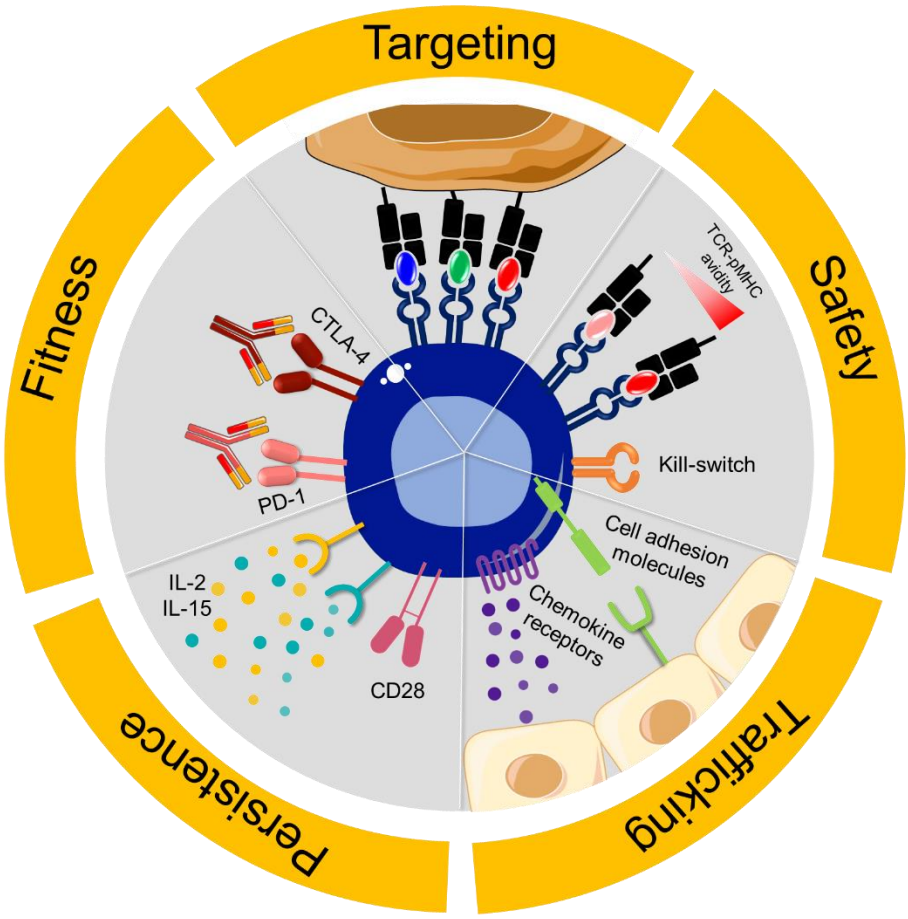

Figure 5-4. Combination therapies for successful tumour clearance. Benefits of immunotherapy with CR24 TCR-transduced T cells could be further boosted by combination therapies with other FDA-approved agents to ensure an optimised and effective on-target killing of all heterogeneous tumour cells, while remaining safe and controllable. *Adapted from*[326].

5.4. Concluding remarks

The immune system possesses two key abilities that nominate it as the best candidate for future therapeutic elimination of cancer: (1) the inherent capability to detect and destroy malignant cells and (2) the capacity to remember such transformations. The last decade has seen immunotherapies cure patients with historically untreatable cancers. In this thesis, I focused on investigating the immunotherapeutic potential HLA A2-restricted, broadly cancer-specific T cells and their TCRs. I have improved the detection of antigen-specific T cells with pMHC multimers reagents and developed an “epitope discovery pipeline” to discover novel therapeutically-relevant receptors and their cognate targets. My investigation led to the discovery of cross-reactive multipronged TCRs that mediated tumour clearance in a stage IV melanoma. No pathologies associated to Melan-A/BST2/IMP-2 cross-reactive TCRs were observed.

I believe that the future of cancer immunotherapy lies in multipronged cancer-specific cross-reactive TCRs, such as CR24 TCR (TRAV12-2 TRAJ8 CDR3α: CAVQKLVF, TRBV6-5 TRBD2 TRBJ2-7 CDR3β: CASSYSFTEATYEQYF) as off-the-shelf cellular products. To confirm absolute safety of suggested CR24-TCR products, full safety profiles must be generated, as well as a structural analysis of the TCR/ligand binding to fully understand the mechanisms of cross-reactivity. As the ethical dispute over genetic engineering resolves, it is plausible to think that a combination of TCR gene transfer and knock-out of negative regulators of the immune response holds the promise of positive treatment outcomes in the clinic and I look forward to seeing how this exciting field develops in the near future.

– References –

1. Janeway, C. A., Travers, P., Walport, M. & Capra, J. D. *Immuno Biology*. (Garland Science, Taylor & Francis Group, 1999).
2. Chiossone, L., Dumas, P.-Y., Vienne, M. & Vivier, E. Natural killer cells and other innate lymphoid cells in cancer. *Nat. Rev. Immunol.* **18**, 671–688 (2018).
3. de Visser, K. E., Eichten, A. & Coussens, L. M. Paradoxical roles of the immune system during cancer development. *Nat. Rev. Cancer* **6**, 24–37 (2006).
4. Curiel, T. J. *et al.* Specific recruitment of regulatory T cells in ovarian carcinoma fosters immune privilege and predicts reduced survival. *Nat. Med.* **10**, 942–949 (2004).
5. Pagès, F. *et al.* Immune infiltration in human tumors: a prognostic factor that should not be ignored. *Oncogene* **29**, 1093–1102 (2010).
6. Fridman, W. H., Pagès, F., Sautès-Fridman, C. & Galon, J. The immune contexture in human tumours: impact on clinical outcome. *Nat. Rev. Cancer* **12**, 298–306 (2012).
7. Fridman, W. H. *et al.* Prognostic and predictive impact of intra- and peritumoral immune infiltrates. *Cancer Res.* **71**, 5601–5 (2011).
8. Shankaran, V. *et al.* IFNγ and lymphocytes prevent primary tumour development and shape tumour immunogenicity. *Nature* **410**, 1107–1111 (2001).
9. Krueger, A., Zie, N., Tara, ¸ & Łyszkiewicz, M. T Cell Development by the Numbers. *Trends Immunol.* **38**, 128–139 (2017).
10. Hara, T. *et al.* Predominant activation and expansion of V gamma 9-bearing gamma delta T cells in vivo as well as in vitro in Salmonella infection. *J. Clin. Invest.* **90**, 204–10 (1992).
11. Nielsen, M. M., Witherden, D. A. & Havran, W. L. γδ T cells in homeostasis and host defence of epithelial barrier tissues. *Nat. Rev. Immunol.* **17**, 733 (2017).
12. Godfrey, D. I., Uldrich, A. P., McCluskey, J., Rossjohn, J. & Moody, D. B. The burgeoning family of unconventional T cells. *Nat. Immunol.* **16**, 1114–1123 (2015).
13. Chi, A. W., Bell, J. J., Zlotoff, D. A. & Bhandoola, A. Untangling the T branch of the hematopoiesis tree. *Curr. Opin. Immunol.* **21**, 121–126 (2009).
14. Haynes, B. F. & Heinly, C. S. Early human T cell development: analysis of the human thymus at the time of initial entry of hematopoietic stem cells into the fetal thymic microenvironment. *J. Exp. Med.* **181**, 1445–58 (1995).
15. Kurd, N. & Robey, E. A. T-cell selection in the thymus: a spatial and temporal perspective. *Immunol. Rev.* **271**, 114–126 (2016).
16. Singer, A. & Bosselut, R. CD4⁄CD8 Coreceptors in Thymocyte Development, Selection, and Lineage Commitment: Analysis of the CD4⁄CD8 Lineage Decision. *Adv. Immunol.* **83**, 91–131 (2004).
17. Germain, R. N. T-CELL DEVELOPMENT AND THE CD4–CD8 LINEAGE DECISION. *Nat. Rev. Immunol.* (2002). doi:10.1038/nri798
18. Carpenter, A. C. & Bosselut, R. Decision checkpoints in the thymus. *Nat. Immunol.* **11**, 666–673 (2010).
19. Yanagi, Y. *et al.* A human T cell-specific cDNA clone encodes a protein having extensive homology to immunoglobulin chains. *Nature* **308**, 145–149 (1984).
20. Hedrick, S. M., Cohen, D. I., Nielsen, E. A. & Davis, M. M. Isolation of cDNA clones

encoding T cell-specific membrane-associated proteins. *Nature* **308**, 149–153 (1984).

21. Arstila, T. P. *et al.* A direct estimate of the human alphabeta T cell receptor diversity. *Science* **286**, 958–61 (1999).
22. Turner, S. J., Doherty, P. C., McCluskey, J. & Rossjohn, J. Structural determinants of T-cell receptor bias in immunity. *Nat. Rev. Immunol.* **6**, 883–894 (2006).
23. Schatz, D. G. & Ji, Y. Recombination centres and the orchestration of V(D)J recombination. *Nat. Rev. Immunol.* **11**, 251–263 (2011).
24. Arya, R. & Bassing, C. H. V(D)J Recombination Exploits DNA Damage Responses to Promote Immunity. *Trends Genet.* **33**, 479–489 (2017).
25. Roth, D. B. V(D)J Recombination: Mechanism, Errors, and Fidelity. *Microbiol. Spectr.* **2**, (2014).
26. Serana, F. *et al.* dentification of a public CDR3 motif and a biased utilization of T-cell receptor V beta and J beta chains in HLA-A2/Melan-A-specific T-cell clonotypes of melanoma patients. *J. Transl. Med.* **7**, 21 (2009).
27. Gauss, G. H. & Lieber, M. R. Mechanistic constraints on diversity in human V(D)J recombination. *Mol. Cell. Biol.* **16**, 258–69 (1996).
28. Bories, J. C., Demengeot, J., Davidson, L. & Alt, F. W. Gene-targeted deletion and replacement mutations of the T-cell receptor beta-chain enhancer: the role of enhancer elements in controlling V(D)J recombination accessibility. *Proc. Natl. Acad. Sci. U. S. A.* **93**, 7871–6 (1996).
29. Lee, Y. N. *et al.* Differential utilization of T cell receptor TCR/TCR locus variable region gene segments is mediated by accessibility. *PNAS* **106**, 17487–17492 (2009).
30. Ndifon, W. *et al.* Chromatin conformation governs T-cell receptor Jβ gene segment usage. *PNAS* **109**, 15865–15870 (2012).
31. Melenhorst, J. J. *et al.* Contribution of TCR-beta locus and HLA to the shape of the mature human Vbeta repertoire. *J. Immunol.* **180**, 6484–9 (2008).
32. Livak, F., Burtrum, D. B., Rowen, L., Schatz, D. G. & Petrie, H. T. Genetic Modulation of T Cell Receptor Gene Segment Usage during Somatic Recombination. *J. Exp. Med.* **192**, 1191–1196 (2000).
33. Elhanati, Y., Sethna, Z., Callan, C. G., Mora, T. & Walczak, A. M. Predicting the spectrum of TCR repertoire sharing with a data-driven model of recombination. *Immunol. Rev.* **284**, 167–179 (2018).
34. Engel, I. & Hedrick, S. M. Site-directed mutations in the VDJ junctional region of a T cell receptor β chain cause changes in antigenic peptide recognition. *Cell* **54**, 473–484 (1988).
35. Katayama, C. D., Eidelman, F. J., Duncan, A., Hooshmand, F. & Hedrick, S. M. Predicted complementarity determining regions of the T cell antigen receptor determine antigen specificity. *EMBO J.* **14**, 927–38 (1995).
36. Rudolph, M. G. & Wilson, I. A. The specificity of TCR/pMHC interaction. *Curr. Opin. Immunol.* **14**, 52–65 (2002).
37. Gras, S. *et al.* Reversed T Cell Receptor Docking on a Major Histocompatibility Class I Complex Limits Involvement in the Immune Response. *Immunity* **45**, 749–760 (2016).

38. Rossjohn, J. *et al.* T Cell Antigen Receptor Recognition of Antigen-Presenting Molecules. *Annu. Rev. Immunol* **33**, 169–200 (2015).
39. Mazza, C. *et al.* How much can a T-cell antigen receptor adapt to structurally distinct antigenic peptides? *EMBO J.* **26**, 1972–1983 (2007).
40. Chothia, C., Boswell, D. R. & Lesk, A. M. The outline structure of the T-cell alpha beta receptor. *EMBO J.* **7**, 3745–55 (1988).
41. Davis, M. M. The evolutionary and structural 'logic' of antigen receptor diversity. *Semin. Immunol.* **16**, 239–243 (2004).
42. Nikolich-Žugich, J., Slifka, M. K. & Messaoudi, I. The many important facets of T-cell repertoire diversity. *Nat. Rev. Immunol.* **4**, 123–132 (2004).
43. Valitutti, S., Müller, S., Cella, M., Padovan, E. & Lanzavecchia, A. Serial triggering of many T-cell receptors by a few peptide–MHC complexes. *Nature* **375**, 148–151 (1995).
44. BEVAN, M. J. In a radiation chimaera, host H–2 antigens determine immune responsiveness of donor cytotoxic cells. *Nature* **269**, 417–418 (1977).
45. Vacchio, M. S. & Bosselut, R. What Happens in the Thymus Does Not Stay in the Thymus: How T Cells Recycle the CD4+-CD8+ Lineage Commitment Transcriptional Circuitry To Control Their Function. *J. Immunol.* **196**, 4848–56 (2016).
46. Klein, L., Kyewski, B., Allen, P. M. & Hogquist, K. A. Positive and negative selection of the T cell repertoire: what thymocytes see (and don't see). *Nat. Publ. Gr.* **14**, 377–391 (2014).
47. Wang, F., Huang, C. Y. & Kanagawa, O. Rapid deletion of rearranged T cell antigen receptor (TCR) Valpha-Jalpha segment by secondary rearrangement in the thymus: role of continuous rearrangement of TCR alpha chain gene and positive selection in the T cell repertoire formation. *Proc. Natl. Acad. Sci. U. S. A.* **95**, 11834–9 (1998).
48. Xing, Y. & Hogquist, K. A. T-cell tolerance: central and peripheral. *Cold Spring Harb. Perspect. Biol.* **4**, a006957 (2012).
49. Heath, W. R. & Carbone, F. R. Cross-Presentation, dendritic Cells, Tolerance and Immunity. *Annu. Rev. Immunol.* **19**, 47–64 (2001).
50. Heath, W. R. & Carbone, F. R. Cross-presentation in viral immunity and self-tolerance. *Nat. Rev. Immunol.* **1**, 126–134 (2001).
51. Kurts, C., Kosaka, H., Carbone, F. R., Miller, J. F. A. P. & Heath, W. R. Class I–restricted Cross-Presentation of Exogenous Self-Antigens Leads to Deletion of Autoreactive CD8+ T Cells. *J. Exp. Med.* **186**, 239–245 (1997).
52. von Boehmer, H. & Hafen, K. Minor but not major histocompatibility antigens of thymus epithelium tolerize precursors of cytolytic T cells. *Nature* **320**, 626–628 (1986).
53. Sigal, L. J., Crotty, S., Andino, R. & Rock, K. L. Cytotoxic T-cell immunity to virus-infected non-haematopoietic cells requires presentation of exogenous antigen. *Nature* **398**, 77–80 (1999).
54. Huang, A. *et al.* Role of bone marrow-derived cells in presenting MHC class I-restricted tumor antigens. *Science (80-.).* **264**, 961–965 (1994).
55. Wolfers, J. *et al.* Tumor-derived exosomes are a source of shared tumor rejection antigens for CTL cross-priming. *Nat. Med.* **7**, 297–303 (2001).

56. Madura, F. *et al.* Structural basis for ineffective T-cell responses to MHC anchor residue-improved “heteroclitic” peptides. *Eur. J. Immunol.* **45**, 584–591 (2015).
57. Eckle, S. B., Turner, S. J., Rossjohn, J. & McCluskey, J. Predisposed αβ T cell antigen receptor recognition of MHC and MHC-I like molecules? *Curr. Opin. Immunol.* **25**, 653–659 (2013).
58. Dendrou, C. A., Petersen, J., Rossjohn, J. & Fugger, L. HLA variation and disease. *Nat. Rev. Immunol.* (2018). doi:10.1038/nri.2017.143
59. Robinson, J. *et al.* IMGT/HLA and IMGT/MHC: sequence databases for the study of the major histocompatibility complex. *Nucleic Acids Res.* **31**, 311–4 (2003).
60. Sewell, A. K. Why must T cells be cross-reactive? *Nat. Rev. Immunol.* **12**, 669–677 (2012).
61. Pereyra, F. *et al.* The Major Genetic Determinants of HIV-1 Control Affect HLA Class I Peptide Presentation. *Science (80-.).* **330**, 1551–1557 (2010).
62. Fellay, J. *et al.* A Whole-Genome Association Study of Major Determinants for Host Control of HIV-1. *Science (80-.).* **317**, 944–947 (2007).
63. Kiepiela, P. *et al.* Dominant influence of HLA-B in mediating the potential co-evolution of HIV and HLA. *Nature* **432**, 769–775 (2004).
64. de Groot, N. G. *et al.* AIDS-protective HLA-B*27/B*57 and chimpanzee MHC class I molecules target analogous conserved areas of HIV-1/SIVcpz. *Proc. Natl. Acad. Sci.* **107**, 15175–15180 (2010).
65. Scorza Smeraldi, R. *et al.* HLA-associated susceptibility to AIDS: HLA B35 is a major risk factor for Italian HIV-infected intravenous drug addicts. *Hum. Immunol.* **22**, 73–9 (1988).
66. Chowell, D. *et al.* Patient HLA class I genotype influences cancer response to checkpoint blockade immunotherapy. *Science* **359**, 582–587 (2018).
67. Sharpe, A. H. & Freeman, G. J. THE B7–CD28 SUPERFAMILY. *Nat. Rev. Immunol.* **2**, 116–126 (2002).
68. Janeway, C. A. & Bottomly, K. Signals and signs for lymphocyte responses. *Cell* **76**, 275–285 (1994).
69. Wang, B., Maile, R., Greenwood, R., Collins, E. J. & Frelinger, J. A. Naive CD8 + T Cells Do Not Require Costimulation for Proliferation and Differentiation into Cytotoxic Effector Cells . *J. Immunol.* **164**, 1216–1222 (2000).
70. Huff, W. X., Kwon, J. H., Henriquez, M., Fetcko, K. & Dey, M. The Evolving Role of CD8+CD28- Immunosenescent T Cells in Cancer Immunology. *Int. J. Mol. Sci.* **20**, (2019).
71. Chen, L. & Flies, D. B. Molecular mechanisms of T cell co-stimulation and co-inhibition. *Nat. Rev. Immunol.* **13**, 227–42 (2013).
72. Sewell Clement, A. K. *et al.* CD8 Controls T Cell Cross-Reactivity. *J. Immunol. by guest* (2017). doi:10.4049/jimmunol.1001480
73. Hochweller, K. *et al.* Dendritic cells control T cell tonic signaling required for responsiveness to foreign antigen. *Proc. Natl. Acad. Sci. U. S. A.* **107**, 5931–6 (2010).
74. Malissen, B., Grégoire, C., Malissen, M. & Roncagalli, R. Integrative biology of T cell activation. *Nat. Immunol.* **15**, 790–797 (2014).
75. Tsun, A. *et al.* Centrosome docking at the immunological synapse is controlled by Lck

signaling. *J. Cell Biol.* **192**, 663–74 (2011).

76. Huppa, J. B. & Davis, M. M. T-cell-antigen recognition and the immunological synapse. *Nat. Rev. Immunol.* **3**, 973–983 (2003).
77. Smith-Garvin, J. E., Koretzky, G. A. & Jordan, M. S. T cell activation. *Annu. Rev. Immunol.* **27**, 591–619 (2009).
78. Gálvez, J., Gálvez, J. J. & García-Peñarrubia, P. Is TCR/pMHC Affinity a Good Estimate of the T-cell Response? An Answer Based on Predictions From 12 Phenotypic Models. *Front. Immunol.* **10**, 349 (2019).
79. Davis, M. M. *et al.* LIGAND RECOGNITION BY αβ T CELL RECEPTORS. *Annu. Rev. Immunol.* **16**, 523–544 (1998).
80. Aleksic, M. *et al.* Different affinity windows for virus and cancer-specific T-cell receptors: Implications for therapeutic strategies. *Eur. J. Immunol.* **42**, 3174–3179 (2012).
81. Holler, P. D. & Kranz, D. M. Quantitative Analysis of the Contribution of TCR/pepMHC Affinity and CD8 to T Cell Activation. *Immunity* **18**, 255–264 (2003).
82. Cole, D. K. *et al.* Human TCR-Binding Affinity is Governed by MHC Class Restriction. *J. Immunol.* **178**, 5727–5734 (2007).
83. Krogsgaard, M. *et al.* Evidence that Structural Rearrangements and/or Flexibility during TCR Binding Can Contribute to T Cell Activation. *Mol. Cell* **12**, 1367–1378 (2003).
84. Alam, S. M. *et al.* Qualitative and quantitative differences in T cell receptor binding of agonist and antagonist ligands. *Immunity* **10**, 227–237 (1999).
85. Laugel, B. *et al.* Different T cell receptor affinity thresholds and CD8 coreceptor dependence govern cytotoxic T lymphocyte activation and tetramer binding properties. *J. Biol. Chem.* **282**, 23799–810 (2007).
86. Martinez, R. J. & Evavold, B. D. Lower Affinity T Cells are Critical Components and Active Participants of the Immune Response. *Front. Immunol.* **6**, 468 (2015).
87. Čemerski, S. *et al.* The Stimulatory Potency of T Cell Antigens Is Influenced by the Formation of the Immunological Synapse. *Immunity* **26**, 345–355 (2007).
88. Katz, Z. B., Novotná, L., Blount, A. & Lillemeier, B. F. A cycle of Zap70 kinase activation and release from the TCR amplifies and disperses antigenic stimuli. *Nat. Immunol.* **18**, 86–95 (2017).
89. Trebak, M. & Kinet, J. P. Calcium signalling in T cells. *Nature Reviews Immunology* **19**, 154–169 (2019).
90. Chen, J.-L. *et al.* Ca 2+ Release from the Endoplasmic Reticulum of NY-ESO-1–Specific T Cells Is Modulated by the Affinity of TCR and by the Use of the CD8 Coreceptor . *J. Immunol.* **184**, 1829–1839 (2010).
91. Mescher, M. F. *et al.* Signals required for programming effector and memory development by CD8+ T cells. *Immunol. Rev.* **211**, 81–92 (2006).
92. Kaech, S. M., Wherry, E. J. & Ahmed, R. Effector and memory T-cell differentiation: implications for vaccine development. *Nat. Rev. Immunol.* **2**, 251–262 (2002).
93. Lee, L. Y.-H. *et al.* Memory T cells established by seasonal human influenza A infection cross-react with avian influenza A (H5N1) in healthy individuals. *J. Clin. Invest.* **118**, 3478–

90 (2008).

94. Su, L. F., Kidd, B. A., Han, A., Kotzin, J. J. & Davis, M. M. Virus-Specific CD4+ Memory-Phenotype T Cells Are Abundant in Unexposed Adults. *Immunity* **38**, 373–383 (2013).
95. Farber, D. L., Yudanin, N. A. & Restifo, N. P. Human memory T cells: generation, compartmentalization and homeostasis. *Nat. Rev. Immunol.* **14**, 24–35 (2014).
96. Mason, D. A very high level of crossreactivity is an essential feature of the T-cell receptor. *Immunol. Today* **19**, 395–404 (1998).
97. Regner, M. & Article, R. Cross-reactivity in T-cell antigen recognition. *Immunol. Cell Biol.* **79**, 91–100 (2001).
98. Zarnitsyna, V. I., Evavold, B. D., Schoettle, L. N., Blattman, J. N. & Antia, R. Estimating the Diversity, Completeness, and Cross-Reactivity of the T Cell Repertoire. *Front. Immunol.* **4**, 485 (2013).
99. Wooldridge, L. *et al.* A single autoimmune T cell receptor recognizes more than a million different peptides. *J. Biol. Chem.* **287**, 1168–77 (2012).
100. McDonald, B. D., Bunker, J. J., Erickson, S. A., Oh-Hora, M. & Bendelac, A. Crossreactive αβ T Cell Receptors Are the Predominant Targets of Thymocyte Negative Selection. *Immunity* **43**, 859–869 (2015).
101. Chao, D. L., Davenport, M. P., Forrest, S. & Perelson, A. S. The effects of thymic selection on the range of T cell cross-reactivity. *Eur. J. Immunol.* **35**, 3452–3459 (2005).
102. Reiser, J.-B. *et al.* CDR3 loop flexibility contributes to the degeneracy of TCR recognition. *Nat. Immunol.* **4**, 241–247 (2003).
103. Baker, B. M., Scott, D. R., Blevins, S. J. & Hawse, W. F. Structural and dynamic control of T-cell receptor specificity, cross-reactivity, and binding mechanism. *Immunol. Rev.* **250**, 10–31 (2012).
104. Hanahan, D. & Weinberg, R. A. Hallmarks of cancer: the next generation. *Cell* **144**, 646–74 (2011).
105. Moore, P. S. & Chang, Y. Why do viruses cause cancer? Highlights of the first century of human tumour virology. *Nat. Rev. Cancer* **10**, 878–889 (2010).
106. McLaughlin-Drubin, M. E. & Münger, K. The Human Papillomavirus E7 Oncoprotein. *Virology* **384**, 335 (2009).
107. Farrell, P. J. Epstein–Barr Virus and Cancer. *Annu. Rev. Pathol. Mech. Dis.* **14**, 29–53 (2019).
108. van der Bruggen, P. *et al.* A gene encoding an antigen recognized by cytolytic T lymphocytes on a human melanoma. *Science* **254**, 1643–7 (1991).
109. Melo, D. H. *et al.* Expression of cancer/testis antigens MAGE-A, MAGE-C1, GAGE and CTAG1B in benign and malignant thyroid diseases. *Oncol. Lett.* **14**, 6485–6496 (2017).
110. Hemminger, J. A. *et al.* The cancer-testis antigen NY-ESO-1 is highly expressed in myxoid and round cell subset of liposarcomas. *Mod. Pathol.* **26**, 282–288 (2013).
111. Theobald, M., Biggs, J., Dittmer, D., Levine, A. J. & Sherman, L. A. Targeting p53 as a general tumor antigen. *Proc. Natl. Acad. Sci. U. S. A.* **92**, 11993–7 (1995).
112. Robbins, P. F. *et al.* A mutated beta-catenin gene encodes a melanoma-specific antigen

recognized by tumor infiltrating lymphocytes. *J. Exp. Med.* **183**, 1185–92 (1996).

113. Wu, J. *et al.* TSNAdb: A Database for Tumor-specific Neoantigens from Immunogenomics Data Analysis. *Genomics. Proteomics Bioinformatics* **16**, 276–282 (2018).
114. Wang, Q. J. *et al.* Identification of T-cell Receptors Targeting KRAS-mutated Human Tumors. *Cancer Immunol. Res.* **4**, 204 (2016).
115. Southall, P. J. *et al.* Immunohistological distribution of 5T4 antigen in normal and malignant tissues. *Br. J. Cancer* **61**, 89–95 (1990).
116. Gold, P. & Freedman, S. O. Specific carcinoembryonic antigens of the human digestive system. *J. Exp. Med.* **122**, 467–81 (1965).
117. Karan, D., Johansson, S., Lin, M.-F. & Batra, S. Expression of tumor-associated glycoprotein-72 (TAG-72) antigen in human prostatic adenocarcinomas. *Oncol. Rep.* **8**, 1123–1126 (2001).
118. Reynolds, S. R. *et al.* Stimulation of CD8+ T cell responses to MAGE-3 and Melan A/MART-1 by immunization to a polyvalent melanoma vaccine. *Int. J. Cancer* **72**, 972–976 (1997).
119. Schreibelt, G. *et al.* Effective Clinical Responses in Metastatic Melanoma Patients after Vaccination with Primary Myeloid Dendritic Cells. *Clin. Cancer Res.* **22**, 2155–66 (2016).
120. Levesque, M., Hu, H., Diamandis, E. P. & D'Costa, M. Prostate-Specific antigen expression by various tumors. *J. Clin. Lab. Anal.* **9**, 123–128 (1995).
121. Iqbal, N. & Iqbal, N. Human Epidermal Growth Factor Receptor 2 (HER2) in Cancers: Overexpression and Therapeutic Implications. *Mol. Biol. Int.* **2014**, 852748 (2014).
122. Oka, Y., Tsuboi, A., Elisseeva, O., Udaka, K. & Sugiyama, H. WT1 as a Novel Target Antigen for Cancer Immunotherapy. *Curr. Cancer Drug Targets* **2**, 45–54 (2002).
123. Soares, M. & Finn, O. J. MUC1 mucin as a target for immunotherapy of cancer: Muc1 based immunotherapeutic strategies. in *Cancer Immunology* 101–122 (Springer Netherlands, 2001). doi:10.1007/978-94-017-0963-7_6
124. Wang, M., Yin, B., Wang, H. Y. & Wang, R.-F. Current advances in T-cell-based cancer immunotherapy. *Immunotherapy* **6**, 1265–78 (2014).
125. Gulley, J. L. *et al.* Role of Antigen Spread and Distinctive Characteristics of Immunotherapy in Cancer Treatment. *J. Natl. Cancer Inst.* **109**, (2017).
126. Chen, D. S. & Mellman, I. Review Oncology MeetsImmunology: The Cancer-Immunity Cycle. (2013). doi:10.1016/j.immuni.2013.07.012
127. Kudo-Saito, C., Schlom, J. & Hodge, J. W. Induction of an antigen cascade by diversified subcutaneous/intratumoral vaccination is associated with antitumor responses. *Clin. Cancer Res.* **11**, 2416–26 (2005).
128. Nesslinger, N. J. *et al.* A viral vaccine encoding prostate-specific antigen induces antigen spreading to a common set of self-proteins in prostate cancer patients. *Clin. Cancer Res.* **16**, 4046–56 (2010).
129. Mulders, P. F., De Santis, M., Powles, · Thomas & Fizazi, K. Targeted treatment of metastatic castration-resistant prostate cancer with sipuleucel-T immunotherapy. *Cancer Immunol. Immunother.* **64**, 655–663 (2015).

130. Butterfield, L. H. Cancer vaccines. *BMJ* **350**, h988 (2015).
131. Nakagawa, M., Greenfield, W., Moerman-Herzog, A. & Coleman, H. N. Cross-Reactivity, Epitope Spreading, and De Novo Immune Stimulation Are Possible Mechanisms of Cross-Protection of Nonvaccine Human Papillomavirus (HPV) Types in Recipients of HPV Therapeutic Vaccines. *Clin. Vaccine Immunol.* **22**, 679–687 (2015).
132. Wang, R.-F. & Wang, H. Y. Immune targets and neoantigens for cancer immunotherapy and precision medicine. *Cell Res.* **27**, 11–37 (2017).
133. Marty, R. *et al.* MHC-I Genotype Restricts the Oncogenic Mutational Landscape. *Cell* **171**, 1272-1283.e15 (2017).
134. Legut, M. & Sewell, A. K. Designer T-cells and T-cell receptors for customized cancer immunotherapies. *Curr. Opin. Pharmacol.* **41**, 96–103 (2018).
135. Tan, M. P. *et al.* T cell receptor binding affinity governs the functional profile of cancer-specific CD8+ T cells. *Clin. Exp. Immunol.* **180**, 255–70 (2015).
136. Tan, M. P. *et al.* Human leucocyte antigen class I-redirected anti-tumour CD4 $^{+}$ T cells require a higher T cell receptor binding affinity for optimal activity than CD8 $^{+}$ T cells. *Clin. Exp. Immunol.* **187**, 124–137 (2017).
137. Kim, R., Emi, M. & Tanabe, K. Cancer immunoediting from immune surveillance to immune escape. *Immunology* **121**, 1–14 (2007).
138. Pizzi, M., Boi, M., Bertoni, F. & Inghirami, G. Emerging therapies provide new opportunities to reshape the multifaceted interactions between the immune system and lymphoma cells. *Leukemia* **30**, 1805–1815 (2016).
139. Zamora, A. E., Crawford, J. C. & Thomas, P. G. Hitting the Target: How T Cells Detect and Eliminate Tumors. *J. Immunol.* **200**, 392–399 (2018).
140. Chen, D. S. & Mellman, I. Elements of cancer immunity and the cancer–immune set point. *Nature* **541**, 321–330 (2017).
141. Sharpe, M. & Mount, N. Genetically modified T cells in cancer therapy: opportunities and challenges. *Dis. Model. Mech.* **8**, 337–350 (2015).
142. Concha-Benavente, F. & Ferris, R. L. Reversing EGFR Mediated Immunoescape by Targeted Monoclonal Antibody Therapy. *Front. Pharmacol.* **8**, 332 (2017).
143. Cai, L. *et al.* Defective HLA class I antigen processing machinery in cancer. *Cancer Immunol. Immunother.* **67**, 999–1009 (2018).
144. Kvistborg, P. & Yewdell, J. W. Enhancing responses to cancer immunotherapy. *Science* **359**, 516–517 (2018).
145. Ruiz-Cabello, F. & Garrido, F. HLA and cancer: from research to clinical impact. *Immunol. Today* **19**, 539–542 (1998).
146. Dunn, G. P., Bruce, A. T., Ikeda, H., Old, L. J. & Schreiber, R. D. Cancer immunoediting: from immunosurveillance to tumor escape. *Nat. Immunol.* **3**, 991–998 (2002).
147. Ehrlich, P. Ueber den jetzigen Stand der Karzinomforschung. *Dutch J. Med.* **5**, 273–290 (1909).
148. Couzin-Frankel, J. Breakthrough of the year 2013. Cancer immunotherapy. *Science* **342**, 1432–3 (2013).

149. Lockyer, N. *Nobel Prize in Physiology or Medicine 2018*. (Nature, 2018).
150. Kantoff, P. W. *et al.* Sipuleucel-T Immunotherapy for Castration-Resistant Prostate Cancer. *N. Engl. J. Med.* **363**, 411–422 (2010).
151. Garg, A. D., Coulie, P. G., Van den Eynde, B. J. & Agostinis, P. Integrating Next-Generation Dendritic Cell Vaccines into the Current Cancer Immunotherapy Landscape. *Trends Immunol.* **38**, 577–593 (2017).
152. Sahin, U. *et al.* Personalized RNA mutanome vaccines mobilize poly-specific therapeutic immunity against cancer. *Nature* **547**, 222–226 (2017).
153. van der Burg, S. H., Arens, R., Ossendorp, F., van Hall, T. & Melief, C. J. M. Vaccines for established cancer: overcoming the challenges posed by immune evasion. *Nat. Rev. Cancer* **16**, 219–233 (2016).
154. Maugh, T. H. FDA approves hepatitis B vaccine. *Science* **214**, 1113 (1981).
155. Siddiqui, M. A. A. & Perry, C. M. Human Papillomavirus Quadrivalent (types 6, 11, 16, 18) Recombinant Vaccine (Gardasil??). *Drugs* **66**, 1263–1271 (2006).
156. Zhai, L. & Tumban, E. Gardasil-9: A global survey of projected efficacy. *Antiviral Res.* **130**, 101–109 (2016).
157. Brown, S. D. *et al.* Neo-antigens predicted by tumor genome meta-analysis correlate with increased patient survival. *Genome Res.* **24**, 743–50 (2014).
158. Giannakis, M. *et al.* Genomic Correlates of Immune-Cell Infiltrates in Colorectal Carcinoma. *Cell Rep.* **17**, 1206 (2016).
159. Rajasagi, M. *et al.* Systematic identification of personal tumor-specific neoantigens in chronic lymphocytic leukemia. *Blood* **124**, (2014).
160. Tran, E. *et al.* Immunogenicity of somatic mutations in human gastrointestinal cancers. *Science* **350**, 1387–90 (2015).
161. Ott, P. A. *et al.* An Immunogenic Personal Neoantigen Vaccine for Melanoma Patients. *Nature* **547**, 217 (2017).
162. Nicholaou, T. *et al.* Immunoediting and persistence of antigen-specific immunity in patients who have previously been vaccinated with NY-ESO-1 protein formulated in ISCOMATRIX™. *Cancer Immunol. Immunother.* **60**, 1625–1637 (2011).
163. Guo, Y., Lei, K. & Tang, L. neoantigen vaccine Delivery for Personalized Anticancer immunotherapy. *Front. Immunol.* **9**, 1499 (2018).
164. Yadav, M. *et al.* Predicting immunogenic tumour mutations by combining mass spectrometry and exome sequencing. *Nature* **515**, 572–576 (2014).
165. Sang, M. *et al.* Melanoma-associated antigen genes – An update. *Cancer Lett.* **302**, 85–90 (2011).
166. Hu, Z., Ott, P. A. & Wu, C. J. Towards personalized, tumour-specific, therapeutic vaccines for cancer. *Nat. Rev. Immunol.* (2017). doi:10.1038/nri.2017.131
167. Salgaller, M. L., Marincola, F. M., Cormier, J. N. & Rosenberg, S. A. Immunization against epitopes in the human melanoma antigen gp100 following patient immunization with synthetic peptides. *Cancer Res.* **56**, 4749–57 (1996).
168. Tran, E. *et al.* Cancer Immunotherapy Based on Mutation-Specific CD4+ T Cells in a

Patient with Epithelial Cancer. *Science (80-.).* **344**, 641–645 (2014).

169. Kaufman, J., Tian, S., Gregori, L. & Adorini, D. L. Spreading Determines the Hierarchy of Determinant The Frequency of High Avidity T Cells. *J Immunol Ref.* **166**, 7144–7150 (2001).
170. Cole, D. K. *et al.* Modification of MHC anchor residues generates heteroclitic peptides that alter TCR binding and T cell recognition. *J. Immunol.* **185**, 2600–10 (2010).
171. Valmori, D. *et al.* Enhanced Generation of Specific Tumor-Reactive CTL In Vitro by Selected Melan-A/MART-1 Immunodominant Peptide Analogues. *J. Immunol.* **160**, 1750–1758 (1998).
172. Romero, P. *et al.* CD8 + T-Cell Response to NY-ESO-I: Relative Antigenicity and in Vitro Immunogenicity of Natural and Analogue Sequences. *Clin. Cancer Res.* **7**, 766–772 (2001).
173. Parkhurst, M. R. *et al.* Improved induction of melanoma-reactive CTL with peptides from the melanoma antigen gp100 modified at HLA-A*0201-binding residues. *J. Immunol.* **157**, 2539–48 (1996).
174. Bakker, A. B. *et al. ANALOGUES OF CTL EPITOPES WITH IMPROVED MHC CLASS-I BINDING CAPACITY ELICIT ANTI-MELANOMA CTL RECOGNIZING THE WILD-TYPE EPITOPE*. *Int. J. Cancer* **70**, (Wiley-Liss, Inc, 1997).
175. Ruella, M. & Kalos, M. Adoptive immunotherapy for cancer. *Immunol. Rev.* **257**, 14–38 (2014).
176. Perez, S. A. *et al.* A new era in anticancer peptide vaccines. *Cancer* **116**, NA-NA (2010).
177. Ekeruche-Makinde, J. *et al.* T-cell receptor-optimized peptide skewing of the T-cell repertoire can enhance antigen targeting. *J. Biol. Chem.* **287**, 37269–37281 (2012).
178. Galloway, S. A. E. *et al.* Peptide Super-agonist enhances T-cell Responses to Melanoma. *Front. Immunol.* **10**, 319 (2019).
179. Vijayalakshmi Ayyar, B., Arora, S. & O'kennedy, R. Coming-of-Age of Antibodies in Cancer Therapeutics. *Trends Pharmacol. Sci.* **36**, 1009–1028 (2016).
180. Hodi, F. S. *et al.* Improved Survival with Ipilimumab in Patients with Metastatic Melanoma. *N. Engl. J. Med.* **363**, 711–723 (2010).
181. Ribas, A. *et al.* Association of Pembrolizumab With Tumor Response and Survival Among Patients With Advanced Melanoma. *JAMA* **315**, 1600 (2016).
182. Garon, E. B. *et al.* Pembrolizumab for the Treatment of Non–Small-Cell Lung Cancer. *N. Engl. J. Med.* **372**, 2018–2028 (2015).
183. Paz-Ares, L. *et al.* Pembrolizumab plus Chemotherapy for Squamous Non–Small-Cell Lung Cancer. *N. Engl. J. Med.* **379**, 2040–2051 (2018).
184. Wolchok, J. D. *et al.* Nivolumab plus Ipilimumab in Advanced Melanoma. *N. Engl. J. Med.* **369**, 122–133 (2013).
185. Motzer, R. J. *et al.* Nivolumab versus Everolimus in Advanced Renal-Cell Carcinoma. *N. Engl. J. Med.* **373**, 1803–13 (2015).
186. Ansell, S. M. *et al.* PD-1 Blockade with Nivolumab in Relapsed or Refractory Hodgkin's Lymphoma. *N. Engl. J. Med.* **372**, 311–319 (2015).

187. Weinstock, C. *et al.* U.S. Food and Drug Administration Approval Summary: Atezolizumab for Metastatic Non–Small Cell Lung Cancer. *Clin. Cancer Res.* **23**, 4534–4539 (2017).
188. Kaufman, H. L. *et al.* Updated efficacy of avelumab in patients with previously treated metastatic Merkel cell carcinoma after ≥1 year of follow-up: JAVELIN Merkel 200, a phase 2 clinical trial. *J. Immunother. cancer* **6**, 7 (2018).
189. Syed, Y. Y. Durvalumab: First Global Approval. *Drugs* **77**, 1369–1376 (2017).
190. Migden, M. R. *et al.* PD-1 Blockade with Cemiplimab in Advanced Cutaneous Squamous-Cell Carcinoma. *N. Engl. J. Med.* **379**, 341–351 (2018).
191. Xu, C. *et al.* Comparative safety of immune checkpoint inhibitors in cancer: systematic review and network meta-analysis. *BMJ* **363**, k4226 (2018).
192. Sandigursky, S. & Mor, A. Immune-Related Adverse Events in Cancer Patients Treated With Immune Checkpoint Inhibitors. *Curr. Rheumatol. Rep.* **20**, 65 (2018).
193. Phan, G. Q. & Rosenberg, S. A. Adoptive cell transfer for patients with metastatic melanoma: The potential and promise of cancer immunotherapy. *Cancer Control* **20**, 289–297 (2013).
194. McGranahan, N. *et al.* Clonal neoantigens elicit T cell immunoreactivity and sensitivity to immune checkpoint blockade. *Science* **351**, 1463–9 (2016).
195. Kather, J. N. *et al.* Topography of cancer-associated immune cells in human solid tumors. *Elife* **7**, (2018).
196. Postow, M. A. *et al.* Peripheral T cell receptor diversity is associated with clinical outcomes following ipilimumab treatment in metastatic melanoma. *J. Immunother. cancer* **3**, 23 (2015).
197. Burges, A. *et al.* Effective Relief of Malignant Ascites in Patients with Advanced Ovarian Cancer by aTrifunctional Anti-EpCAM Â Anti-CD3 Antibody: A Phase I/II Study. *Clin. cancer Res.* **13**, 3899–3905 (2007).
198. Zhu, M. *et al.* Blinatumomab, a Bispecific T-cell Engager (BiTE®) for CD-19 Targeted Cancer Immunotherapy: Clinical Pharmacology and Its Implications. *Clin. Pharmacokinet.* **55**, 1271–1288 (2016).
199. Oates, J., Hassan, N. & Jakobsen, B. ImmTACs for targeted cancer therapy: Why, what, how, and which. *Mol. Immunol.* **67**, 67–74 (2015).
200. Zhang, H. *et al.* ImmTAC/Anti-PD-1 antibody combination to enhance killing of cancer cells by reversing regulatory T-cell-mediated immunosuppression. *Immunology* **155**, 238–250 (2018).
201. Boudousquie, C. *et al.* Polyfunctional response by ImmTAC (IMCgp100) redirected CD8 $^{+}$ and CD4 $^{+}$ T cells. *Immunology* **152**, 425–438 (2017).
202. Yu, L. & Wang, J. T cell-redirecting bispecific antibodies in cancer immunotherapy: recent advances. *J. Cancer Res. Clin. Oncol.* **145**, 941–956 (2019).
203. Krishnamurthy, A. & Jimeno, A. Bispecific antibodies for cancer therapy: A review. *Pharmacol. Ther.* **185**, 122–134 (2018).
204. Porzsolt, F. *et al.* Deficient IFNa production in hairy cell leukemia. *Blut* **52**, 185–190 (1986).
205. Klapper, J. A. *et al.* High-dose interleukin-2 for the treatment of metastatic renal cell

carcinoma. *Cancer* **113**, 293–301 (2008).

206. Goldstein, D. & Laszlo, J. The Role of Interferon in Cancer Therapy: A Current Perspective. *CA. Cancer J. Clin.* **38**, 258–277 (1988).
207. Waldmann, T. A. Cytokines in Cancer Immunotherapy. *Cold Spring Harb. Perspect. Biol.* **10**, a028472 (2018).
208. Baldo, B. A. Side Effects of Cytokines Approved for Therapy. *Drug Saf.* **37**, 921–943 (2014).
209. Tang, L. *et al.* Enhancing T cell therapy through TCR-signaling-responsive nanoparticle drug delivery. *Nat. Biotechnol.* **36**, 707–716 (2018).
210. Stephan, M. T., Stephan, S. B., Bak, P., Chen, J. & Irvine, D. J. Synapse-directed delivery of immunomodulators using T-cell-conjugated nanoparticles. *Biomaterials* **33**, 5776–87 (2012).
211. Stephan, M. T., Moon, J. J., Um, S. H., Bershteyn, A. & Irvine, D. J. Therapeutic cell engineering with surface-conjugated synthetic nanoparticles. *Nat. Med.* **16**, 1035–1041 (2010).
212. Schwartzentruber, D. J. *et al.* gp100 Peptide Vaccine and Interleukin-2 in Patients with Advanced Melanoma. *N. Engl. J. Med.* **364**, 2119–2127 (2011).
213. Atkins, M. B. *et al.* Phase III trial comparing concurrent biochemotherapy with cisplatin, vinblastine, dacarbazine, interleukin-2, and interferon alfa-2b with cisplatin, vinblastine, and dacarbazine alone in patients with metastatic malignant melanoma (E3695): a trial coordinated by the Eastern Cooperative Oncology Group. *J. Clin. Oncol.* **26**, 5748–54 (2008).
214. Maker, A. V. *et al.* Tumor Regression and Autoimmunity in Patients Treated With Cytotoxic T Lymphocyte–Associated Antigen 4 Blockade and Interleukin 2: A Phase I/II Study. *Ann. Surg. Oncol.* **12**, 1005–1016 (2005).
215. Young, P. A., Morrison, S. L. & Timmerman, J. M. Antibody-Cytokine Fusion Proteins for Treatment of Cancer: Engineering Cytokines for Improved Efficacy and Safety. *Semin. Oncol.* **41**, 623–636 (2014).
216. Rosenberg, S. A. *et al.* Durable complete responses in heavily pretreated patients with metastatic melanoma using T-cell transfer immunotherapy. *Clin. Cancer Res.* **17**, 4550–7 (2011).
217. Burton, A. L. *et al.* Prognostic Significance of Tumor Infiltrating Lymphocytes in Melanoma. *Am. Surg.* **77**, 188–192 (2011).
218. Lee, N., Zakka, L. R. & Schatton, T. Tumour-infiltrating lymphocytes in melanoma prognosis and cancer immunotherapy. *Pathology* **48**, 177–187 (2016).
219. Stumpf, M. *et al.* Intraepithelial CD8-positive T lymphocytes predict survival for patients with serous stage III ovarian carcinomas: relevance of clonal selection of T lymphocytes. *Br. J. Cancer* **101**, 1513–1521 (2009).
220. Li, J., Wang, J., Chen, R., Bai, Y. & Lu, X. The prognostic value of tumor-infiltrating T lymphocytes in ovarian cancer. *Oncotarget* **8**, 15621–15631 (2017).
221. Naito, Y. *et al.* CD8+ T cells infiltrated within cancer cell nests as a prognostic factor in

human colorectal cancer. *Cancer Res.* **58**, 3491–4 (1998).

222. Huang, H.-S. *et al.* Prognostic impact of tumor infiltrating lymphocytes on patients with metastatic urothelial carcinoma receiving platinum based chemotherapy. *Sci. Rep.* **8**, 7485 (2018).
223. Meng, Q. *et al.* Neoepitope targets of tumour-infiltrating lymphocytes from patients with pancreatic cancer. *Br. J. Cancer* 1 (2018). doi:10.1038/s41416-018-0262-z
224. Schreiber, R. D., Old, L. J. & Smyth, M. J. Cancer Immunoediting: Integrating Immunity's Roles in Cancer Suppression and Promotion. *Science (80-.).* **331**, 1565–1570 (2011).
225. Dudley, M. E. *et al.* Adoptive Cell Transfer Therapy Following Non-Myeloablative but Lymphodepleting Chemotherapy for the Treatment of Patients With Refractory Metastatic Melanoma. *J. Clin. Oncol.* **23**, 2346–2357 (2005).
226. Donia, M. *et al.* Characterization and Comparison of 'Standard' and 'Young' Tumour-Infiltrating Lymphocytes for Adoptive Cell Therapy at a Danish Translational Research Institution. *Scand. J. Immunol.* **75**, 157–167 (2012).
227. Gattinoni, L., Powell, D. J., Rosenberg, S. A. & Restifo, N. P. Adoptive immunotherapy for cancer: building on success. *Nat. Rev. Immunol.* **6**, 383–393 (2006).
228. Wrzesinski, C. *et al.* Increased intensity lymphodepletion enhances tumor treatment efficacy of adoptively transferred tumor-specific T cells. *J. Immunother.* **33**, 1–7 (2010).
229. Crump, M. *et al.* Outcomes in refractory diffuse large B-cell lymphoma: Results from the international SCHOLAR-1 study. *Blood* (2017). doi:10.1182/blood-2017-03-769620
230. Maude, S. L. *et al.* Tisagenlecleucel in Children and Young Adults with B-Cell Lymphoblastic Leukemia. *N. Engl. J. Med.* **378**, 439–448 (2018).
231. Qin, H. *et al.* Preclinical Development of Bivalent Chimeric Antigen Receptors Targeting Both CD19 and CD22. (2018). doi:10.1016/j.omto.2018.10.006
232. Shah, N. N., Maatman, T., Hari, P. & Johnson, B. Multi Targeted CAR-T Cell Therapies for B-Cell Malignancies. *Front. Oncol.* (2019). doi:10.3389/fonc.2019.00146
233. Zhou, H. *et al.* The efficacy and safety of anti-CD19/CD20 chimeric antigen receptor- T cells immunotherapy in relapsed or refractory B-cell malignancies:a meta-analysis. *BMC Cancer* **18**, 929 (2018).
234. Brentjens, R. J. *et al.* Safety and persistence of adoptively transferred autologous CD19-targeted T cells in patients with relapsed or chemotherapy refractory B-cell leukemias. *Blood* **118**, 4817–28 (2011).
235. Porter, D. L. *et al.* Chimeric antigen receptor T cells persist and induce sustained remissions in relapsed refractory chronic lymphocytic leukemia. *Sci. Transl. Med.* **7**, 303ra139 (2015).
236. Jackson, H. J., Rafiq, S. & Brentjens, R. J. Driving CAR T-cells forward. *Nat. Rev. Clin. Oncol.* **13**, 370–383 (2016).
237. Curran, K. J. *et al.* Enhancing Antitumor Efficacy of Chimeric Antigen Receptor T Cells Through Constitutive CD40L Expression. *Mol. Ther.* **23**, 769–778 (2015).
238. Rafiq, S. *et al.* Targeted delivery of a PD-1-blocking scFV by CAR-T cells enhances anti-tumor efficacy in vivo. *Nat. Biotechnol.* **36**, 847–858 (2018).

239. Yeku, O. O., Purdon, T. J., Koneru, M., Spriggs, D. & Brentjens, R. J. Armored CAR T cells enhance antitumor efficacy and overcome the tumor microenvironment. *Sci. Rep.* **7**, 10541 (2017).
240. Legut, M., Dolton, G., Mian, A. A., Ottmann, O. & Sewell, A. CRISPR-mediated TCR replacement generates superior anticancer transgenic T-cells. *Blood* blood-2017-05-787598 (2017). doi:10.1182/blood-2017-05-787598
241. Linette, G. P. *et al.* Cardiovascular toxicity and titin cross-reactivity of affinity-enhanced T cells in myeloma and melanoma. *Blood* **122**, 863–71 (2013).
242. D 'angelo, S. P., Tap, W. D., Schwartz, G. K. & Carvajal, R. D. Sarcoma Immunotherapy: Past Approaches and Future Directions. *Sarcoma* 1–13 (2014). doi:10.1155/2014/391967
243. Hirayama, A. V. & Turtle, C. J. Toxicities of CD19 CAR-T cell immunotherapy. *Am. J. Hematol.* **94**, S42–S49 (2019).
244. Rius, C. *et al.* Peptide-MHC Class I Tetramers Can Fail To Detect Relevant Functional T Cell Clonotypes and Underestimate Antigen-Reactive T Cell Populations. *J. Immunol.* **200**, 2263–2279 (2018).
245. Masters, J. R. & Stacey, G. N. Changing medium and passaging cell lines. *Nat. Protoc.* (2007). doi:10.1038/nprot.2007.319
246. van den Berg, H. A. *et al.* Cellular-Level Versus Receptor-Level Response Threshold Hierarchies in T-Cell Activation. *Front. Immunol.* **4**, (2013).
247. Price, D. A. *et al.* Antigen-specific release of β-chemokines by anti-HIV-1 cytotoxic T lymphocytes. *Curr. Biol.* **8**, 355–358 (1998).
248. Ekeruche-Makinde, J. *et al.* Peptide length determines the outcome of TCR/peptide-MHCI engagement. *Blood* **121**, 1112–1123 (2013).
249. Wooldridge, L. *et al.* Interaction between the CD8 coreceptor and major histocompatibility complex class I stabilizes T cell receptor-antigen complexes at the cell surface. *J. Biol. Chem.* **280**, 27491–27501 (2005).
250. Lissina, A. *et al.* Protein kinase inhibitors substantially improve the physical detection of T-cells with peptide-MHC tetramers. *J. Immunol. Methods* **340**, 11–24 (2009).
251. Haney, D. *et al.* Isolation of viable antigen-specific CD8+ T cells based on membrane-bound tumor necrosis factor (TNF)-α expression. *J. Immunol. Methods* **369**, 33–41 (2011).
252. Bagaev, D. V. *et al.* VDJviz: a versatile browser for immunogenomics data. *BMC Genomics* **17**, 453 (2016).
253. Shugay, M. *et al.* VDJdb: a curated database of T-cell receptor sequences with known antigen specificity. *Nucleic Acids Res.* **46**, D419–D427 (2018).
254. Richardson, M. W. *et al.* Mode of Transmission Affects the Sensitivity of Human Immunodeficiency Virus Type 1 to Restriction by Rhesus TRIM5. *J. Virol.* **82**, 11117–11128 (2008).
255. Sanjana, N. E., Shalem, O. & Zhang, F. Improved vectors and genome-wide libraries for CRISPR screening. *Nat. Methods* **11**, 783–784 (2014).
256. Kozak, M. Point mutations define a sequence flanking the AUG initiator codon that modulates translation by eukaryotic ribosomes. *Cell* (1986). doi:10.1016/0092-

8674(86)90762-2

257. Meier, J. A., Zhang, F. & Sanjana, N. E. GUIDES: sgRNA design for loss-of-function screens. *Nat. Methods* **14**, 831–832 (2017).

258. Deltcheva, E. *et al.* CRISPR RNA maturation by trans-encoded small RNA and host factor RNase III. *Nature* **471**, 602–7 (2011).

259. Jinek, M. *et al.* A Programmable Dual-RNA–Guided DNA Endonuclease in Adaptive Bacterial Immunity. *Science (80-.).* **337**, 816–821 (2012).

260. Altman, J. D. *et al.* Phenotypic Analysis of Antigen-Specific T Lymphocytes. *Science (80-.).* **274**, 94–96 (1996).

261. Bentzen, A. K. *et al.* Large-scale detection of antigen-specific T cells using peptide-MHC-I multimers labeled with DNA barcodes. *Nat. Biotechnol.* **34**, 1037–1045 (2016).

262. Batard, P. *et al.* Dextramers: New generation of fluorescent MHC class I/peptide multimers for visualization of antigen-specific CD8+ T cells. *J. Immunol. Methods* **310**, 136–148 (2006).

263. Newell, E. W., Klein, L. O., Yu, W. & Davis, M. M. Simultaneous detection of many T-cell specificities using combinatorial tetramer staining. *Nat. Methods* **6**, 497–499 (2009).

264. Hadrup, S. R. *et al.* Parallel detection of antigen-specific T-cell responses by multidimensional encoding of MHC multimers. *Nat. Methods* **6**, 520–526 (2009).

265. Dolton, G. *et al.* More tricks with tetramers: A practical guide to staining T cells with peptide-MHC multimers. *Immunology* **146**, 11–22 (2015).

266. Wooldridge, L. *et al.* Tricks with tetramers: how to get the most from multimeric peptide-MHC. *Immunology* **126**, 147–64 (2009).

267. Dolton, G. *et al.* Comparison of peptide-major histocompatibility complex tetramers and dextramers for the identification of antigen-specific T cells. *Clin. Exp. Immunol.* **177**, 47–63 (2014).

268. Tungatt, K. *et al.* Antibody stabilization of peptide-MHC multimers reveals functional T cells bearing extremely low-affinity TCRs. *J. Immunol.* **194**, 463–74 (2015).

269. Crawford, F., Kozono, H., White, J., Marrack, P. & Kappler, J. Detection of Antigen-Specific T Cells with Multivalent Soluble Class II MHC Covalent Peptide Complexes. *Immunity* **8**, 675–682 (1998).

270. Stone, J. D., Chervin, A. S. & Kranz, D. M. T-cell receptor binding affinities and kinetics: impact on T-cell activity and specificity. *Immunology* **126**, 165–176 (2009).

271. Huang, J. *et al.* Detection, phenotyping, and quantification of antigen-specific T cells using a peptide-MHC dodecamer. *Proc. Natl. Acad. Sci. U. S. A.* **113**, E1890-7 (2016).

272. Sabatino, J. J., Huang, J., Zhu, C., Evavold, B. D. & Evavold, B. D. High prevalence of low affinity peptide-MHC II tetramer-negative effectors during polyclonal CD4+ T cell responses. *J. Exp. Med.* **208**, 81–90 (2011).

273. Derby, M. A., Wang, J., Margulies, D. H. & Berzofsky, J. A. Two intermediate-avidity cytotoxic T lymphocyte clones with a disparity between functional avidity and MHC tetramer staining. *Int. Immunol.* **13**, 817–24 (2001).

274. Dougan, S. K. *et al.* Transnuclear TRP1-Specific CD8 T Cells with High or Low Affinity

TCRs Show Equivalent Antitumor Activity. *Cancer Immunol. Res.* **1**, 99–111 (2013).

275. Martinez, R. J., Andargachew, R., Martinez, H. A. & Evavold, B. D. Low-affinity CD4+ T cells are major responders in the primary immune response. *Nat. Commun.* **7**, 13848 (2016).
276. McKinney, E. F., Lee, J. C., Jayne, D. R., Lyons, P. A. & Smith, K. G. T-cell exhaustion, co-stimulation and clinical outcome in autoimmunity and infection. *Nature* **523**, 612–616 (2015).
277. Khan, N., Cobbold, M., Cummerson, J. & Moss, P. A. H. Persistent viral infection in humans can drive high frequency low-affinity T-cell expansions. *Immunology* **131**, 537–48 (2010).
278. Potter, T. A., Rajan, T. V., Dick, R. F. & Bluestone, J. A. Substitution at residue 227 of H–2 class I molecules abrogates recognition by CD8-dependent, but not CD8-independent, cytotoxic T lymphocytes. *Nature* **337**, 73–75 (1989).
279. Daniels, M. A. & Jameson, S. C. Critical role for CD8 in T cell receptor binding and activation by peptide/major histocompatibility complex multimers. *J. Exp. Med.* **191**, 335–46 (2000).
280. Wooldridge, L. *et al.* Anti-CD8 Antibodies Can Inhibit or Enhance Peptide-MHC Class I (pMHCI) Multimer Binding: This Is Paralleled by Their Effects on CTL Activation and Occurs in the Absence of an Interaction between pMHCI and CD8 on the Cell Surface. *J. Immunol.* **171**, 6650–6660 (2003).
281. Wooldridge, L. *et al.* Anti-coreceptor antibodies profoundly affect staining with peptide-MHC class I and class II tetramers. *Eur. J. Immunol.* **36**, 1847–1855 (2006).
282. Melenhorst, J. J. *et al.* Detection of low avidity CD8+ T cell populations with coreceptor-enhanced peptide-major histocompatibility complex class I tetramers. **338**, 31–39 (2008).
283. Guillaume, P. *et al.* Soluble major histocompatibility complex-peptide octamers with impaired CD8 binding selectively induce Fas-dependent apoptosis. *J. Biol. Chem.* **278**, 4500–9 (2003).
284. Weichsel, R. *et al.* Profound Inhibition of Antigen-Specific T-Cell Effector Functions by Dasatinib. *Clin. Cancer Res.* **14**, 2484–2491 (2008).
285. Dolton, G. *et al.* Optimized Peptide–MHC Multimer Protocols for Detection and Isolation of Autoimmune T-Cells. *Front. Immunol.* **9**, 1378 (2018).
286. Kawakami, Y. *et al.* Cloning of the gene coding for a shared human melanoma antigen recognized by autologous T cells infiltrating into tumor. *Proc. Natl. Acad. Sci. U. S. A.* **91**, 3515–9 (1994).
287. Coulie, P. G. *et al.* A new gene coding for a differentiation antigen recognized by autologous cytolytic T lymphocytes on HLA-A2 melanomas. *J. Exp. Med.* **180**, 35–42 (1994).
288. Ellebaek, E. *et al.* Adoptive cell therapy with autologous tumor infiltrating lymphocytes and low-dose Interleukin-2 in metastatic melanoma patients. *J. Transl. Med.* **10**, 169 (2012).
289. Andersen, R. *et al.* Long-Lasting Complete Responses in Patients with Metastatic Melanoma after Adoptive Cell Therapy with Tumor-Infiltrating Lymphocytes and an

Attenuated IL2 Regimen. *Clin. Cancer Res.* **22**, 3734–3745 (2016).

290. Donia, M., Larsen, S. M., Met, Ö. & Svane, I. M. Simplified protocol for clinical-grade tumor-infiltrating lymphocyte manufacturing with use of the Wave bioreactor. *Cytotherapy* **16**, 1117–1120 (2014).
291. Bianchi, V. MOLECULAR AND CELLULAR BASIS OF T CELL RESPONSES TO MELANOMA ANTIGENS. (Cardiff University, 2016).
292. Schwartz, L. H. *et al.* RECIST 1.1-Update and clarification: From the RECIST committee. *Eur. J. Cancer* **62**, 132–7 (2016).
293. Simon, S. *et al.* TCR Analyses of Two Vast and Shared Melanoma Antigen-Specific T Cell Repertoires: Common and Specific Features. *Front. Immunol.* **9**, 1962 (2018).
294. Skowera, A. *et al.* CTLs are targeted to kill beta cells in patients with type 1 diabetes through recognition of a glucose-regulated preproinsulin epitope. *J. Clin. Invest.* **118**, 3390–402 (2008).
295. Purbhoo, M. A. *et al.* The HLA A*0201-restricted hTERT(540-548) peptide is not detected on tumor cells by a CTL clone or a high-affinity T-cell receptor. *Mol. Cancer Ther.* **6**, 2081–91 (2007).
296. Donia, M. *et al.* PD-1 $^{+}$ Polyfunctional T Cells Dominate the Periphery after Tumor-Infiltrating Lymphocyte Therapy for Cancer. *Clin. Cancer Res.* **23**, 5779–5788 (2017).
297. Drake, D. R. & Braciale, T. J. Cutting edge: lipid raft integrity affects the efficiency of MHC class I tetramer binding and cell surface TCR arrangement on CD8+ T cells. *J. Immunol.* **166**, 7009–13 (2001).
298. Whelan, J. A. *et al.* Specificity of CTL interactions with peptide-MHC class I tetrameric complexes is temperature dependent. *J. Immunol.* **162**, 331–337 (1999).
299. Davidson, B. *et al.* VICKZ2 protein expression in ovarian serous carcinoma effusions is associated with poor survival. *Hum. Pathol.* **45**, 1520–1528 (2014).
300. Li, Y. *et al.* p62/IMP2 stimulates cell migration and reduces cell adhesion in breast cancer. *Oncotarget* **6**, 32656–32668 (2015).
301. Kim, H.-Y., Ha Thi, H. T. & Hong, S. IMP2 and IMP3 cooperate to promote the metastasis of triple-negative breast cancer through destabilization of progesterone receptor. *Cancer Lett.* **415**, 30–39 (2018).
302. Barghash, A., Helms, V. & Kessler, S. M. Overexpression of *IGF2* mRNA-Binding Protein 2 (IMP2/p62) as a Feature of Basal-like Breast Cancer Correlates with Short Survival. *Scand. J. Immunol.* **82**, 142–143 (2015).
303. He, X. *et al.* IGF2BP2 Overexpression Indicates Poor Survival in Patients with Acute Myelocytic Leukemia. *Cell. Physiol. Biochem.* **51**, 1945–1956 (2018).
304. Degrauwe, N. *et al.* The RNA Binding Protein IMP2 Preserves Glioblastoma Stem Cells by Preventing let-7 Target Gene Silencing. *Cell Rep.* **15**, 1634–1647 (2016).
305. Dai, N. *et al.* IGF2 mRNA binding protein-2 is a tumor promoter that drives cancer proliferation through its client mRNAs IGF2 and HMGA1. *Elife* **6**, e27155 (2017).
306. Cohen, G. B. *et al.* Clonotype Tracking of TCR Repertoires during Chronic Virus Infections. *Virology* **304**, 474–484 (2002).

307. Koning, D. *et al.* In vitro expansion of antigen-specific CD8(+) T cells distorts the T-cell repertoire. *J. Immunol. Methods* **405**, 199–203 (2014).
308. Miconnet, I. *et al.* Large TCR Diversity of Virus-Specific CD8 T Cells Provides the Mechanistic Basis for Massive TCR Renewal after Antigen Exposure. *J. Immunol.* **186**, 7039–7049 (2011).
309. Price, D. A. *et al.* Avidity for antigen shapes clonal dominance in CD8+ T cell populations specific for persistent DNA viruses. *J. Exp. Med.* **202**, 1349–61 (2005).
310. Akondy, R. S. *et al.* The yellow fever virus vaccine induces a broad and polyfunctional human memory CD8+ T cell response. *J. Immunol.* **183**, 7919–30 (2009).
311. Blom, K. *et al.* Temporal dynamics of the primary human T cell response to yellow fever virus 17D as it matures from an effector- to a memory-type response. *J. Immunol.* **190**, 2150–8 (2013).
312. de Melo, A. B. *et al.* T-Cell Memory Responses Elicited by Yellow Fever Vaccine are Targeted to Overlapping Epitopes Containing Multiple HLA-I and -II Binding Motifs. *PLoS Negl. Trop. Dis.* **7**, e1938 (2013).
313. Wieten, R. W. *et al.* A Single 17D Yellow Fever Vaccination Provides Lifelong Immunity; Characterization of Yellow-Fever-Specific Neutralizing Antibody and T-Cell Responses after Vaccination. (2016). doi:10.1371/journal.pone.0149871
314. Wieten, R. W. *et al.* 17D yellow fever vaccine elicits comparable long-term immune responses in healthy individuals and immune-compromised patients. *J. Infect.* **72**, 713–722 (2016).
315. Elong Ngono, A. *et al.* Protective Role of Cross-Reactive CD8 T Cells Against Dengue Virus Infection. *EBioMedicine* **13**, 284–293 (2016).
316. Saron, W. A. A. *et al. Flavivirus* serocomplex cross-reactive immunity is protective by activating heterologous memory CD4 T cells. *Sci. Adv.* **4**, eaar4297 (2018).
317. Reynolds, C. J. *et al.* T cell immunity to Zika virus targets immunodominant epitopes that show cross-reactivity with other Flaviviruses. *Sci. Rep.* **8**, 672 (2018).
318. Bovay, A. *et al.* T cell receptor alpha variable 12-2 bias in the immunodominant response to Yellow fever virus. *Eur. J. Immunol.* **48**, 258–272 (2018).
319. Huang, J. *et al.* The kinetics of two-dimensional TCR and pMHC interactions determine T-cell responsiveness. doi:10.1038/nature08944
320. Alexander-Miller, M. *et al.* Selective expansion of high- or low-avidity cytotoxic T lymphocytes and efficacy for adoptive immunotherapy. *PNAS* **93**, 4102–4107 (2013).
321. Zhong, S. *et al.* T-cell receptor affinity and avidity defines antitumor response and autoimmunity in T-cell immunotherapy. *PNAS* **110**, 6973–6978 (2013).
322. Hodi, F. S. *et al.* Biologic activity of cytotoxic T lymphocyte-associated antigen 4 antibody blockade in previously vaccinated metastatic melanoma and ovarian carcinoma patients. *Proc. Natl. Acad. Sci.* (2003). doi:10.1073/pnas.0830997100
323. Robbins, P. F. *et al.* Cutting edge: persistence of transferred lymphocyte clonotypes correlates with cancer regression in patients receiving cell transfer therapy. *J. Immunol.* **173**, 7125–30 (2004).

324. Dudley, M. E. *et al.* Cancer Regression and Autoimmunity in Patients After Clonal Repopulation with Antitumor Lymphocytes. *Science (80-.).* **298**, 850–854 (2002).
325. Huang, J. *et al.* T cells associated with tumor regression recognize frameshifted products of the CDKN2A tumor suppressor gene locus and a mutated HLA class I gene product. *J. Immunol.* **172**, 6057–64 (2004).
326. Legut, M. Genome Editing Approaches for Development of Pan-Population. (Cardiff University, 2017).
327. Zhou, J., Dudley, M. E., Rosenberg, S. A. & Robbins, P. F. Persistence of multiple tumor-specific T-cell clones is associated with complete tumor regression in a melanoma patient receiving adoptive cell transfer therapy. *J. Immunother.* **28**, 53–62 (2005).
328. Parmley, S. F. & Smith, G. P. Antibody-selectable filamentous fd phage vectors: affinity purification of target genes. *Gene* **73**, 305–318 (1988).
329. Koeppel, F. *et al.* Whole exome sequencing for determination of tumor mutation load in liquid biopsy from advanced cancer patients. *PLoS One* **12**, e0188174 (2017).
330. Pasetto, A. *et al.* Tumor- and Neoantigen-Reactive T-cell Receptors Can Be Identified Based on Their Frequency in Fresh Tumor. *Cancer Immunol. Res.* **4**, 734–43 (2016).
331. Matsushita, H. *et al.* Cancer exome analysis reveals a T-cell-dependent mechanism of cancer immunoediting. *Nature* **482**, 400–404 (2012).
332. Yossef, R. *et al.* Enhanced detection of neoantigen-reactive T cells targeting unique and shared oncogenes for personalized cancer immunotherapy. *JCI insight* **3**, (2018).
333. Rizvi, N. A. *et al.* Cancer immunology. Mutational landscape determines sensitivity to PD-1 blockade in non-small cell lung cancer. *Science* **348**, 124–8 (2015).
334. Reichel, J. *et al.* Flow sorting and exome sequencing reveal the oncogenome of primary Hodgkin and Reed-Sternberg cells. *Blood* **125**, 1061–72 (2015).
335. Restifo, N. P. *et al.* Loss of Functional Beta2-Microglobulin in Metastatic Melanomas From Five Patients Receiving Immunotherapy. *JNCI J. Natl. Cancer Inst.* **88**, 100–108 (1996).
336. Kalaora, S. *et al.* Combined Analysis of Antigen Presentation and T-cell Recognition Reveals Restricted Immune Responses in Melanoma. (2018). doi:10.1158/2159-8290.CD-17-1418
337. Gros, A. *et al.* Prospective identification of neoantigen-specific lymphocytes in the peripheral blood of melanoma patients. *Nat. Med.* **22**, 433–438 (2016).
338. Patel, S. J. *et al.* Identification of essential genes for cancer immunotherapy. *Nature* **548**, 537–542 (2017).
339. Wheeler, S. Identifying a novel γδ T-cell stress ligand : Potential for cancer immunotherapy. (Cardiff University, 2017).
340. Crowther, M. D. Novel Unconventional T-cells in Response to Bacteria and Cancer. (Cardiff University, 2018).
341. Boder, E. T. & Wittrup, K. D. Yeast surface display for screening combinatorial polypeptide libraries. *Nat. Biotechnol.* (1997). doi:10.1038/nbt0697-553
342. Zhang, G. L. *et al.* Machine learning competition in immunology - Prediction of HLA class I binding peptides. *Journal of Immunological Methods* (2011).

doi:10.1016/j.jim.2011.09.010

343. Houghten, R. A. *et al.* Mixture-based synthetic combinatorial libraries. *Journal of Medicinal Chemistry* (1999). doi:10.1021/jm990174v

344. Pinilla, C. *et al. Combinatorial Peptide Libraries as an Alternative Approach to the Identification of Ligands for Tumor-reactive Cytolytic T Lymphocytes 1*. *CANCER RESEARCH* **61**, (2001).

345. Zhao, Y. *et al.* Combinatorial Peptide Libraries and Biometric Score Matrices Permit the Quantitative Analysis of Specific and Degenerate Interactions Between Clonotypic TCR and MHC Peptide Ligands. *J. Immunol.* (2001). doi:10.4049/jimmunol.167.4.2130

346. Szomolay, B. *et al.* Identification of human viral protein-derived ligands recognized by individual MHCI-restricted T-cell receptors. *Immunol. Cell Biol.* **94**, 573–582 (2016).

347. Olsen, L. R. *et al.* TANTIGEN: a comprehensive database of tumor T cell antigens. *Cancer Immunol. Immunother.* (2017). doi:10.1007/s00262-017-1978-y

348. Andersen, R. S. *et al.* Dissection of T-cell Antigen Specificity in Human Melanoma. *Cancer Res.* **72**, 1642–1650 (2012).

349. Theaker, S. M. Developing peptide vaccines for breast cancer. (Cardiff University, 2018).

350. Purbhoo, M. A. *et al.* The human CD8 coreceptor effects cytotoxic T cell activation and antigen sensitivity primarily by mediating complete phosphorylation of the T cell receptor zeta chain. *J. Biol. Chem.* **276**, 32786–92 (2001).

351. Macosko, E. Z. *et al.* Highly Parallel Genome-wide Expression Profiling of Individual Cells Using Nanoliter Droplets. *Cell* **161**, 1202–1214 (2015).

352. McDaniel, J. R., DeKosky, B. J., Tanno, H., Ellington, A. D. & Georgiou, G. Ultra-high-throughput sequencing of the immune receptor repertoire from millions of lymphocytes. *Nat. Protoc.* **11**, 429–442 (2016).

353. Cole, D. K. *et al.* Structural Mechanism Underpinning Cross-reactivity of a CD8+ T-cell Clone That Recognizes a Peptide Derived from Human Telomerase Reverse Transcriptase. *J. Biol. Chem.* **292**, 802–813 (2017).

354. Macdonald, W. A. *et al.* T Cell Allorecognition via Molecular Mimicry. *Immunity* **31**, 897–908 (2009).

355. Gras, S. *et al.* The Shaping of T Cell Receptor Recognition by Self-Tolerance. *Immunity* **30**, 193–203 (2009).

356. Madura, F. *et al.* Structural basis for ineffective T-cell responses to MHC anchor residue-improved "heteroclitic" peptides. *Eur. J. Immunol.* **45**, 584–91 (2015).

357. Hundemer, M. *et al.* Identification of a new HLA-A2–restricted T-cell epitope within HM1.24 as immunotherapy target for multiple myeloma. *Exp. Hematol.* **34**, 486–496 (2006).

358. Jalili, A. *et al.* Induction of HM1.24 peptide–specific cytotoxic T lymphocytes by using peripheral-blood stem-cell harvests in patients with multiple myeloma. *Blood* **106**, 3538–3545 (2005).

359. Harada, T. & Ozaki, S. Targeted therapy for HM1.24 (CD317) on multiple myeloma cells. *Biomed Res. Int.* **2014**, 965384 (2014).

360. Kawai, S. *et al.* Interferon-α enhances CD317 expression and the antitumor activity of anti-

CD317 monoclonal antibody in renal cell carcinoma xenograft models. *Cancer Sci.* **99**, 2461–2466 (2008).

361. Walter-Yohrling, J. *et al.* Identification of Genes Expressed in Malignant Cells That Promote Invasion. *Cancer Res.* **63**, 1101–1105 (2003).
362. Becker, M. *et al.* Distinct gene expression patterns in a tamoxifen-sensitive human mammary carcinoma xenograft and its tamoxifen-resistant subline MaCa 3366/TAM. *Mol. Cancer Ther.* **4**, 151–170 (2005).
363. Cai, D. *et al.* Up-regulation of bone marrow stromal protein 2 (BST2) in breast cancer with bone metastasis. *BMC Cancer* **9**, 102 (2009).
364. Cole, D. K. *et al.* Germ line-governed recognition of a cancer epitope by an immunodominant human T-cell receptor. *J. Biol. Chem.* **284**, 27281–9 (2009).
365. Lloyd, A. Gene Editing in T-cells and T-cell Targets. (2016).
366. Hruz, T. *et al.* Genevestigator V3: A Reference Expression Database for the Meta-Analysis of Transcriptomes. *Adv. Bioinformatics* **2008**, 1–5 (2008).
367. Johnson, L. A. *et al.* Gene transfer of tumor-reactive TCR confers both high avidity and tumor reactivity to nonreactive peripheral blood mononuclear cells and tumor-infiltrating lymphocytes. *J. Immunol.* **177**, 6548–59 (2006).
368. Tyler, E. M., Jungbluth, A. A., Gnjatic, S., O'Reilly, R. J. & Koehne, G. Cancer-Testis Antigen 7 Expression and Immune Responses Following Allogeneic Stem Cell Transplantation for Multiple Myeloma. *Cancer Immunol. Res.* (2014). doi:10.1158/2326-6066.cir-13-0174
369. Friedman, R. S., Spies, A. G. & Kalos, M. Identification of naturally processed CD8 T cell epitopes from prostein, a prostate tissue-specific vaccine candidate. (2004). doi:10.1002/eji.200324768
370. Musiyenko, A., Bitko, V. & Barik, S. Ectopic expression of miR-126*, an intronic product of the vascular endothelial EGF-like 7 gene, regulates prostein translation and invasiveness of prostate cancer LNCaP cells. *J. Mol. Med.* (2008). doi:10.1007/s00109-007-0296-9
371. Pin, E. *et al.* Identification of a Novel Autoimmune Peptide Epitope of Prostein in Prostate Cancer. (2016). doi:10.1021/acs.jproteome.6b00620
372. Bernhard, H. *et al.* Recognition of human renal cell carcinoma and melanoma by HLA-A2-restricted cytotoxic T lymphocytes is mediated by shared peptide epitopes and up-regulated by interferon-. *Scand. J. Immunol.* (1996). doi:10.1046/j.1365-3083.1996.d01-304.x
373. Comoli, P. *et al.* BCR-ABL-specific T-cell therapy in Ph+ ALL patients on tyrosine-kinase inhibitors. *Blood* (2017). doi:10.1182/blood-2016-07-731091
374. Anderson, L. D. *et al.* Identification of MAGE-C1 (CT-7) epitopes for T-cell therapy of multiple myeloma. *Cancer Immunol. Immunother.* (2011). doi:10.1007/s00262-011-1009-3
375. Kiessling, A. *et al.* Identification of an HLA-A*0201-restricted T-cell epitope derived from the prostate cancer-associated protein prostein. *Br. J. Cancer* (2004). doi:10.1038/sj.bjc.6601642

376. Prickett, T. D. *et al.* Durable Complete Response from Metastatic Melanoma after Transfer of Autologous T Cells Recognizing 10 Mutated Tumor Antigens. *Cancer Immunol. Res.* **4**, 669–678 (2016).
377. Santoiemma, P. P. & Powell, D. J. Tumor infiltrating lymphocytes in ovarian cancer. (2015). doi:10.1080/15384047.2015.1040960
378. Fujita, K. *et al.* Prolonged disease-free period in patients with advanced epithelial ovarian cancer after adoptive transfer of tumor-infiltrating lymphocytes. *Clin. Cancer Res.* **1**, 501–7 (1995).
379. Figlin, R. A. *et al.* Multicenter, randomized, phase III trial of CD8(+) tumor-infiltrating lymphocytes in combination with recombinant interleukin-2 in metastatic renal cell carcinoma. *J. Clin. Oncol.* **17**, 2521–9 (1999).
380. Gonzalez-Galarza, F. F., Christmas, S., Middleton, D. & Jones, A. R. Allele frequency net: a database and online repository for immune gene frequencies in worldwide populations. *Nucleic Acids Res.* **39**, D913–D919 (2011).
381. Goto, T. *et al.* A novel membrane antigen selectively expressed on terminally differentiated human B cells. *Blood* **84**, 1922–30 (1994).
382. Shigematsu, Y. *et al.* Overexpression of the transmembrane protein BST-2 induces Akt and Erk phosphorylation in bladder cancer. *Oncol. Lett.* **14**, 999–1004 (2017).
383. Yokoyama, T. *et al.* Plasma membrane proteomics identifies bone marrow stromal antigen 2 as a potential therapeutic target in endometrial cancer. *Int. J. Cancer* **132**, 472–484 (2013).
384. Wang, W. *et al.* HM1.24 (CD317) is a novel target against lung cancer for immunotherapy using anti-HM1.24 antibody. *Cancer Immunol. Immunother.* **58**, 967–976 (2009).
385. Mukai, S. *et al.* Overexpression of Transmembrane Protein BST2 is Associated with Poor Survival of Patients with Esophageal, Gastric, or Colorectal Cancer. *Ann. Surg. Oncol.* **24**, 594–602 (2017).
386. Barghash, A. *et al.* Elevated expression of the IGF2 mRNA binding protein 2 (IGF2BP2/IMP2) is linked to short survival and metastasis in esophageal adenocarcinoma. *Oncotarget* **7**, 49743–49750 (2016).
387. Madjo, U. *et al.* LC3C Contributes to Vpu-Mediated Antagonism of BST2/Tetherin Restriction on HIV-1 Release through a Non-canonical Autophagy Pathway. *Cell Rep.* **17**, 2221–2233 (2016).
388. Arias, J. F. *et al.* Tetherin antagonism by Vpu protects HIV-infected cells from antibody-dependent cell-mediated cytotoxicity. *Proc. Natl. Acad. Sci. U. S. A.* **111**, 6425–30 (2014).
389. Sayeed, A. *et al.* Aberrant Regulation of the BST2 (Tetherin) Promoter Enhances Cell Proliferation and Apoptosis Evasion in High Grade Breast Cancer Cells. *PLoS One* **8**, e67191 (2013).
390. Mahauad-Fernandez, W. D., Borcherding, N. C., Zhang, W. & Okeoma, C. M. Bone Marrow Stromal Antigen 2 (BST-2) DNA Is Demethylated in Breast Tumors and Breast Cancer Cells. *PLoS One* **10**, e0123931 (2015).
391. Wenzel, J. *et al.* Type I Interferon–Associated Recruitment of Cytotoxic Lymphocytes. *Am.*

J. Clin. Pathol. **124**, 37–48 (2005).

392. Bell, J. L. *et al.* Insulin-like growth factor 2 mRNA-binding proteins (IGF2BPs): post-transcriptional drivers of cancer progression? *Cell. Mol. Life Sci.* **70**, 2657–2675 (2013).
393. Boudoukha, S., Cuvellier, S. & Polesskaya, A. Role of the RNA-Binding Protein IMP-2 in Muscle Cell Motility. *Mol. Cell. Biol.* **30**, 5710–5725 (2010).
394. Suda, T., Tsunoda, T., Daigo, Y., Nakamura, Y. & Tahara, H. Identification of human leukocyte antigen-A24-restricted epitope peptides derived from gene products upregulated in lung and esophageal cancers as novel targets for immunotherapy. *Cancer Sci.* **98**, 1803–1808 (2007).
395. Echchakir, H. *et al.* Evidence for in situ expansion of diverse antitumor-specific cytotoxic T lymphocyte clones in a human large cell carcinoma of the lung. *Int. Immunol.* **12**, 537–546 (2000).
396. WEYNANTS, P. *et al.* Derivation of Tumor-specific Cytolytic T-Cell Clones from Two Lung Cancer Patients with Long Survival. *Am. J. Respir. Crit. Care Med.* **159**, 55–62 (1999).
397. Slingluff, C. L. *et al.* Cytotoxic T-lymphocyte response to autologous human squamous cell cancer of the lung: epitope reconstitution with peptides extracted from HLA-Aw68. *Cancer Res.* **54**, 2731–7 (1994).
398. Karanikas, V. *et al.* High Frequency of Cytolytic T Lymphocytes Directed against a Tumor-specific Mutated Antigen Detectable with HLA Tetramers in the Blood of a Lung Carcinoma Patient with Long Survival. *Cancer Res.* **61**, 5144–50 (2001).
399. Kawakami, Y. & Rosenberg, S. A. Human tumor antigens recognized by T-cells. *Immunol. Res.* **16**, 313–339 (1997).
400. Bolotin, D. A. *et al.* MiXCR: software for comprehensive adaptive immunity profiling. *Nat. Methods* **12**, 380–381 (2015).
401. Matzinger, P. & Bevan, M. J. Why do so many lymphocytes respond to major histocompatibility antigens? *Cell. Immunol.* **29**, 1–5 (1977).
402. Jerne, N. K. The somatic generation of immune recognition. *Eur. J. Immunol.* **1**, 1–9 (1971).
403. Harkiolaki, M. *et al.* T Cell-Mediated Autoimmune Disease Due to Low-Affinity Crossreactivity to Common Microbial Peptides. *Immunity* **30**, 348–357 (2009).
404. Birnbaum, M. E. *et al.* Deconstructing the Peptide-MHC Specificity of T Cell Recognition. *Cell* **157**, 1073–1087 (2014).
405. Bridgeman, J. S., Sewell, A. K., Miles, J. J., Price, D. A. & Cole, D. K. Structural and biophysical determinants of αβ T-cell antigen recognition. *Immunology* **135**, 9–18 (2012).
406. Yin, Y. & Mariuzza, R. A. The Multiple Mechanisms of T Cell Receptor Cross-reactivity. *Immunity* **31**, 849–851 (2009).
407. Rudolph, M. G., Stanfield, R. L. & Wilson, I. A. HOW TCRS BIND MHCS, PEPTIDES, AND CORECEPTORS. *Annu. Rev. Immunol.* **24**, 419–466 (2006).
408. Kraj, P., Pacholczyk, R. & Ignatowicz, L. αβTCRs Differ in the Degree of Their Specificity for the Positively Selecting MHC/Peptide Ligand. *J. Immunol.* **166**, 2251–2259 (2001).
409. Reiser, J.-B. *et al.* Crystal structure of a T cell receptor bound to an allogeneic MHC

molecule. *Nat. Immunol.* **1**, 291–297 (2000).

410. Luz, J. G. *et al.* Structural comparison of allogeneic and syngeneic T cell receptor-peptide-major histocompatibility complex complexes: a buried alloreactive mutation subtly alters peptide presentation substantially increasing V(beta) Interactions. *J. Exp. Med.* **195**, 1175–86 (2002).
411. Borbulevych, O. Y. *et al.* T Cell Receptor Cross-reactivity Directed by Antigen-Dependent Tuning of Peptide-MHC Molecular Flexibility. *Immunity* **31**, 885–896 (2009).
412. Wilson, D. B. *et al.* Specificity and degeneracy of T cells. *Mol. Immunol.* **40**, 1047–1055 (2004).
413. Madura, F. *et al.* TCR-induced alteration of primary MHC peptide anchor residue. *Eur. J. Immunol.* **49**, eji.201948085 (2019).
414. Riley, T. P. *et al.* T cell receptor cross-reactivity expanded by dramatic peptide–MHC adaptability. *Nat. Chem. Biol.* (2018). doi:10.1038/s41589-018-0130-4
415. Welsh, R. M. & Selin, L. K. No one is naive: the significance of heterologous T-cell immunity. *Nat. Rev. Immunol.* **2**, 417–426 (2002).
416. Francis, T. *On the Doctrine of Original Antigenic Sin*. *Source: Proceedings of the American Philosophical Society* **104**, (1960).
417. Klenerman, P. *et al.* Cytotoxic T-cell activity antagonized by naturally occurring HIV-1 Gag variants. *Nature* **369**, 403–407 (1994).
418. Selin, L. K. *et al.* CD8 memory T cells: cross-reactivity and heterologous immunity. *Semin. Immunol.* **16**, 335–347 (2004).
419. Townsend, A. R. & Skehel, J. J. The influenza A virus nucleoprotein gene controls the induction of both subtype specific and cross-reactive cytotoxic T cells. *J. Exp. Med.* **160**, 552–63 (1984).
420. Selin, L. K., Nahill, S. R. & Welsh, R. M. Cross-reactivities in memory cytotoxic T lymphocyte recognition of heterologous viruses. *J. Exp. Med.* **179**, 1933–43 (1994).
421. Friberg, H. *et al.* Memory CD8+ T cells from naturally acquired primary dengue virus infection are highly cross-reactive. *Immunol. Cell Biol.* **89**, 122–9 (2011).
422. Urbani, S. *et al.* The impairment of CD8 responses limits the selection of escape mutations in acute hepatitis C virus infection. *J. Immunol.* **175**, 7519–29 (2005).
423. Cornberg, M. *et al.* CD8 T Cell Cross-Reactivity Networks Mediate Heterologous Immunity in Human EBV and Murine Vaccinia Virus Infections. *J. Immunol.* **184**, 2825–2838 (2010).
424. Clute, S. C. *et al.* Cross-reactive influenza virus-specific CD8+ T cells contribute to lymphoproliferation in Epstein-Barr virus-associated infectious mononucleosis. *J. Clin. Invest.* **115**, 3602–12 (2005).
425. Vali, B. *et al.* Characterization of cross-reactive CD8+ T-cell recognition of HLA-A2-restricted HIV-Gag (SLYNTVATL) and HCV-NS5b (ALYDVVSKL) epitopes in individuals infected with human immunodeficiency and hepatitis C viruses. *J. Virol.* **85**, 254–63 (2011).
426. Acierno, P. M. *et al.* Cross-reactivity between HLA-A2-restricted FLU-M1:58-66 and HIV p17 GAG:77-85 epitopes in HIV-infected and uninfected individuals. *J. Transl. Med.* **1**, 3

(2003).

427. Kennedy, P. T. F. *et al.* The influence of T cell cross-reactivity on HCV-peptide specific human T cell response. *Hepatology* **43**, 602–611 (2006).

428. Wedemeyer, H., Mizukoshi, E., Davis, A. R., Bennink, J. R. & Rehermann, B. Cross-reactivity between hepatitis C virus and Influenza A virus determinant-specific cytotoxic T cells. *J. Virol.* **75**, 11392–400 (2001).

429. Varela-Calvino, R., Skowera, A., Arif, S. & Peakman, M. Identification of a Naturally Processed Cytotoxic CD8 T-Cell Epitope of Coxsackievirus B4, Presented by HLA-A2.1 and Located in the PEVKEK Region of the P2C Nonstructural Protein. *J. Virol.* **78**, 13399–13408 (2004).

430. Hiemstra, H. S. *et al.* Cytomegalovirus in autoimmunity: T cell crossreactivity to viral antigen and autoantigen glutamic acid decarboxylase. *Proc. Natl. Acad. Sci. U. S. A.* **98**, 3988–91 (2001).

431. Ou, D., Mitchell, L. A., Metzger, D. L., Gillam, S. & Tingle, A. J. Cross-reactive rubella virus and glutamic acid decarboxylase (65 and 67) protein determinants recognised by T cells of patients with Type I diabetes mellitus. *Diabetologia* **43**, 750–762 (2000).

432. Yang, J. *et al.* A Novel Approach of Identifying Immunodominant Self and Viral Antigen Cross-Reactive T Cells and Defining the Epitopes They Recognize. *Front. Immunol.* **9**, 2811 (2018).

433. Lang, H. L. E. *et al.* A functional and structural basis for TCR cross-reactivity in multiple sclerosis. *Nat. Immunol.* **3**, 940–943 (2002).

434. JOHNSTON, A., GUDJONSSON, J. E., SIGMUNDSDOTTIR, H., LOVE, T. J. & VALDIMARSSON, H. Peripheral blood T cell responses to keratin peptides that share sequences with streptococcal M proteins are largely restricted to skin-homing CD8+ T cells. *Clin. Exp. Immunol.* **138**, 83–93 (2004).

435. Voelter, V. *et al.* Characterization of Melan-A reactive memory CD8+ T cells in a healthy donor. *Int. Immunol.* **20**, 1087–1096 (2008).

436. Antunes, D. A. *et al.* Interpreting T-Cell Cross-reactivity through Structure: Implications for TCR-Based Cancer Immunotherapy. *Front. Immunol.* **8**, 1210 (2017).

437. Morgan, R. A. *et al.* Cancer Regression and Neurological Toxicity Following Anti-MAGE-A3 TCR Gene Therapy. *J. Immunother.* **36**, 133–151 (2013).

438. Morgan, R. A. *et al.* Cancer regression in patients after transfer of genetically engineered lymphocytes. *Science* **314**, 126–9 (2006).

439. Zang, Y.-W., Gu, X.-D., Xiang, J.-B. & Chen, Z.-Y. Clinical application of adoptive T cell therapy in solid tumors. *Med. Sci. Monit.* **20**, 953–9 (2014).

440. Raman, M. C. C. *et al.* Direct molecular mimicry enables off-target cardiovascular toxicity by an enhanced affinity TCR designed for cancer immunotherapy. *Sci. Rep.* **6**, 18851 (2016).

441. Singh, N. K. *et al.* Emerging Concepts in TCR Specificity: Rationalizing and (Maybe) Predicting Outcomes. *J. Immunol.* **199**, 2203–2213 (2017).

442. Mendes, M. F. A., Antunes, D. A., Rigo, M. M., Sinigaglia, M. & Vieira, G. F. Improved

structural method for T-cell cross-reactivity prediction. *Mol. Immunol.* **67**, 303–310 (2015).

443. Antunes, D. A. *et al.* Structural in silico analysis of cross-genotype-reactivity among naturally occurring HCV NS3-1073-variants in the context of HLA-A*02:01 allele. *Mol. Immunol.* **48**, 1461–1467 (2011).
444. Dash, P. *et al.* Quantifiable predictive features define epitope-specific T cell receptor repertoires. *Nature* **547**, 89–93 (2017).
445. Glanville, J. *et al.* Identifying specificity groups in the T cell receptor repertoire. *Nature* **547**, 94–98 (2017).
446. Bentzen, A. K. *et al.* T cell receptor fingerprinting enables in-depth characterization of the interactions governing recognition of peptide–MHC complexes. *Nat. Biotechnol. 2018 3612* **36**, 1191 (2018).
447. Cole, D. K. *et al.* Hotspot autoimmune T cell receptor binding underlies pathogen and insulin peptide cross-reactivity. *J. Clin. Invest.* **126**, 2191–204 (2016).
448. Schober, K. *et al.* Orthotopic replacement of T-cell receptor α- and β-chains with preservation of near-physiological T-cell function. *Nat. Biomed. Eng.* 1 (2019). doi:10.1038/s41551-019-0409-0
449. Macosko, E. Z. *et al.* Highly Parallel Genome-wide Expression Profiling of Individual Cells Using Nanoliter Droplets. *Cell* **161**, 1202–1214 (2015).
450. Schuster, S. J. *et al.* Chimeric Antigen Receptor T Cells in Refractory B-Cell Lymphomas. *N. Engl. J. Med.* **377**, 2545–2554 (2017).
451. Maude, S. L. *et al.* Efficacy of Humanized CD19-Targeted Chimeric Antigen Receptor (CAR)-Modified T Cells in Children and Young Adults with Relapsed/Refractory Acute Lymphoblastic Leukemia. *Blood* **128**, (2016).
452. Roybal, K. T. *et al.* Engineering T Cells with Customized Therapeutic Response Programs Using Synthetic Notch Receptors Article Engineering T Cells with Customized Therapeutic Response Programs Using Synthetic Notch Receptors. *Cell* **167**, 419-432.e16 (2016).
453. Morsut, L. *et al.* Engineering Customized Cell Sensing and Response Behaviors Using Synthetic Notch Receptors. *Cell* (2016). doi:10.1016/j.cell.2016.01.012
454. Greco, R. *et al.* Improving the safety of cell therapy with the TK-suicide gene. *Front. Pharmacol.* (2015). doi:10.3389/fphar.2015.00095
455. Antonio, D. S. *et al.* Inducible Apoptosis as a Safety Switch for Adoptive Cell Therapy. *N Engl J Med* **365**, 1673–83 (2011).
456. Lim, W. A. & June, C. H. The Principles of Engineering Immune Cells to Treat Cancer. *Cell* **168**, 724–740 (2017).
457. Wiek, C. *et al.* Identification of amino acid determinants in CYP4B1 for optimal catalytic processing of 4-ipomeanol. *Biochem. J.* (2015). doi:10.1042/BJ20140813
458. Mensali, N. *et al.* Preclinical assessment of transiently TCR redirected T cells for solid tumour immunotherapy. *Cancer Immunol. Immunother.* 1–9 (2019). doi:10.1007/s00262-019-02356-2
459. Giraldo, N. A. *et al.* The clinical role of the TME in solid cancer. *Br. J. Cancer* 1 (2018). doi:10.1038/s41416-018-0327-z

460. Petrova, V., Annicchiarico-Petruzzelli, M., Melino, G. & Amelio, I. The hypoxic tumour microenvironment. *Oncogenesis* (2018). doi:10.1038/s41389-017-0011-9
461. Shrimali, R. K. *et al.* Antiangiogenic agents can increase lymphocyte infiltration into tumor and enhance the effectiveness of adoptive immunotherapy of cancer. *Cancer Res.* (2010). doi:10.1158/0008-5472.CAN-10-0153
462. Rosen, L. S. VEGF-Targeted Therapy: Therapeutic Potential and Recent Advances. *Oncologist* (2005). doi:10.1634/theoncologist.10-6-382
463. Corti, A., Curnis, F., Rossoni, G., Marcucci, F. & Gregorc, V. Peptide-mediated targeting of cytokines to tumor vasculature: The NGR-hTNF example. *BioDrugs* (2013). doi:10.1007/s40259-013-0048-z
464. Kershaw, M. H. *et al.* Redirecting Migration of T Cells to Chemokine Secreted from Tumors by Genetic Modification with CXCR2. *Hum. Gene Ther.* (2002). doi:10.1089/10430340260355374
465. Peng, W. *et al.* Transduction of tumor-specific T cells with CXCR2 chemokine receptor improves migration to tumor and antitumor immune responses. *Clin. Cancer Res.* (2010). doi:10.1158/1078-0432.CCR-10-0712
466. Riley, R. S., June, C. H., Langer, R. & Mitchell, M. J. Delivery technologies for cancer immunotherapy. *Nat. Rev. Drug Discov.* **18**, 175–196 (2019).
467. Mi, Y., Hagan, C. T., Vincent, B. G. & Wang, A. Z. Emerging Nano-/Microapproaches for Cancer Immunotherapy. *Advanced Science* (2019). doi:10.1002/advs.201801847
468. Schmid, D. *et al.* T cell-targeting nanoparticles focus delivery of immunotherapy to improve antitumor immunity. *Nat. Commun.* (2017). doi:10.1038/s41467-017-01830-8
469. Garrido, G. *et al.* Upregulation of HLA Class I Expression on Tumor Cells by the Anti-EGFR Antibody Nimotuzumab. *Front. Pharmacol.* (2017). doi:10.3389/fphar.2017.00595
470. Ramakrishnan, M. S. *et al.* Nimotuzumab, a promising therapeutic monoclonal for treatment of tumors of epithelial origin. *MAbs* **1**, 41–8
471. Schietinger, A. *et al.* Tumor-Specific T Cell Dysfunction Is a Dynamic Antigen-Driven Differentiation Program Initiated Early during Tumorigenesis. *Immunity* (2016). doi:10.1016/j.immuni.2016.07.011
472. Im, S. J. *et al.* Defining CD8 + T cells that provide the proliferative burst after PD-1 therapy. *Nature* (2016). doi:10.1038/nature19330
473. Lee, S. & Schmitt, C. A. The dynamic nature of senescence in cancer. *Nature Cell Biology* (2019). doi:10.1038/s41556-018-0249-2
474. Rosenberg, S. A. IL-2: the first effective immunotherapy for human cancer. *J. Immunol.* **192**, 5451–8 (2014).
475. Weng, J. *et al.* IL-15 enhances the antitumor effect of human antigen-specific CD8+ T cells by cellular senescence delay. *Oncoimmunology* (2016). doi:10.1080/2162402X.2016.1237327
476. Mullinax, J. E. *et al.* Combination of Ipilimumab and Adoptive Cell Therapy with Tumor-Infiltrating Lymphocytes for Patients with Metastatic Melanoma. *Front. Oncol.* (2018). doi:10.3389/fonc.2018.00044

– Annexe 1 – Supplementary figures

Melan-A/MART1 (Length: 375 nucleotides)

TCTAGAGCCGCCACCATGCCCAGGGAGGACGCCCACTTTATCTACGGCTACCCCAAGAAGGGCCACGGCCACAG
CTATACCACCGCCGAGGAGGCCGCCGGAATTGGCATCCTGACCGTGATCCTGGGCGTGCTGCTGCTGATCGGCT
GCTGGTATTGCAGGAGAAGGAACGGCTACAGGGCCCTGATGGACAAGAGCCTGCACGTGGGCACACAGTGCGCC
CTGACCAGAAGATGCCCCCAGGAGGGCTTCGACCACAGGGACAGCAAGGTGAGCCTGCAGGAAAAGAACTGCGA
GCCTGTGGTGCCCAATGCCCCTCCTGCCTACGAGAAGCTGAGCGCCGAGCAGAGCCCCCCTCCTTATAGCCCCCT
CGAG

BST2/CD317/Tetherin (Length: 561 nucleotides)

TCTAGAGCCGCCACCATGGCCAGCACCAGCTACGACTACTGCAGGGTGCCCATGGAGGACGGCGACAAGAGATG
TAAACTGCTGCTGGGCATCGGCATCCTCGTGCTGCTGATCATCGTGATCCTGGGCGTCCCCCTGATCATCTTCACC
ATCAAGGCCAACAGCGAAGCCTGCAGGGACGGCCTGAGAGCCGTGATGGAGTGCAGGAACGTGACCCACCTGCT
GCAGCAGGAGCTGACCGAAGCCCAGAAGGGATTCCAGGACGTGGAGGCTCAGGCCGCCACCTGCAACCACACCG
TGATGGCCCTGATGGCCAGCCTGGACGCCGAAAAGGCCCAGGGCCAGAAGAAGGTGGAGGAGCTGGAGGGCGA
GATCACAACCCTCAACCACAAGCTGCAGGACGCCAGCGCCGAGGTGGAAAGACTGAGAAGGGAGAACCAGGTGC
TGTCCGTGAGGATCGCCGACAAGAAGTACTACCCTAGCAGCCAGGATAGCAGCAGCGCCGCTGCTCCTCAGCTGC
TGATCGTGCTGCTGGGCCTGAGCGCCCTGCTGCAGCTCGAG

IF2B2/IMP-2/VICKZ (Length: 1818 nucleotides)

TCTAGAGCCGCCACCATGATGAATAAGCTGTATATTGGCAACCTCTCCCCTGCTGTGACCGCCGACGACCTCAGGC
AGCTGTTTGGCGACAGAAAACTCCCCCTCGCCGGACAGGTGCTCCTCAAGTCCGGCTATGCCTTTGTGGACTATC
CTGATCAGAACTGGGCCATCAGAGCCATCGAGACCCTGAGCGGCAAAGTGGAGCTGCATGGCAAGATTATGGAGG
TGGACTACTCCGTCAGCAAGAAGCTGAGGTCCAGGAAGATCCAAATCAGGAACATCCCCCCCCCATCTGCAGTGGG
AAGTGCTCGACGGCCTGCTGGCCCAATATGGAACCGTGGAAAACGTGGAGCAGGTGAACACAGACACAGAGACC
GCCGTGGTCAATGTCACATACGCCACCAGGGAAGAGGCTAAGATCGCCATGGAGAAGCTGAGCGGCCACCAGTTC
GAGAACTATAGCTTTAAGATCAGCTACATCCCCGATGAGGAGGTGTCCAGCCCTAGCCCCCCCCAAAGAGCTCAG
AGGGGCGACCACAGCAGCAGAGAACAGGGCCATGCTCCTGGCGGAACAAGCCAGGCCAGGCAGATCGACTTTCC
CCTGAGGATTCTGGTGCCCACCCAGTTCGTGGGAGCTATCATCGGCAAAGAGGGCCTCACCATCAAGAACATCAC
AAAGCAGACACAGTCCAGGGTCGACATCCATAGGAAGGAGAACTCCGGCGCTGCCGAAAAACCCGTCACCATTCA
CGCCACCCCCGAGGGCACAAGCGAAGCCTGCAGGATGATCCTGGAGATCATGCAGAAGGAGGCCGACGAAACCA
AGCTGGCCGAGGAGATCCCCCTGAAGATTCTGGCCCACAACGGCCTGGTGGGAAGACTGATTGGCAAGGAGGGC
AGGAACCTGAAGAAAATCGAGCACGAGACCGGCACAAAAATCACCATCAGCTCCCTCCAGGACCTGTCCATCTATA
ACCCTGAGAGGACCATCACCGTGAAGGGCACCGTCGAGGCCTGTGCCAGCGCCGAAATTGAAATCATGAAAAAGC
TGAGAGAGGCCTTCGAAAATGATATGCTGGCCGTGAACCAGCAGGCTAATCTGATCCCCGGACTCAACCTGAGCG
CCCTGGGCATCTTCAGCACCGGACTGTCCGTCCTGTCCCCCCCTGCTGGACCTAGAGGAGCTCCCCCTGCCGCTC
CCTATCACCCCTTTACCACCCACTCCGGCTACTTCTCCTCCCTGTACCCCCACCATCAGTTCGGACCCTTTCCCCA
CCATCACTCCTACCCTGAACAGGAGATCGTGAATCTGTTTATTCCCACACAGGCCGTGGGCGCCATCATCGGAAAA
AAGGGCGCCCACATTAAGCAACTGGCCAGATTCGCTGGCGCTTCCATCAAGATCGCCCCTGCTGAGGGACCCGAC
GTGAGCGAAAGGATGGTCATCATCACCGGCCCCCCCGAAGCCCAGTTCAAAGCCCAGGGCAGAATTTTCGGCAAG
CTCAAGGAGGAAAACTTCTTCAATCCTAAGGAGGAGGTGAAGCTGGAGGCCCACATTAGGGTGCCTTCCTCCACC
GCTGGAAGGGTCATCGGCAAGGGAGGAAAGACCGTCAACGAGCTGCAAAATCTGACATCCGCCGAGGTGATCGT
CCCTAGGGACCAGACCCCCGATGAGAACGAGGAAGTGATCGTCAGGATCATCGGCCACTTCTTCGCTTCCCAGAC
CGCCCAGAGGAAGATCAGGGAGATCGTGCAGCAAGTCAAGCAGCAAGAACAAAAGTATCCTCAGGGCGTCGCCTC
CCAGAGGAGCAAACTCGAG

Supplementary figure 1. DNA sequences synthesised and cloned into the lentiviral vector pELNS. Constructs were optimised for *H. sapiens*. Key: Xba I, Xho I, Kozak sequence.

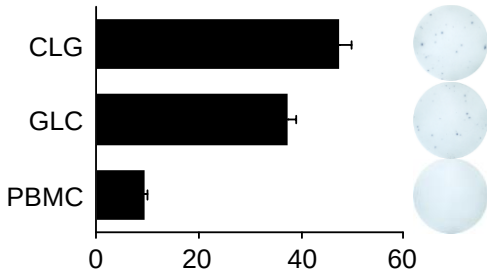

Supplementary figure 2. ***Ex vivo*** **detection of antigen-specific CD8⁺ T cells by ELISPOT.** Donor 0439 PBMC was pre-screened for T cell activation against stimulation with HLA A2-restricted EBV virus peptides. *Ex vivo* PBMC were incubated with CLGGLLTMV and GLCTLVAML peptides at 10^{-5}M overnight, followed by IFNγ ELISpot quantification. Unpulsed PBMC were used as negative control. Experiments were done in duplicate. Deviation from mean is shown. Representative ELISpot images used for quantification are shown.

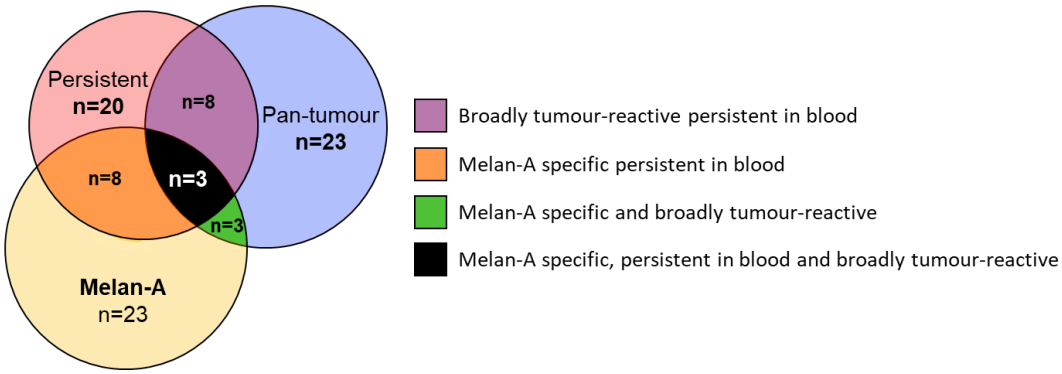

Supplementary figure 3. Summary of TCRβ clonotypes described in section 4.2.3. MM909.24 TIL were viable sorted based on reactivity (%TNF CD07α) towards autologous melanoma and other cancer cell lines from diverse tissue origins, followed by TCRβ chain sequencing. Analysis showed n=23 TCRβ chains respond to the patient autologous melanoma line and one other cancer cell line (pan tumour, (●)). 8/23 TCRβ chains were also identified in patient PBMC following complete remission (●). In Chapter 3, n=23 Melan-A specific TCRβ chains were described (Melan-A, (●)). Of these, 8/23 TCRβ chains were also identified to be persistent in blood 6 months after TIL infusion (●); more importantly, 3/23 Melan-A specific TCRβ chains were also observed to react towards other tumour cell lines (●). A total of n=3 TCRβ chains were found to be Melan-A specific, persistent in blood and broadly tumour reactive (●).

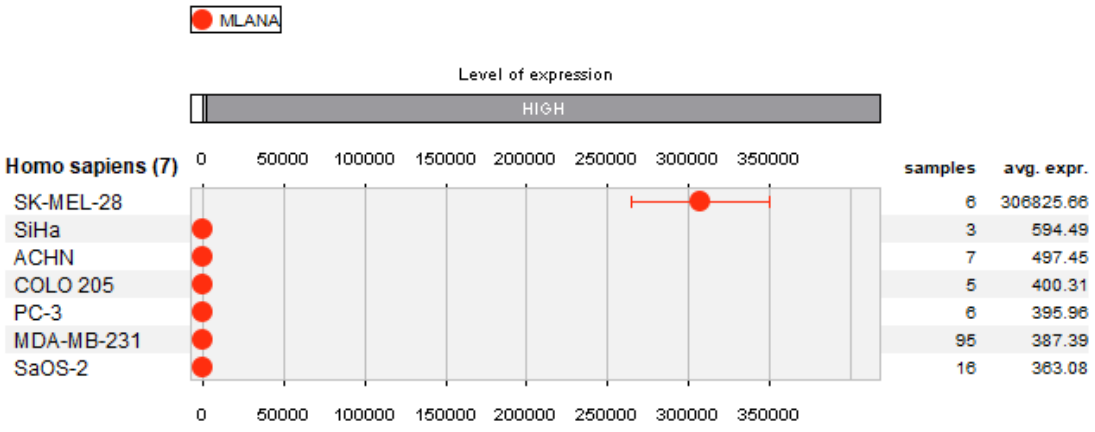

Supplementary figure 4. MLANA Gene expression pattern in tumour cell lines. Data extracted from *Genevestigtor*[366]. Gene expression encoding for Melan-A protein on the indicated commercial cell lines. Expression is based on RNAseq data from numerous public repositories. The cell line SK-MEL-28 from a melanoma origin was used as positive control for MLANA gene expression.

A. MM909.24

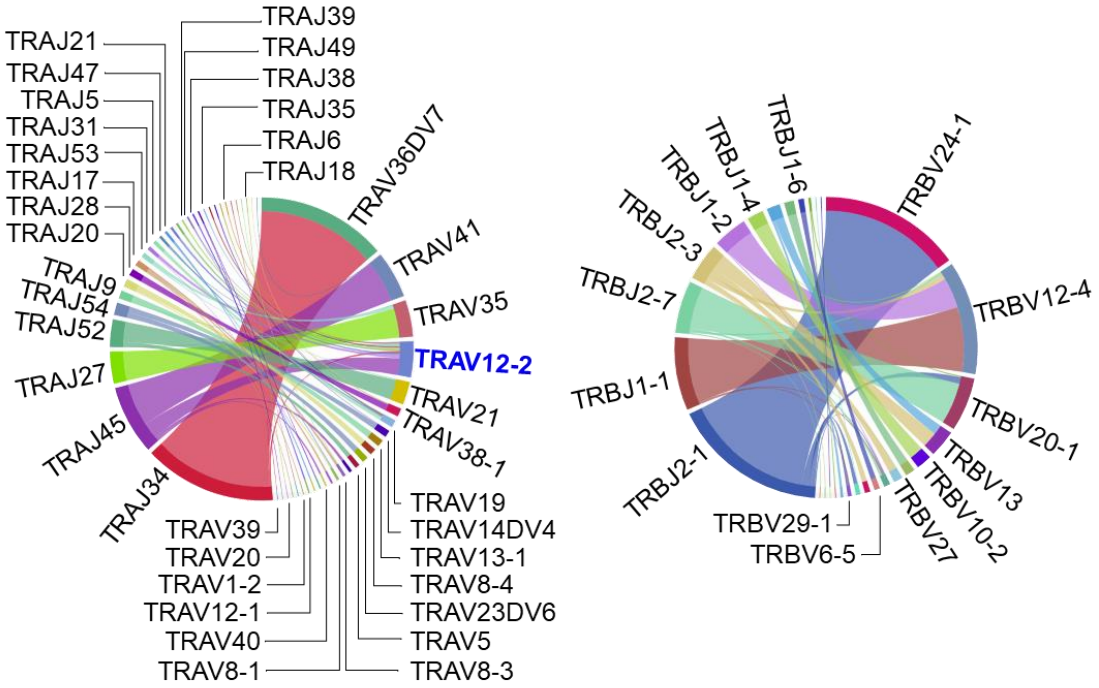

B. MDA MB 231

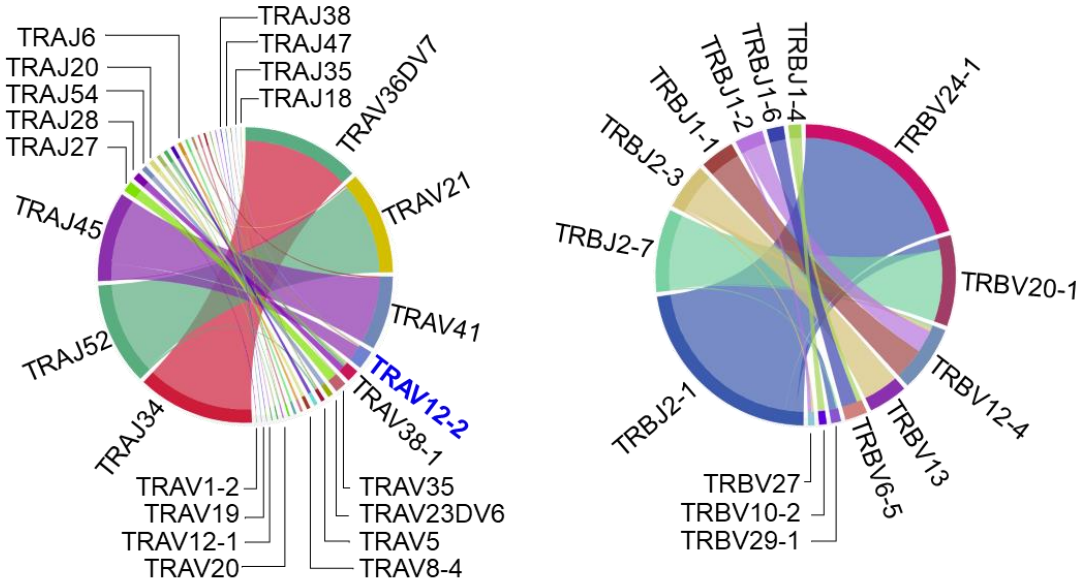

Figure continues next page

C. MCF-7

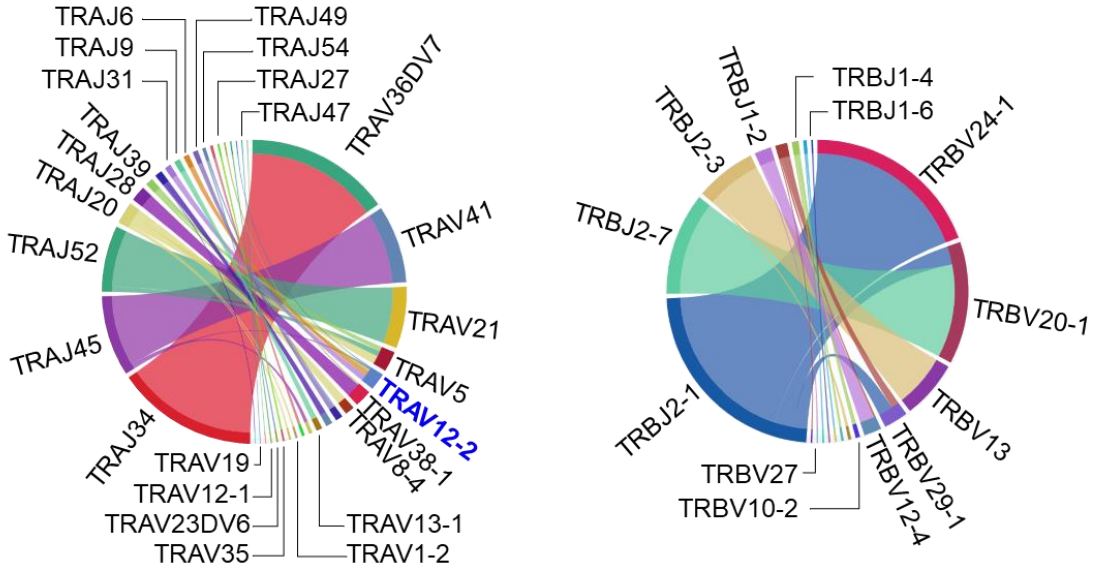

D. MS 751

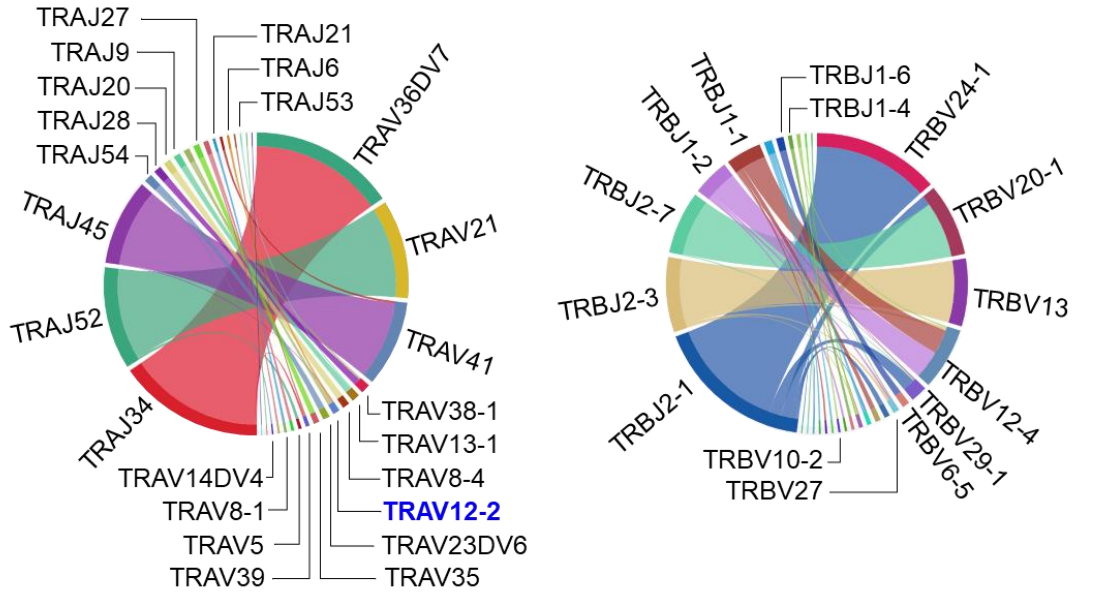

Figure continues next page

E. LnCap

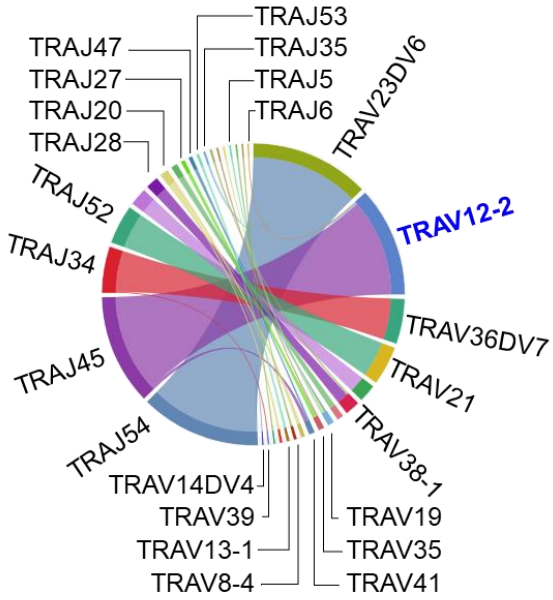

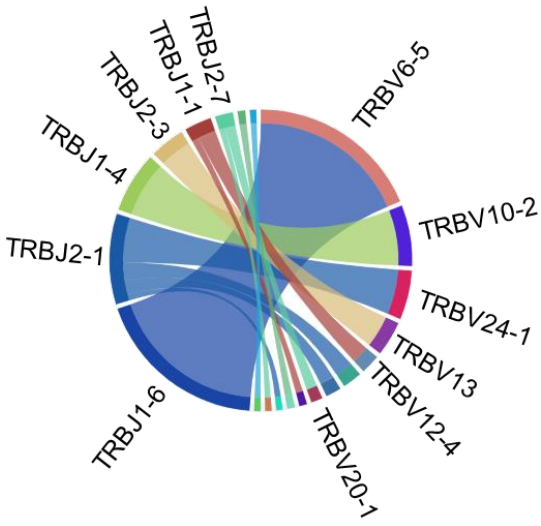

F. SaOS

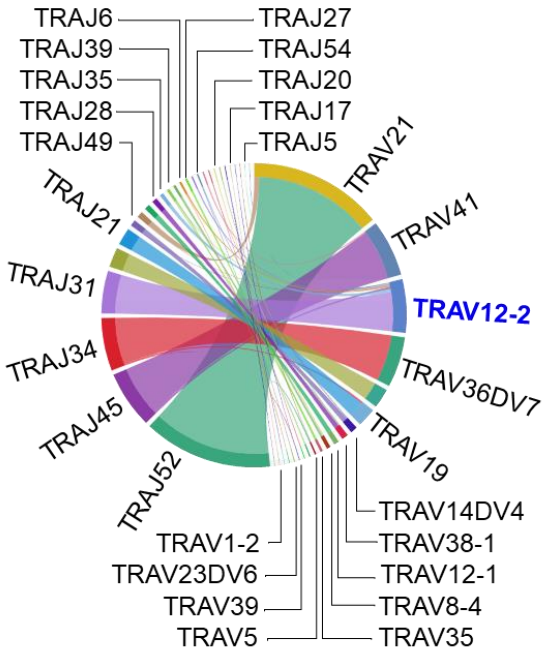

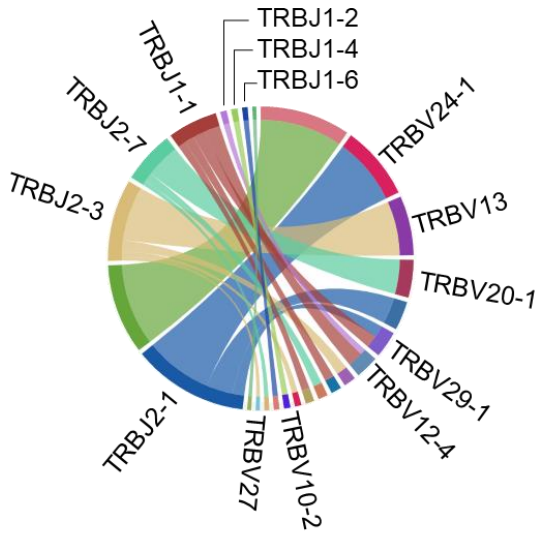

Figure continues next page

G. H69

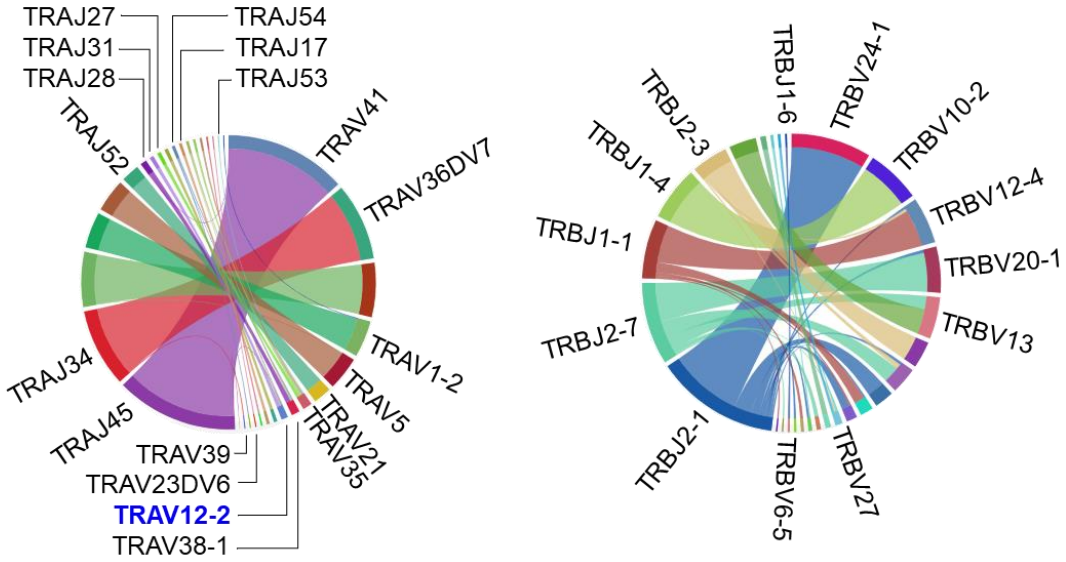

H. COLO 205

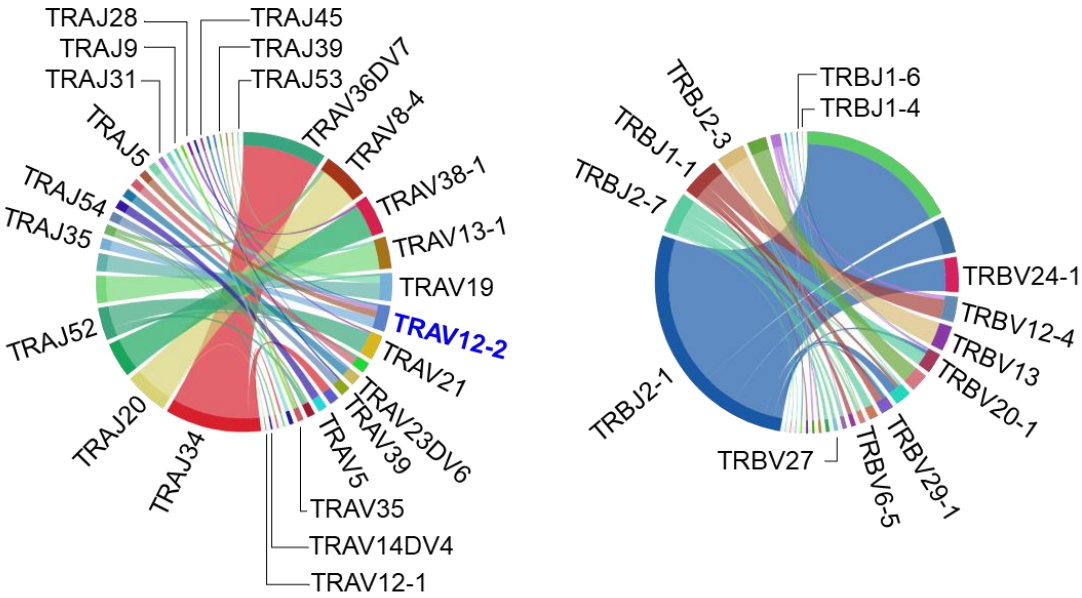

Figure continues next page

I. RCC17

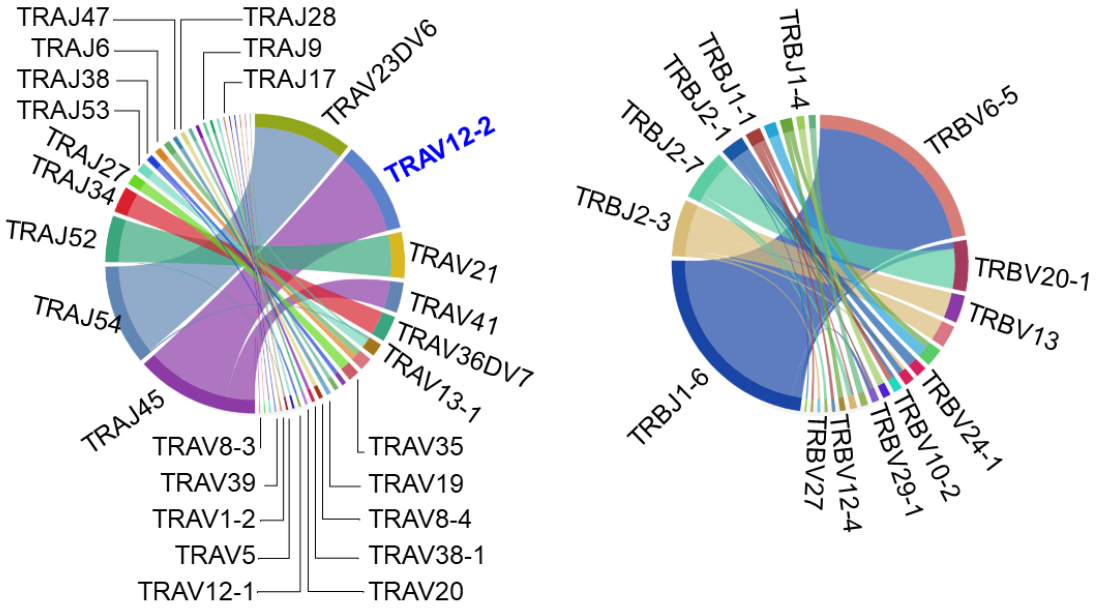

Supplementary figure 5. **Clonotypic architecture of MM909.24 tumour-reactive TILs.** Rearranged gene usages of TCRα (left) and TCRβ (right) in autologous tumour-reactive TILs **(A)** present in the non-melanoma reactive sorts MDA-MB-231 **(B)**, MCF-7 **(C)**, MS 751 **(D)**, LnCap **(E)**, SaOS **(F)**, H69 **(G)**, COLO 205 **(H)** and RCC17 **(I)**. TRAV12-2 gene usage is highlighted in **blue**.

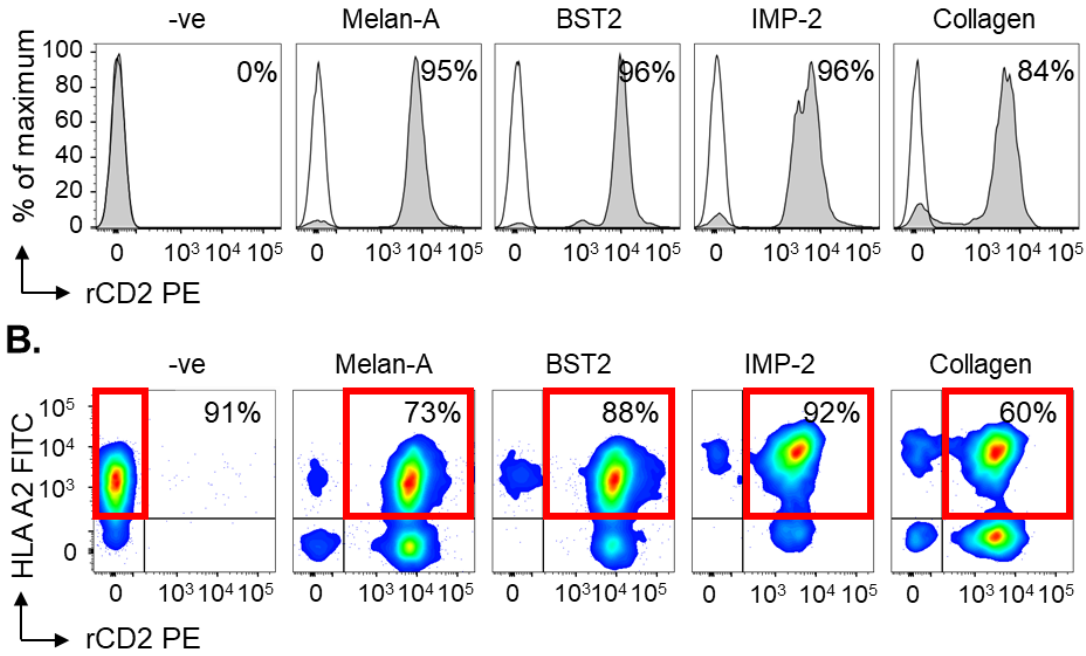

Supplementary figure 6. **Expression of transgenes in MOLT3 cell line.** Surface antibody staining of MOLT3 cells untransduced (-ve) or transduced with a construct co-expressing Melan-A, BST2, IMP-2 or collagen (as negative control) transgenes with mouse rCD2 transgene as marker **(A)** and a construct containing the HLA A2 transgene **(B)**. % of fluorescent cells is indicated at the top right of the panel. Cells were gated on exclusion of dead (Vivid$^+$) cells.

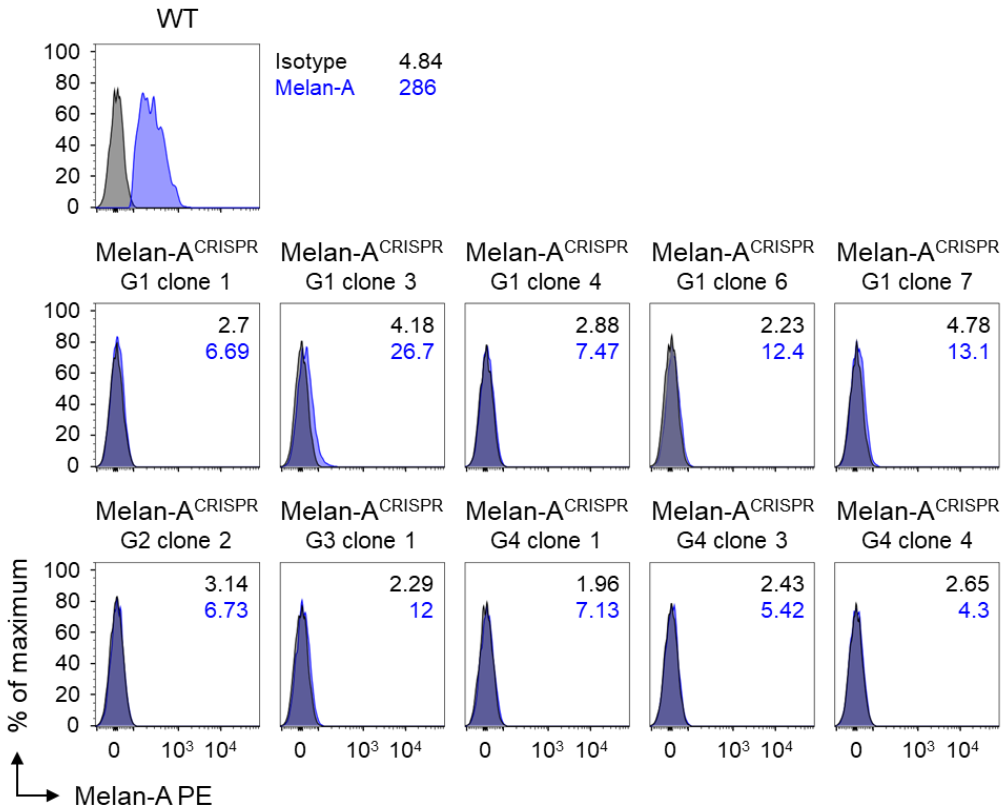

Supplementary figure 7. **Antibody staining of MM909.24 Melan-A^{CRISPR} clones.** Intracellular antibody staining using rabbit anti-Melan-A primary antibody and anti-rabbit PE secondary antibody, of MM909.24 clones after Melan-A abrogation using CRISPR/Cas9 technology. Melan-A-deficient clones were pulled together into the "MM909.24 Melan-A^{CRISPR} cell line" described in the main text for experimentation. Melan-A^{CRISPR} G1 clone 3 was not included in the pull.

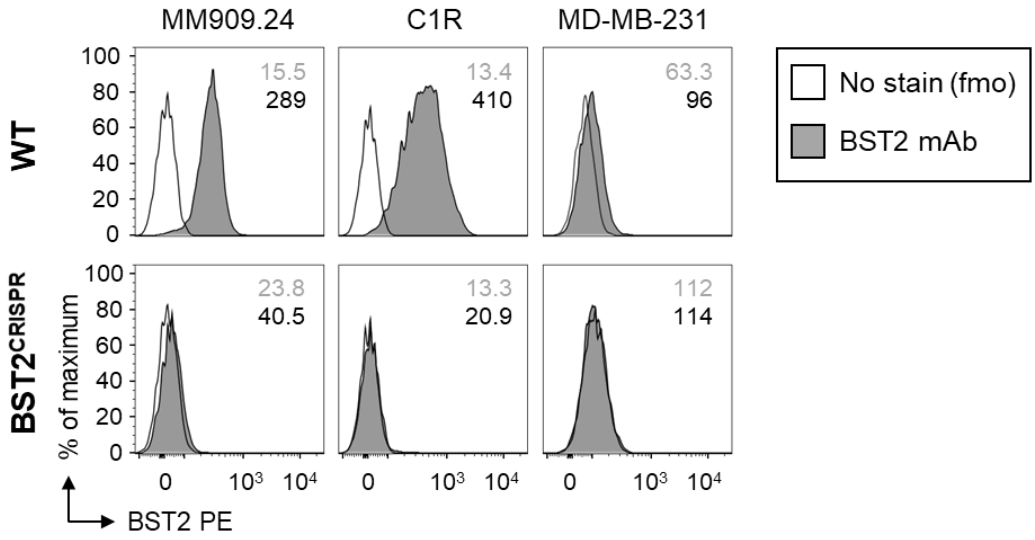

Supplementary figure 8. CRISPR/Cas9 abrogation of BST2 in cancer cell lines. Surface antibody staining of wild type (WT) MM909.24, C1R and MDA-MB-231 cell lines and electroporated with the Neon® transfection system for CRISPR/Cas9-mediated abrogation of BST2 expression (BST2^{CRISPR}) following the parameters shown in Table 2-15. BST2^{CRISPR} cell lines were viably sorted on Aria based on negative expression of BST2 and grown as a line.

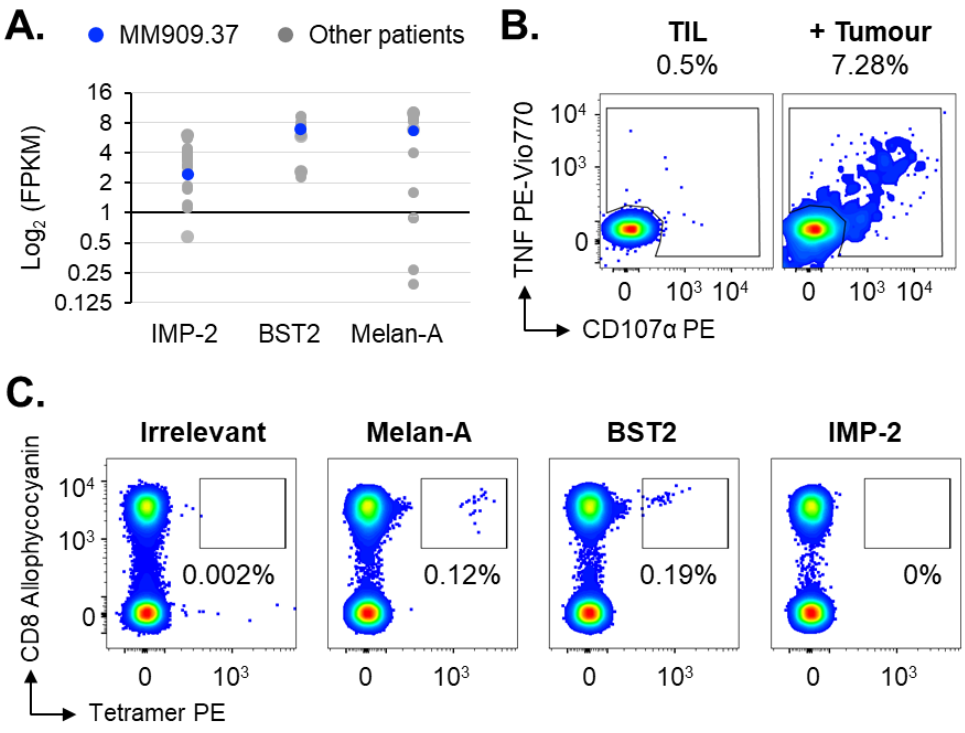

Supplementary figure 9. Patient's MM909.37 TIL infusion product exhibits Melan-A and BST2 T cell responses. **(A)** Normalised and log_2 transformed gene transcript levels of IMP-2, BST2 and Melan-A genes expressed in FPKM units (Fragments per kilobase of exon per million reads mapped) in other malignant melanoma patient samples. Melan-A^{high} BST2^{high} IMP-2^{low} expressing tumour from patient MM909.37 is shown in blue. Data was collected and processed by *Thomas Walley*. **(B)** TAPI staining of the original TIL infusion product following 4h co-incubation with autologous tumour. Gates were set on single lymphocytes and live CD3$^+$ CD8$^+$ CD14^{neg} CD19^{neg} cells. % of TNF and CD107a is displayed. **(C)** TIL infusion product from patient MM909.37 was stained with HLA A2-Melan-A$_{26-35}$ (EAAGIGILTV), BST2$_{22-31}$ (LLLGIGILVL) and IMP-2$_{367-376}$ (NLSALGIFST) tetramers. Gates were set on single lymphocytes and live CD3$^+$CD14^{neg}CD19^{neg} cells. The percentage of CD8$^+$Tet$^+$ T cells is shown for each gate. Irrelevant tetramer made with human telomerase reverse transcriptase (hTERT$_{540–548}$, ILAKFLHWL) was used to set the gates.

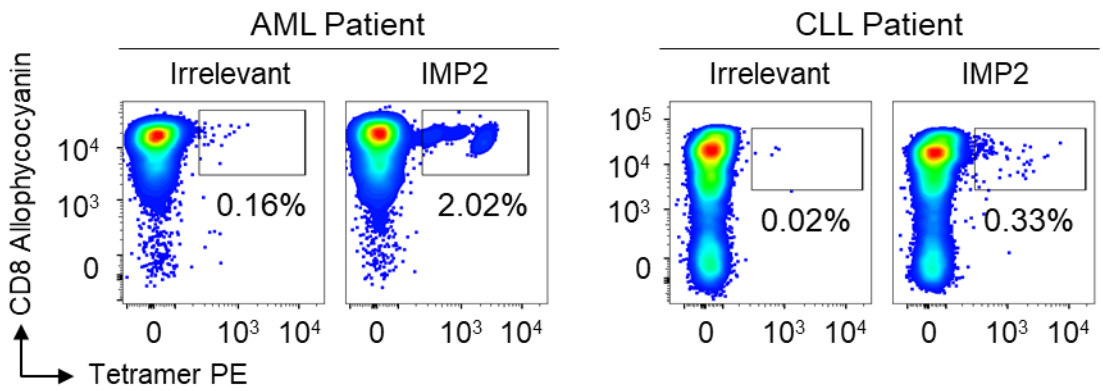

Supplementary figure 10. Acute Myeloid Leukemia (AML) and Chronic Lymphocytic Leukemia (CLL) patients exhibit IMP-2 T cell responses. (A) PBMC extracted from patients suffering from AML or CLL was stained with HLA A2-IMP-$2_{367-376}$ (NLSALGIFST) tetramer. Gates were set on single lymphocytes and live $CD3^{+}CD14^{neg}$ $CD19^{neg}$ cells. The percentage of $CD8^{+}Tet^{+}$ T cells is shown for each gate. Irrelevant tetramer made with human telomerase reverse transcriptase ($hTERT_{540–548}$, ILAKFLHWL) was used to set the gates. *Data courtesy of Sarah Galloway*.

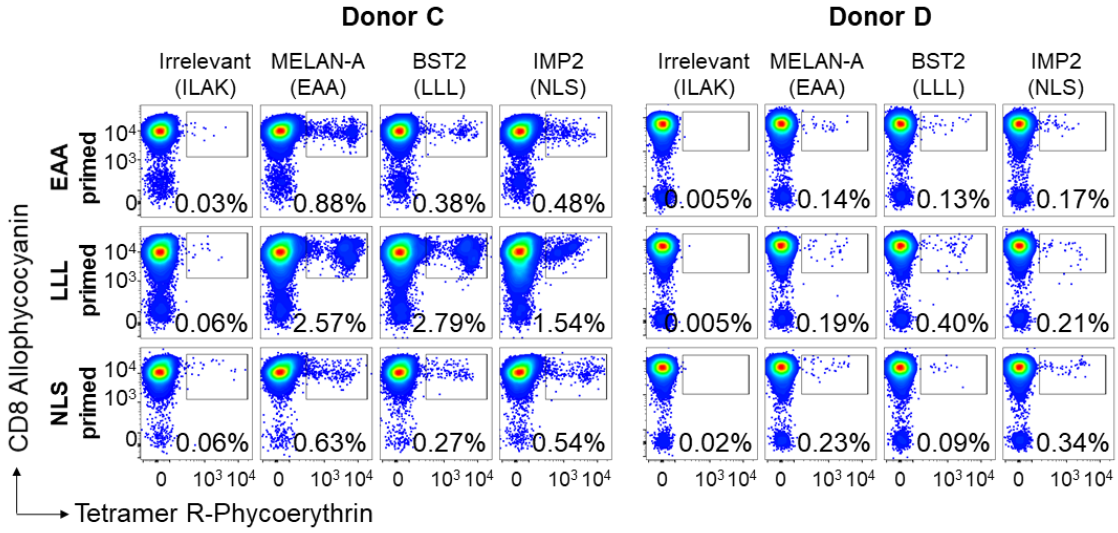

Supplementary figure 11. Priming of healthy HLA-A2 PBMC with peptide results in increased numbers of Melan-A, BST2 and IMP-2 $tetramer^{+}$ cells. CD8+ T cells from two donors were primed with HLA-A2-restricted Melan-A_{26-35} (EAAGIGILTV), $BST2_{22-31}$ (LLLGIGILVL) or IMP-$2_{367-376}$ (NLSALGIFST) peptides, followed by tetramer staining with each epitope after 2 weeks in culture. Irrelevant tetramer made with $hTERT_{540–548}$ was used to set the gates. Gates were set on single lymphocytes and live $CD3^{+}CD14^{neg}CD19^{neg}$ cells. The percentage of $CD8^{+}Tet^{+}$ T cells is shown for each gate.

– Annexe 2 – Supplementary Tables

Supplementary table 1. RNAseq TCRβ sequences from HLA A2-Melan-A tetramer⁺ sorted TILs from patient MM909.24. Shared TCRβ sequences between sorts are displayed in grey. Unique TCRβ sequences to sort are displayed in blue. The described GLG motif is underlined.

Sample	Frequency (%)	CDR3β	V gene	J gene
Standard	66.67	CASSFAGTDTQYF	TRBV27	TRBJ2-3
	12.96	CAWSQMGLGTEAFF	TRBV30	TRBJ1-1
	9.26	CASSYSFTEATYEQYF	TRBV6-5	TRBJ2-7
	5.56	CASSYVGLGSPLHF	TRBV6-3	TRBJ1-6
	5.56	CASSWAGPVEQYF	TRBV12-4	TRBJ2-7
Optimised	63.66	CASSFAGTDTQYF	TRBV27	TRBJ2-3
	4.45	CASSLQGLGRNAFF	TRBV28	TRBJ1-1
	3.83	CAWSQMGLGTEAFF	TRBV30	TRBJ1-1
	3.00	CASSLTGLGQPQHF	TRBV28	TRBJ1-5
	2.90	CATSDRGQGANWDEQFF	TRBV24-1	TRBJ2-1
	2.59	CASSWAGPVEQYF	TRBV12-4	TRBJ2-7
	2.48	CSVEGSLGRALRANEQFF	TRBV29-1	TRBJ2-1
	2.17	CSEGSPYNEQFF	TRBV20-1	TRBJ2-1
	1.86	CASSRGAFYNEQFF	TRBV28	TRBJ2-1
	1.66	CASSLGLAGNEQYF	TRBV27	TRBJ2-7
	1.14	CASSYSFTEATYEQYF	TRBV6-5	TRBJ2-7
	1.14	CASSQEPNWNTEAFF	TRBV4-1	TRBJ1-1
	1.14	CASSPAGLGQPQHF	TRBV6-3	TRBJ1-5
	1.14	CASSNGFHFNTLYF	TRBV27	TRBJ2-3
	1.14	CASSLHPTYQPQHF	TRBV7-6	TRBJ1-5
	1.04	CASSQASPGDEQFF	TRBV4-2	TRBJ2-1
	0.72	CAWSSQGLGQPQHF	TRBV30	TRBJ1-5
	0.72	CASSFVLAGGGYF	TRBV28	TRBJ2-7
	0.72	CSNQPQHF	TRBV15	TRBJ1-5
	0.62	CAWKGLGYSYEQYF	TRBV30	TRBJ2-7
	0.62	CASSTGQGFTEAFF	TRBV6-1	TRBJ1-1
	0.62	CSAPQTGLGQPQHF	TRBV20-1	TRBJ1-5
	0.62	CASTLGGGTEAFF	TRBV12-4	TRBJ1-1

Supplementary table 2. Persistent TCRβ sequences in blood post-treatment from tumour-reactive TILs in patient MM909.24. *Data courtesy of Dr. Attaf.*

CDR3β	TIL	PBMC
CSARDLLAETYEQYF	28.670%	8.897%
CASSNTGGYTQYF	8.129%	1.059%
CASSQGGQPKRSGNTIYF	7.450%	0.371%
CASSDTYYGYTF	4.540%	0.019%
CSAREDGGQTYEQYF	3.365%	0.817%
CASNQFRQGIRSYEQYF	1.267%	1.207%
CSARDLLAETYEQYF	1.026%	8.897%
CASSLGEGSPGELFF	0.455%	0.019%
CATSDRGQGANWDEQFF	0.343%	7.262%
CASSNGFHFNTLYF	0.115%	22.381%
CASSLAGYEQYF	0.061%	0.223%
CASTLGGGTEAFF	0.044%	14.302%
CASTPGSLYYGYTF	0.041%	0.186%
CASSLHHEQYF	0.034%	0.149%
CASSEARGLAEFTDTQYF	0.027%	0.093%
CATSDRGLNTGELFF	0.017%	1.263%
CASSAGGALTGELFF	0.017%	0.056%
CASSPTTGLKTRSGYTF	0.010%	3.826%
CASSYSFTEATYEQYF	0.003%	0.093%
CSARDLLAETYEQYF	0.003%	8.897%

Supplementary table 3. TCRβ sequences from RNAseq of HLA A2-IMP-2 tetramer⁺ sorted PBMC from donor 0439. Shared TCRβ sequences between sorts are displayed in grey. Unique TCRβ sequences to sort are displayed in blue.

Sample	Frequency (%)	V segment	J segment	CDR3β
Standard	36.70	TRBV7-2	TRBJ1-5	CASSPETGIGGQPQHF
	20.79	TRBV20-1	TRBJ2-7	CSARQGQGFLYEQYF
	12.12	TRBV27	TRBJ2-2	CASSFEGNTGELFF
	10.26	TRBV4-1	TRBJ1-2	CASSQVGQAIYGYTF
	5.46	TRBV7-9	TRBJ2-7	CASSTLRYEQYF
	3.76	TRBV4-1	TRBJ2-1	CASSPLVGSYNEQFF
	3.02	TRBV20-1	TRBJ2-4	CRAGGLAGALSYF
	2.59	TRBV5-1	TRBJ2-7	CASSFEGLSYEQYF
	1.90	TRBV4-1	TRBJ2-1	CASSPLGGSYNEQFF
	1.43	TRBV13	TRBJ2-1	CASSSLRRGDNEQFF
	0.89	TRBV20-1	TRBJ2-4	CSAGGLAGALSYF
	0.66	TRBV7-2	TRBJ2-1	CASSLASVTFAAEQFF
	0.43	TRBV3-1	TRBJ1-6	CASSQAPPVITGSPLHF
Optimised	14.57	TRBV29-1	TRBJ2-7	CSVEDRGVSYEQYF
	14.16	TRBV7-2	TRBJ1-5	CASSPETGIGGQPQHF
	8.28	TRBV12-5	TRBJ1-1	CASGLDIHAFF
	7.37	TRBV18	TRBJ2-1	CASSPLDNWEQFF
	6.82	TRBV7-9	TRBJ2-7	CASSLEVTYEQYF
	6.50	TRBV7-9	TRBJ1-3	CASSLAGEGGNTIYF
	6.32	TRBV20-1	TRBJ2-7	CSARQGQGFLYEQYF
	6.24	TRBV27	TRBJ1-2	CASSEGQNYGYTF
	3.70	TRBV27	TRBJ1-2	CASSLGGSYGYTF
	3.67	TRBV20-1	TRBJ2-2	CSARYDTGELFF
	3.47	TRBV27	TRBJ2-2	CASSFEGNTGELFF
	3.44	TRBV4-1	TRBJ1-2	CASSQVGQAIYGYTF
	2.83	TRBV3-1	TRBJ1-1	CASSPTGTEAFF
	2.13	TRBV7-9	TRBJ2-7	CASSTLRYEQYF
	1.72	TRBV4-1	TRBJ2-1	CASSPLVGSYNEQFF
	1.17	TRBV7-9	TRBJ1-2	CASSLAGGYGYTF
	1.11	TRBV3-1	TRBJ1-1	CASSIAEQIGEAFF
	1.02	TRBV20-1	TRBJ2-4	CSAGGLAGALSYF
	0.79	TRBV24-1	TRBJ2-1	CATQTSGGFNEQFF
	0.73	TRBV5-1	TRBJ2-7	CASSFEGLSYEQYF
	0.70	TRBV7-6	TRBJ2-7	CASSFSDFGNEQYF
	0.55	TRBV6-1	TRBJ2-7	CASETGRRFYEQYF
	0.55	TRBV19	TRBJ1-2	CASIPGQGNGYTF
	0.44	TRBV27	TRBJ2-2	CASSPGQGMAGELFF
	0.41	TRBV5-6	TRBJ1-2	CASTLEGSSGYGYTF
	0.29	TRBV20-1	TRBJ2-7	CSAEREISYEQYF
	0.26	TRBV7-2	TRBJ2-1	CASSLASVTFAAEQFF
	0.26	TRBV4-1	TRBJ2-1	CASSQPSGAVNNEQFF
	0.17	TRBV7-8	TRBJ1-6	CASSLGGGLYNSPLHF
	0.17	TRBV13	TRBJ2-1	CASSSLRRGDNEQFF
	0.17	TRBV15	TRBJ1-1	CATSSYGGSGLGTEAFF

Supplementary table 4. TCRβ sequences from RNAseq of HLA A2-BMLF1 tetramer+ sorted PBMC from donor 4. Shared TCRβ sequences between sorts are displayed in grey. Unique TCRβ sequences to sort are displayed in blue.

Sample	Frequency (%)	CDR3β	V gene	J gene
Standard	99.96	CSVGTGGTNEKLFF	TRBV29-1	TRBJ1-4
	0.04	CASTKTREKLYF	TRBV27	TRBJ2-7
Optimised	99.92	CSVGTGGTNEKLFF	TRBV29-1	TRBJ1-4
	0.08	CASTKTREKLYF	TRBV27	TRBJ2-7

Supplementary table 5. TCRβ sequences from RNAseq of HLA A2-LMP2A tetramer+ sorted PBMC from donor 5. Shared TCRβ sequences between sorts are displayed in grey. Unique TCRβ sequences to sort are displayed in blue.

Sample	Frequency (%)	CDR3β	V gene	J gene
Standard	99.46	CASSEDGMNTEAFF	TRBV10-2	TRBJ1-1
	0.23	CSATGLAGLGEQFF	TRBV20-1	TRBJ2-1
	0.15	CASSGTGGKTQYF	TRBV7-2	TRBJ2-5
	0.10	CASSPVGGSSGNTIYF	TRBV28	TRBJ1-3
	0.07	CASNPFGAGVSDTQYF	TRBV28	TRBJ2-3
Optimised	36.50	CASSGTGGKTQYF	TRBV7-2	TRBJ2-5
	26.24	CASSPVGGSSGNTIYF	TRBV28	TRBJ1-3
	24.44	CASSEDGMNTEAFF	TRBV10-2	TRBJ1-1
	12.83	CASNPFGAGVSDTQYF	TRBV28	TRBJ2-3

Supplementary table 6. TCRβ sequences from RNAseq of HLA A2- BMLF1 tetramer+ sorted PBMC from donor 3205. Shared TCRβ sequences between sorts are displayed in grey. Unique TCRβ sequences to sort are displayed in blue.

Sample	Frequency (%)	CDR3β	V gene	J gene
Standard	56.10	CASSLMGGPNYGYTF	TRBV7-2	TRBJ1-2
	43.90	CASSLVNTGELFF	TRBV11-3	TRBJ2-2
Optimised	65.64	CSVGGYGTNEKLFF	TRBV29-1	TRBJ1-4
	18.12	CASSPGQVLPGEQYF	TRBV2	TRBJ2-7
	3.34	CSVGTGGTNEKLFF	TRBV29-1	TRBJ1-4
	3.28	CASSEDAGLGAYGYTF	TRBV2	TRBJ1-2
	2.47	CSVGTYGTNEKLFF	TRBV29-1	TRBJ1-4
	2.18	CSARDSAIGANPERNYGYTF	TRBV20-1	TRBJ1-2
	1.65	CSARDRVGNGYTF	TRBV20-1	TRBJ1-2
	0.85	CASSDPGILPGPQHF	TRBV2	TRBJ1-5
	0.59	CSARDRVGNTIYF	TRBV20-1	TRBJ1-3
	0.44	CASSPGTAEKLFF	TRBV10-2	TRBJ1-4
	0.38	CASSQSPGGVEFF	TRBV14	TRBJ2-1
	0.33	CSARDRVGNGYTF	TRBV20-1	TRBJ1-2
	0.32	CSVNRGFYGYTF	TRBV29-1	TRBJ1-2
	0.26	CSATKSGTGELGGYTF	TRBV20-1	TRBJ1-2
	0.11	CAIEGGQSYEQYF	TRBV10-3	TRBJ2-7
	0.02	CASSSWDKNTEVFF	TRBV15	TRBJ1-1
	0.02	CASSVGELAGGLDTQYF	TRBV9	TRBJ2-3

Supplementary table 7. TCRβ sequences from RNAseq of HLA A2- BMLF1 tetramer+ sorted PBMC from donor 0439. Shared TCRβ sequences between sorts are displayed in grey. Unique TCRβ sequences to sort are displayed in blue.

Sample	Frequency (%)	CDR3β	V gene	J gene
Standard	29.04	CASTFKESIVNTEAFF	TRBV7-9	TRBJ1-1
	19.81	CSASGYSNQPQHF	TRBV20-1	TRBJ1-5
	13.73	CASSWAAPGEQFF	TRBV19	TRBJ2-1
	12.85	CASSPGTGGNSPLHF	TRBV5-1	TRBJ1-6
	6.49	CASSSQGQGHVNTEAFF	TRBV7-9	TRBJ1-1
	6.46	CASSLKQSGHYQETQYF	TRBV12-4	TRBJ2-5
	5.62	CASSLASGNSYEQYF	TRBV11-2	TRBJ2-7
	2.30	CASSLHRAEAFF	TRBV5-4	TRBJ1-1
	2.10	CASSPGTVATGELFF	TRBV5-1	TRBJ2-2
	0.94	CASSDYLAPTDTQYF	TRBV2	TRBJ2-3
	0.65	CASSGGGGHYGYTF	TRBV9	TRBJ1-2
Optimised	3.73	CASRGSGEKLFF	TRBV6-6	TRBJ1-4
	2.95	CASSVQGSGTYGYTF	TRBV9	TRBJ1-2
	2.69	CASSYSSTEAFF	TRBV6-5	TRBJ1-1
	2.49	CASSLLGQAYGYTF	TRBV28	TRBJ1-2
	2.17	CASSRQGDEKLFF	TRBV6-6	TRBJ1-4
	2.07	CSVEAGGNQPQHF	TRBV29-1	TRBJ1-5
	2.04	CSVLWTEAFF	TRBV29-1	TRBJ1-1
	2.01	CASSLARGGTEAFF	TRBV5-1	TRBJ1-1
	1.97	CASTYGTQYSYGYTF	TRBV3-1	TRBJ1-2
	1.91	CAIMSTSYTEAFF	TRBV10-3	TRBJ1-1
	1.87	CASSFQGGRIGQPQHF	TRBV12-3	TRBJ1-5
	1.84	CASSWGQGSYEQYF	TRBV27	TRBJ2-7
	1.62	CASSLSYGGLLDTEAFF	TRBV5-1	TRBJ1-1
	1.53	CASSSHTGGFGYTF	TRBV7-9	TRBJ1-2
	1.53	CASSSQRNTEAFF	TRBV7-3	TRBJ1-1
	1.52	CASRMDIFRMGNTIYF	TRBV6-1	TRBJ1-3
	1.46	CASSLEPLSGNTIYF	TRBV5-5	TRBJ1-3
	1.44	CASSRGQESPYYGYTF	TRBV5-1	TRBJ1-2
	1.44	CSARGDLRENSPLHF	TRBV20-1	TRBJ1-6
	1.43	CASSSDINYGYTF	TRBV7-8	TRBJ1-2
	1.42	CASSQLTATNYGYTF	TRBV4-1	TRBJ1-2
	1.42	CASSGGIGYGYTF	TRBV7-6	TRBJ1-2
	1.41	CASSLEVGNQPQHF	TRBV5-1	TRBJ1-5
	1.37	CASSQVRGTEAFF	TRBV11-2	TRBJ1-1
	1.35	CASSRDKNYGYTF	TRBV6-5	TRBJ1-2
	1.26	CASSFGRAGNQPQHF	TRBV27	TRBJ1-5
	1.22	CASSVDRNSPLHF	TRBV9	TRBJ1-6
	1.22	CASSQGRLGRYF	TRBV3-1	TRBJ1-3
	1.18	CASSFGSGNTIYF	TRBV12-3	TRBJ1-3
	1.15	CASSPRGRTEAFF	TRBV7-8	TRBJ1-1
	1.15	CSAKRGNTEAFF	TRBV20-1	TRBJ1-1
	1.15	CASSWVNTEAFF	TRBV7-2	TRBJ1-1
	1.09	CASYTGTGGNTIYF	TRBV12-4	TRBJ1-3
	1.09	CASSPTGTEAFF	TRBV3-1	TRBJ1-1
	1.08	CASSENRGKGTEAFF	TRBV7-9	TRBJ1-1

	1.04	CASSPNPGGLNGYTF	TRBV3-1	TRBJ1-2
	1.04	CSARQPGGVDTEAFF	TRBV20-1	TRBJ1-1
	1.03	CSARTLDGYTF	TRBV20-1	TRBJ1-2
	1.03	CSVDRGLNTEAFF	TRBV29-1	TRBJ1-1
	1.01	CASRGFSDQPQHF	TRBV12-3	TRBJ1-5
	0.99	CASSLHGRNYEQYF	TRBV5-4	TRBJ2-7
	0.99	CASSSLNTEAFF	TRBV27	TRBJ1-1
	0.97	CSARETGTRFYEQYF	TRBV20-1	TRBJ2-7
	0.90	CASSQDTRRQPQHF	TRBV3-1	TRBJ1-5
	0.90	CASSVEGETQYF	TRBV9	TRBJ2-5
	0.87	CASSLESGEKLFF	TRBV5-1	TRBJ1-4
	0.86	CASSLEAADNYGYTF	TRBV5-5	TRBJ1-2
	0.86	CASSGGPPAREQYF	TRBV5-5	TRBJ2-7
	0.85	CASSPGPGETQYF	TRBV7-2	TRBJ2-5
	0.82	CASSLKQAGGAKNIQYF	TRBV7-9	TRBJ2-4
	0.81	CASSLAGQGDNYEQYF	TRBV5-1	TRBJ2-7
	0.80	CASSLDGTPFYEQYF	TRBV5-1	TRBJ2-7
	0.80	CASSLGRGYEQYF	TRBV5-1	TRBJ2-7
	0.78	CASSEYVRGGNTIYF	TRBV25-1	TRBJ1-3
	0.78	CASSWGTPSYEQYF	TRBV5-1	TRBJ2-7
	0.77	CASSLLGISADTQYF	TRBV5-1	TRBJ2-3
	0.75	CATSNNVGQTQYF	TRBV15	TRBJ2-3
	0.68	CASSLRDRRTTDTQYF	TRBV5-1	TRBJ2-3
	0.66	CASSSGQPNTGELFF	TRBV5-1	TRBJ2-2
	0.66	CASSRQGLETQYF	TRBV11-2	TRBJ2-5
Optimised	0.66	CASSLARSGGTDTQYF	TRBV7-9	TRBJ2-3
	0.66	CASSQGSLNTEAFF	TRBV4-1	TRBJ1-1
	0.65	CASSSGVYYGYTF	TRBV11-2	TRBJ1-2
	0.64	CASSLAGAGLPEAFF	TRBV7-8	TRBJ1-1
	0.63	CASSLAGDTGELFF	TRBV5-5	TRBJ2-2
	0.62	CASSSRDGYQNTEAFF	TRBV12-3	TRBJ1-1
	0.61	CASSAPPGTQYF	TRBV7-2	TRBJ2-3
	0.59	CASSLAGQGALSRQYF	TRBV12-4	TRBJ2-7
	0.59	CASGLGTSYNEQFF	TRBV5-1	TRBJ2-1
	0.58	CSARDQSLAKNIQYF	TRBV20-1	TRBJ2-4
	0.57	CASSEGSTWDSYGYTF	TRBV6-1	TRBJ1-2
	0.57	CASSLYSRAAGQPQHF	TRBV5-6	TRBJ1-5
	0.56	CASSREWNTEAFF	TRBV5-1	TRBJ1-1
	0.54	CATSDRQSRSGELFF	TRBV24-1	TRBJ2-2
	0.51	CSVKWGAGELFF	TRBV29-1	TRBJ2-2
	0.49	CASSQGLSGGLSYNEQFF	TRBV3-1	TRBJ2-1
	0.48	CASSQDGGSSYNEQFF	TRBV4-2	TRBJ2-1
	0.47	CSASLAGGPFQETQYF	TRBV20-1	TRBJ2-5
	0.46	CSARYQAGTETQYF	TRBV20-1	TRBJ2-5
	0.43	CSARPGGGSQSYEQYF	TRBV20-1	TRBJ2-7
	0.42	CASSANKVSGGPDNEQFF	TRBV9	TRBJ2-1
	0.42	CASSLVGTEAFF	TRBV7-9	TRBJ1-1
	0.42	CASSLAGAPSGEQYF	TRBV5-1	TRBJ2-7
	0.42	CASSYGAGEDTQYF	TRBV6-5	TRBJ2-3
	0.41	CASSLAWGRDYTEAFF	TRBV5-1	TRBJ1-1

	0.41	CASSSIRGQGYEQYF	TRBV7-9	TRBJ2-7
	0.39	CASSFEASVSTDTQYF	TRBV11-2	TRBJ2-3
	0.39	CASSEGPYTGELFF	TRBV6-1	TRBJ2-2
	0.35	CASASGANTGELFF	TRBV5-5	TRBJ2-2
	0.33	CSATDRVTGNTEAFF	TRBV20-1	TRBJ1-1
	0.32	CASTTGTGGGEQYF	TRBV12-4	TRBJ2-7
	0.31	CASSQGFGNTEAFF	TRBV19	TRBJ1-1
	0.28	CASCQVRGTEAFF	TRBV11-2	TRBJ1-1
	0.27	CSVPSGGANTGELFF	TRBV29-1	TRBJ2-2
	0.24	CASSPSHGLNTGELFF	TRBV7-9	TRBJ2-2
	0.24	CASSQSGAGGPYEQYF	TRBV16	TRBJ2-7
	0.24	CASSPSWDLQETQYF	TRBV4-1	TRBJ2-5
	0.23	CASSLVGVPNYGYTF	TRBV5-6	TRBJ1-2
	0.22	CASSDGAGTWDTQYF	TRBV6-1	TRBJ2-3
	0.20	CARRSWGASEQFF	TRBV27	TRBJ2-1
	0.19	CASSQTGGTEAFF	TRBV12-3	TRBJ1-1
	0.19	CASSSRDSYEQYF	TRBV7-9	TRBJ2-7
	0.18	CASSFLAENNEQFF	TRBV27	TRBJ2-1
Optimised	0.18	CASSLRNTEAFF	TRBV12-3	TRBJ1-1
	0.18	CASSLGGAEAFF	TRBV5-4	TRBJ1-1
	0.13	CSAPRTGRLDTEAFF	TRBV20-1	TRBJ1-1
	0.13	CASTSGTGTGELFF	TRBV5-1	TRBJ2-2
	0.13	CASSPNGVETQYF	TRBV6-1	TRBJ2-5
	0.11	CASSQMSGGAYNEQFF	TRBV14	TRBJ2-1
	0.11	CAISDGQGPYEQYF	TRBV10-3	TRBJ2-7
	0.10	CASSTGTSGGTDTQYF	TRBV5-1	TRBJ2-3
	0.10	CASSYGDSYEQYF	TRBV7-9	TRBJ2-7
	0.09	CASSQGSLNTEAFF	TRBV4-1	TRBJ1-1
	0.08	CASSALPAGGITGELFF	TRBV19	TRBJ2-2
	0.06	CASSPSPSLRGKVTYNEQFF	TRBV7-8	TRBJ2-1
	0.06	CASSLGSHTEAFF	TRBV5-5	TRBJ1-1
	0.06	CASSYSVPALGNTIYF	TRBV6-2	TRBJ1-3
	0.06	CASSTGQGASNEKLFF	TRBV7-9	TRBJ1-4
	0.05	CASTFKESIVNTEAFF	TRBV7-9	TRBJ1-1
	0.05	CASSPLDNWEQFF	TRBV18	TRBJ2-1

Supplementary table 8. TCRα sequences from RNAseq of HLA A2-NS4B tetramer⁺ sorted PBMC from donor 0345. Shared TCRβ sequences between sorts are displayed in grey. Unique TCRβ sequences to sort are displayed in blue.

Sample	Frequency (%)	CDR3β	V gene	J gene
Standard	51.44	CALSPSGNTGKLIF	TRAV16	TRAJ37
	17.81	CAVGGGKLIF	TRAV12-2	TRAJ23
	14.26	CAVSNYQLIW	TRAV12-2	TRAJ33
	6.27	CVASGTYKYIF	TRAV12-2	TRAJ40
	2.97	CAVGNDKIIF	TRAV12-2	TRAJ30
	2.64	CAENSGGYQKVTF	TRAV13-2	TRAJ13
	1.98	CAVNSDGQKLLF	TRAV12-2	TRAJ16
	1.48	CAFPESNFGNEKLTF	TRAV38-1	TRAJ48
	1.15	CAVGDDKIIF	TRAV12-2	TRAJ30
Optimised	34.67	CAVSNYQLIW	TRAV12-2	TRAJ33
	13.71	CAVGGGKLIF	TRAV12-2	TRAJ23
	7.76	CALSPSGNTGKLIF	TRAV16	TRAJ37
	5.95	CAVGNDKIIF	TRAV12-2	TRAJ30
	3.1	CVASGTYKYIF	TRAV12-2	TRAJ40
	2.98	CASIGGGRRALTF	TRAV25	TRAJ5
	2.98	CAVIGDKIIF	TRAV12-2	TRAJ30
	4.66	CAVGDDKIIF	TRAV12-2	TRAJ30
	2.85	CATGDDKIIF	TRAV12-2	TRAJ30
	2.72	CAVNSGTDSWGKLQF	TRAV12-2	TRAJ24
	2.07	CIVRGDSWGKLQF	TRAV26-1	TRAJ24
	1.81	CAVNSDGQKLLF	TRAV12-2	TRAJ16
	1.55	CAMRETTASDGQKLLF	TRAV14DV4	TRAJ16
	1.55	CAADGQKLLF	TRAV25	TRAJ16
	1.42	CASMDSNYQLIW	TRAV1-2	TRAJ33
	1.42	CAVGTDKLIF	TRAV12-2	TRAJ34
	1.29	CGTDISGYSTLTF	TRAV30	TRAJ11
	1.29	CAVIAGKSTF	TRAV12-2	TRAJ27
	1.16	CAFPESNFGNEKLTF	TRAV38-1	TRAJ48
	1.16	CAVNAAGTSYDKVIF	TRAV12-2	TRAJ50
	0.91	CVVADDKIIF	TRAV12-1	TRAJ30
	0.65	CAASDTNAGGTSYGKLTF	TRAV29DV5	TRAJ52
	0.65	CAPSQGGSEKLVF	TRAV12-2	TRAJ57
	0.39	CAVRWENSGYALNF	TRAV8-6	TRAJ41
	0.39	CAGRREKLTF	TRAV35	TRAJ48
	0.39	CAVNNARLMF	TRAV12-2	TRAJ31
	0.26	CAVSDDKIIF	TRAV12-2	TRAJ30

Supplementary table 9. TCRβ sequences from RNAseq of HLA A2-NS4B tetramer+ sorted PBMC from donor 0345. Shared TCRβ sequences between sorts are displayed in grey. Unique TCRβ sequences to sort are displayed in blue.

Sample	Frequency (%)	CDR3β	V gene	J gene
Standard	51.46	CSASHRAGNEQYF	TRBV20-1	TRBJ2-7
	33.62	CATGLAGGNEQFF	TRBV15	TRBJ2-1
	5.21	CATSRGQAYEQYF	TRBV15	TRBJ2-7
	2.84	CASSPGTGTYEQYF	TRBV27	TRBJ2-7
	2.29	CASSPGQAYEQYF	TRBV3-1	TRBJ2-7
	2.13	CASSLSDRVGEQYF	TRBV5-1	TRBJ2-7
	1.03	CASSERGSNQPQHF	TRBV27	TRBJ1-5
	0.71	CASRQQGGTEAFF	TRBV6-5	TRBJ1-1
	0.71	CSASAADTDTQYF	TRBV20-1	TRBJ2-3
Optimised	34.5	CATGLAGGNEQFF	TRBV15	TRBJ2-1
	33.29	CSASHRAGNEQYF	TRBV20-1	TRBJ2-7
	10.41	CATSRGQAYEQYF	TRBV15	TRBJ2-7
	4.54	CASSPGTGTYEQYF	TRBV27	TRBJ2-7
	3.74	CASSPGQAYEQYF	TRBV3-1	TRBJ2-7
	2.07	CASSLSSSTGPTDTQYF	TRBV28	TRBJ2-3
	1.9	CSVDVGAYEQYF	TRBV29-1	TRBJ2-7
	1.84	CASSQGQAYEQYF	TRBV4-1	TRBJ2-7
	1.15	CSAFRDFSYEQYF	TRBV20-1	TRBJ2-7
	1.09	CASSQGLAGVHEQFF	TRBV27	TRBJ2-1
	0.92	CASSLDWRGADSPLHF	TRBV5-1	TRBJ1-6
	0.92	CSALAGAFYEQYF	TRBV20-1	TRBJ2-7
	0.86	CASSVLRGRQGAWGEKLFF	TRBV7-3	TRBJ1-4
	0.75	CASSRGGTGDQPQHF	TRBV27	TRBJ1-5
	0.75	CSVDGRTGINEQFF	TRBV29-1	TRBJ2-1
	0.52	CASSPGLAGGLASTDTQYF	TRBV3-1	TRBJ2-3
	0,40	CASRQQGGTEAFF	TRBV6-5	TRBJ1-1
	0.35	CASSQGERFGNEQFF	TRBV4-1	TRBJ2-1

Supplementary table 10. **HLA class I typing of tumour cell lines.** HLA information for commercially available tumour lines was extracted from the TRON database (http://celllines.tron-mainz.de/). HLA typing for patients enrolled in the ACT clinical trial MM909 was provided by the CCIT centre.

	Tumour cell line	HLA A	HLA B	HLA C
Tumours from ACT clinical trial	MM909.11	01:01, 03:01	15:01, 40:01	03:04, 03:04
	MM909.22	01:01, 01:01	44:02, 08:01	07:01, 05:01
	MM909.24	02:01, 30:02	40:02, 40:02	03:04, 03:04
	MM909.37	02:01, 02:01	40:02, 44:02	03:04, 04:01
	MM909.45	01:01, 24:02	13:02, 37:01	06:02, 06:02
Commercially available tumour lines	A 2780	26:03, 26:03	49:01, 37:04	07:01, 02:02
	ACHN	26:01, 26:01	49:01, 49:01	07:01, 07:01
	C1R	Null	Null	04:01, 04:01
	COLO205	02:01, 01:01	07:02, 08:01	07:01, 07:01
	LnCap	01:01, 02:01	08:01, 37:04	07:01, 06:02
	MCF-7	02:01, 02:01	18:01, 35:01	05:01, 05:01
	MDA-MB-231	02:01, 02:17	40:01, 41:04	02:02, 17:01
	MOLT3	01:01, 25:01	16:01, 57:01	06:02, 12:03
	MS 751	02:01, 24:02	35:03, 40:01	03:04, 12:03
	PC-3	24:02, 01:01	55:01, 13:02	01:01, 06:02
	RCC17	02:01, 24:02,	Not available	Not available
	SaOS	02:01, 24:02	13:02, 44:02	06:02, 07:04
	SiHa	24:02, 24:02	40:02, 40:02	03:04, 03:04

Supplementary table 11. Frequency of autologous tumour-reactive tetramer⁺ TCRs. Summary of TCRα (A) and TCRβ (B) clonotypes appearing in the HLA A2-EAAGIGILTV, A2-LLLGIGILVL and/or A2-NLSALGIFST tetramer⁺ sorts that have been previously observed in autologous tumour-reactive sorts

	% frequency in sort				% frequency in sort		
CDR3α	**EAA**	**LLL**	**NLS**	**CDR3β**	**EAA**	**LLL**	**NLS**
CAVQTDKLIF	1.14	0.21	20.93	CATSDRGQGANWDEQFF	26.24	0.99	33.80
CAGTKGGTSYGKLTF	0.13	0.04	3.40	CASTLGGGTEAFF	1.01	0.17	0.10
CAVNSGGGADGLTF	7.34	0.75	0.06	CASSSSDTDTQYF	0.53	0.05	0.87
CAARGAQKLVF	12.21	0.05	0.15	CARRTLVIVRRFYSGNTIYF	0.24	0.46	0.20
CAERLAGGTSYGKLTF	0.09	0.10	0.29	CSEGSPYNEQFF	1.74	0.16	12.96
CAVGLAPQAAGNKLTF	7.12	0.10	0.37	CSVEGSLGRALRANEQFF	7.21	0.37	15.19
CAVNNARLMF	1.54	6.1	0.4	CASSWAGPVEQYF	1.75	0.21	0.20
CAGQGYGKSTF	0.02	-	0.19	CSATGLAGLGEQFF	1.48	34.57	0.24
CAVSIGFGNVLHC	4.45	-	0.24	CSGQANTEAFF	8.73	1.50	0.97
CAVSSSDYKLSF	0.02	-	0.15	CATSDLLLAGGRSSYNEQFF	0.30	0.06	0.01
CAASEGGGFKTIF	0.04	-	0.23	CASSQGLAGSNEQFF	0.24	0.28	0.06
CAFMNPGAGSYQLTF	0,15	-	2.12	CSARDLLAETYEQYF	0.29	-	0.15
CAGGGGGADGLTF	1.16	-	0.03	CASSPTTGLKTRSGYTF	0.43	-	0.23
CAVGGGADGLTF	0.03	0.68	-	CASSLGIISGQPQHF	0.04	-	0.40
CAVPDPENFVF	1.23	-	0.02	CASSYVGLGSPLHF	0.07	-	0.01
CAVSNAGNMLTF	2.52	-	0.03	CASSNGFHFNTLYF	0.61	-	0.41
CAVNKAARQLTF	0.26	0.12	-	CASSFAGTDTQYF	0.52	-	0.41
CALSEADTGRRALTF	-	-	0.04	CASSQGLLLDNEQFF	0.5	-	0.55
CAGQEGSGGSNYKLTF	-	-	0.02	CSVGPGSTGELFF	0.24	-	0.02
CAVPMYSGGGADGLTF	-	-	1.39	CASSLGEGSPGELFF	0.04	-	0.04
CAVPGDKIIF	0.01	-	-	CASSSPMDSGDTDTQYF	0.06	-	0.02
CLLGGSGGGADGLTF	0.02	-	-	CASSYWGLALNIQYF	0.05	-	1.91
CALTEEYGNKLVF	-	-	0.07	CATHGGEKLFF	0.02	-	-
CAVHTGGFKTIF	0.15	-	-	CSARDTTWGLEQYF	0.06	-	-
CALDNYGQNFVF	0.02	-	-	CATKPSGSTDTQYF	0.11	-	-
CAQAAGNKLTF	-	-	0.25	CASSEYTSGNQPQHF	-	0.15	-
CGSNTGNQFYF	0.06	-	-	CASSQEQLAGPEQYF	0.06		-
CAVNGGNKLVF	0.01	-	-	CSARDLIGSQTYEQYF	-	0.04	-
CAVQARPRGSTLGRLYF	-	-	0.02	CASSNTGGYTQYF	-	-	0.03
CAMREGIGNQFYF	-	-	0.07	CASSFLSGAGAETQYF	-	-	0.02
CAVHNARLMF	-	-	0.07	CASSFPEGRLYNEQFF	-	-	0.26
CAMREEGAQKLVF	0.05	-	-	CASSEAASGRPQTF	0.49	-	-
CAVDGGTDKLIF	-	-	0.09				
CALDSNYQLIW	0.17	-	-				

Supplementary table 12. Candidate peptide sequences from MARIA CPL scan ranked in order of recognition likelihood.

#	Sequence	Protein	Abreviation	UniProt
1	MLTFWLVALV	Isoform 9 of Multidrug resistance-associated protein 1	MRP1	P33527-9
2	ITTQTGYSLA	Mucin-16	MUC-16	Q8WXI7
3	LTAGTLLLLT	Serine protease hepsin	HEPS	P05981
4	IVTGVLVGVA	Isoform 3 of Carcinoembryonic antigen-related cell adhesion molecule 3	CEACAM3	P40198-3
5	ILQGFLVMLA	Isoform 2 of Canalicular multispecific organic anion transporter 2	MRP3	O15438-2
6	LSSNIIIHPS	Isoform 2 of Coiled-coil domain-containing protein 110	CC110	Q8TBZ0-2
7	ISAVVGILLV	Receptor tyrosine-protein kinase erbB-2	ERBB2	P04626
8	MSAQIASGMA	Chain A, Proto-oncogene Tyrosine-protein Kinase	SRC	P12931
9	ILSVVTSALV	anaplastic lymphoma kinase Ki-1 variant	NPM1	P06748
10	ILTGSLVALC	STEAP family member 1B isoform 1	STEAP1B	Q6NZ63
11	VLSNVLSGLI	sarcoma antigen 1	SAGE1	Q9NXZ1
12	LISNIKEMIT	calcium-activated chloride channel regulator 2 preproprotein	CLCA2	Q9UQC9
13	IMIGVLVGVA	carcinoembryonic antigen-related cell adhesion molecule 5	CEACAM5	P06731
14	IIQGIDSFVI	myeloblastin	PRTN3	P24158
15	ALSSVGLHMT	squamous cell carcinoma antigen recognized by T-cells 3 isoform X1	SART3	Q15020
16	MLMQWGQFLD	melanoma-associated antigen	MG50	Q92626
17	ITTQTGSPGA	Mucin-16	MUC-16	Q8WXI7
18	ILAGVYALII	P protein	P protein	Q04671
19	GVAGVGAGLA	myeloid leukaemia cell differentiation protein	Mcl-1	Q07820
20	NTAGISQYLQ	kinase insert domain receptor	FLK-1	P35968.2
21	ITTQTGPHGA	Mucin-16	MUC-16	Q8WXI7
22	IIAQTSLGLQ	mucin 5AC	MUC5AC	P98088
23	IKAAIGCGIV	DNA topoisomerase 2-alpha	TOP2A	P11388
24	LQQNVDVFAA	ankyrin repeat domain-containing protein 30A	NY-BR-1	Q9BXX3
25	LLSNEVIWLD	kinesin-like protein	KIF20A	O95235
26	MSQGILSPPA	kinesin-like protein	KIF20A	O95235
27	LLASIAAGLS	Lymphocyte antigen 6 complex	LY6K	Q17RY6
28	NLAAVGLFPA	insulin-like growth factor 2 mRNA-binding protein 1 isoform 1	IGF2BP1	Q9NZI8
29	MLAGSVVIVV	anoctamin-7	Ano7	Q6IWH7
30	LEPQISQGLV	platelet-derived growth factor receptor	PDGF-R	P09619
31	LTTNTGLQMW	melanoma-associated chondroitin sulfate proteoglycan	MCSP	Q6UVK1
32	LLTSVLVTTT	Mucin-16	MUC-16	Q8WXI7